BRNO UNIVERSITY OF TECHNOLOGY
VYSOKÉ UČENÍ TECHNICKÉ V BRNĚ

FACULTY OF MECHANICAL ENGINEERING
FAKULTA STROJNÍHO INŽENÝRSTVÍ

HEAT TRANSFER AND FLUID FLOW LABORATORY
LABORATOŘ PŘENOSU TEPLA A PROUDĚNÍ

APPLICATION OF POLYMERIC HOLLOW-FIBER MEMBRANES IN AIR FILTRATION
VYUŽITÍ POLYMERNÍCH MEMBRÁN NA BÁZI DUTÝCH VLÁKEN K FILTRACI VZDUCHU

DOCTORAL THESIS
DIZERTAČNÍ PRÁCE

AUTHOR — **Ing. Pavel Bulejko**
AUTOR PRÁCE

SUPERVISOR — **prof. Ing. Tomáš Svěrák, CSc.**
ŠKOLITEL

BRNO 2019

Abstract

Hollow-fiber membranes (HFMs) have widely been applied to many liquid treatment applications such as wastewater treatment, membrane contactors/bioreactors, membrane distillation etc. Despite the fact that HFMs are widely used for gas separation from gas mixtures, their use for mechanical filtration of aerosols is very scarce. This work studied filtration performance of polypropylene HFMs including filtration efficiency, pressure drop and pressure drop evolution with long-term dust loading. Filtration efficiency was measured using different challenging aerosols including micronized titanium dioxide powder and aerosolized ammonium sulfate. Pressure drop was measured in various configurations, including different HFM area and fiber diameter. Pressure drop evolution with long-term particle loading was carried out using a challenge dust as defined in ANSI/ASHRAE 52.2 standard. Mathematical models developed for prediction of air filtration efficiency and membrane permeability/pressure drop were compared applying them on the structural parameters of the HFMs. These membranes are characteristic of pore diameters of about 90 nm and relatively low porosity, thus high potential for nanoparticle removal from air. Furthermore, analysis on cake pressure drop and evaluation of energy demands for fun operation were done and compared with theoretically predicted values. Finally, an attempt to estimate life-cycle cost of air filtration using HFMs was outlined.

Abstrakt

Membrány z dutých vláken jsou široce využívány v aplikacích týkajících se úpravy kapalin jako např. při čištění odpadních vod, v membránových kontaktorech a bioreaktorech, membránové destilaci apod. I když jsou často využívány při separacích směsí plynů, je jejich použití pro mechanickou filtraci aerosolů velmi vzácné. Tato práce se zabývá filtrací vzduchu pomocí polypropylenových membrán z dutých vláken včetně jejich filtrační účinnosti, tlakových ztrát a také zanášením při dlouhodobé filtraci. Filtrační účinnost byla proměřena za použití různých aerosolů jako TiO_2 a síran amonný. Tlakové ztráty byly měřeny při různých konfiguracích, tj. různé filtrační ploše a průměru vlákna membrány. Zanášení membrán bylo testováno použitím normovaného prachu definovaného normou ANSI/ASHRAE 52.2. Predikční modely pro filtrační účinnost a permeabilitu/tlakovou ztrátu membrány byly aplikovány na parametry membrán z dutých vláken a porovnány. Tyto membrány mají velikost pórů kolem 90 nm a poměrně nízkou porositu a tím vysoký potenciál pro separaci nanočástic ze vzduchu. Dále byla provedena analýza filtračního koláče a vyhodnocení energetických nároků a porovnány s teoretickými modely. V závěru práce je nastíněn odhad ceny životního cyklu při filtraci pomocí těchto membrán.

Keywords

Air filtration, hollow-fiber membrane, aerosol, filtration efficiency, pressure drop, fouling, filtration cake, dust-holding capacity, energy consumption, life-cycle cost

Klíčová slova

Filtrace vzduchu, membrána z dutých vláken, aerosol, filtrační účinnost, tlaková ztráta, zanášení, filtrační koláč, kapacita zadržení prachu, spotřeba energie, náklady na životní cyklus

BULEJKO, P. *Application of polymeric hollow-fiber membranes in air filtration*. Brno: Brno University of Technology, Faculty of Mechanical Engineering, 2019. 139 pp., Supervisor: prof. Ing. Tomáš Svěrák, CSc.

Declaration

Hereby I declare that the doctoral thesis "Application of polymeric hollow-fiber membranes in air filtration" is my own work under supervision of prof. Ing. Tomáš Svěrák, CSc. and that all literature sources were quoted completely and correctly.

Brno……..

……

Ing. Pavel Bulejko

Acknowledgement

I would like to sincerely thank my supervisor prof. Ing. Tomáš Svěrák, CSc. for his patience, motivation, friendly attitude, free hand in the work and ceaseless encouragement. I would also like to thank prof. Ing. Jaroslav Horský, CSc. (in memoriam) and prof. Ing. Miroslav Raudenský, CSc. who have allowed the establishment of our chemical engineering group and supported us financially.

I would like to sincerely thank prof. Ing. Mirko Dohnal, DrSc. for valuable discussions on the topic of hollow-fiber membranes and membrane separations generally. A lot of thanks also go to ZENA Membranes s.r.o. for providing me with hollow-fiber membranes and for cooperation on this work. I must also express my sincere gratitude to head of the Energy Institute of the Faculty of Mechanical Engineering, doc. Ing. Jiří Pospíšil, Ph.D., for providing me with the necessary facilities for particle concentration measurement. I would also like to thank Ing. Jakub Ondráček, Ph.D. from Laboratory of Aerosol Chemistry and Physics of the Academy of Sciences of the Czech Republic for rendering the measurements of filtration efficiency of closed hollow-fiber membrane modules using their experimental facilities, which comprise one chapter of this thesis.

Great thanks also go to all people from Heat Transfer and Fluid Flow Laboratory for their help with many problems I came across when dealing with this work, mainly in experimental part. Among others I would like to praise my colleagues from our "chemical band" especially Ing. Ondřej Krištof and Ing. et Bc. Pavel Kejík for their help, advices, sophisticated and productive talks on (not only) the topic in Na Devadesátce pub and for creating a very good friendly atmosphere with a lot of fun which lighten myself during some for me difficult times. Last but not least, I would like to thank my family for their never-ending support.

Finally, I would like to thank God who has presented me with patience, will, tirelessness and perseverance and all those attributes necessary for accomplishment of every target not only in this work but also in whole life.

Contents

1 Introduction

1.1 Problem background

Air filtration is used in a plethora of applications such as air pollution control, emission reduction, respiratory protection for human and processing of hazardous materials. The rising awareness of environmental agencies and the general public for a cleaner environment is forcing many industrial companies to consider a filtration process in their plants. Another driving force for a progress in air filtration field is the increasing need for a clean air environment in many advanced industries. Such industries include micro/electronics, medical applications, pharmaceutical production, biological research, gas turbine and nuclear energy installations and others. With increasing development of nanotechnologies, the filtration of airborne nanoparticles has become a significant issue due to their large production in material synthesis and combustion processes. Nanoparticles are particles with at least one dimension smaller than 100 nm. In an airborne form, they pose a significant health risk due to their high mobility and toxicity caused by a large specific surface. They may also lead to a new hazard and risks to the environment. Aerosol filtration has been widely studied both experimentally and theoretically and models for fibrous filter media are well developed and documented [1–3]. Several works reviewed the use of air filters for nanoparticle removal. For example, Wang and Otani [4] focused on fibrous filters and their performance while Shaffer and Rengasamy [5] reviewed respiratory protection against airborne nanoparticles. More recently, stricter environmental and safety standards have led to higher performance filters in the traditional respirator and industrial air filtration markets. Therefore, we can observe a growing impact of membranes in air filtration applications over the last two decades [6].

Membrane air filtration is an exciting development which is nowadays considered the most efficient physical method for airborne particle separation. Traditional commercial air filters such as glass fiber or melt-blown based filters provide low filtration efficiencies for particle sizes between 100 and 500 nm. This is due to large diameters of their fibers, mostly in the order of tens to hundreds of micrometers, compared to airborne particle sizes. It is thus necessary to increase the filter thickness to enhance the filtration efficiency, which in turn dramatically increases the pressure drop [7]. The development of high efficiency air filters is mainly dependent on an understanding of the most penetrating particles. The removal of such particles was significantly improved using membranes based on nanofibers. However, even high-efficiency particulate air filters (HEPA) can remove only 99.97% of particles which means that a very small fraction can still escape the filter. As these particles are very small, they are most dangerous and easily inhaled [8]. Therefore, the removal of these should be prioritized. Another issue arising from application of fibrous filters is the filtration regime they operate in. Vast majority of fibrous filters operate in a deep bed filtration regime. These filters cannot be regenerated which is a significant shortcoming. From this point of view, membrane filters which operate in a surface filtration regime are significantly advantageous because their cleaning is very simple using various techniques such as vibration/shaking, back-pulse/back-blow or blowing the membrane surface. Even though the initial pressure drop of such a membrane can be higher compared to deep-bed filter, its life cycle is significantly prolonged. Then, it is a tradeoff between the energy use which is higher for operating the membranes and recycling/disposal possibilities which in turn are very limited for deep bed filters. The recycling is also important due to environmental issues being raised more and more

intensely. Nowadays, due to large amount of used filters, there are concerns about the impact of the filter disposal. Therefore, there is a trend towards manufacturing of filters with longer lifetimes and filters which are cleanable. These filters mitigate the environmental impact by reducing their volume disposed in landfills or incineration plants [9]. Such membranes which are already very well-known and extensively applied to a large industrial scale could be hollow-fiber membranes (HFMs).

HFMs, first patented by Mahon in 1966 [10], possess several advantages. The hollow fiber geometry offers a larger active membrane area per unit volume of the membrane module resulting in a greater process intensification. Moreover, hollow fibers provide a good mechanical support and easy handling during module fabrication and process operation [11] as well as their cleaning. This is a tremendous challenge when dealing with filters based on extremely fine nanofibers which can jeopardize the robustness of the filter, thus requiring a mechanical support. The excellent mass transfer caused by the hollow fiber geometry have led to various commercial applications in different fields such as medical (blood fractionation), water purification/desalination, micro/ultrafiltration, reverse osmosis, liquid/liquid and liquid/solid separation, gas separation, hemodialysis and so on [12]. Other applications of HFMs are in various stages of development. Among others, it is air purification and other miscellaneous operations such as air de/humidification [13, 14]. Utilization of HFMs in air treatment, especially in air filtration is quite a new topic which has been scarcely studied. At the very beginning of this thesis proposal in 2015, there was no research work carried out on the air filtration using HFMs. During last year, several works have been done and published by a research group from Singapore [15–17] and China [18]. HFM modules with primary application in air filtration have even recently been found in portfolio of several companies [19–25]. Another company dealing with HFM production is Zena s.r.o. [26]. This company produces HFMs made of polypropylene via dry stretching technique. The main applications of these HFMs are water/wastewater treatment and membrane contactor/bioreactor technology. However, it was suggested to explore how the same HFMs would act as air filters and what air applications would be appropriate for such a filter. Therefore, following objectives were proposed to be solved in the framework of this thesis.

1.2 Research objectives

This work will study air filtration using HFMs. These objectives were specified for the work:

1. Analysis of the current state of the art in the high-efficiency air filtration:
    - overview of air filtration technology, high efficiency filter media;
    - HFMs in air filtration,
    - mathematical modeling of air filtration;
2. Design of experimental apparatus for testing the performance of HFMs;
3. Experimental investigation of HFMs' performance:
    - collection efficiency of different types of HFMs for different particles at different conditions: aerosol from incense stick burning (polydisperse), aerosol of dispersed micronized TiO_2 powder (polydisperse), ammonium sulfate solution generated aerosol (monodisperse and polydisperse), different flowrates and aerosol concentrations;

- pressure drop and pressure drop evolution with long term dust loading using a TiO_2 dust and an ASHRAE A2 dust at different filtration conditions;
- dust holding capacity for various conditions;

4. Life cycle cost estimate of air filtration using HFMs;
5. Comparison of results with other works and filtration materials.

1.3 General definitions and terminology related to this thesis

The definitions are mostly taken from [27].

Aerosols – solid and liquid airborne particles, typically ranging in size from 0.001 to 100 µm.

Air cleaning – removal of gases or vapors from the air.

Air filtration – removal of aerosol contaminants from the air.

Airborne contaminants – gases, vapors, or aerosols.

Arrestance – ability of a filter to capture a mass fraction of coarse test dust.

Collection/filtration efficiency – fraction of entering particles that are retained by the filter.

Dust holding capacity – measurement of the total amount of dust a filter is able to hold during a dust-loading test.

Filter face velocity – air stream velocity just prior to entering the filter.

Filter performance – a description of a filter's collection efficiency, pressure drop, and dust holding capacity over time.

Fractional efficiency – collection efficiency for a given particle size or particle size range.

Life-cycle cost – sum of all filter costs from initial investment to disposal and replacement, including energy and maintenance costs.

Particulate filter – collects aerosol only mechanically or electrostatically:

- *Fibrous* – assembly of fiber randomly laid perpendicular to airflow;
- *High-efficiency* – primarily used to collect particles smaller than 1 µm;
- *Low-efficiency* – primarily used to collect particles larger than 1 µm;
- *Mechanical* – cotton, fiberglass, polyester, polypropylene etc.;
- *Polarized (electret)* – contains electrostatically enhanced fibers.

Pressure drop – a difference in static pressure measured upstream and downstream of a filter. A measure of airflow resistance through the filter.

2 The current state of knowledge

2.1 Background information

Air and other gases filtration seems to be considered as the less important part of the general filtration compared to liquid filtration business. This is not unusual because gas filtration make up only about 15% of the total filtration market. Nonetheless, application of gas filtration can be found almost in every aspect of human activity, some of them are growing in importance. There are several differences between gas and liquid filtration. From the equipment point of view, various and much wider range is employed in liquid filtration. Gas filtration is mostly conducted using a replaceable filter unit which is kept in an appropriate housing. So there is no equivalent complex processing of filters used for liquid suspensions treatment. The next point is the concentration of liquid and gas suspension. Most of the gaseous phase filtration is designed and used for treatment of very dilute suspensions. Gas filtration systems are used for removal very small amount of solid particles or liquid droplets, often much less than 1% from overall continuous gas flow. Typical for gas filtration are large flow rates involved in some applications. Therefore, given installations may require large filtration areas. Gas filtration often involves depth filtration as separation mechanism which is allowed due to low concentrations of feed and which also permit acceptable solid retention volumes [28].

Probably the largest number of air filters is used in the systems controlling indoor air quality (IAQ) in living accommodations (domestic, commercial and institutional) and also in working spaces. Especially of growing interest are clean rooms installations for critical assembly processes. These are now being supplemented by the vent filters controlling discharges from working spaces where potentially hazardous atmospheres are used. These filters are being grouped under the term HVAC (heating, ventilation and air conditioning) and are basic means for improvement of IAQ. Filters designed for the treatment of air are divided into three categories:

1. *Primary filters* – are designed for capturing the majority of larger particles of 5–10 μm in size and have high holding capacity. These filters are able to work with relatively high airflow velocities.
2. *Second-stage filters* – these have finer media for trapping and retaining smaller particles which passed through the primary filter i.e. smaller than 5 μm.
3. *Ultrafine filters* – final stage filters are of very high efficiencies i.e. 99.95% or more, even for submicron particles. The high efficiency particulate air (HEPA) and ultra-low penetration air (ULPA) filters belong to this group. These employ a high density medium made of synthetic spun fibers of sub-micrometer diameter in the form of closely pleated pack. Air velocity is limited to about 0.03 $m \cdot s^{-1}$ [29].

2.1.1 Air filtration equipment

The filters currently employed for gas cleaning at ambient temperatures come in two broad types delineated by their shape, i.e.:

1. *Cylindrical:*
   - a bag filter, hanging from the top of its housing,
   - a cylindrical core fixed inside a concentric housing and formed of a molded cylinder of bonded fibers or granules,

- a single piece of thin medium folded in a shape of concertina to fill the housing;

2. *Flat panel consisting of a rectangular frame that carries either:*
   - a thick pad of filter medium or,
   - a set of pockets or (Fig. 2.1b),
   - a piece of pleated filter medium (Fig. 2.1d).

a)  b)  c)  d) 

Fig. 2.1: *Compact (a), pocket (b)* **[30]***, bag (c) and mini-pleated (d) filter* **[31]**

The filter cartridge, whether yarn wound, bonded fiber (or granules), or pleated sheet, has taken much of the filtration market. This is mainly due to its ability to offer finer levels of filtration which is a demanded trend. This trend is also leading to the use of membrane media in pleated cartridge applications. The cartridge is used in critical air filtration applications, especially compressed air production, but numerically is more common in baghouse utilizations.

In volume terms, the greater part of air filtration is probably undertaken by the panel filters used to protect building ventilation systems and the internals of large engines especially gas turbines. These usually are formed of a rectangular frame carrying some filter medium fitted in a matching space in a dividing wall between the ambient air and the required clean zone. The filter medium in its simplest form is a thin pad of a nonwoven material. This has, however, only limited capacity in terms of air flow and particle retention. More often, it is in the form of a layer of a pleated sheet material or of a set of pockets protruding backwards away from the front of the frame (Fig. 2, the second from the left). Most recently, and of rapidly growing occurrence, there are V-block panels formed of sets of V-shaped zones with its sides made of smaller panels of filter media made of mini-pleats (Fig. 2, the first from the left). These panels are available in a wide range of materials and matches the HEPA/ULPA and ASHRAE standards [28].

A building's HVAC system is absolutely critical to its IAQ. An HVAC system must be properly designed and installed, commissioned, operated and maintained to produce maximum results. It must also prevent sick building syndrome at the same time. Ventilation is naturally a large part of HVAC system and also of creating a healthy indoor environment. The next important factor for IAQ is maintenance. The costs associated with health problems and productivity loss can be far greater than the savings coming from not performing needed maintenance. To ensure maximum efficiency, there should be continuous monitoring of the ventilation and humidity control systems as well as watchful water and moisture control. HVAC system efficiency also benefits from semiannual monitoring, testing, adjusting and rebalancing. Prior to any construction or remodeling, systems should also be washed out and construction should be isolated from buildings occupants by space, time or barrier to minimize infiltration of pollutants into the workspace [32].

2.1.2 Mechanisms of particle deposition

Several different collection mechanisms take place during filtration of aerosols. These are mainly mechanical means of separation, i.e. inertial impaction, interception and diffusion (Brownian motion). Furthermore, it can be electrostatic attraction typical for electret filters, i.e. filters posing electric charge to enhance their efficiency, and gravitational settling occurring for larger particles. In this work, only mechanical means of separation are considered (Fig. 2.2a). The prediction of overall efficiency is based on efficiency of a single fiber which is based on individual mechanisms.

The inertial impaction occurs when particle carried by an air stream passing around a fiber deviates due to its inertia from the streamline and collides with the fiber. The interception effect is due to the finite size of particles. Assumed that the particles follow the air flow streamlines, interception occurs when a particle comes within one particle radius from the fiber surface. Interception may play an important role for nanoparticles filtered using a filter with a very small fiber diameter. The diffusion mechanism is typical for very small particles undergoing random Brownian motion which then collide with the fiber and are captured. Generally, the relative contributions of diffusion and particle inertia to deposition are functions mainly of particle diameter, gas velocity and fiber diameter. Particle inertia contributes to separation of large particles whereas diffusion dominates under 100 nm. The particle inertia and Brownian motion are weak for the medium size particles [33]. As a consequence, the collection efficiency of a fibrous filter has a minimum value (Fig. 2.2b) which is the most penetrating particle size (MPPS). In reality, filtration efficiency (η) is determined as follows:

$$\eta = 1 - \frac{C_{\text{down}}}{C_{\text{up}}} \tag{2.1}$$

where C_{down} and C_{up} are the particle concentration downstream and upstream of the filter, respectively. Another important parameter used mainly for comparing different filters is a filter figure of merit also referred to as quality factor (QF) which is the ratio of filter penetration to filter pressure drop (Δp):

$$QF = \frac{-\ln(1-\eta)}{\Delta p} \tag{2.2}$$

The filtration mechanisms together with the mathematical modelling and prediction models for filtration efficiency are described in chapter 3 in a greater detail.

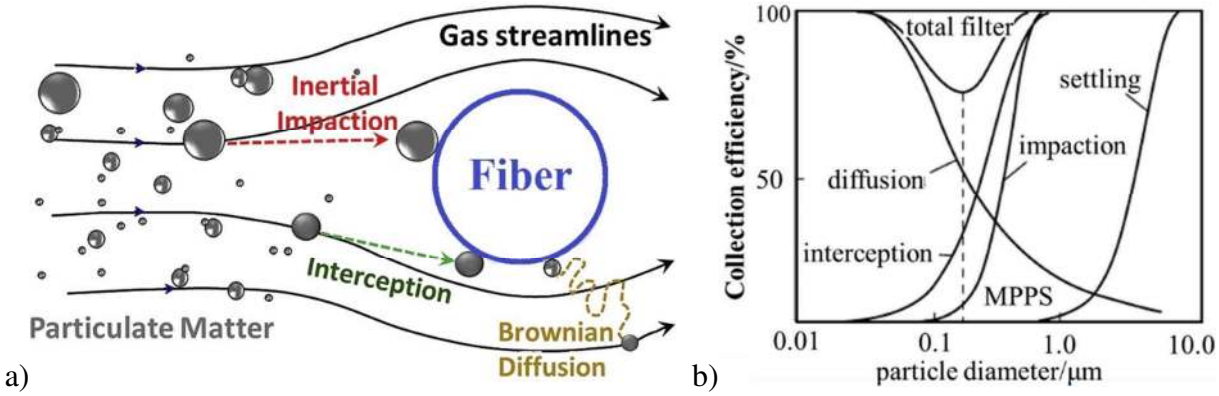

Fig. 2.2: *Individual collection mechanisms (a – adopted and adjusted from* **[34]***) and filtration efficiency for individual single-fiber mechanisms and total efficiency (b)* **[7]**

2.1.3 Air filtration applications

The avoiding of contaminating material has been and continues to be more demanding. The efficiency of cleaning should be greater and the cut-point of solid particle separation should be lower. Typical sizes of common air contaminants and a comparison of different equipment for particulate matter mitigation with air filtration are shown in Fig. 2.3. In general, the main applications of gas filtration are:

- respirators and breathing air systems,
- compressed air production, typically for pneumatic and hospital air systems,
- critical working atmosphere venting and control, including provision of cleanrooms,
- general building ventilation and air conditioning,
- vehicle cabin air filtration, including atmosphere control in buses, trains, airplanes etc.,
- mobile engines air intakes and exhausts (especially for diesel engines),
- process air cleaning, where the air is a process input or coolant,
- demisting of gas streams free of water or oil droplets.

Not included in that list are process exhausts especially where these come from chemical reactions like ore roasting, heating furnaces, i.e. where the exhausts are hot and usually heavily laden with suspended solids.

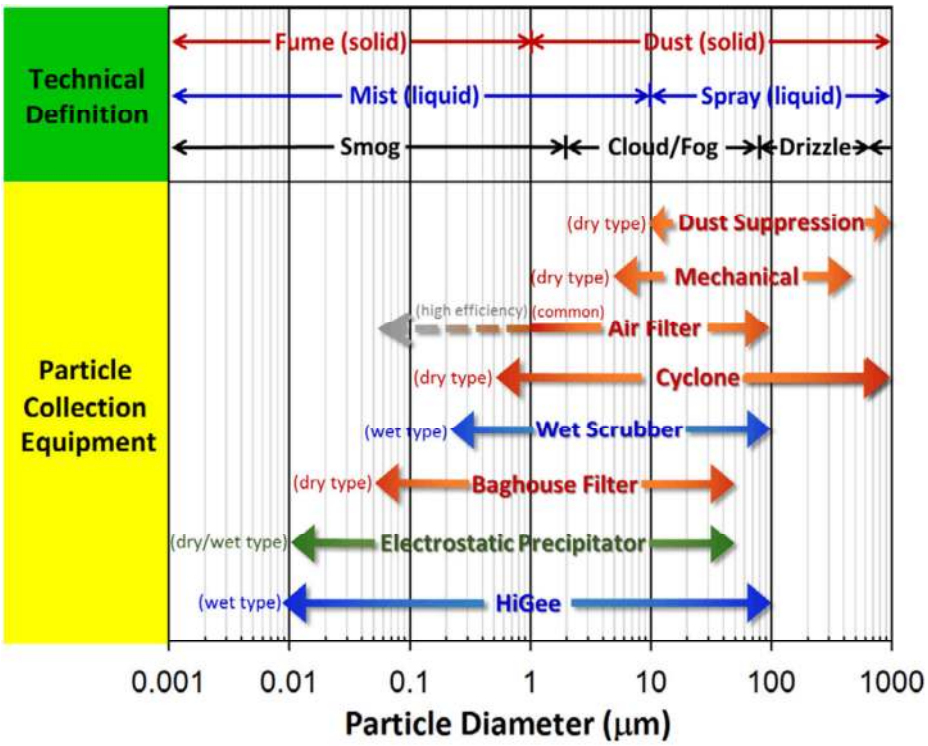

Fig. 2.3: *A relationship between various types of particulate control equipment and their applicable particle size of collection* **[34]**

Concerning the membrane air filters, these are ideal in a number of medical and biopharmaceutical applications. The low pressure drop, ULPA efficiency and hydrophobic membrane properties are essential in surgical and hospital airway management, protecting both patient and equipment. Depending on the particular requirements, the membrane may be treated to enhance its oleophobic properties. In biopharmaceutical manufacturing membrane filters are used

to vent gases produced during fermentation and cell culture. These vent filters require absolute barrier to microorganism in aerosol. Cleanrooms and other industrial applications benefit from membranes as well. When combined with suitable support layers, membrane based filter media have very low off-gassing. This is essential in the critical microelectronics cleanroom environments. HEPA and ULPA filters provide absolute protection for cleanrooms. They are designed to be installed for the lifetime of cleanroom. Pre-filters are used to capture the majority of particles in the airstream and reduce the load on the membrane filters. Membranes are also utilized in a growing number of air filtration applications such as respirators and personal protective equipment. Air filtration membranes are demanded also in applications where risk of exposure to harmful contaminants is present. Another set of common applications for membranes is consumer and industrial vacuum cleaners. There are two types of filters in these applications i.e. those that protect the equipment itself (e.g. vacuum motor) and those that filter the exhaust air. Filters of vacuum cleaner run at very high air velocities compared to other air filtration applications. Membranes can provide high efficiency at these higher airspeeds and the low pressure drop enables the high airflow rates with reduced power consumption. The dust cake on the filter surface can be easily cleaned after use via shaking or water spray and the membrane filter returns nearly back to their original pressure drop and efficiency [6].

2.1.4 Air filtration costs

The pressure drop in the gas stream as it flows through a filter represents an energy loss which has to be made up by the overall system. This is especially in large volume applications such as gas turbine air intakes and process exhausts. Since the more efficient filter media need higher pressure drops to move the air through it, many activities have been put into the development of media with lower pressure drop such as membrane materials in the form of a surface layer made of fine fibers. These materials provide not only a lower energy operation but also give more efficient filtration [28]. Cost associated with air filtration and air-cleaning systems can be divided into three general categories – initial costs (investment), operating (energy, maintenance) and replacement (disposal) as shown in Fig. 2.4a. An example of cost of operating an MERV8 filter is shown in Fig. 2.4b. Although some users might consider only the initial costs when selecting an appropriate filtration system, it is important to take into account all of the life-cycle costs.

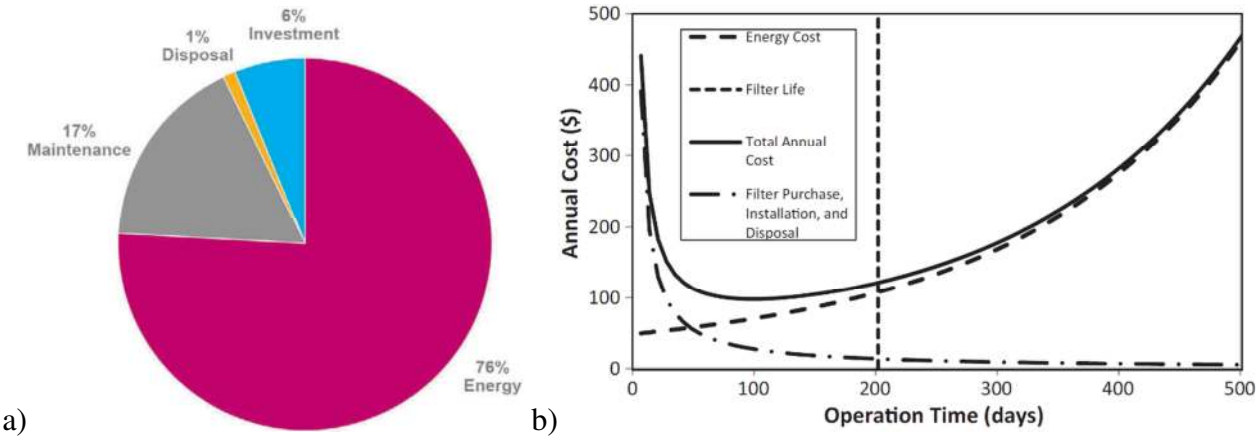

Fig. 2.4: *Air filter life-cycle cost (a)* **[35]** *and an MERV8 pre-filter annual cost (b)* **[36]**

Initial costs include those for original equipment, i.e. the filter rack system, individual filter units and auxiliary accessories, and the direct and indirect costs associated with the installing the system related to the electrical, ducting and the other works. So the total purchase cost of a filtration system is the sum of the costs of the filter rack system, filter units and auxiliary equipment, instruments and controls, taxes, and freight. Particulate filters expenses generally increase as filter efficiency and quality increase. A lower-efficiency may be adequate for some applications and can be used instead of HEPA filter to control the costs while achieving adequate performance. Other factors that influence the initial costs of the system include the volumetric flow rate, contaminant concentrations and humidity. Volumetric flow and pressure drop may be the most important factors because they determine the size of duct and filter rack as well as blower and motor.

Annual *operating costs* include operating labor and materials, replacement filters, maintenance, utilities, waste disposal and equipment depreciation. The costs vary based upon the specific filtration system. Many of these costs should be considered in terms of the present value of money. Operating and maintenance labor costs depend on the filter type, size and operating difficulty of a particular unit. Electrical costs to operate the blowers are directly related to airflow through and pressure drop across the filters.

An important part of *replacement costs* relates to the estimated life of the filtration system. As filter life increases, the cost per operating hour falls. Nonetheless, mechanical filters exposed to contaminated air increase pressure drop across them and this increases costs of consumed electricity to move air using fans. Costs can be minimized by evaluation of the system and selection of the best final pressure drop to replace filters based on extended filter life and minimized power requirements. Factors affecting particulate filter life include contaminant concentration, particle size distributions, airflow rates, filter efficiency and quality. Filter replacement labor costs depend on the number, size and type of filters, their accessibility, how they are held in the filter rack, and other factors affecting labor.

The cost of a standard HEPA filter (610 mm × 610 mm) is approximately 100 to 250 USD. Initial HEPA filter pressure drops are in range 250 to 325 Pa, depending on the design flow rate, fan performance curve and related issues. Maximum pressure drop can be as high as 750 Pa. Operating costs are in the order of 5.40 USD per square meter of floor area per year [27].

2.2 High efficiency air filtration

2.2.1 Air filtration membranes

In 2009, Galka and Saxena of Lydall Filtration [37] published an article [6] about a growing importance of membranes in high efficiency air filtration and focused mainly on, at that time highly used and developed, membranes made of ultra-high molecular weight polyethylene (UPE, Fig. 2.5a) and expanded polytetrafluorethylene (PTFE, Fig. 2.5b). At that time, expanded PTFE membrane filtration media had been used in air filtration for over a decade and a new membrane air filters based on UPE were introduced to the market. Air filters produced with PTFE and UPE membranes possess exceptional efficiency and pressure drop. Performance varies depending on the exact efficiency class of the membrane. PTFE is nearly universally compatible with acid, bases, aqueous solutions and organic solvents and exhibits higher levels of water repellency at

similar permeability levels. The strong carbon-fluorine bond provides excellent thermal resistance (maximum use temperature up to 260 °C). High efficiency PTFE membranes are very thin layers, typically of 10–25 µm thickness (for comparison, microglass filter media has a typical thickness of 300–400 µm). PTFE membranes filter via a surface exclusion mechanism as they are thin and possess few layers of fibrils. They are highly porous but have small depth for particles to be captured and retained within. Therefore, most of the high efficiency air filters is dependent on high dust holding capacity media to be pre-filters. The very next problematic issue of PTFE is consistency as membrane become thinner and the impact of manufacturing process variations. There is also low strength and stiffness that is why they cannot be handled. They must be stretched and laminated to a support layer to provide strength for handling. A protective face layer is often implemented due to low abrasive strength.

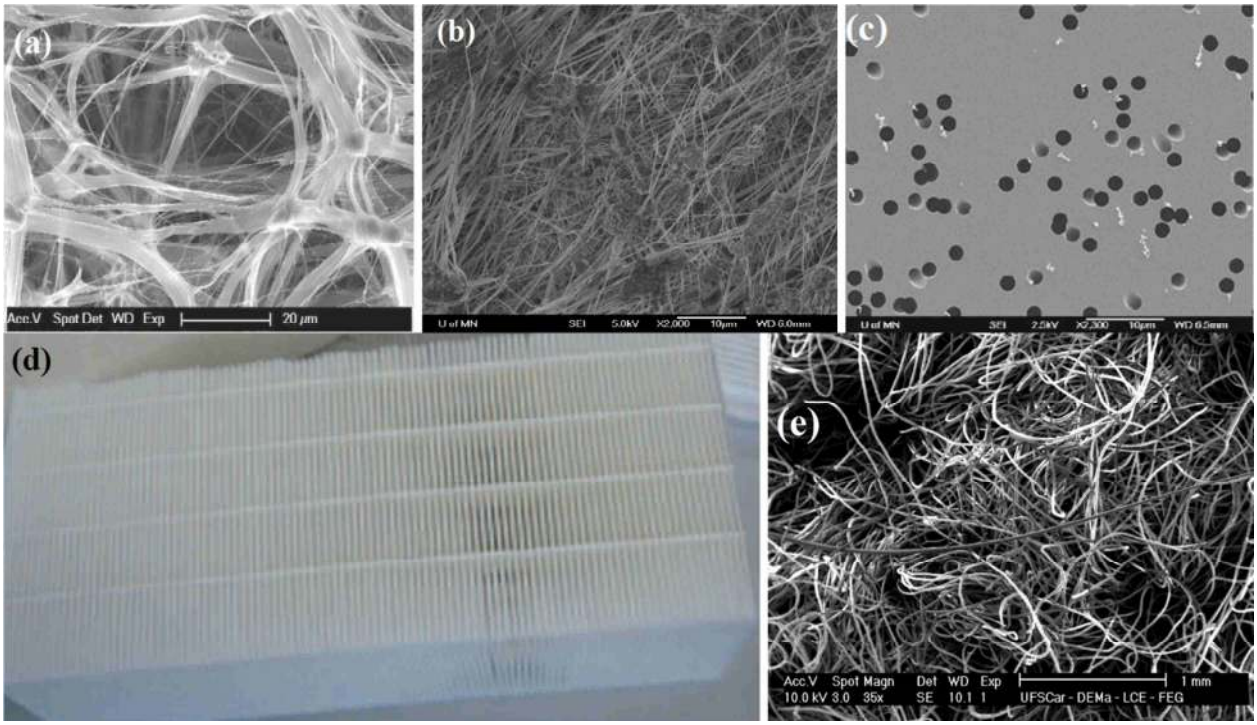

Fig. 2.5: *SEM images of various air filtration membranes: (a) UPE* **[6]***, (b) PTFE* **[38]***, (c) Nuclepore* **[39]***, (d) pleat packs of UPE membranes on thin PET substrates* **[6]** *and (e) SEM image of a PES fibrous filter* **[40]**

The very long linear molecular chain of UPE (10 to 100 times greater than that of normal linear PE) and the absence of chemical groups give the polymer high resistance to radiation energy. UPE membranes may be sterilized using high doses of gamma radiation without significant degradation of structural or filtration properties. With its simple structure consisting of carbon and hydrogen, UPE is an environmentally friendly polymer. It may be incinerated without harmful by-products created by chemical groups within other polymers. UPE membrane thickness varies between 40 and 150 µm depending on efficiency class. The structure is unique as it is composed of a number of fibril layers. It creates a surface loading structure for larger particles while providing depth for high capture and holding capacity of particles not filtered on the surface. The result is higher void space and loading capacity than that of PTFE membranes. The UPE membranes are 3 to 10 times thinner than microglass and are unable to approach the inherent dust holding capacity of

microglass media. An exciting aspect of the UPE air filtration membranes is its inherent structural integrity. This is a result of the combination of large structural and small filtering fibers. With the high toughness and abrasion resistance, the protective face material is not required. UPE membranes are easily produced in the form of a roll as stand-alone films. This creates the flexibility to create composite constructions using a wide range of substrates, e.g. pleated packs (Fig. 2.5d). A PES fibrous filter to compare with structure of the membranes is shown in Fig. 2.5e.

Nuclepore filter (Fig. 2.5c) is another type of membrane. These polycarbonate (PC) membranes possess microscopic circular pores of uniform diameter, approximately perpendicular to the surface. These membranes were used for specific applications such as measuring workplace exposures or air pollution monitoring. Models were developed to predict the filtration efficiency of these membranes based on four mechanisms, i.e. impaction, interception, pore and surface diffusion [41]. These will be considered in a greater detail in chapter 3.

2.2.2 Nanofibrous membranes

Nanostructured materials are at the forefront of today's material research and provide one of the greatest potential for improving performance and capabilities of products in a number of industrial sectors. Nanofibers are one of the most important nanostructures in nanoscience and nanotechnology.

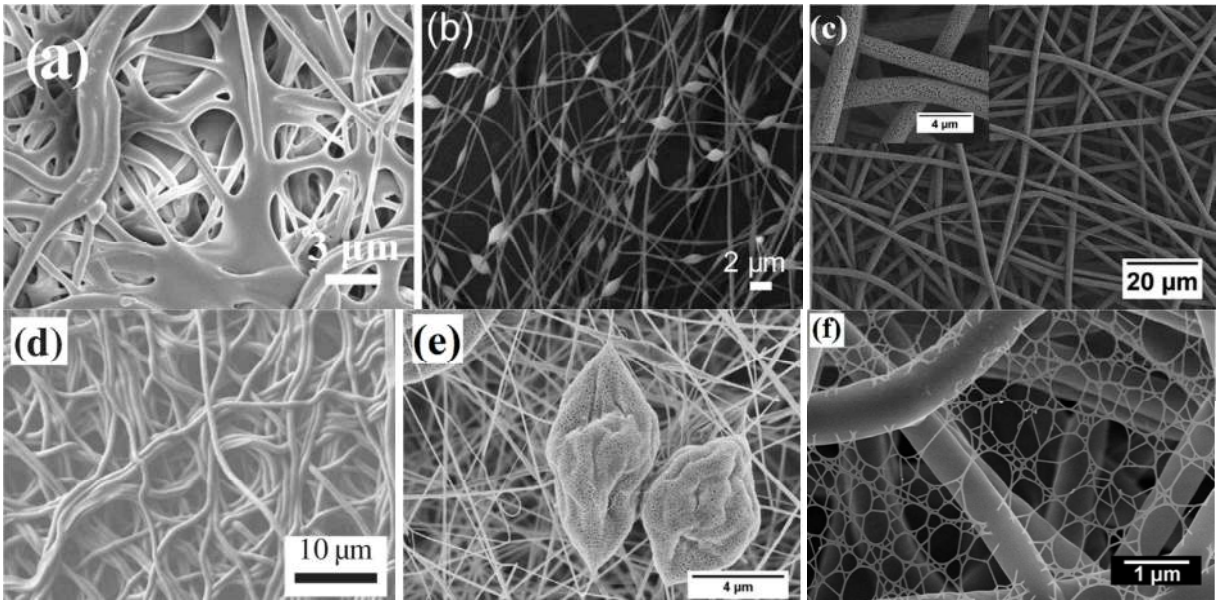

Fig. 2.6: *SEM pictures of various nanofibrous membranes: (a) PVA-PAA* **[42]***, (b) PAN-GO* **[43]***, (c) PLA* **[44]***, (d) PVA-CA* **[45]***, (e) PU/SLS* **[46]**

The most used method for fabrication of nanofibers is electrospinning. Compared to other methods of fiber fabrication such as template synthesis, drawing or phase separation, this method has emerged as a straightforward approach to nanofibers with high specific surface area, high porosities and controllable composition for a wide range of applications [47]. The spectrum of filtration materials made of electrospun nanofibers is extremely broad. They are based on various polymers such as poly(lactic acid) (PLA, Fig. 2.6c) or combination of several polymers, e.g. polyvinylalcohol-poly(acrylic acid) (PVA-PAA, Fig. 2.6a). They can create various structures, composite layers or so called nanonets, i.e. very fine nanofiber nets on the surface of a fibrous

support (Fig. 2.6f). Another option is to combine polymers with inorganic materials such as polyacrylonitril with graphene oxide (PAN-GO, Fig. 2.6b) or addition of surfactants to improve nanofiber morphology such as in polyurethane with sodium laurylsulfonate (PU/SLS, Fig. 2.6f) or PVA with citric acid (Fig. 2.6d). Even though electrospinning of nanofibers and their air filtration applications is fairly a new topic, it has been extensively reviewed in several books or chapters, see e.g. [48–51]. Concerning the newest advances in nanofibrous membranes for air filtration applications, see e.g. [7, 42, 43, 45, 52–66].

2.2.3 Testing of high efficiency air filters

When the highest levels of air purity are required, e.g. in cleanrooms for the pharmacy and food industries or in hospital operating theatres, EPA, HEPA and ULPA filters are the solution. In Europe, these filters are subject to classification according to EN 1822 [67] for filtration efficiency and zero leakage. HEPA and ULPA filters are also subjects to individual tests.

First part describes classification, performance testing and labeling (Table 2.1). EPA/HEPA/ULPA filter classification is based on values for local particle collection efficiencies (local values) and integral efficiency (integral value). Each is assessed on the basis of the most penetrating particle size (MPPS). For the classification of EPA filters, a leak testing is not possible and not necessary. Therefore, no local values as leak detection limits are given for this group. Next part of the standard deals with aerosol production, measuring equipment and particle-count statistics. This section includes the definition of measuring instruments and aerosol generators, and sets out the statistical basis for evaluating low-level particle counts. Third section describes the testing of fractional collection efficiencies and the determination of the particle size for which the efficiency is a minimum (MPPS) of the flat sheet filter medium. Samples of the filter medium are subjected to a defined air flow, to which a test aerosol is added. Partial flows of the test aerosol are sampled upstream and downstream of the test specimen and the particle number concentrations are measured using particle counts methods. From these results, the fractional collection efficiency curve can be plotted and the particle size with the highest penetration (MPPS) can be determined. The results are dependent on the filter medium and the air velocity, and hence product specifications have to be determined.

Table 2.1: *Classification of filters according to EN 1822*

Group	Filter class EN 1822	Filtration efficiency in the MPPS [%]	
		Integral value	Local value
EPA	E10	≥85	-
	E11	≥95	-
	E12	≥95.5	-
HEPA	H13	≥99.95	99.75
	H14	≥99.995	99.975
ULPA	U15	≥99.9995	99.9975
	U16	≥99.99995	99.99975
	U17	≥99.999995	99.9999

2.3 Hollow-fiber membranes in air filtration

Fig. 2.7 shows the principle of HFM separation and dead-end HFM module. HFMs consist of a large number (up to thousands) of hollow fibers with inner diameter in range of tens to several hundreds of microns. This gives a large filtration area in a significantly small volume. The surface area of HFM is about four times larger compared to pleated flat sheet membrane per volume. Although the number of scientific works on development of HFMs for air filtration is very limited, there are companies which already offer HFM air filters in their product portfolio. An overview of published works, products, their features and recommended applications follows.

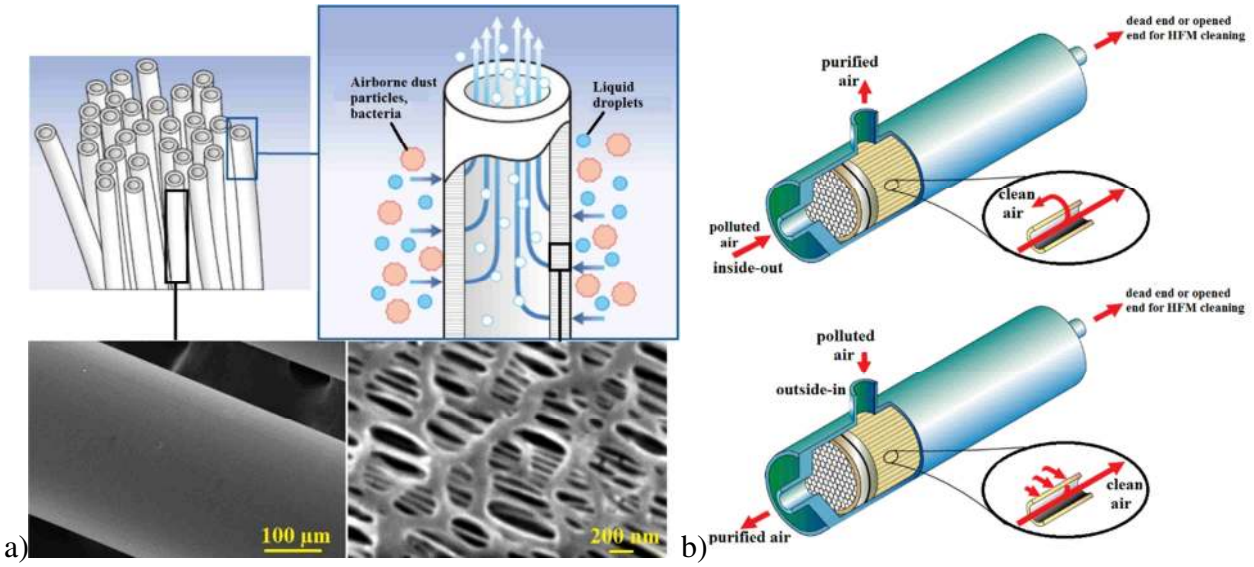

Fig. 2.7: *Principle of air filtration using HFM (a) and principle of a dead-end HFM module (b)*

The very first work on this topic was published in 2017 by Wang et al. [15] who designed high efficiency polyvinylidene fluoride-polyethylene glycol (PVDF-PEG) hollow fibers for separation of ultrafine particles from air. These HFMs (Fig. 2.8) with asymmetric structure were prepared via dry-jet wet spinning. The addition of high molecular weight PEG in spinning dope should have facilitated the formation of loosely connected cross-section and porous outer skin, thus enhancing the gas permeance for air filtration. In the inside-out testing configuration, all HFMs varying in molecular weight of PEG exhibited a high efficiency of 99.999% against a polydisperse NaCl aerosol with a geometric average particle size of ~30 nm. Further, they found out that permeance increased with increase in molecular weight of PEG. The highest molecular weight of PEG was 12000 Da. This HFM had highest quality factor. However, HFM with PEG of 8000 Da had the best mechanical properties. When tested in dead-end filtration, the filtration efficiency increased with increasing air flowrate which is contrary compared to fibrous filters. However, due to generally higher pressure drops, the use was recommended for low flowrate applications.

Another work was carried out by Li et al. in 2017 [16]. In this work, a highly permeable poly(ether sulfone) (PESF) based HFM was prepared via a one-step dry-jet wet spinning. They obtained HFM with a fibrous-like porous substrate and a sieve-like outer layer (Fig. 2.9) and challenged with an ammonium sulfate aerosol with a particle size smaller than 300 nm. Filtration efficiency higher than 99.995% was achieved. Moreover, authors have tested various techniques for membrane regeneration, namely air back purge, water rinse and water backwash. Air back

purge had practically no cleaning effect, while water rinsing regenerated the membrane even though the membrane permeance was slightly lower compared to a new membrane.

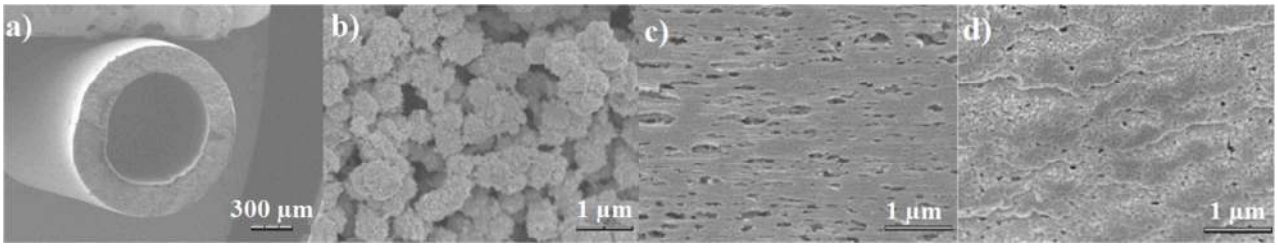

Fig. 2.8: *PVDF-PEG HFMs cross-section (a), cross-section enlarged (b), inner surface (c) and outer surface (d)* **[15]**

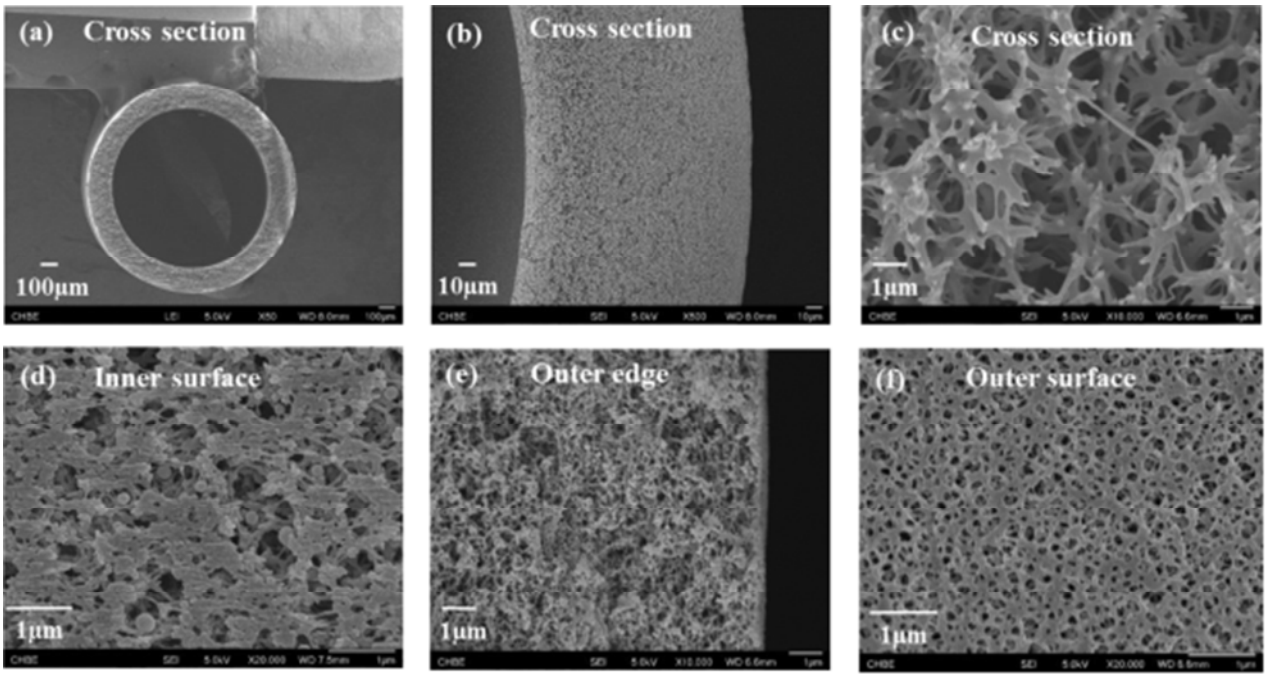

Fig. 2.9: *FESEM images of PES HFMs* **[16]**

Next work published by Wang et al. in 2018 [17] aimed to develop PVDF hollow fibers (Fig. 2.10) with main focus on enhancement of membrane gas permeance. Using dilute PVDF dopes with SiO_2 additives and applying a KOH etching, the nitrogen permeance increased significantly. Moreover, the HFMs showed an efficiency of 99.9999% against both NaCl and diethylhexyl sebacate (DEHS) aerosol. The efficiency remains the same after 36 h of continuous filtration in a highly polluted environment with a very small increase in pressure drop of about 100 Pa.

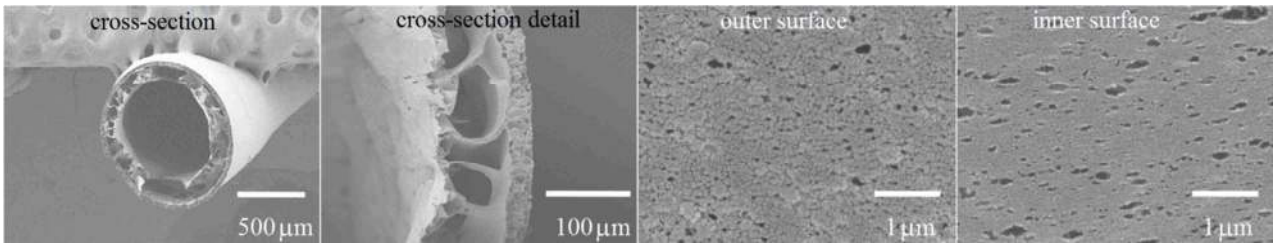

Fig. 2.10: *FESEM images of PVDF-silica HFMs* **[17]**

Last work on HFM air filtration published in 2018 by Xu et al. [18] dealt with development and testing of asymmetric HFMs made of PTFE for removal of ultrafine particles in $PM_{2.5}$. The HFMs were prepared via cold pressing including paste extrusion, stretching and heating. The HFM structure was controlled by reduction ratio, stretching ratio and heating temperature which have influence on morphology, porosity, shrinkage ratio, tensile strength and permeability. The PTFE HFMs had the microstructure of nodes interconnected by fibrils (Fig. 2.11). Such a structure might possess synergistic advantages of porous membranes and fibrous filters with a sieve-like outer layer and a fibrous-like porous substrate. These HFMs achieved filtration efficiency higher than 99% for $PM_{2.5}$ and 90% for $PM_{0.3}$. Moreover, due to the membrane hydrophobicity, they pose a self-cleaning ability and a high dust holding capacity of more than 120 g m^{-2}.

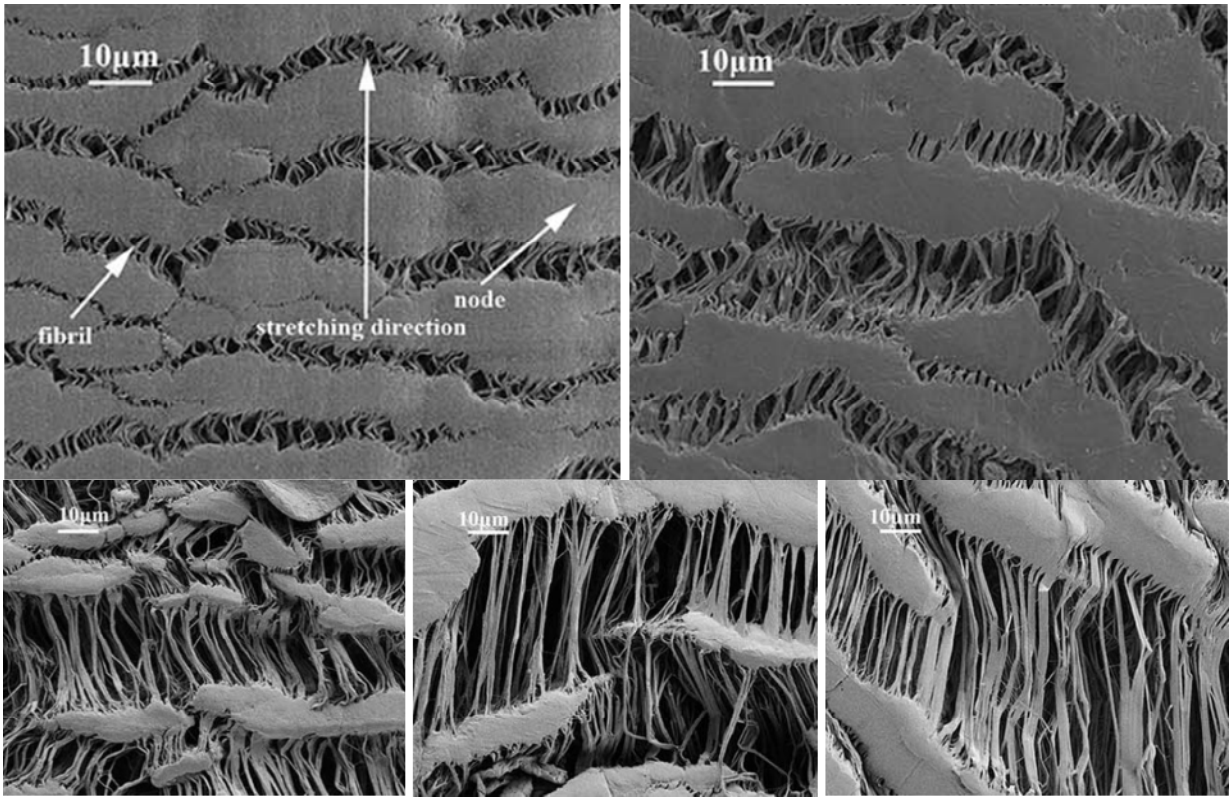

Fig. 2.11: *FESEM images of PTFE HFMs at different stretching ratios* **[18]**

An overview of existing HFM air filters from various companies is listed in Table 2.2. Examples of particular products are shown in Fig. 2.12. Mitsubishi Chemical [22] produces capsule filters (dead-end modules) based on PE HFMs (Fig. 2.12a). Recommended applications are very specific in gas filtration, i.e. sterilized water tank ventilation, clean room and medical device airline and blood testing apparatus. Furthermore, these filters can be used for calibration of particle counters. Koyo Industries Co., Ltd. [23] produces HFM air filters (Fig. 2.12b) able to separate foreign matter and water drips from pipes providing clean air environment. It offers long service life and low pressure loss. It is recommended for precision measuring instruments, analyzing equipment, semiconductor manufacturing, printing and painting equipment, air blow and air pipes of medical, dental, food and optical part equipment. SMC Corp. [21] produces small body, lightweight and large flowrate (Fig. 2.12c) HFM filters suitable for semiconductor, measuring instrument, printing and medical industries. Similar air filter can be found in portfolio

of Pisco Inc. [20]. Kitz Microfilter Corp. [19] produces several types of HFM air filters, i.e. in-line filters similar to those from Koyo or SMC (Fig. 2.12b,c), cartridge types (Fig. 2.12d) and so called air guns (Fig. 2.12e). Typical applications are compressor air cleaning, print board, microelectronic parts and precision machinery. Cole-Parmer [24] produces HFM air filter. The membrane material is a mixed cellulose ester. This membrane is ideal for bioprocessing, fermentation and cell culture applications, mostly used as a sterile barrier when feeding media to a bioreactor. Finally, the membrane from Transforming Technologies [25] is used as filter for ionizing nozzles to provide clean ionized air.

Table 2.12: *An overview of HFMs for air filtration produced by various manufacturers*

Manufacturer/country	HFM material	Pore size (µm)/*particle retention	Filtration efficiency (%)	Max TMP (MPa)	HFM active area (m^2)	Reference
Mitsubishi/ Japan	PE	0.1	n.a.	0.1 – 0.2	0.07 – 0.3	[22]
Koyo Industries/ Japan	PP	0.01*	n.a.	0.25	0.008	[23]
Kitz Microfilter/ Japan	PP	0.01*	99.99	0.5 – 1.0	0.008 – 0.11	[19]
PISCO Inc./USA	n.a.	0.01	99.99	0.25	0.0107 – 0.0215	[20]
SMC Corp./Japan	n.a.	0.01*	99.99	1.0		[21]
Cole-Parmer/USA	MCE	0.2	n.a.	2	0.045	[24]
Transforming Technologies/USA	n.a.	0.01	n.a.	n.a.	n.a.	[25]

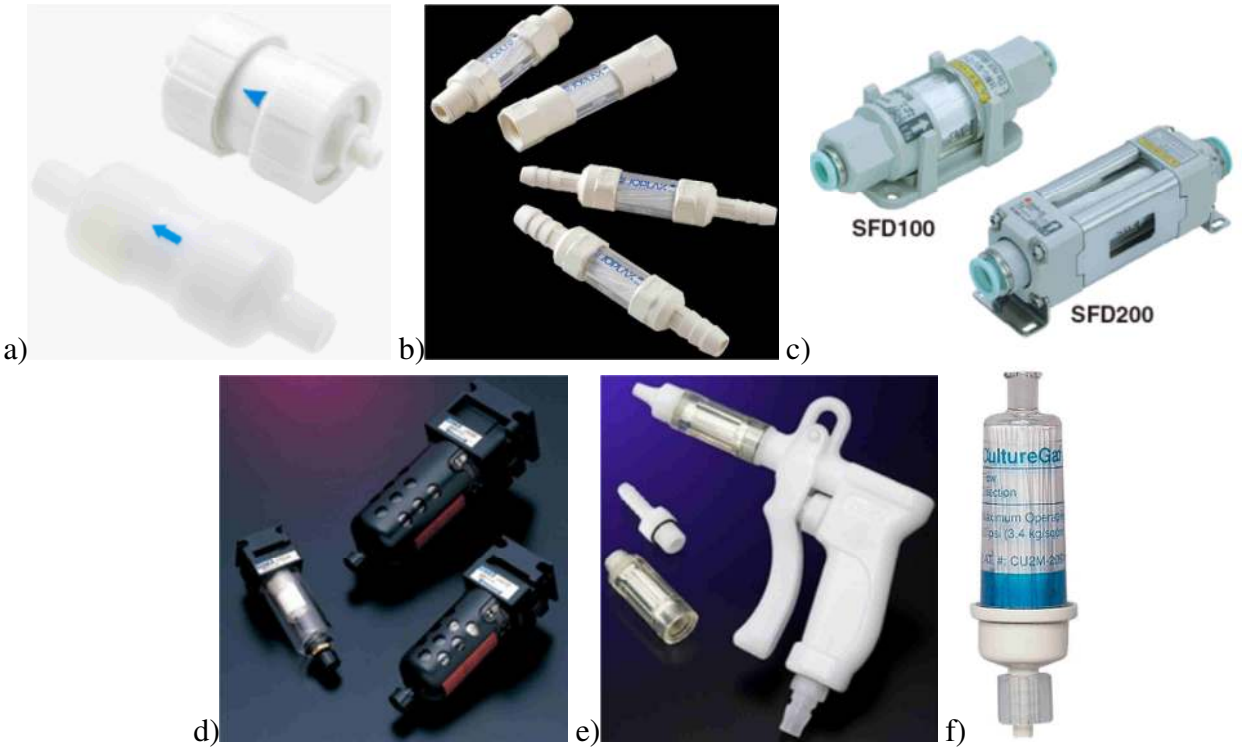

a) b) c) d) e) f)

Fig. 2.11: *HFM modules from various manufacturers: (a) Mitsubishi, (b) Koyo Industries, (c) SMC Corp., (d) Kitz cartridge (e) Kitz air gun, (f) Cole-Parmer*

2.4 Summary of knowledge from the literature review

From the literature review, it is clear that the use of HFMs in air filtration is very scarce and the space for research and development in this field could be of high importance. Due to HFM's compactness, simple production, low weight and high efficiency can be favorably used for specialized applications. However, due to the geometry cannot be used for high volume filtration applications such as HVAC. Several companies have been found to have HFM air filtration products in their portfolio. Nonetheless, these can be used only for low air flowrates. This shortcoming can be eliminated by variations of several HFM parameters, among surface area, porosity and fiber wall thickness, it is especially inner fiber diameter which influences the pressure drop over the length of the hollow fiber lumen. With these options, HFMs can easily be customized for individual air filtration applications.

3 Predicting the air filtration efficiency of hollow-fiber membranes using mathematical models for fibrous and Nuclepore filters[1]

3.1 Introduction

In this chapter, mathematical models developed for prediction of air filtration efficiency of fibrous filters and CPMs are applied on a HFM pore structure. For calculation, we used parameters of symmetric polypropylene HFM produced by ZENA Membranes s.r.o. [26]. From the porous structure of these HFMs (Fig. 3.1), and comparing with a typical structure of a fibrous filter (see e.g., [6, 68–72] and a CPM (see e.g., [73–77]), we can see several similarities but also several main differences. First, the HFM pore structure is composed of longitudinal segments (referred to as collectors) with an average diameter of about 90 nm. These can be considered fibers analogically to fibrous filters. Second, the pore structure contains elliptical pores that are analogical to CPM, which has circular pores. Conversely, HFMs have very high solidity (here 0.48) compared to commercial fibrous filters, which typically have solidity between 0.01 and 0.3 [4]. So with some assumptions, the models for fibrous filters and CPMs can be applied on the HFMs considered in this study. Therefore, the main effort of this work is to compare these models by numerically applying them on HFM assuming that the collection mechanisms are analogical to those considered in fibrous filters and CPMs. Based on single fiber theory developed for fibrous filters, we determined single collector efficiencies (SCE) based on different mechanisms taking place in aerosol filtration. The efficiency results were compared between SCE models for individual mechanisms developed by various researchers. Therefore, this work can also serve as an overview of mathematical models for SCE due to different capturing mechanisms.

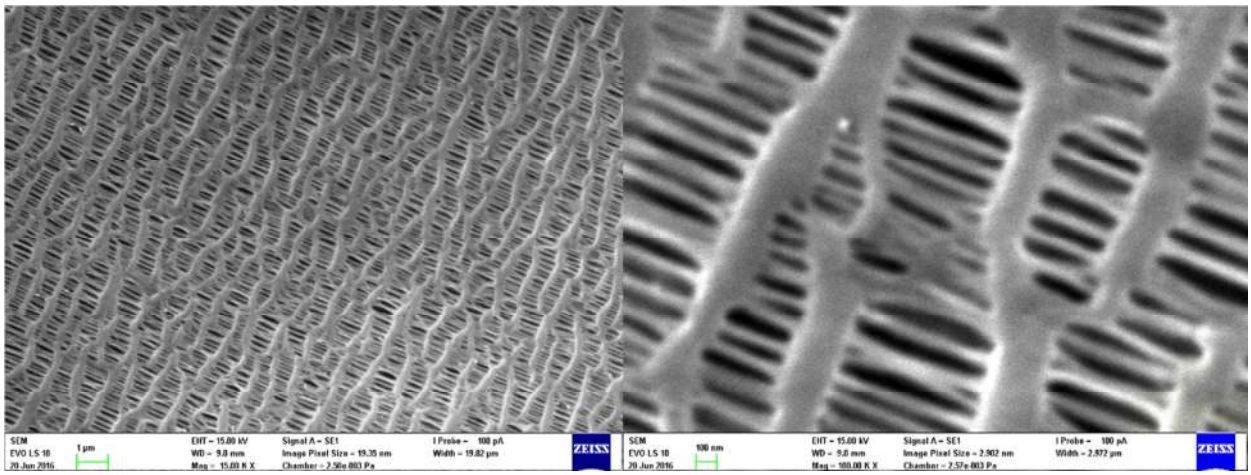

Fig. 3.1: *Polypropylene HFM pore structure*

3.2 Prediction models for air filtration efficiency

Air filtration materials or whole air filtration units are mostly evaluated in terms of filtration efficiency and pressure drop. The former describes the ability of a filter unit to remove particles

[1] A version of this chapter was published as: Bulejko, P. Numerical comparison of prediction models for aerosol filtration efficiency applied on a hollow-fiber membrane pore structure. *Nanomaterials* **2018**, *8*, 447.

from air stream while the latter one is related mainly to energy requirements. The filtration efficiency η is defined as follows:

$$\eta = 1 - \frac{C_{\text{down}}}{C_{\text{up}}} \tag{3.1}$$

where C_{down} and C_{up} are the number of particles downstream and upstream of the filter, respectively.

3.2.1 Efficiency prediction of fibrous filters – SCE approach

Non-woven fibrous filters are composed of fibers, which are randomly oriented even though the orientation is mostly normal to the airflow. The diameter of fibers is mostly not uniform and can be produced from various mostly polymeric materials. The filtration efficiency of fibrous filters may be predicted based on several parameters and assumption of an idealized filter structure. The formula is as follows [2]:

$$\eta = 1 - \exp\left[-\frac{4\alpha\eta_{\text{f}} Z}{\pi(1-\alpha)d_{\text{f}}} \right] \tag{3.2}$$

where α, η_{f}, Z and d_{f} are the filter solidity, SCE, filter thickness and average collector diameter, respectively. The total SCE is a sum of contributions from different collection mechanisms and can be written as follows:

$$\eta_{\text{f}} = (\eta_{\text{I}} + \eta_{\text{R}} + \eta_{\text{D}})\eta_{\text{A}} \tag{3.3}$$

where η_{I}, η_{R}, η_{D} and η_{A} are the single collector efficiencies due to inertial impaction, interception, diffusion and adhesion, respectively. The filtration theory, which is based on three main mechanisms, inertial impaction, interception and diffusion (Fig. 3.2), does not take into account particle-fiber interaction, i.e., the particle rebound and re-entrainment. Therefore, we used Eq. (3.3) to calculate the SCE based on collision efficiency (sum of collection efficiencies due to impaction interception and diffusion) multiplied by the collection efficiency caused by adhesion effects [78, 79].

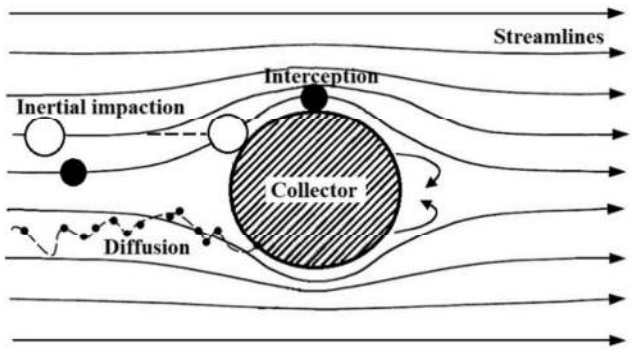

Fig. 3.2: *Schematic presentation of individual collection mechanisms at a single collector*

3.2.1.1 SCE due to Brownian motion

Filtration efficiency due to diffusion (Brownian motion) is a significant part of the overall filtration efficiency. The randomly changing trajectory of very small particles (Fig. 3.2) increases the probability of hitting the collector and their capture by filter. The governing parameter for diffusion mechanism is Peclet number, which is the ratio of convection and diffusion transport rate as follows:

$$Pe = \frac{Ud_{\mathrm{f}}}{D} \tag{3.4}$$

where U is the face velocity and D is the diffusion coefficient of particle calculated as follows:

$$D = \frac{k_{\mathrm{B}} T C_{\mathrm{s}}}{3\pi\mu d_{\mathrm{p}}} \tag{3.5}$$

where k_{B}, T, μ and d_{p} are the Boltzmann constant, absolute temperature, air dynamic viscosity and particle diameter, respectively and C_{s} is the Cunningham slip correction factor:

$$C_{\mathrm{s}} = 1 + Kn\left[1.207 + 0.44\exp\left(-\frac{0.78}{Kn}\right)\right] \tag{3.6}$$

where Kn is the Knudsen number of particle with λ as mean free path of gas molecules:

$$Kn = \frac{2\lambda}{d_{\mathrm{p}}} \tag{3.7}$$

Several relationships have been proposed to predict SCE due to diffusion (η_{D}). For nanoparticles that have high diffusion coefficient, hence smaller Peclet number, Wang et al. [80] gave the following relationship:

$$\eta_{\mathrm{D}} = 0.84 Pe^{-0.43} \tag{3.8}$$

Eq. (3.8) suggests a lower dependence of diffusion efficiency on the Peclet number, though it is in good agreement with experimental data for whole range of Peclet numbers. Another relationship was proposed by Kirsch and Fuchs [81]:

$$\eta_{\mathrm{D}} = 2.7 Pe^{-2/3} \tag{3.9}$$

Eqs. (8) and (9) does not include the effect of flow field distortion at the gas-fiber interface and are independent. Therefore, several researchers proposed different expressions based on theoretical derivation or experimental data. Stechkina et al. [82] proposed following relationship:

$$\eta_{\mathrm{D}} = 2.9 Ku^{-1/3} Pe^{-2/3} + 0.62 Pe^{-1} \tag{3.10}$$

while analysis of Pich [83] and Lee and Liu [84] lead to Eqs. (3.11) and (3.12), respectively:

$$\eta_{\mathrm{D}} = 2.27 Ku^{-1/3} Pe^{-2/3}(1 + 0.62 KnPe^{1/3} Ku^{-1/3}) \tag{3.11}$$

$$\eta_{\mathrm{D}} = 1.6\left(\frac{1-\alpha}{Ku}\right)^{1/3} Pe^{-2/3} \tag{3.12}$$

where Ku is the Kuwabara hydrodynamic factor. The Kuwabara factor compensates the flow field distortion around a collector occurring due to its proximity to neighboring fibers. The Kuwabara factor is a dimensionless parameter and depends only on filter solidity α for $d_{\mathrm{f}} \geq 2$ μm as follows:

$$Ku = -\frac{\ln\alpha}{2} + \alpha - \frac{\alpha^2}{4} - \frac{3}{4} \tag{3.13}$$

As the slip effect becomes significant for filters with fiber diameter smaller than 2 µm (which is true for HFMs considered in this work), Kirsch and Stechkina [85] recommended adding the Knudsen number of fiber (Eq. 3.14) to compensate for the slip effect:

$$Kn_{\mathrm{f}} = \frac{2\lambda}{d_{\mathrm{f}}} \tag{3.14}$$

Thus, for a fiber diameter smaller than 2 µm, the relationship for the Kuwabara factor is:

$$Ku = \frac{2\lambda}{d_{\mathrm{f}}} - \frac{\ln\alpha}{2} + \alpha - \frac{\alpha^2}{4} - \frac{3}{4} \tag{3.15}$$

The same was proposed for the relationships for diffusion efficiency, i.e., modifying using a correction factor accounting for slip flow when the fiber diameter is in the same magnitude as the mean free path of the gas molecules. Using the work of Lee and Liu [84] as a basis (Eq. 3.12), Liu and Rubow [86] corrected this model to consider the slip effect as follows:

$$\eta_{\mathrm{D}} = 1.6\left(\frac{1-\alpha}{Ku}\right)^{1/3} Pe^{-2/3} C_1 \tag{3.16}$$

where C_1 is a constant calculated as follows:

$$C_1 = 1 + 0.388 Kn_{\mathrm{f}}\left[(1-\alpha)\frac{Pe}{Ku}\right]^{1/3} \tag{3.17}$$

However, efficiencies calculated using Eq. (3.16) might exceed unity for very small particles (low Peclet numbers). Therefore, Payet et al. [87] introduced another correction factor, to get the efficiency for very small particles under unity, as follows:

$$\eta_{\mathrm{D}} = 1.6\left(\frac{1-\alpha}{Ku}\right)^{1/3} Pe^{-2/3} C_1 C_2 \tag{3.18}$$

where C_2 is calculated as follows:

$$C_2 = \frac{1}{1 + 1.6\left(\frac{1-\alpha}{Ku}\right)^{1/3} Pe^{-2/3} C_1} \tag{3.19}$$

Note that the constant 1.6 in Eq. (3.12) and the other derived based on the same constant may be substituted with a different value (mostly higher value of 2.6 or 2.9) to obtain a better agreement with experimental data. The commonly used single collector theory was developed for the Kuwabara cell model [88]. This model, however, does not consider possible heterogeneities of filter structure (local porosity variations) related to non-uniform fiber distribution or their size polydispersity [89].

3.2.1.2 SCE due to interception

Interception occurs when a particle following fluid streamline flowing around the collector is in a distance of one particle radius from the collector surface. The interception mechanism is governed by the interception parameter R, which is the ratio of particle to fiber diameter:

$$R = \frac{d_{\mathrm{p}}}{d_{\mathrm{f}}} \tag{3.20}$$

Interception efficiency increases by increasing the interception parameter [90]. Following this, the interception efficiency should be independent of the airflow velocity, which is true for most models developed for SCE due to interception. However, considering the filter fibers as isolated cylinders, the interception efficiency obtained from Lamb's solution of Navier-Stokes equations [91] is dependent on Reynolds number hence airflow velocity. Langmuir [92] derived this relationship for low Reynolds numbers ($Re_f < 1$) as follows:

$$\eta_R = \frac{2(1+R)\ln(1+R) - (1+R) + (1+R)^{-1}}{2(2-\ln Re_f)} \tag{3.21}$$

with Re_f as fiber Reynolds number characterizing flow field around a fiber calculated as follows:

$$Re_f = \frac{d_f U \rho}{\mu} \tag{3.22}$$

where ρ is the fluid density. Majority of mathematical expressions for interception efficiency are based on the Kuwabara cell model [88] and are independent of fluid velocity. Kirsch and Stechkina gave a complete model for SCE due to interception as follows [85]:

$$\eta_R = \frac{1+R}{2Ku}\left[2\ln(1+R) - 1 + \alpha + \left(\frac{1}{1+R}\right)^2\left(1-\frac{\alpha}{2}\right) - \frac{\alpha}{2}(1+R)^2\right] \tag{3.23}$$

This is the basic formula for the SCE due to interception based on the Kuwabara flow field. However, it is a rather long and complicated expression, which Lee and Liu reduced to following simpler forms [84]:

$$\eta_R = \frac{1-\alpha}{Ku}\frac{R^2}{1+R} \tag{3.24}$$

$$\eta_R = 0.6\frac{1-\alpha}{Ku}\frac{R^2}{1+R} \tag{3.25}$$

Eq. (3.24) is valid for $R < 0.2$ and $\alpha < 0.5$. With the assumption that fibers are not oriented perpendicular to the flow direction and for non-uniform fiber distribution, Lee and Liu [84] modified Eq. (3.24) by multiplying it by a coefficient of 0.6. The interception efficiency model can thus be simplified even though it has several limitations, mainly small interception parameter and filter solidity, the latter of which is not too restrictive and can be used for calculations in this work. Several investigators suggested other corrections of Eq. (3.23). For example, Stechkina and Fuchs [93] approximated this relationship by omitting all the terms containing the filter solidity α and obtained the following equation:

$$\eta_R = \frac{1+R}{2Ku}\left[2\ln(1+R) - 1 + \frac{1}{(1+R)^2}\right] \tag{3.26}$$

The limitations are the same as for Eq. (3.22) i.e., R and α must be small. Owing to the omission of filter solidity, the approximation is less accurate with increasing solidity. Therefore, they proposed another modification as follows:

$$\eta_R = 2.4\alpha^{1/3}R^{1.75} \tag{3.27}$$

Lee and Gieseke [94] proposed another modification of Eq. (3.24) as follows:

$$\eta_{\mathrm{R}} = \frac{1-\alpha}{Ku}\frac{R^2}{(1+R)^{\frac{2}{3(1-\alpha)}}} \tag{3.28}$$

None of the prediction models for interception efficiency (Eqs. (3.23)–(3.28)) considers the gas slip effect. Pich [95] proposed a relationship for interception efficiency, considering gas slip, for small Knudsen numbers:

$$\eta_{\mathrm{R}} = \frac{(1+R)^{-1} - (1+R) + 2(1+1.996Kn)(1+R)\ln(1+R)}{2(-0.75-0.5\ln\alpha) + 1.996Kn(-0.5-\ln\alpha)} \tag{3.29}$$

Another relationship considering the gas slip effect was developed by Liu and Rubow [86] who further modified the model of Lee and Liu [84] (Eq. 3.25) by multiplying it by a correction factor for the gas slip as follows:

$$\eta_{\mathrm{R}} = 0.6\frac{1-\alpha}{Ku}\frac{R^2}{1+R}\left(1+\frac{1.996Kn_{\mathrm{f}}}{R}\right) \tag{3.30}$$

3.2.1.3 SCE due to inertial impaction

Inertial impaction takes place in higher airflow velocities for particles with a larger diameter (mostly larger than 1 μm depending on conditions) due to their higher inertia, which causes them to follow a different trajectory than that of airflow streamlines. The streamlines near the collector abruptly changes. The particle thus separates from the streamlines and hits the collector. Collection efficiency due to inertial impaction depends on Stokes' number characterizing the particle inertia, which is defined as follows:

$$Stk = \frac{d_{\mathrm{p}}^2 \rho_{\mathrm{p}} C_{\mathrm{s}} U}{18\mu d_{\mathrm{f}}} \tag{3.31}$$

where ρ_{p} is the particle density. If the Stokes' number is higher than unity, the particles separate from streamlines and hit the collector. On the other hand, for Stokes' number lower than one, the inertia effect will not take place. Several formulae have been derived for SCE due to inertial impaction. The most often used relationship is that proposed by Stechkina et al. [82]:

$$\eta_{\mathrm{I}} = \frac{Stk}{4Ku^2}\left(29.6-28\alpha^{0.62}\right)R^2 - 27.5R^{2.8} \tag{3.32}$$

for $0.0035 < \alpha < 0.111$ and $0.01 < R < 0.4$, while for $R > 0.4$, the relationship is modified as follows:

$$\eta_{\mathrm{I}} = \frac{Stk}{2Ku^2} \tag{3.33}$$

Landahl and Hermann [96] proposed a relationship based on experimental data for $Re_{\mathrm{f}} > 10$. However, as suggested by Saleh et al. [97], this equation may also be used for $Re_{\mathrm{f}} < 2$. The relationship is as follows:

$$\eta_{\mathrm{I}} = \frac{Stk^3}{Stk^3 + 0.77Stk^2 + 0.22} \tag{3.34}$$

Fuchs gave another relationship for impaction efficiency as follows [1]:

$$\eta_{\mathrm{I}} = \frac{Stk^2}{(Stk+0.25)^2} \tag{3.35}$$

while Gougeon et al. [98] and Friedlander [99] proposed empirical Eqs. (3.36) and (3.37), respectively:

$$\eta_{\mathrm{I}} = 0.039 Stk^{1.5} \tag{3.36}$$

$$\eta_{\mathrm{I}} = 0.075\, Stk^{6/5} \tag{3.37}$$

Eqs. (3.36) and (3.37) are valid for $0.0263 < Re_{\mathrm{f}} < 0.25$ and $0.5 < Stk < 4.1$ and $\mathrm{Re_f} < 1$, $0.8 < Stk < 2$ and $R < 0.2$, respectively. Zhu et al. [100] derived a relationship with no restrictions concerning Stk, Re_{f} and α as follows:

$$\eta_{\mathrm{I}} = \frac{2R(1-\alpha)Stk\sqrt{\alpha} + (1-\alpha)\alpha Stk^2}{Ku} \tag{3.38}$$

Several researchers proposed models accounting for the effect of fiber and particle Reynolds number on the SCE due to inertial impaction. Suneja and Lee [101] derived a relationship for $1 < Re_{\mathrm{f}} < 60$ and $1 < Stk < 20$ as follows:

$$\eta_{\mathrm{I}} = \left[1 + \frac{1.53 - 0.23\ln Re_{\mathrm{f}} + 0.0167\ln^2 Re_{\mathrm{f}}}{Stk}\right]^{-2} \tag{3.39}$$

Ilias and Douglas [102] theoretically investigated inertial aerosol deposition on an isolated cylinder by solving time dependent Navier-Stokes equations. They proposed a correlation for $30 < Re_{\mathrm{f}} < 40000$ and $0.07 < Stk < 5$ as follows:

$$\eta_{\mathrm{I}} = \frac{Stk^3 + 1.622 \cdot 10^{-4} Stk^{-1}}{1.031 Stk^3 + (1.14 + 0.04044 \ln Re_{\mathrm{f}}) Stk^2 + 0.01479 \ln Re_{\mathrm{f}} + 0.2013} \tag{3.40}$$

3.2.1.4 SCE due to adhesion

For adhesion efficiency, several authors proposed empirical relationships for varying material combinations, with different ranges of Reynolds and Stokes numbers. Based on experimental results, an expression for adhesion efficiency was proposed by Ptak and Jaroszczyk as follows [103]:

$$\eta_{\mathrm{A}} = \frac{190}{(Re_{\mathrm{pp}} Stk)^{0.68} + 190} \tag{3.41}$$

where Re_{pp} is the particle Reynolds number calculated as follows:

$$Re_{\mathrm{pp}} = \frac{d_{\mathrm{p}} U \rho_{\mathrm{p}}}{\mu} \tag{3.42}$$

Re_{pp} is not the standard fluid dynamics Reynolds number, it uses the particle density ρ_{p} for the calculation [104]. Eq. (3.41) was accurate for $1 < Stk < 120$ and $0.4 < \mathrm{Re_f} < 5.75$.

3.2.2 Efficiency prediction of membrane filters – CPM approach

CPMs are thin PC membranes with circular pores. The theoretical prediction of the filtration efficiency is based on several mechanisms similar to fibrous filters but with physically different meanings (Fig. 3.3).

The theoretical impaction efficiency η_{I} for Nuclepore filters can be calculated using the model proposed by Pich [105] as follows:

$$\eta_{\mathrm{I}} = \frac{2\eta_{\mathrm{I}}'}{1+\xi} - \frac{\eta_{\mathrm{I}}'^2}{(1+\xi)^2} \tag{3.43}$$

where η_{I}' and ξ are calculated as follows:

$$\eta_{\mathrm{I}}' = 2Stk\sqrt{\xi} + 25Stk^2 \exp\left(-\frac{1}{Stk\sqrt{\xi}}\right) - 2Stk^2\xi \tag{3.44}$$

$$\xi = \frac{\sqrt{\varepsilon}}{1-\sqrt{\varepsilon}} \tag{3.45}$$

where ε is the membrane porosity and Stk is the Stokes number and is calculated as follows:

$$Stk = \frac{d_{\mathrm{p}}^2 \rho_{\mathrm{p}} C_{\mathrm{c}} U}{9\mu d_{\mathrm{o}}} \tag{3.46}$$

with C_{c} as the slip correction factor and calculated as follows [1]:

$$C_{\mathrm{c}} = 1 + 2.49\frac{\lambda}{d_{\mathrm{p}}} + 0.84\frac{\lambda}{d_{\mathrm{p}}}\exp\left(-0.44\frac{d_{\mathrm{p}}}{\lambda}\right) \tag{3.47}$$

The diffusion efficiency in pores η_{D} can be calculated as follows [106]:

$$\eta_{\mathrm{D}} = 2.56N_{\mathrm{D}}^{2/3} - 1.2N_{\mathrm{D}} - 0.177N_{\mathrm{D}}^{4/3} \tag{3.48}$$

if $N_{\mathrm{D}} < 0.01$ or

$$\begin{aligned}\eta_{\mathrm{D}} &= 1 - 0.819\exp(-3.657N_{\mathrm{D}}) - 0.098\exp(-22.305N_{\mathrm{D}}) \\ &- 0.032\exp(-56.95N_{\mathrm{D}}) - 0.016\exp(-107.6N_{\mathrm{D}})\end{aligned} \tag{3.49}$$

if $N_{\mathrm{D}} > 0.01$, where N_{D} is:

$$N_{\mathrm{D}} = \frac{4ZD\varepsilon}{d_{\mathrm{o}}^2 U} \tag{3.50}$$

where D is diffusion coefficient calculated according to Eq. (3.5) and d_{o} is the pore diameter. The interception efficiency on pore opening η_{R} can be calculated using the model suggested by Spurny et al. [106]:

$$\eta_{\mathrm{R}} = R_{\mathrm{o}}(2 - R_{\mathrm{o}}) \tag{3.51}$$

where R_{o} is the interception parameter for capillary pore filters calculated as follows:

$$R_{\mathrm{o}} = \frac{d_{\mathrm{p}}}{d_{\mathrm{o}}} \tag{3.52}$$

Nanoparticles can also deposit on the front surface of Nuclepore filters when particles are smaller than 100 nm and face velocity is low. The surface-diffusion efficiency η_{DS} can be calculated using the expression proposed by Manton [107]:

$$\eta_{\mathrm{DS}} = 1 - \exp\left[\frac{-\beta_1\delta^{2/3}}{1 + (\beta_1/\beta_2)\delta^{7/15}}\right] \tag{3.53}$$

where $\beta_2 = 4.5$ and β_1 and δ are coefficients that are calculated as follows:

$$\beta_1 = 4.57 - 6.46\varepsilon + 4.58\varepsilon^2 \tag{3.54}$$

$$\delta = \frac{2D\sqrt{\varepsilon}}{d_o U} \tag{3.55}$$

The total efficiency η is calculated as follows:

$$\eta = 1-(1-\eta_I)(1-\eta_D)(1-\eta_R)(1-\eta_{DS}) \tag{3.56}$$

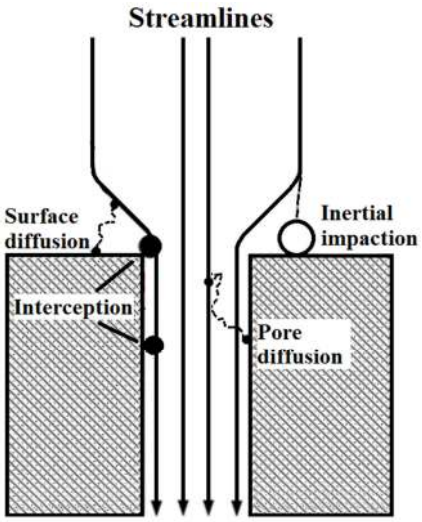

Fig. 3.3: *Schematic filtration mechanisms involved in separation on a CPM*

3.3 Materials and methods

HFM is a special type of membrane geometry. HFM modules are characterized by compactness as they contain a high filtration area within a small volume. Fig. 3.4 shows a HFM pore structure. As mentioned above, two different approaches were chosen. One is based on SCE (Fig. 3.4a) and the other based on a capillary pore approach using models developed for predicting the efficiency of Nuclepore filters considering pore dimensions (Fig. 3.4b). Based on the SEM images, dimensions of individual collectors (Fig. 3.4a) and pores (Fig. 3.4b) were determined using Stream Motion software (Olympus Corporation, Shinjuku, Japan). Using these dimensions, a weighted average size of collector (pore) $d_{f(o)}$ was calculated as follows:

$$d_{f(o)} = \frac{\sum_{i=1}^{N} n_i d_{f(o)i}}{N_{f(o)}} \tag{3.57}$$

where $d_{f(o)i}$ is an individual collector (pore) size, n_i is the number of collectors/pores with a given size $d_{f(o)i}$ and $N_{f(o)}$ is the number of all measured collectors/pores, i.e., number of measurements obtained from the SEM pictures. The average collector/pore size is thus a weighted average of 125 values. The weighted average pore size was calculated using pore dimensions of the elliptical shape (the major and minor axes). The largest particle able to penetrate through the membrane is mostly given by the smaller pore dimension (i.e., that of minor axe). However, due to the random motion and shape of particles, some particles larger than the minor axe length can penetrate through the membrane. Therefore, the weighted average was calculated using both axes' dimensions, giving a larger average pore size. This step ensures that the results of the predicted efficiencies will not be overrated. The main parameters of the membrane structure and conditions

for which the models were compared are shown in Table 3.1. For the model comparison, we also used the standard deviation of pore and collector average diameter to depict uncertainty bounds. For the sake of brevity, this was done for final results only, i.e. overall efficiency.

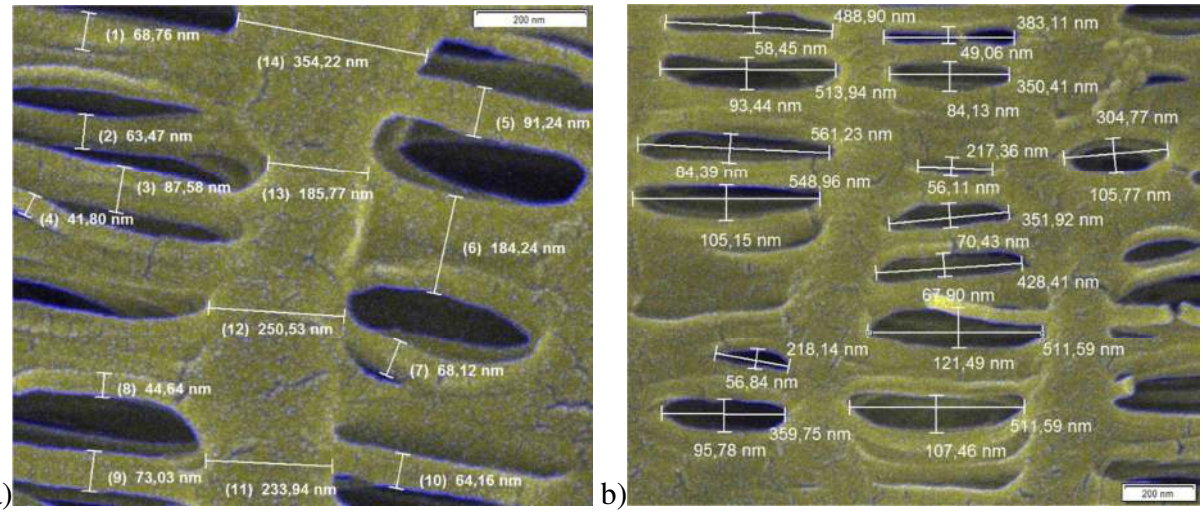

Fig. 3.4: *Evaluation of collector diameter (a) and pore size (b) from SEM images using Stream Motion software*

Table 3.1: *Parameters of HFM pore structure and conditions used for calculations*

Fiber wall thickness, Z (μm)	36
Average pore size, d_o (nm)	205 ± 157
Average collector diameter, d_f (nm)	90 ± 83
Solidity, α (%)	48
Porosity, ε (%)	52
Temperature, T (K)	296.15
Air density, ρ (kg m^{-3})	1.21
Air dynamic viscosity, μ (Pa s)	$1.83 \cdot 10^{-5}$
Particle density, ρ_p (kg m^{-3})	1060
Mean free path of air molecules, λ (nm)	67.3

3.4 Results and discussion

In this section, results obtained using different models are compared when applied on the parameters of the HFM pores structure. Two different approaches were used as mentioned in the previous section, i.e., the approach based on models developed for fibrous filters and a model for membrane filters.

3.4.1 SCE approach

3.4.1.1 SCE due to inertial impaction

Fig. 3.5 shows SCE due to the inertial impaction based on different models for a face velocity of 5 cm/s (a) and 20 cm/s (b) in relation to *Stk*. Stokes number is a governing parameter of inertial impaction mechanism based on which one can decide if the inertial impaction mechanism

dominates at conditions adopted in a filtration process. Moreover, the use of *Stk* is more appropriate compared to the relation of efficiency to particle diameter. *Stk* relates to the particle diameter itself, particle density, collector diameter, face velocity and other parameters governing the mechanisms taking place during aerosol filtration (Eq. 3.31).

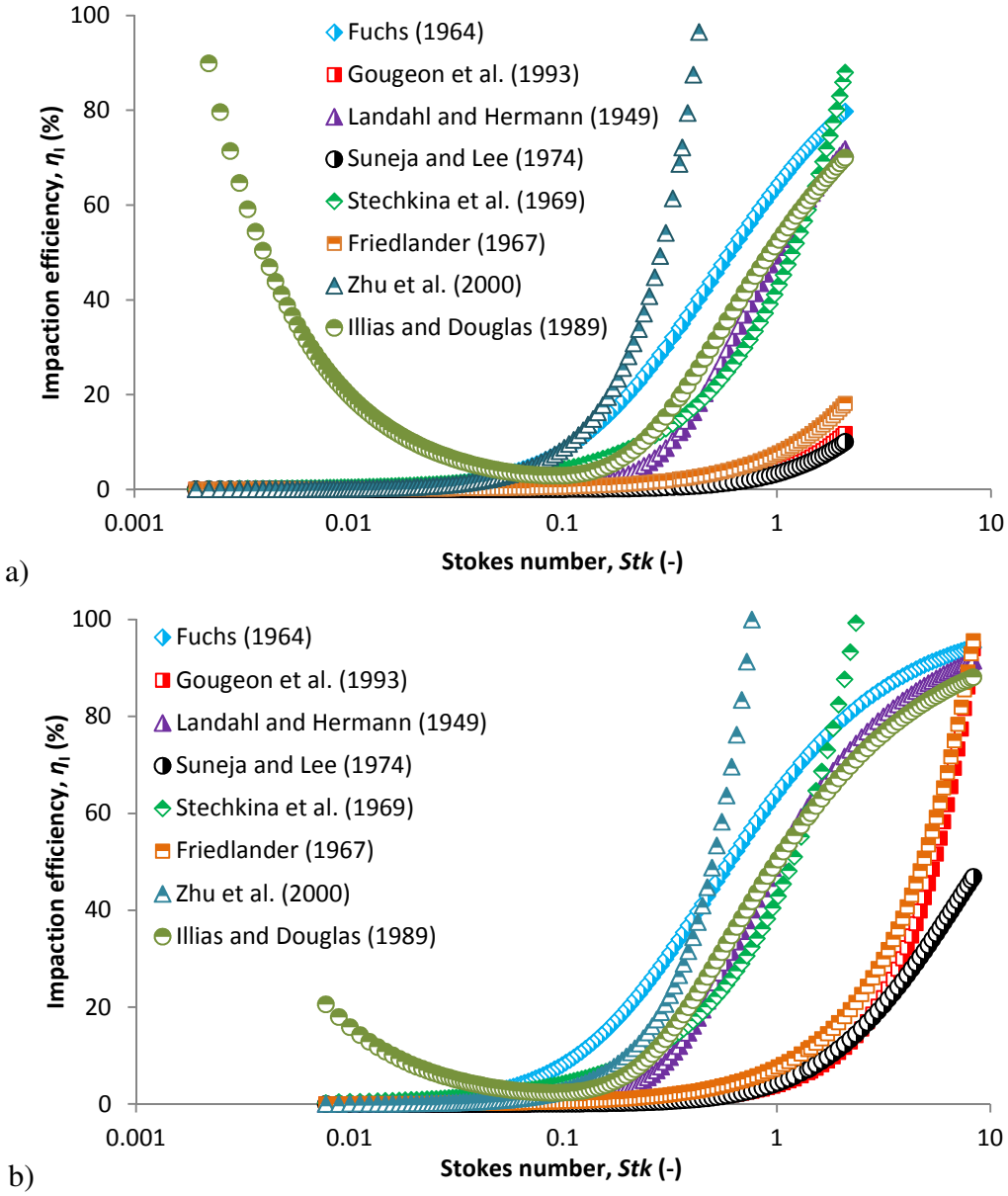

Fig. 3.5: *Comparison of impaction efficiency based on different models and airflow velocity of 5 cm/s (a) and 20 cm/s (b) in relation to Stokes number*

3.4.1.2 SCE due to interception

Fig. 3.6a shows a single fiber efficiency due to the interception mechanism in relation to interception parameter. Interception may play an important role in nanoparticle filtration if the collector diameters are small [41] and starts to dominate at an interception parameter of 0.1 [108]. This is true for most of the models except for that derived by Pich (Eq. 3.29) [95] which predicts high interception efficiencies also for very small interception parameters under 0.1 corresponding to particle sizes smaller than 10 nm (supplementary Fig. S3.3). The Eq. (3.29) was derived for small fiber Knudsen numbers which is not fulfilled for the given collector diameter. Therefore, the

Knudsen number is higher and the model overrates the results to lower particle sizes. Liu and Rubow [86] derived another relationship (Eq. 3.30) considering the gas slip effect, which is more appropriate for very small collector diameters. The interception mechanism is independent of face velocity, which is the main difference from inertial impaction and Brownian motion. This is, however, not true for model of Langmuir (Eq. 3.21) [92] where the interception efficiency is also dependent on the fiber Reynolds number which is given by the face velocity (Fig. 3.6b).

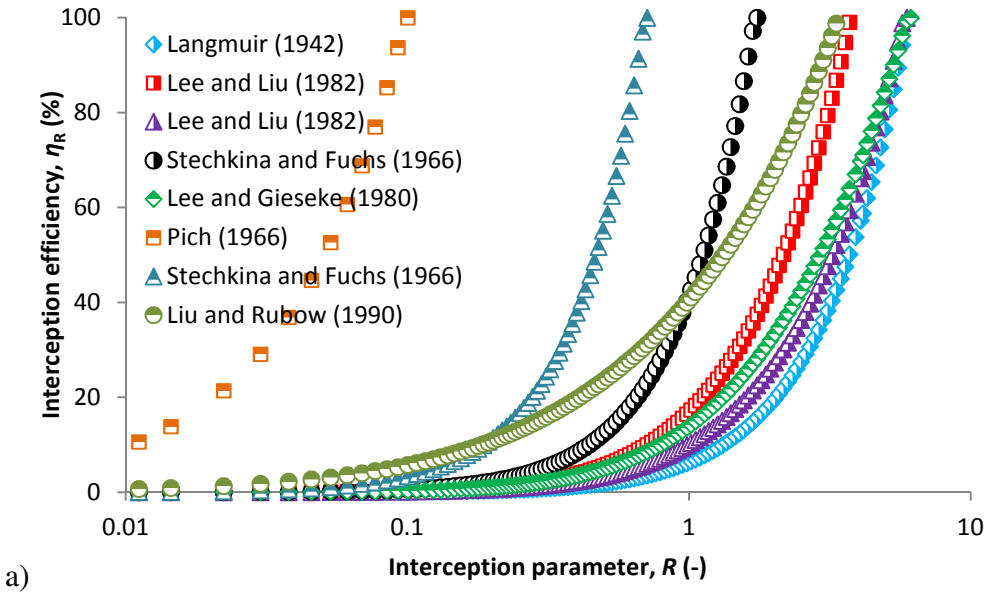

a)

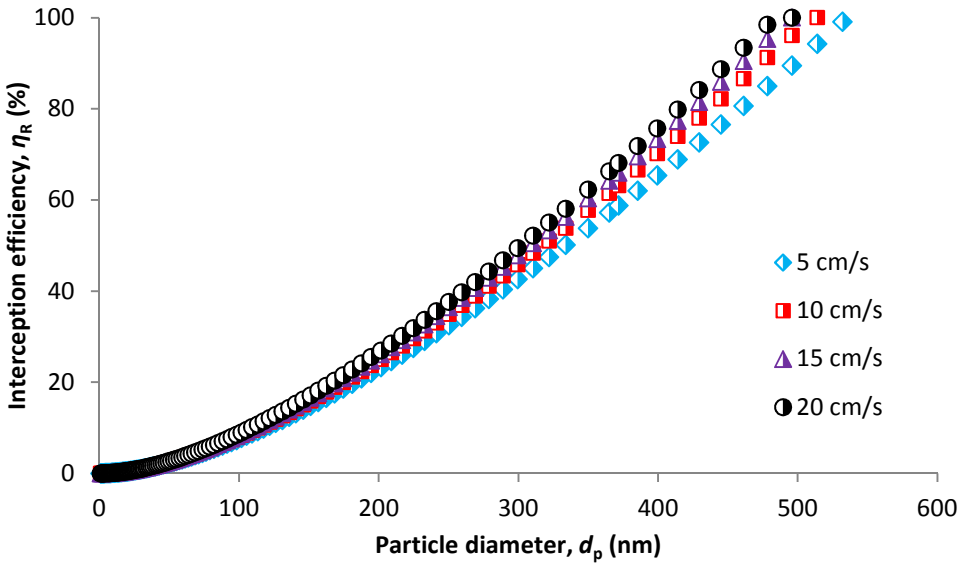

b)

Fig. 3.6: *(a) SCE due to interception based on various models in relation to interception parameter and (b) comparison of SCE due to interception at different face velocities based on Langmuir model (Eq. 3.21)*

3.4.1.3 SCE due to Brownian motion

Brownian motion (diffusion) is another important mechanism occurring when separating particles from air. Unlike for inertial impaction, this mechanism is enhanced at very small face velocities and for very small particles that are mostly under 100 nm in size. The governing parameter for

Brownian motion is the Peclet number, which is the ratio of convection to diffusion transport rate. SCE due to diffusion increases with a decreasing Peclet number, i.e., decreasing particle size (Fig. 3.7). With increasing airflow velocity, the Peclet number is shifted to higher values which diminishes the capturing effect caused by random motions of particles (compare Fig. 3.7a,b). Therefore, with increasing velocity, the SCE due to diffusion decreases and is shifted to lower particle sizes. Comparison of efficiency/particle size curves by face velocity calculated using different models are shown in supplementary material in Fig. S3.4, a comparison of individual models is in Fig. S3.5. The most appropriate model for SCE due to diffusion is Eq. (3.18). This model developed by Payet et al. [87] covers even very small particles for which the other models give an efficiency that is higher than 1 (Fig. 3.7).

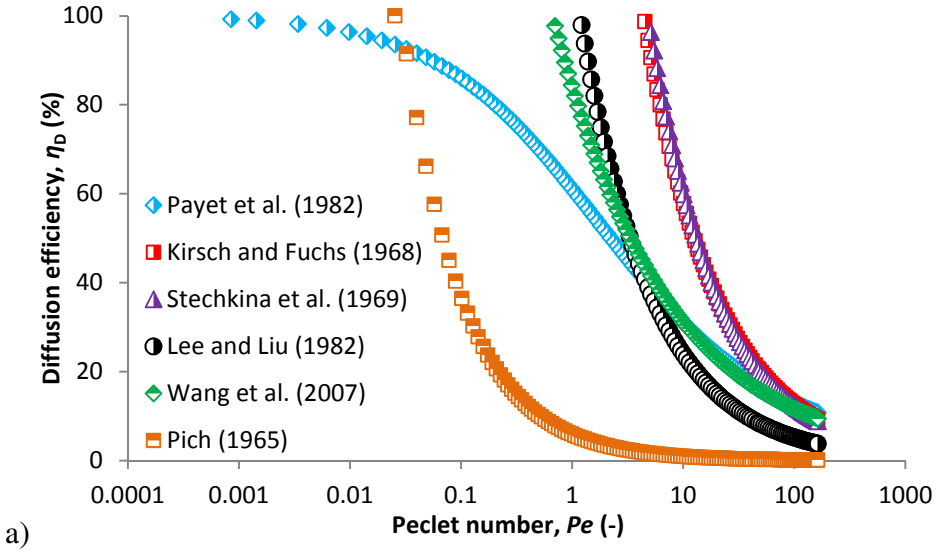

a)

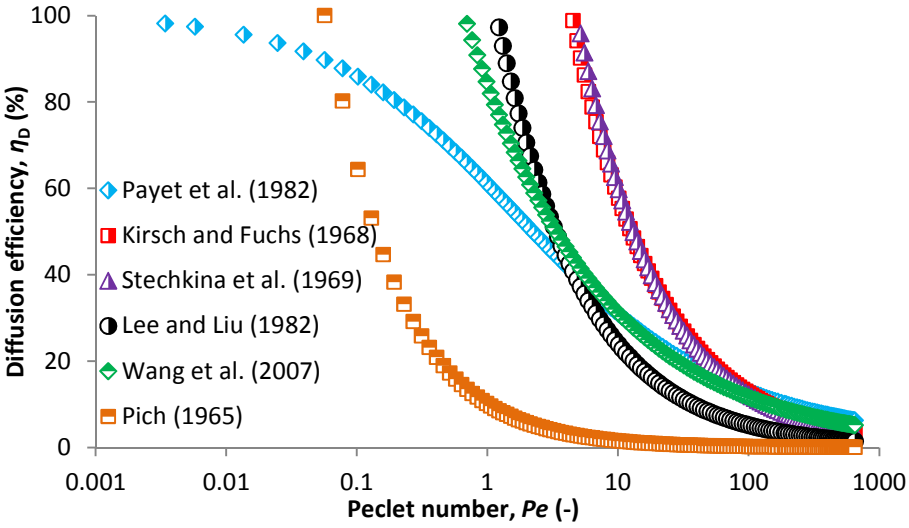

b)

Fig. 3.7: *Comparison of SCE due to diffusion mechanisms based on different models for an airflow velocity of 5 cm/s (a) and 20 cm/s (b) in relation to the Peclet number*

Fig. 3.8 shows adhesion efficiency in relation to particle size based on the model developed by Ptak and Jaroszczyk [103] (Eq. 3.41). This mechanism is not often considered in theoretical predictions. However, we also use this model to completely describe the mechanical capture of particles in which adhesion plays an important role due to re-entrain and rebound effects. We also

calculated single fiber efficiency according to Eq. (3.3), which is the product of collision efficiency (a sum of SCE due to impaction interception and diffusion) and adhesion efficiency presented by the values predicted using Eq. (3.41). Adhesion efficiency is mostly higher for smaller particles and lower face velocities as shown in Fig. 3.8. This is given by adhesion energy between a particle and a fiber as follows:

$$E = \frac{H d_\mathrm{p}}{6 a_0^2} \tag{3.58}$$

where H is the Hamaker constant and a_0 is the adhesion distance. Adhesion energy is directly proportional to the particle size, therefore, higher energy is necessary to keep a larger particle attached to the fiber. It is similar for face velocity, which is mostly assumed the same as the impact velocity of the particle colliding with the fiber surface. The impact velocity should be less than the critical velocity v derived from the adhesion energy given as follows [78]:

$$v < \sqrt{\frac{H}{4\pi\rho_\mathrm{p} a_0 d_\mathrm{p}^2}} \tag{3.59}$$

The Hamaker constant can be calculated as follows [78, 109]:

$$H = \frac{3}{4} k_\mathrm{B} T \left(\frac{\varphi_1 - \varphi_3}{\varphi_1 + \varphi_3}\right)\left(\frac{\varphi_2 - \varphi_3}{\varphi_2 + \varphi_3}\right) + \frac{3h\vartheta_\mathrm{e}}{8\sqrt{2}} \frac{\left(n_1^2 - n_3^2\right)\left(n_2^2 - n_3^2\right)}{\sqrt{\left(n_1^2 + n_3^2\right)\left(n_2^2 + n_3^2\right)}\left[\sqrt{\left(n_1^2 + n_3^2\right)} + \sqrt{\left(n_2^2 + n_3^2\right)}\right]} \tag{3.60}$$

where φ is the static dielectric constant, n is the refractive index, h is the Planck constant and ϑ_e is the main electronic absorption frequency typically around 3×10^{15} s^{-1}. The subscript notation 1, 2 and 3 of ε and n indicate the particle, membrane surface and fluid, respectively. The typical value of Hamaker constant ranges between 10^{-19} and 10^{-20} [110]. However, significant influence will also have particle surface charges, which can cause the membrane to act as an electret filter, so the particles may be captured due to electrostatic forces. In this work however, we focus on the mechanical means of filtration only, so this effect is not considered.

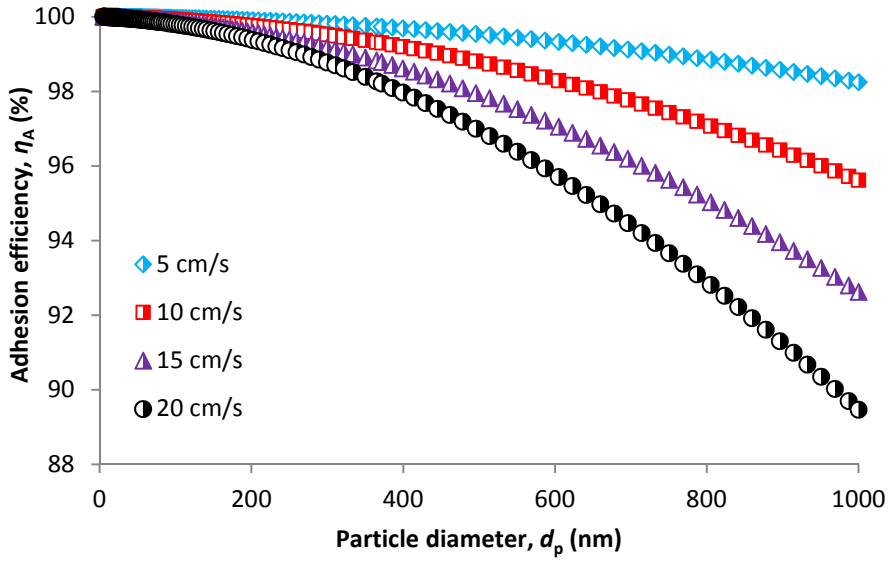

Fig. 3.8: *Collection efficiency due to the adhesion effect*

3.4.1.4 Overall SCE and overall filtration efficiency

Overall SCE is shown in Fig. 3.9a. This is a typical shape of efficiency/particle size curve with a minimum corresponding to most penetrating particle size (MPPS). The left-hand side of the

minimum is governed by the diffusion mechanism while interception and inertial impaction are responsible for the right-hand side. However, the curves in Fig. 3.9a correspond only to one single filter fiber, i.e., one collector of the HFM structure (Fig. 3.4a). To get an overall membrane efficiency, it is necessary to recalculate the SCE to a whole membrane structure using Eq. (3.2).

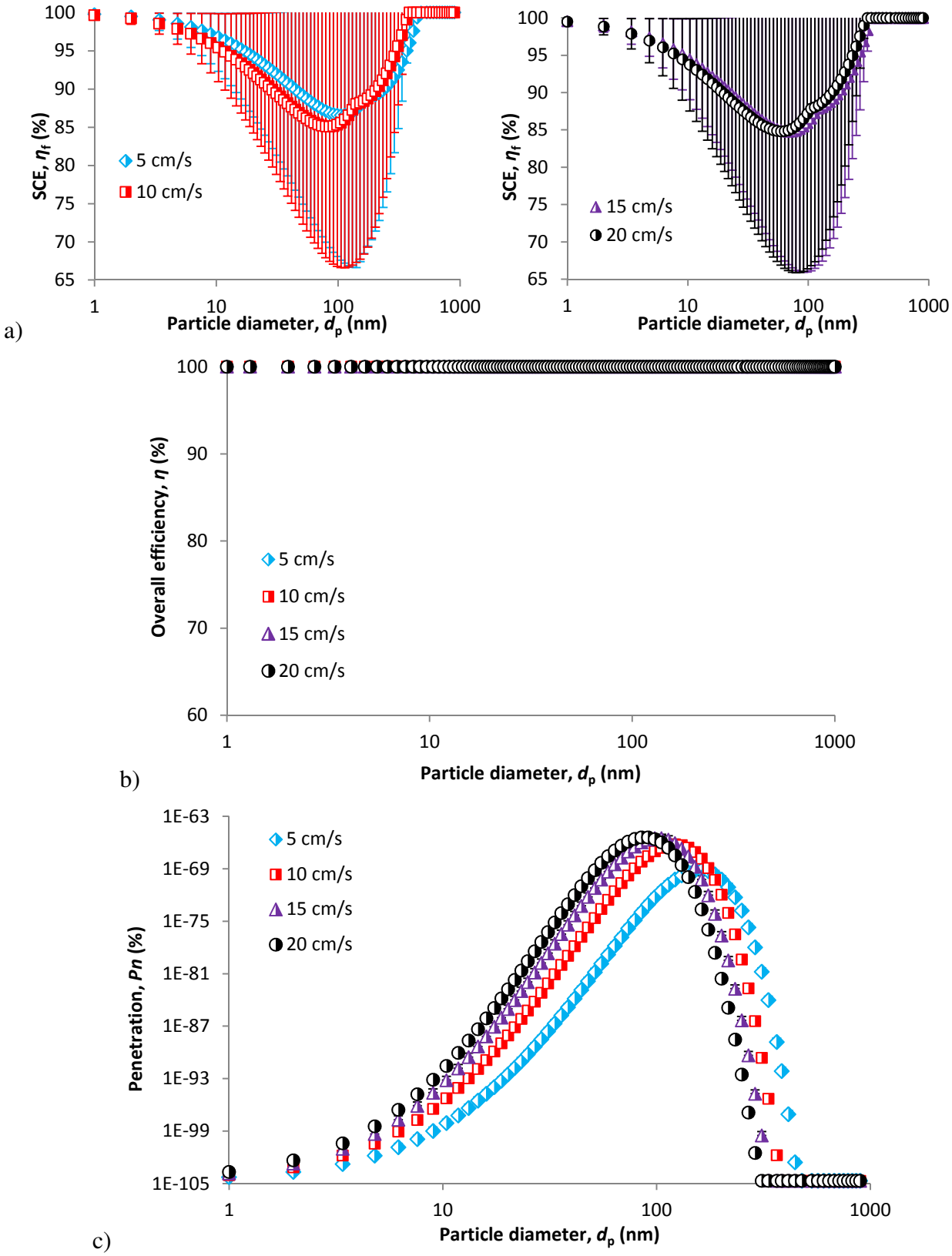

Fig. 3.9: *Single collector efficiency (a), overall filter efficiency (b) and overall penetration (c)*

The results are shown in Fig. 3.9b,c. After recalculating, we get 100% removal efficiency for all particle sizes (Fig. 3.9b). Fig. 3.9c shows the same expressed as penetration, i.e., the amount of particles which can penetrate through the membrane, which is in order of 10^{-66} which is practically equaled to zero. The results shown in Fig. 3.9a are single collector efficiencies calculated using models for diffusion (Eq. 3.18), interception (Eq. 3.21), impaction (Eq. 3.35) and adhesion (Eq. 3.41). So it is an example of one selected combination of models for individual mechanism. The other was not calculated as it was assumed that the result would be the same or would vary somewhere in the order of 10^{-70}, which is negligible.

The main reason for these results is the high solidity of the HFM structure, which is 0.48, while most of the fibrous filters have solidity between 0.01–0.3 [4] and most of the models are developed for this solidity range. Moreover, the membrane collector diameter is very small, giving a very dense structure. If we look at Fig. 3.4a, we can see collector diameters of about 100 nm in size. The thickness of the membrane wall is 36 µm. This means that there are about 360 such layers in the membrane wall creating a dense network that is very hard for particles to penetrate. Therefore, the results seem to be reasonable. In practice, this membranes could serve as absolute filters which are used for aerosols which must have 100% removal efficiency. Such aerosols include some radioactive particles, toxic aerosols and viruses.

3.4.2 CPM approach

The approach based on membrane pore size instead of membrane fiber diameter is presented in this section. Inertial impaction is stronger for larger particles at higher velocities, which is in accordance with theory. However, the model of Pich [105] is less accurate as it does not consider the possible sieving effect in membrane filters i.e., complete capture of particles on the membrane surface for particles larger than membrane pore size. This is obvious from Fig. 3.10. The membrane pore size considered in the calculations is 205 nm (Table 3.1). If circular pores are assumed, which is a simplification in the model, we should obtain 100% efficiency for particles above 205 nm regardless of the face velocity. This is not seen to be true from Fig. 3.10.

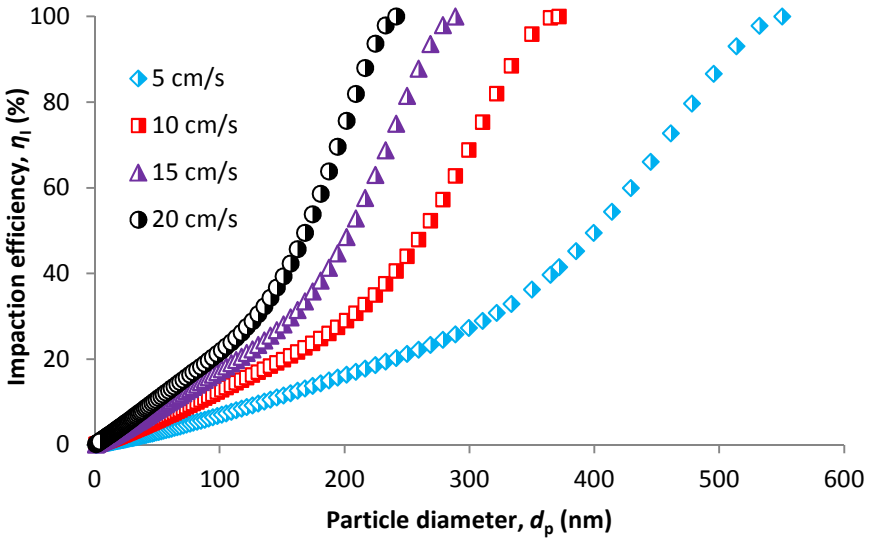

Fig. 3.10: *Impaction efficiency based on CPM model*

More plausible results are obvious for interception efficiency (Fig. 3.11). The interception efficiency increases up to a particle size of 202 nm with an efficiency of 99.97%. For a particle

size of 209 nm (slightly larger than pore size), efficiency is 100% which is reasonable. Therefore, the model proposed by Spurny et al. (Eq. 3.51) [106] seems to be accurate for the structure of polypropylene HFMs.

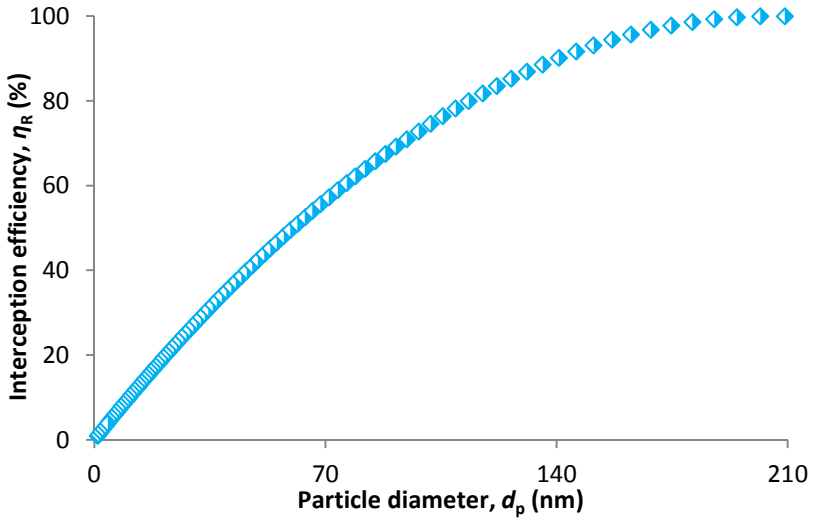

Fig. 3.11: *Interception efficiency based on CPM model*

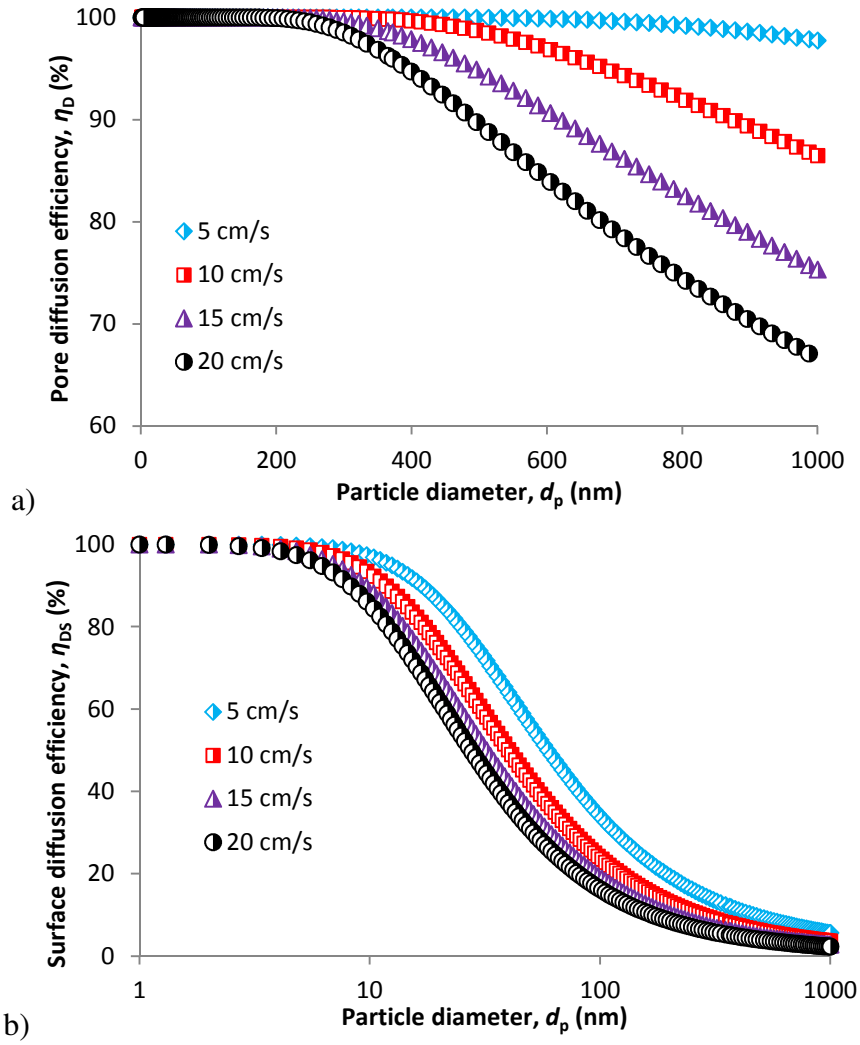

Fig. 3.12: *Collection efficiency due to diffusion in pores (a) and on the membrane surface (b)*

Diffusion is an important part of the overall efficiency. We can distinguish between diffusion capture in pores and diffusion capture on membrane surface (Fig. 3.3). Prediction models were developed for both (Eqs. (48) and (53)). Fig. 3.12a shows pore diffusion efficiency. To talk about diffusion capture within membrane pore structure is possible only for particles smaller than the largest pore size (i.e., smaller than 205 nm). Larger particles will only be a subject to surface diffusion capture (Fig. 3.12b) which is possible for whole particle size range. From Fig. 3.12a, a similar problem for the model for impaction efficiency is obvious. While efficiency for impaction should be 100% for particles above 205 nm, pore diffusion should be equaled to zero because no particle larger than 205 nm can penetrate the pore structure, so there is no diffusion capture of these particles.

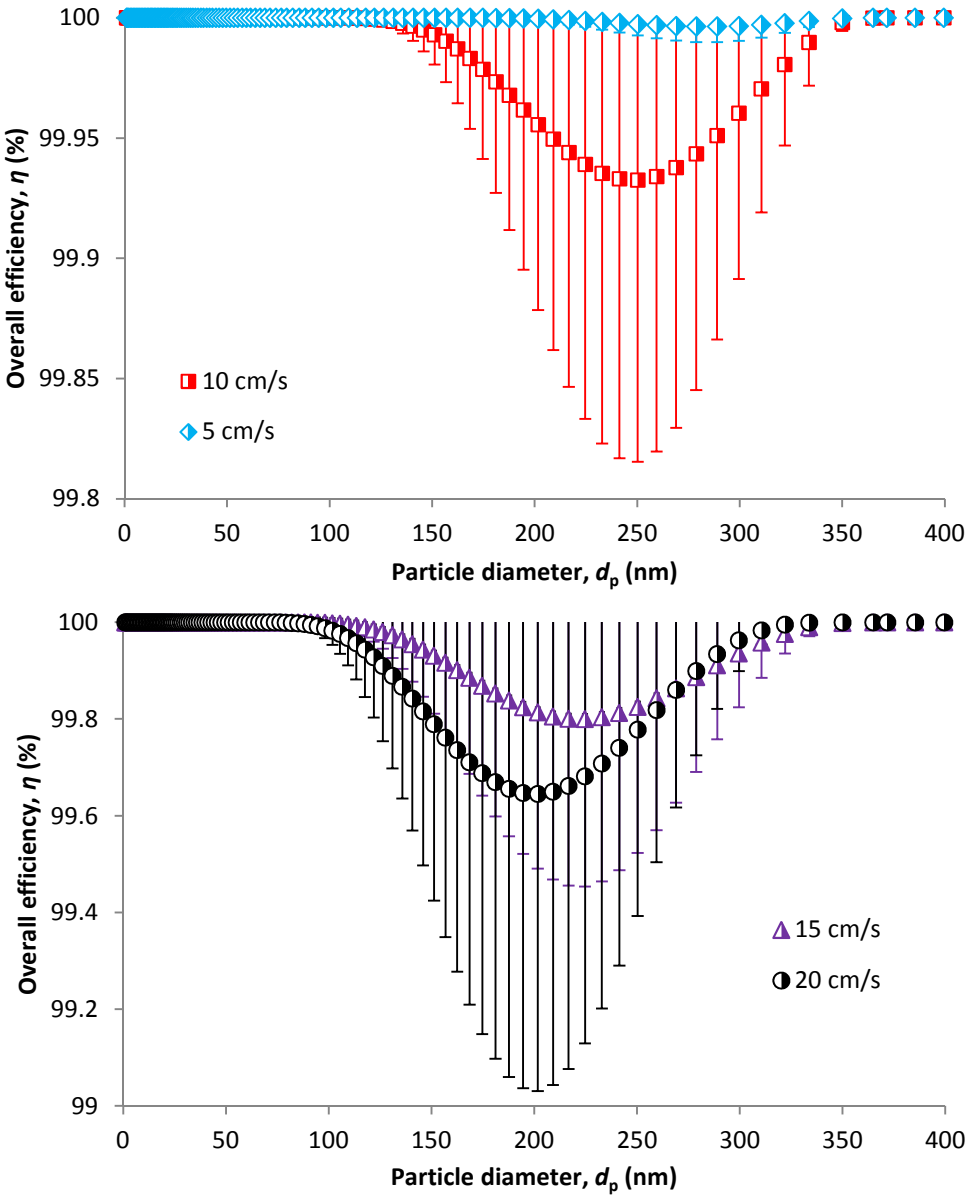

Fig. 3.13: *Overall efficiency in relation to particle size based on CPM model for a velocity of 5 and 10 cm/s (a) and 15 and 20 cm/s (b)*

Overall efficiency is predicted based on the models for individual mechanisms and calculated using Eq. (3.56). Fig. 3.13 shows 99.997% MPPS (290 nm) efficiency at a velocity of 5 cm/s. With increasing velocity, the efficiency for MPPS decreases. However, it is still in the range of

99.7% at a velocity of 20 cm/s. MPPS is shifted to smaller particle size with velocity. It is 250, 225 and 202 nm for 10, 15 and 20 cm/s, respectively. This model gives more realistic results compared to the model for fibrous filters, where unconditional 100% efficiency was obtained for all face velocities.

3.5 Conclusion

Prediction models for air filtration efficiency of fibrous and membrane filters were numerically compared by applying an HFM pore structure. With some assumptions, these models can be used for predictions of the aerosol separation efficiency of HFMs. Fibrous filter models give 100% efficiency no matter what level of face velocity, i.e., zero penetration. This is given by very small collectors in membrane structure similarly to nanofibrous filters. Compared to nanofibrous filters, HFMs have a very high solidity of 0.48. The HFM structure is very dense and the calculations can overestimate, as most of the models predict filter efficiency for solidity up to 0.3. CPM models predict efficiencies that are more realistic. Penetration up to 0.00014% was calculated for a face velocity of 20 cm/s. CPM models seem to give more plausible results for these HFMs, however, an experimental verification should be appropriate to compare accuracy of both approaches. However, this is rather a suggestion for another study, as this verification would probably be challenging, concerning experimental work. Thus, it would also be possible to empirically develop a new accurate model for HFMs.

4 Air filtration performance of hollow-fiber membranes in removal of ultrafine particles from incense stick burning[2]

4.1 Introduction

The main aim of this chapter is to characterize the filtration performance of symmetric polypropylene HFMs (0.4 to 0.8 m^2 filtration area) for nanoparticle removal. Transmembrane pressure and fractional filtration efficiency for particles in 18–100 nm range were determined. The tested HFMs were then compared using quality factor (*QF*) for individual particle sizes at a permeate velocity of 5, 10 and 15 cm/s.

4.2 Underlying phenomena

Aerosol particles carried by an air stream can be retained by a filter through different mechanisms. These mechanisms depend on the filtration conditions and mainly properties of the aerosol to be filtered particularly on particle-size distribution. Generally, collection efficiency (η) can be calculated as follows:

$$\eta = 1 - \frac{C_{\text{down}}}{C_{\text{up}}} \tag{4.1}$$

where C_{down} and C_{up} are the particle concentrations downstream and upstream of the filter, respectively. Theoretical prediction of filter efficiency is based on efficiency of a single collector (refer to Fig. 3.2) which is defined as the ratio of the number of particles collected to the number of particles in the volume of air geometrically demarcated by the collector. The collection efficiency thus depends on geometrical parameters of the filter, particles and also flow characteristics during filtration. To assess which mechanism dominates the collection for given conditions, evaluation in terms of several dimensionless parameters characterizing the filtration conditions is often appropriate as these parameters are a function of collection efficiency:

$$\eta = \eta(Re, Pe, Stk, R, G) \tag{4.2}$$

where *Re*, *Pe*, *Stk* are the Reynolds, Peclet and Stokes number, respectively and *R* and *G* are the interception and sedimentation parameter, respectively. Gravitation settling can contribute to particle capture but it can be neglected for nanoparticles [4, 111, 112]. To characterize the flow field around the collectors, Reynolds number, which is the ratio of inertia to viscous forces, is often used:

$$Re_{\text{f}} = \frac{d_{\text{f}} U \rho}{\mu} \tag{4.3}$$

where d_{f} is the average collector diameter, U is the face velocity, ρ and μ are the air density and dynamic viscosity, respectively. The same can be used to characterize the flow field around the particle, which is the particle-fluid Reynolds number. The relationship is the same as Eq. (4.3) but the particle diameter d_{p} and the particle velocity relative to the gas flow U_{p} are used:

[2] A version of this chapter was published as: Bulejko, P.; Dohnal, M.; Pospíšil, J.; Svěrák, T. Air filtration performance of symmetric polypropylene hollow-fiber membranes for nanoparticle removal. *Separation and Purification Technology.* **2018**, *197*, 122–128.

$$Re_{\mathrm{p}} = \frac{d_{\mathrm{p}} U_{\mathrm{p}} \rho}{\mu} \tag{4.4}$$

For calculation of Re_{p}, we assumed $U = U_{\mathrm{p}}$.

The diffusion mechanism is characteristic for particles undergoing a Brownian motion which then hit the collectors and are captured. Diffusion dominates when nanoparticles are filtered. To consider the relative importance of convection and diffusion, the Peclet number is used:

$$Pe = \frac{U d_{\mathrm{f}}}{D} \tag{4.5}$$

where D is the diffusion coefficient of particle calculated as follows:

$$D = \frac{k_{\mathrm{B}} T C_{\mathrm{s}}}{3\pi\mu d_{\mathrm{p}}} \tag{4.6}$$

where k_{B} and T are the Boltzmann constant and absolute temperature, respectively and C_{s} is the Cunningham slip correction factor:

$$C_{\mathrm{s}} = 1 + Kn\left[1.207 + 0.44\exp\left(-\frac{0.78}{Kn}\right)\right] \tag{4.7}$$

where Kn is the Knudsen number of particle with λ as mean free path of gas molecules:

$$Kn = \frac{2\lambda}{d_{\mathrm{p}}} \tag{4.8}$$

The interception effect assumes that particles follow the airflow streamlines. Interception occurs if the particle center is in a distance of one particle radius from the collector surface. Interception plays an important role in nanoparticle filtration for small collector diameters [41]. So called interception parameter is used to assess influence of interception mechanism which is the ratio of particle and collector diameter:

$$R = \frac{d_{\mathrm{p}}}{d_{\mathrm{f}}} \tag{4.9}$$

Inertial impaction is related to the flow field around the particle and dominates when particle inertia causes the particle to separate from airflow streamlines adjacent to the collector. The particle thus follows different trajectory and collides with the collector [113]. Stokes' number Stk characterizes the particle inertia and is defined as follows:

$$Stk = \frac{d_{\mathrm{p}}^2 \rho_{\mathrm{p}} C_{\mathrm{s}} U}{18\mu d_{\mathrm{f}}} \tag{4.10}$$

where ρ_{p} is the particle density. If Stk is higher than unity, particles separate from streamlines and hit the collector. Conversely, for Stk lower than unity, the particles move along streamlines and the inertial effect does not take place. For high Reynolds numbers, the inertia effect is more appreciable as the streamlines adjacent to the collector turn around more rapidly.

4.3 Materials and methods

4.3.1 Hollow-fiber membranes

Three various types of low cost polypropylene HFMs from Zena Membranes s.r.o. Brno, Czechia [26] were tested (Table 4.1). These HFMs are manufactured via dry stretching of hollow fibers

with no waste. HFMs are often characterized by packing density. The membrane packing density a_M is the fraction of the cross-sectional area of a fiber over the cross-sectional area of a HFM bundle. The relationship can be written using the fiber outer diameter (D_o) and bundle (module) inner diameter (D_{bi}) as follows [114]:

$$a_M = N_f \frac{D_o^2}{D_{bi}^2} \tag{4.11}$$

where N_f is the number of fibers in the bundle. HFMs have narrow pore-size distributions (measured using a Quantachrome 3Gzh capillary flow porometer, pore size range 0.01–500 µm) with most pores within a size range of 85–105 nm (Fig. 4.1). Fig. 4.2a shows a single hollow fiber from a Zeiss EVO LS10 scanning electron microscope with shell side porous surface overview and the detail of porous morphology in Fig. 4.2b. The SEM images were used to measure collector diameters of HFMs (Table 4.1).

Table 4.1: *Parameters of HFMs*

HFMs	P50	P60	P80
Fiber outer diameter, D_o (µm)	300	300	620
Fiber inner diameter, D_i (µm)	228	228	474
Fiber wall thickness, Z (µm)	36	36	73
Number of fibers, N_f	1380	1380	300
HFMs net length, L (mm)	730	730	730
Membrane packing density, a_M (%)	46	46	43
Bundle inner diameter, D_{bi} (mm)	16.4	16.4	16.4
HFM surface area, A (m^2)	0.95	0.95	0.43
Initial *TMP* (5 cm/s) (Pa)	543.2 ± 3.3	558.6 ± 3.6	284.6 ± 2.7
Average pore size, d_o (nm)	94	87	95
Porosity, ε (%)	52	52	54
Average collector diameter, d_f (nm)	130	90	112

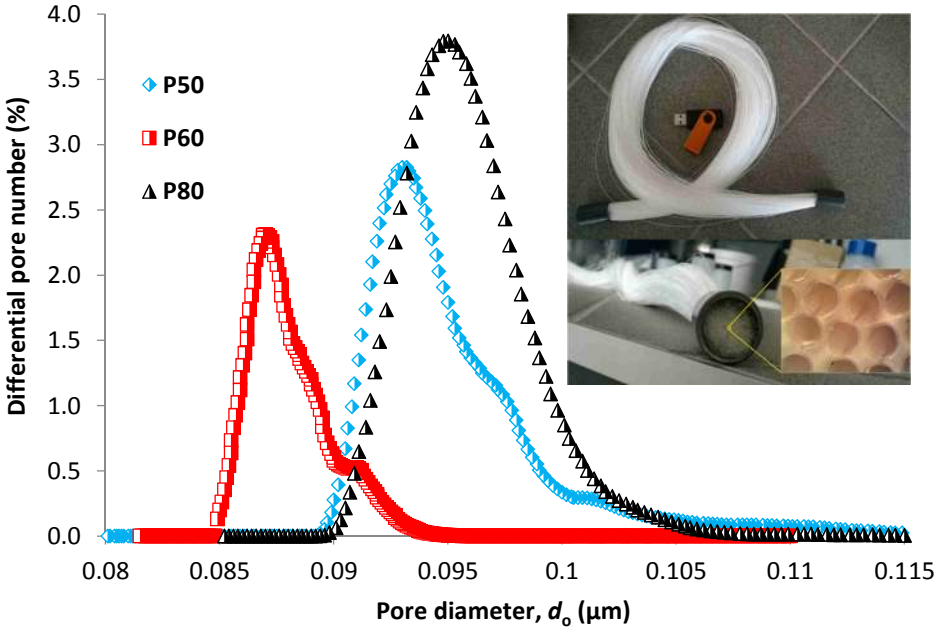

Fig. 4.1: *A picture of the HFM and pore-size distributions of tested HFMs*

HFMs P50 and P60 have the same parameters – P50 is an earlier generation of P60. They differ in their methods of preparation, which are not described here. However, both P50 and P60 were measured to assess if there were significant differences between them. Fouling of HFMs by aerosol particles was then observed using a JEOL JSM-7600F scanning electron microscope.

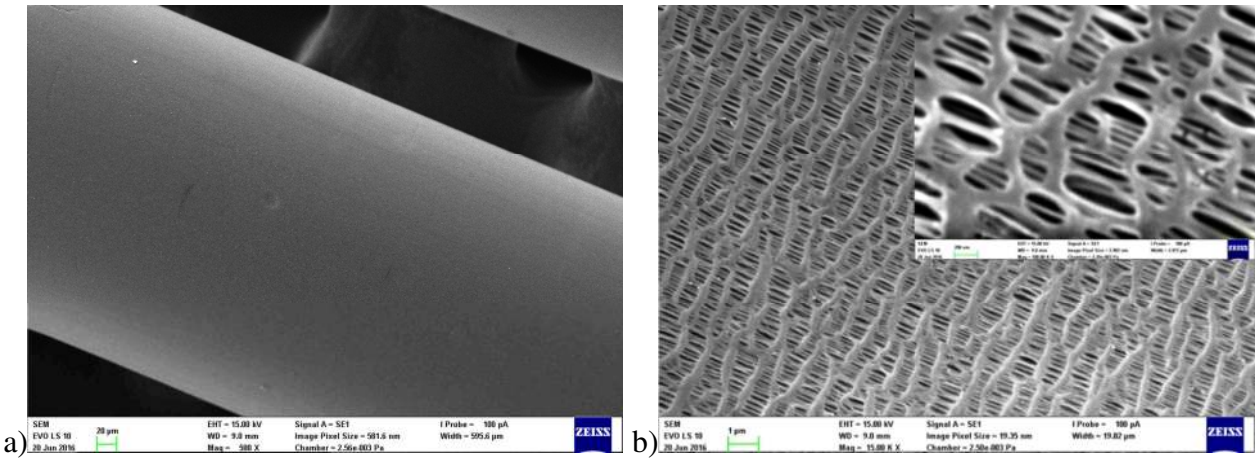

Fig. 4.2: *SEM of HFM shell side: a view of a single fiber (a) and a detail of porous surface (b)*

4.3.2 Experimental conditions

Filtration experiments were carried out in a glass chamber with 260 dm^3 volume connected to a suction pipe (1), to which the HFM bundle was linked (Fig. 4.3a, a real photograph of the setup shown in supplementary Fig. S4.00). The suction pipe was provided with a velocity probe (8), a thermocouple (10) and a differential pressure sensor (12). The airflow through the HFM was provided by a ventilator (11). The particles which passed through the membrane (downstream side), carried by airflow inside the pipe, were sampled via the sampling spot (9) using a TSI SMPS 3080 electrostatic classifier connected to a CPC 3775 particle counter (6) with a scanning time of 45 s and a retrace time of 15 s. The particle sizer was linked to a laptop with software for data management (5).

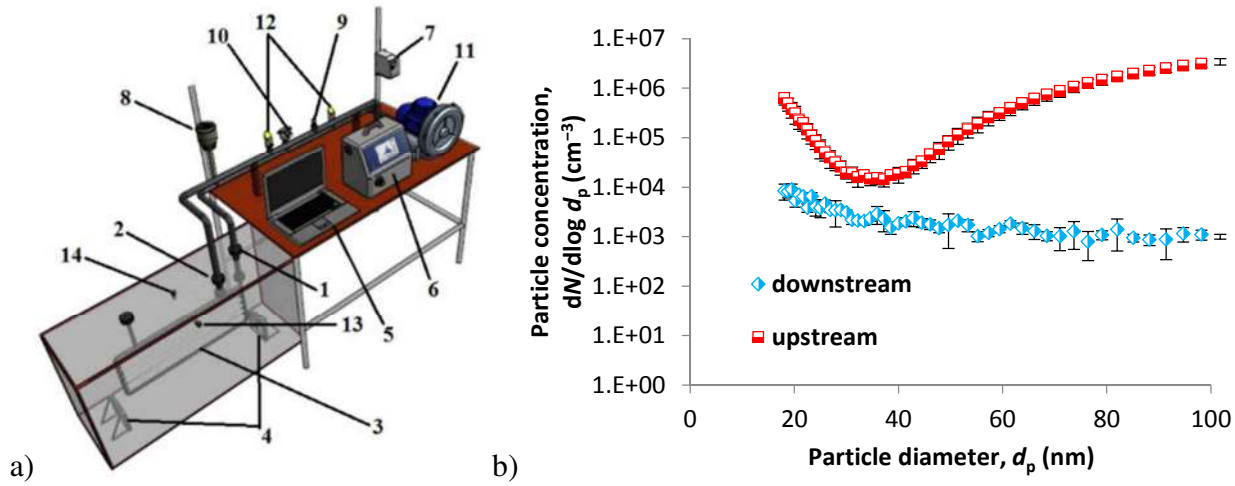

a) b)

Fig. 4.3: *A simplified scheme of the experimental setup (a) and upstream/downstream aerosol particle size/concentration profile (b)*

A polydisperse aerosol was generated inside the chamber by burning incense sticks (HEM Opium incense sticks, Mumbai, India). The aerosol penetration was measured at a permeate velocity of 5, 10 and 15 cm/s. All the upstream aerosols had similar particle size distribution with geometric average particle size of 70 ± 3 nm. Fig. 4.3b shows an upstream/downstream particle size/concentration profile.

4.3.3 Evaluating the filtration performance

Air filtration materials or whole air filtration units are mostly evaluated in terms of filtration efficiency and pressure drop. The former describes the ability of a filter unit to remove particles from an air stream while the latter is mainly related to energy requirements. The filtration efficiency η is generally defined by Eq. (4.1). The measurement of particle concentrations upstream and downstream consisted of a series of six particle counting instances according to the scheme in Table 4.2. The number of particles was measured sequentially downstream and upstream while each upstream and downstream concentration was measured three times.

Table 4.2: *Measuring cycle for particle concentrations counted sequentially upstream/downstream*

upstream				C_{up1}	C_{up2}	C_{up3}
downstream	C_{down1}	C_{down2}	C_{down3}			

The average of three concentrations upstream and downstream were then used to calculate the efficiency according to following equation:

$$\eta_{1,i} = 1 - \frac{C_{\text{down1},i}}{\frac{C_{\text{up1},i} + C_{\text{up2},i} + C_{\text{up3},i}}{3}} \tag{4.12}$$

Possible fluctuations of upstream particle concentration were thus treated to avoid significant data distortion. The efficiency calculated using Eq. (4.12) was determined for a given particle size in 48 channel resolution. The average efficiencies of individual HFMs were compared using the analysis of variance (ANOVA). Non-parametric ANOVA was chosen after testing the data normality using the Shapiro-Wilk test which proved that the efficiency data are not governed by normal distribution (the test results are shown in supplementary material, Fig. S4.0). The efficiency data were compared using the Kruskal-Wallis test in two ways, i.e. with permeate velocity and HFM type as a categorization variable. Using this test it was possible to discover whether changing the permeate velocity has significant influence on the filtration efficiency or if the individual HFMs differs significantly among each other (at the same velocity) at a significance level of 0.05.

Another important quantity was the pressure loss caused by the filtration medium, which is chiefly related to energy requirements thus greatly affecting the price of the overall filtration process. To be consistent with the terminology used for membrane processes which the usage of HFMs falls into, we use the term “transmembrane pressure” (*TMP*) for difference between feed and permeate pressure. *TMP* is significantly influenced by the filtration media’s permeability. This can be estimated using the Darcy equation, which includes the fluid flow in a porous structure of a filtration medium in relation to the pressure drop and fluid velocity (U) [40, 115]:

$$\frac{TMP}{Z} = \frac{\mu}{k} U \tag{4.13}$$

where Z is the filter thickness (here fiber wall thickness), μ is the fluid viscosity and k is the permeability of the membrane. The overall filtration performance is mostly assessed using the quality factor (QF) which includes filter efficiency in relation to transmembrane pressure:

$$QF = \frac{-\ln(1-\eta)}{TMP} \tag{4.14}$$

Filters of better quality have a higher QF, i.e. they have higher filtration efficiency and/or lower TMP.

4.4 Results and discussion

4.4.1 Transmembrane pressure of HFMs

Here we distinguish between TMP and dead-end pressure (p_{de}). TMP is the pressure difference between the upstream and downstream sides of the membrane. The dead-end pressure is a pressure difference between the atmosphere and negative pressure at the dead-end potting created by the ventilator at the vacuum pipe. A differential pressure sensor was connected to the dead-end potting of the HFM bundle and the difference compared to the atmosphere was measured at different airflow velocities at the vacuum side. A pressure difference is caused by the airflow in the hollow fiber lumen induced by the ventilator. Through this measurement we obtained the information if the HFM was active throughout the full length of the fibers and obtained information about the real participation of the membrane surface area on the filtration. The results are shown in Fig. 4 for both TMP and dead-end pressure. TMP (at 5 cm/s) was highest for P60 (558.6 Pa), followed by P50 (543.2 Pa) and P80 (284.6 Pa). Dead-end pressure was the opposite of the TMP i.e. P80 > P50 > P60 and were 34.1, 6.6, and 2.1 Pa, respectively. This order was expected as a higher TMP caused lower dead-end pressure due to pressure loss in the length of the fiber lumen. Conversely, at lower TMP, higher dead-end pressure was expected as the pressure losses through the fiber length were lower mainly due to larger fiber diameters, as in P80.

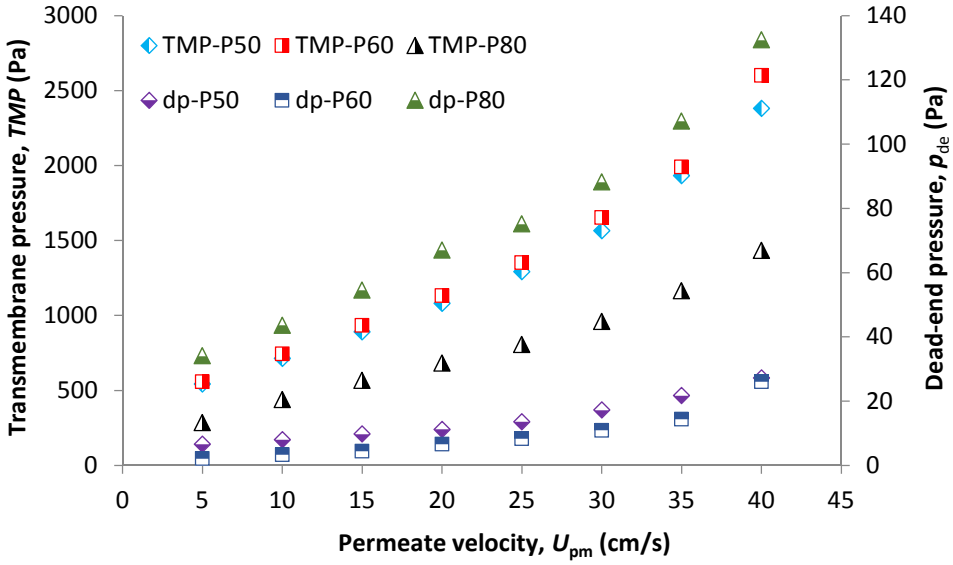

Fig. 4.4: *Transmembrane pressure and dead-end pressure vs. permeate velocity of clean HFMs*

The *TMP* of the tested HFMs was one order of magnitude lower (for the corresponding airflow velocities) than those reported by Wang et al. [15] who prepared HFMs of PVDF-PEG for air purification. Compared to filters made of non-woven, our HFMs had significantly higher *TMP* than those reported by Hung and Leung [116] who tested nanofiber filters with *TMP* in the range of 5.4 to 74 Pa (at 5 cm/s) but comparable to HEPA filters tested by Bortolassi et al. [115] which had their *TMP* in the range from 269 to 418 Pa (at 5 cm/s). Nonetheless, it should be noted that this is a comparison of two completely different filter geometries which should be considered demonstrative for the velocity of 5 cm/s. Parameters such as filtration area, filter thickness, packing density, and fiber diameter are not and generally cannot be taken into account as some of these parameters have totally different physical meaning (for example, the fiber diameter of non-woven filters and of HFM, or non-woven filter thickness and HFM fiber wall thickness). Therefore, it is more appropriate to compare filters using the quality factor *QF*, which considers the basic characteristics of air filters, such as filtration efficiency and pressure drop.

Generally, very small fiber diameters create higher airflows accompanied by high *TMP* and pressure loss throughout the fiber length due to space restriction. The Reynolds number in a single fiber will inherently be lower than one, characteristic of laminar flow. Therefore, the use of this type of membrane is recommended for low-volume applications or for pressure air purification.

4.4.2 Filtration efficiency

Fig. 4.5 shows the fractional efficiency of tested HFMs in relation to permeate velocity. All the curves have a typical shape, each with a minimum which is the most penetrating particle size (MPPS). The highest efficiency (above 79% for MPPS) was observed at the lowest air flow velocity of 5 cm/s. The MPPS efficiencies were 79.07% (35.9 nm), 86.54% (37.2 nm) and 86.31% (40.0 nm) for P50 (Fig. 4.5a), P60 (Fig. 4.5b) and P80 (Fig. 4.5c), respectively. Here, we can see an expected trend for the tested HFMs, i.e. the highest MPPS efficiency for P60 followed by P80 and P50 (Fig. 4.6).

The typical curve shape is caused by different mechanisms acting at the same time. Usually the left side of the minima is dominated by the particle Brownian motion [117]. This is in accordance with the Peclet number which was very low (under 30, refer to supplementary material Fig. S4.1) for whole investigated particle size range (20–100 nm). Moreover, the flow field around the particles was laminar as the particle Reynolds number was lower than one (Fig. S4.2). The right hand side is usually dominated by inertial impaction. However, as the minima are under 100 nm size, we can expect stronger effect of interception. Interception parameter was higher than 0.1 for each HFM (Fig. S4.3) which is the region where the interception starts to dominate [108]. Moreover, in the absence of significant external forces, interception governs the deposition only if inertial impaction is negligible [113]. The inertial force becomes appreciable in transition flow regime where Re_f is in the range of 1 to 15 [4]. As a consequence the streamlines approaching a collector turn around more rapidly. As the collector Reynolds number was significantly lower than one (the order of 10^{-3}, Fig. S4.4) for each HFM and Stokes' number lower than one (the highest value of about 0.16, Fig. S4.5) inertial impaction at the present experimental conditions can be neglected.

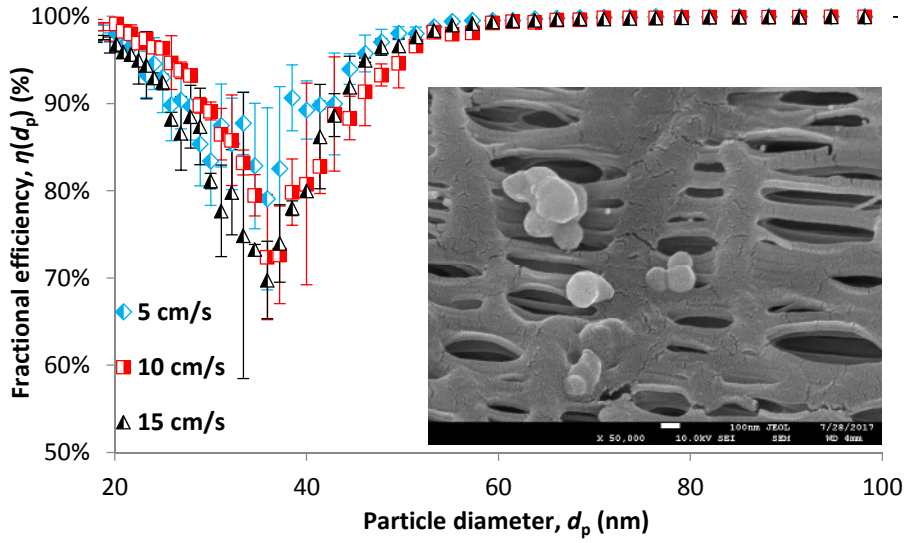

a)

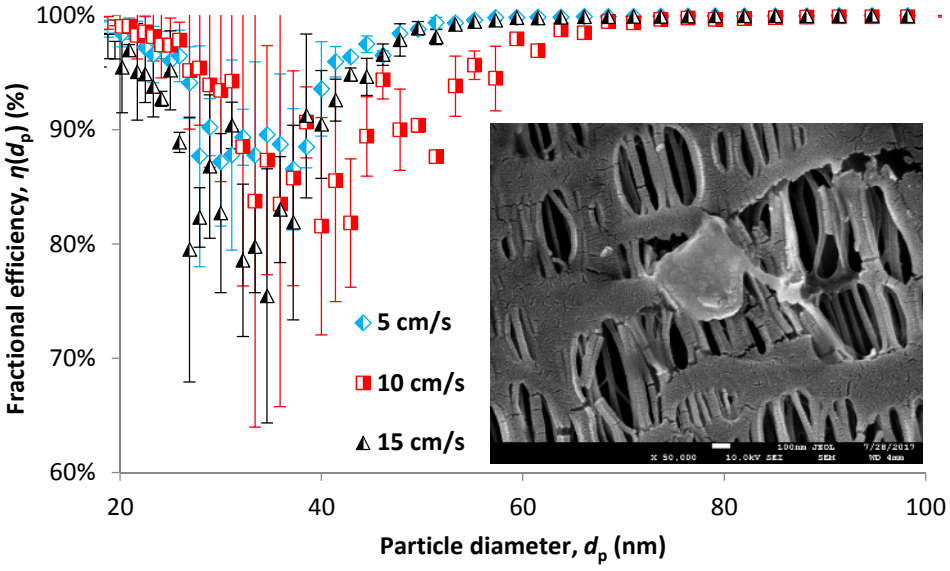

b)

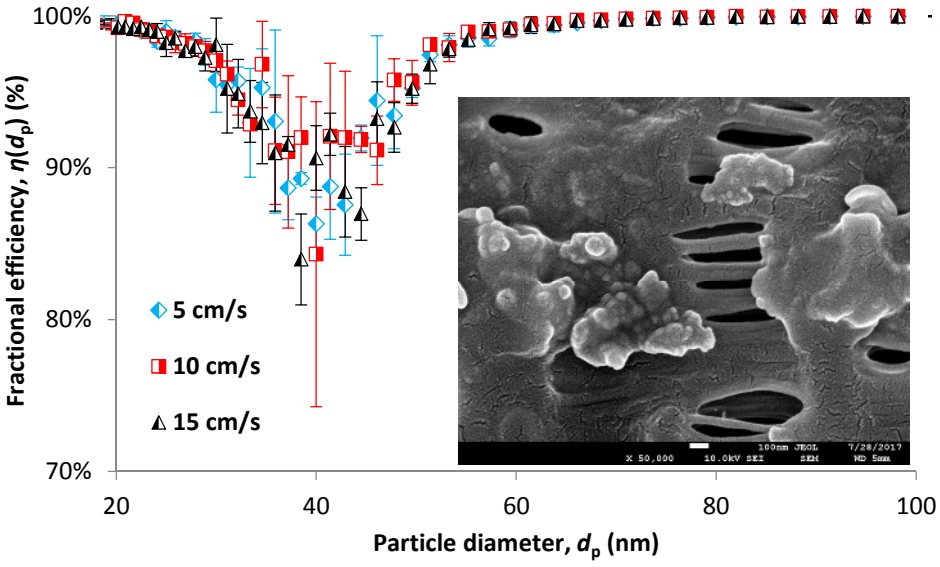

c)

Fig. 4.5: *Filtration efficiency in relation to particle size for different HFMs with a SEM picture of fouled surface for P50 (a), P60 (b) and P80 (c)*

Fig. 4.5 further shows decreasing filtration efficiency with increasing permeate velocity. This is in agreement with previous works focused on fibrous filters [118–122] but in contradiction to very recent work on air filtration using PVDF-PEG HFMs by Wang et al. [15]. The authors attributed this to the asymmetric structure of these HFMs where the high flowrate could enhance aerosol deposition through direct impaction and Brownian motion, thus decreasing the penetration of particles. As the tested HFMs are symmetrical, the mechanism of particle collection is rather similar to that of fibrous filters. Even though the fiber walls are very thin (tens of microns), they have a porous structure similar to a fibrous filter medium (Fig. 4.2b), like a net of randomly distributed fibers (collectors).

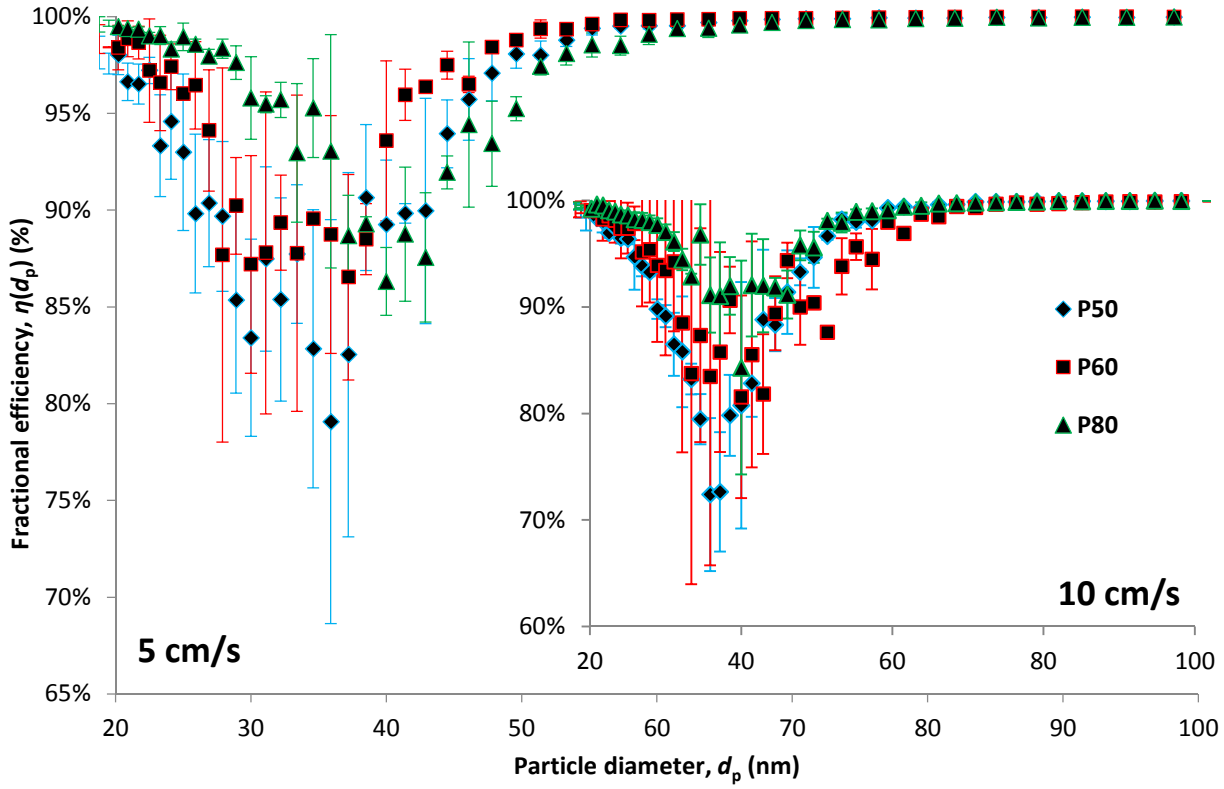

Fig. 4.6: *Comparison of all HFMs at 5 cm/s and 10 cm/s*

At higher velocities, the influence of convection prevails, thus weakening the diffusion. There is less time for a particle to collide with an obstacle within the pore structure via Brownian diffusion [118]. This is, however, true for larger particles where Stokes' number is higher than one. As the interception parameter increases with particle size, we can expect increased influence of interception deposition mainly for particles above 60 nm as these are captured from more 99.9%.

Table 4.3: *Filtration performance characteristics of individual HFMs in relation to permeate velocity*

HFM	P50			P60			P80		
Permeate velocity, U_{pm} (cm/s)	5	10	15	5	10	15	5	10	15
MPPS (nm)	35.9	35.9	35.9	37.2	40.0	34.6	40.0	40.0	38.5
Efficiency, η(MPPS) (%)	79.07	72.40	69.76	86.54	81.56	75.45	86.31	84.30	83.96

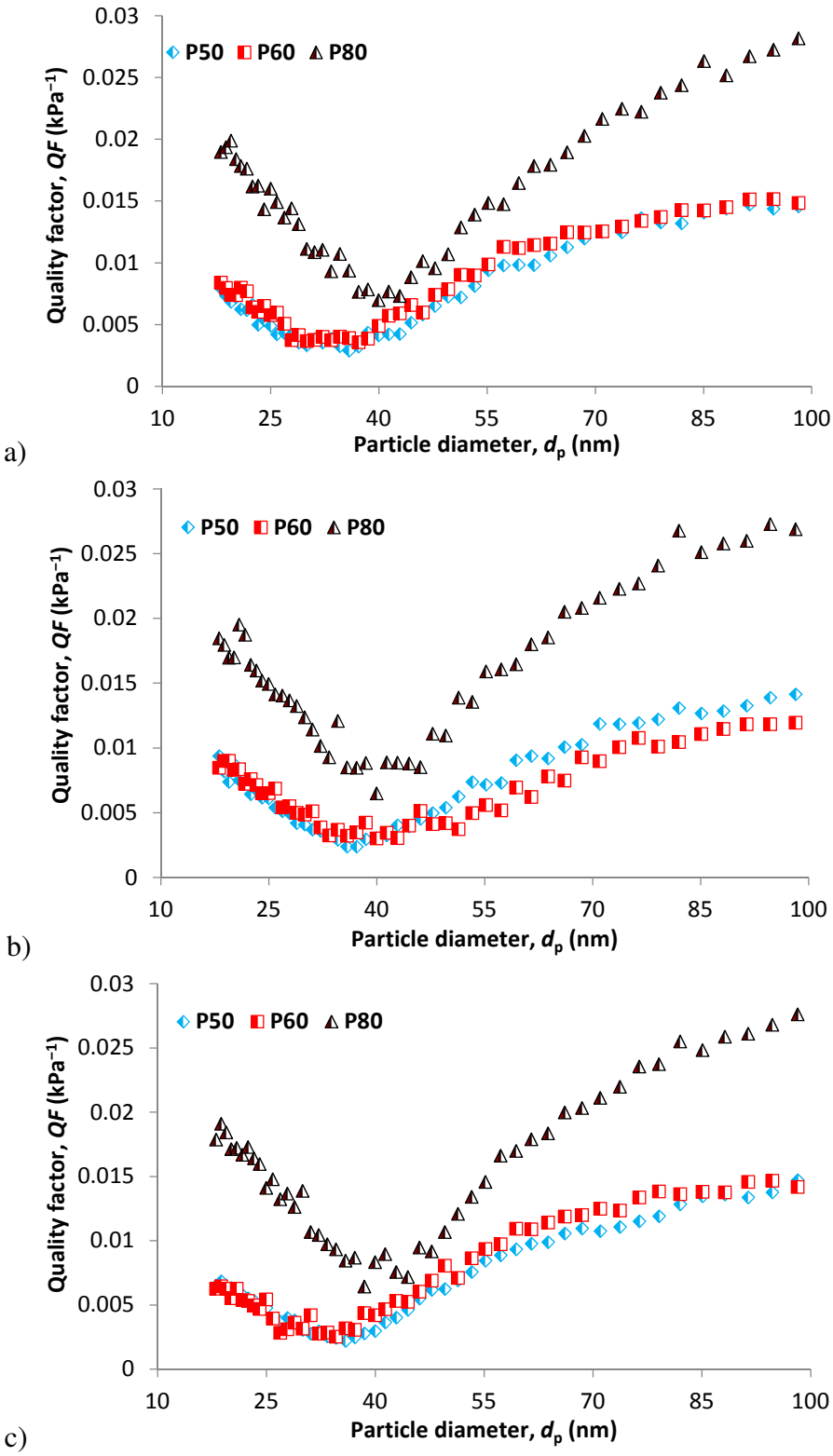

Fig. 4.7: *Quality factor vs particle diameter at a permeate velocity of 5 cm/s (a), 10 cm/s (b) and 15 cm/s (c)*

Table 4.3 shows an overview of efficiencies and MPPS for tested HFMs at different velocities. MPPS remains the same with permeate velocity for P50 and P80. This is contrary to the work of Chen et al. [123] who studied Nuclepore filters, and also to the theoretical predictions of Jung et al. [124]. Jung et al. [124] attributed this to the increased impaction mechanism at higher velocity

(and thus decreased Brownian motion) which was even enhanced with increased dust loading. Here, we have observed practically no change in MPPS, which may be attributed to competitive behavior of the interception and diffusion mechanisms with increasing velocity as all the MPPS belong to the area were Brownian diffusion dominates. Another reason for this may be the influence of fiber wall thickness, which is related to pore diffusion. From Table 4.3, a slight upward trend can be seen for MPPS with thicker fiber walls (P50/60 < P80). For thicker walls, a higher residence time for particles is achieved [123] and the diffusion deposition is enhanced. This is mainly true for smaller particles. With increasing velocity, larger particles can penetrate more easily due to the combination of interception and diffusion.

4.4.3 HFM fouling

Fig. 4.5 also shows surface HFMs after air filtration. The HFM pore structure was fouled by aerosol particles in varying intensity. Some of the particles are captured on the membrane surface separately (Fig. 4.5a,b), while some of them form a film-like layer (visible in Fig. 4.5c) caused by particles merging, probably due to air humidity (laboratory conditions were a temperature of 23 °C and humidity of about 55%). At this level of air humidity, increased adhesion forces among generated particles can occur, forming agglomerates (clearly visible in Fig. 4.5c). From these pictures it is clear that surface filtration dominates but mainly for larger particles above 100 nm. Particles under 100 nm will inherently be captured inside the HFM fiber wall via the diffusion mechanism. This is the opposite of what happens with fibrous filters, in which depth filtration is the main separation mechanism for whole particle size ranges [44, 115, 119, 125–127].

4.4.4 Quality factor of tested HFMs

Fig. 4.7 compares the tested HFMs using *QF* at different permeate velocities as calculated using Eq. (4.14). P80 has the highest *QF* in the whole particle size range at each tested permeate velocity which is due mainly to lower *TMP*. P50 and P60 are comparable or P60 is slightly higher. Comparing the *QF* for MPPS, P80 is still the highest (7.0 kPa^{-1}), followed by P60 (3.7 kPa^{-1}) and P50 (2.9 kPa^{-1}) at 5 cm/s. P80 remains still highest also for the other velocities.

QF was higher than those reported by Wang et al. (2017) for PVDF-PEG HFMs, which had their *QF* in the range of 2 kPa^{-1} for a particle size of 30 nm and a velocity of 9.2 cm/s. *QF* results correspond to or are lower when compared to electrospun polyurethane nanofiber filters, for an MPPS of 70 nm and a face velocity of 5.7 cm/s [128]. They are also lower when compared to Nylon 6 nanofiber filters for an MPPS of 120 nm and 5 cm/s [116]. Lastly, they are comparable to the nanosized/porous polylactic acid composite fibrous membranes (MPPS of 260 nm, 14.1 cm/s) reported by Wang and Pan [44] and higher than 4-layer oleophylic glass fiber filters (average aerosol particle size of 900 nm, 10 cm/s) as reported by Chang et al. [126].

4.5 Conclusion

The air filtration performance of polypropylene HFMs was investigated. Due to their high efficiency, HFMs may be used for special applications in which low volume flowrates are involved.

Based on the results presented above, the following conclusions were made:

- The results show high efficiency for removal of submicron particles. The MPPS were in the range of 34 to 40 nm with high efficiency at a velocity of 5 cm/s and decreased in the following order: P60 > P80 > P50 (for MPPS). With increasing permeate velocity, the MPPS efficiency decreased down to 69% (15 cm/s). Nonetheless, for particle sizes above 60 nm, the efficiency remained practically unchanged no matter the permeate velocity.
- *TMP* is rather higher compared to fibrous air filters. P50 and P60 are almost the same as they have the same parameters and were around 560 Pa at 5 cm/s. P80, with double the fiber diameter though half the filtration area, had *TMP* of 285 Pa at the same permeate velocity, which is comparable to fibrous HEPA filters. *TMP* remains the main problem to practical applicability as this parameter determines the energy consumption of the overall filtration process.
- Polypropylene HFMs were further compared in terms of *QF,* which is often appropriate. *QF* was comparable with fibrous filters and the other HFMs reported previously mainly for MPPS of P80 while rather higher for larger particle sizes (those above 60 nm). P60 had a higher efficiency compared to P80 though a lower *QF* due mainly to higher *TMP*.

5 Air filtration performance of hollow-fiber membranes in removal of submicron TiO_2 aerosol[3]

5.1 Introduction

The main aim of this chapter was to determine filtration efficiency characteristics for particle size range from 100 to 600 nm using a test dust of TiO_2 particles with a modal particle size of 340 nm. TiO_2 was previously used to model pressure drop evolution during fouling in water filtration [129] and also to assess air filtration performance of multilayered electrospun polylactide membranes [8]. Therefore, we chose TiO_2 as model particles for this study. The influence of permeate velocity and amount of testing dust was studied. Finally, we studied membrane fouling and pressure drop evolution with time and observed the fouled HFMs using SEM.

5.2 Materials and methods

5.2.1 Experimental setup

Filtration was carried out in a chamber of 70 dm^3 volume (Fig. 5.1) where a HFM was placed. The HFM was connected to a fan using a pipe. The pipe was provided with an EE660 velocity probe (VP) and an Omega PX277-05D5V differential pressure sensor (Δp). The second output of the differential pressure sensor was connected to the chamber thus obtaining pressure drop caused by the HFM. Micronized titanium dioxide (titanium white pigment, Fig. 5.2a) was used as a test dust (particle-size distribution shown in Fig. 5.2b measured using a Malvern Mastersizer 2000 laser diffraction analyzer). TiO_2 dust was used due to an easier and faster formation of dust environment. Particles generated from a solution such as polystyrene latex, NaCl or DEHS could not be used because it was necessary to create a stable particle dispersion in a very short time and in an appropriate concentration in the whole volume of the chamber. The production of particles using a generator is slow and the concentrations are rather low. Using this method, it was practically impossible to create required amount of airborne particles in the chamber, also due to their sedimentation. Two or more generators/nebulizers in parallel would help to provide high aerosol concentrations. Unfortunately, these were not available. Therefore, we used TiO_2 powder which was dispersed using a pressure air nozzle (see further).

The test dust was fed through an opening on the chamber wall (the upstream concentration profiles shown in Fig. 5.2c). It was not possible to use dust feeder because, unlike in the planar filter testing, there was not any air stream inside the chamber and the fed dust just fell down without any dispersion. To ensure adequate homogeneous dust dispersion into the chamber it was necessary to use pressure air. The weighed amount of dust was dispersed from a small dish using pressure air driven through an ejector (Fig. 5.1). The dust was thus uniformly dispersed in the chamber. Particles which passed through the membrane, carried by the airflow inside the pipe, are sampled using a TSI SMPS 3080 electrostatic classifier connected to a CPC 3775 particle counter. The particle sizer was linked to a laptop with software for data management.

[3] A version of this chapter was published as: Bulejko, P.; Svěrák, T.; Dohnal, M.; Pospíšil, J. Aerosol filtration using hollow-fiber membranes: Effect of permeate velocity and dust amount on separation of submicron TiO_2 particles. *Powder Technology.* **2018**, *340*, 344–353.

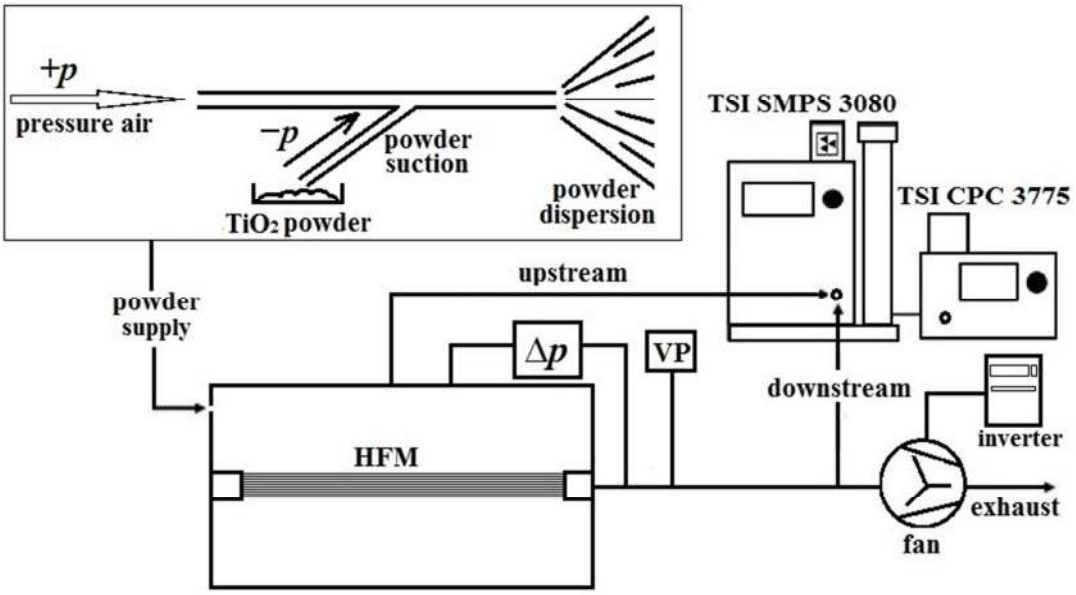

Fig. 5.1: *A scheme of the experimental setup*

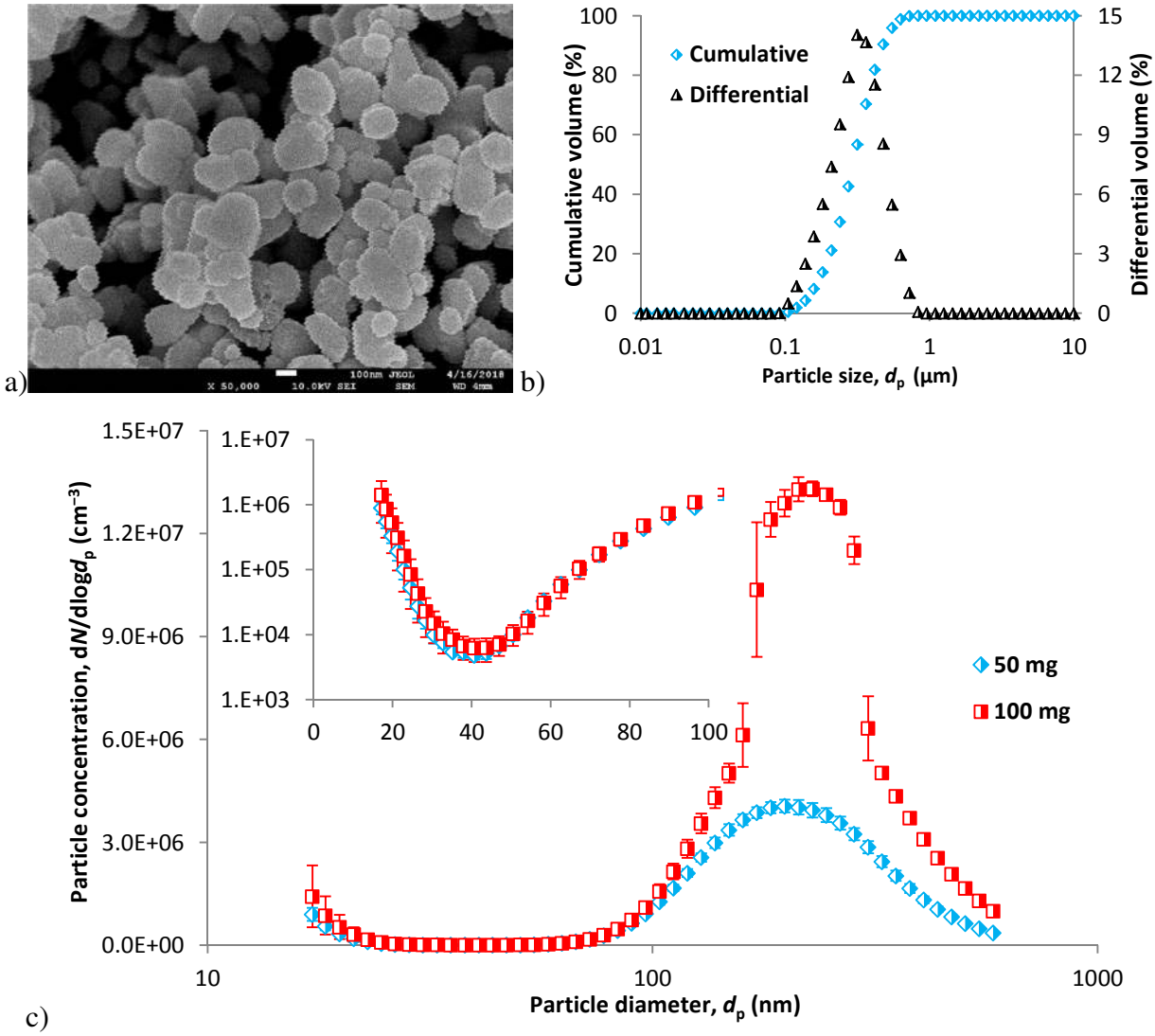

Fig. 5.2: *TiO_2 particles used as a test dust (a), particle size distribution of testing dust (b) and upstream concentration profile of the same at two different amounts of TiO_2 (c)*

5.2.2 Hollow-fiber membranes

Polypropylene HFMs (Fig. 5.3a) produced by ZENA Membranes s.r.o. [26] were tested on filtration performance. Parameters of HFM are shown in Table 5.1. They have a narrow pore-size distribution (Fig. 5.3b) with majority of pores within a size range of 90–100 nm (measured using a Quantachrome 3Gzh capillary flow porometer). Fig. 5.4 shows a single hollow fiber shell side (Fig. 5.4a) with a detail of the membrane porous structure (Fig. 5.4b,c). The strength of the membrane fibers is 2N/fiber (measured using a LabTest 6.0051 tensile testing machine).

Table 5.1: *HFMs' parameters*

Fiber outer diameter, D_o (µm)	620
Fiber wall thickness, Z (µm)	60
Number of fibers, N_f	300
HFM net length, L (mm)	730
HFM surface area, A (m^2)	0.43
Initial Δp at 0.2 m/s (Pa)	700
Permeability, k ($m^3m^{-2}h^{-1}bar^{-1}$)	240
Average pore size, d_o (nm)	276
Average collector diameter, d_f (nm)	112
Porosity, ε (%)	54

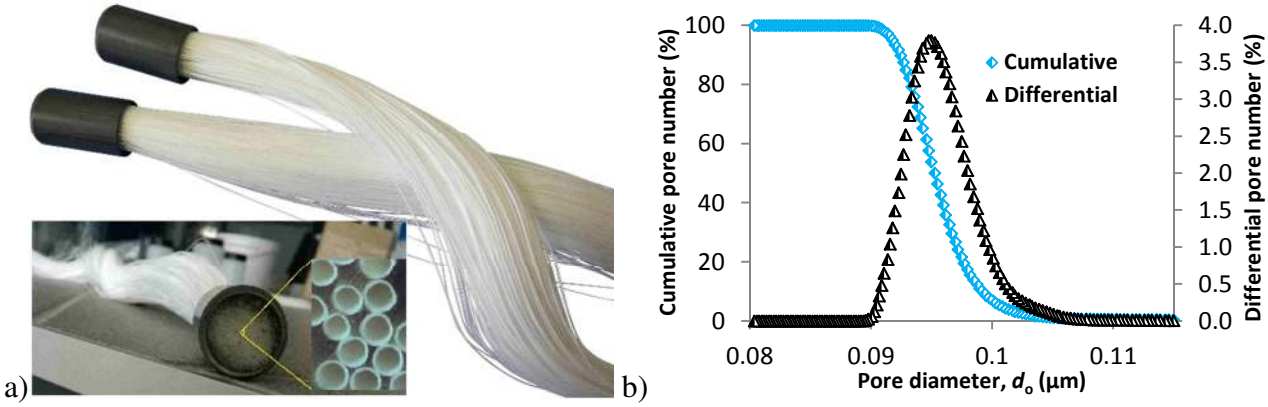

Fig. 5.3: *A HFM bundle (a) and a pore-size distribution of HFM (b)*

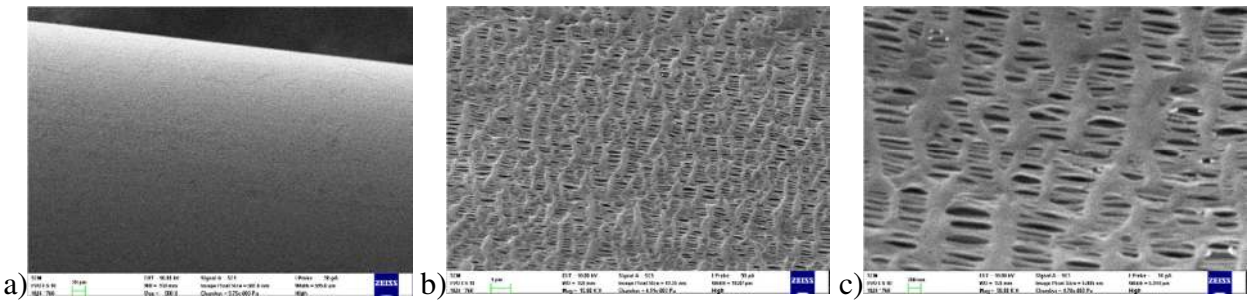

Fig. 5.4: *SEM of HFM shell side: a single fiber (a), porous surface (b) and porous structure morphology in detail*

5.2.3 Evaluating the filtration performance

Air filtration materials or whole air filtration units are mostly evaluated in terms of filtration efficiency and pressure drop. The former describes the ability of a filter unit to remove particles from an air stream while the latter is mainly related to energy requirements. The filtration efficiency η is generally defined as follows:

$$\eta = 1 - \frac{C_{\text{down}}}{C_{\text{up}}} \tag{5.1}$$

where C_{down} and C_{up} are the number of particles downstream and upstream of the filter, respectively.

The measurement consisted of several steps. First, we measured several times upstream particle concentration to assess the reproducibility of dust dispersion. It was necessary to use the same air pressure at the inlet to the ejector to obtain reproducible particle size distribution of the dispersed TiO_2 powder upstream of the HFM. We did seven measurements of upstream particle concentration and calculated average and standard deviation. These values were then used to calculate the filtration efficiency. This was carried out for two dust weights of 50 and 100 mg. After dust dispersion in the chamber, the fan was turned on and immediately measured the particle size profile at downstream side of HFM. The downstream particle concentration was measured seven times. The efficiency data were tested on normality (for results, refer to supplementary material Fig. S5.1 and S5.2) using the Shapiro-Wilk test which confirmed that the data are not governed by normal distribution. Therefore, non-parametric ANOVA was used to compare the efficiency data. Using the Mann-Whitney test, it is possible to discover whether the efficiency is changing under varying conditions, i.e. different permeate velocity and upstream dust concentration.

Another important quantity was the pressure drop caused by the filtration medium, which is chiefly related to energy requirements which greatly affect the price of the overall filtration process. Here the pressure drop is considered as a sum of transmembrane pressure (*TMP*) (i.e. pressure gradient over the membrane wall) and fiber length pressure loss (i.e. pressure gradient over the length of the hollow fiber lumen). *TMP* is significantly influenced by the filtration media's permeability. This can be estimated using the Darcy's equation, which includes the fluid flow in a porous structure of a filtration medium in relation to *TMP* and fluid velocity (*U*) [130, 131]:

$$\frac{TMP}{Z} = \frac{\mu}{k} U \tag{5.2}$$

where Z is the filter thickness (here fiber wall thickness), μ is the fluid viscosity and k is the permeability of the membrane. The gas pressure drop in the bore of follow fibers can be estimated using Hagen-Poiseuille equation. Although this equation originates from incompressible fluid, it can be derived for gas flow using ideal gas state equation as [132]:

$$\frac{\mathrm{d}p^2}{\mathrm{d}x} = -\frac{256\mu JTR_{\text{m}}}{\pi D_{\text{i}}^4} \tag{5.3}$$

where p is the random local pressure, x is the random position on the fiber, D_{i} is the hollow fiber inner diameter, J is the gas molar flowrate in the hollow fiber lumen, T is the gas temperature and R_{m} is the molar gas constant. The overall pressure drop evolution with fouling was recorded. We

did a 90 h experiment with a dust dose of 0.2 g/h at a permeate velocity of 20 cm/s. Membrane samples for SEM analysis were taken after 25, 50 and 90 h of fouling. Then, we increase the dust dose to 2 g/h and observed the pressure drop increase in time. The overall filtration performance is mostly assessed using the quality factor (*QF*) which includes filter efficiency in relation to filter overall pressure losses:

$$QF = \frac{-\ln(1-\eta)}{\Delta p} \tag{5.4}$$

Filters of better quality have a higher *QF*, i.e. they have higher filtration efficiency and/or lower pressure losses.

5.3 Results and discussion

5.3.1 Pressure gradient

Pressure drop of the tested HFMs is rather higher even for small filtration velocities (Fig. 5.5). It is 640 Pa at 20 cm/s for clean membrane of 0.43 m^2 filtration area. This is caused by the very small pore size (Fig. 5.3b) but also the membrane geometry. The overall HFM pressure drop is a total of *TMP* which is the pressure loss over the membrane wall and pressure drop over the length of the fiber. This problem was the focus of many works, e.g. [132–134]. Due to very small fiber diameter, higher airflows are accompanied by high pressure drop due to very small fiber diameter. Generally, Reynolds number in a single fiber will inherently be lower than one characteristic of laminar flow. Achieving higher Reynolds numbers will inherently cause such pressures which the membrane material would no longer withstand causing fibers' rupture. Therefore, the use of this type of membrane is recommended for low-volume applications. This problem, however, can partially be eliminated by increasing the membrane filtration area by connecting individual membrane bundles into larger scale modules, see also [26]. This technology is thus easily scalable (refer to supplementary material, Fig. S5.0).

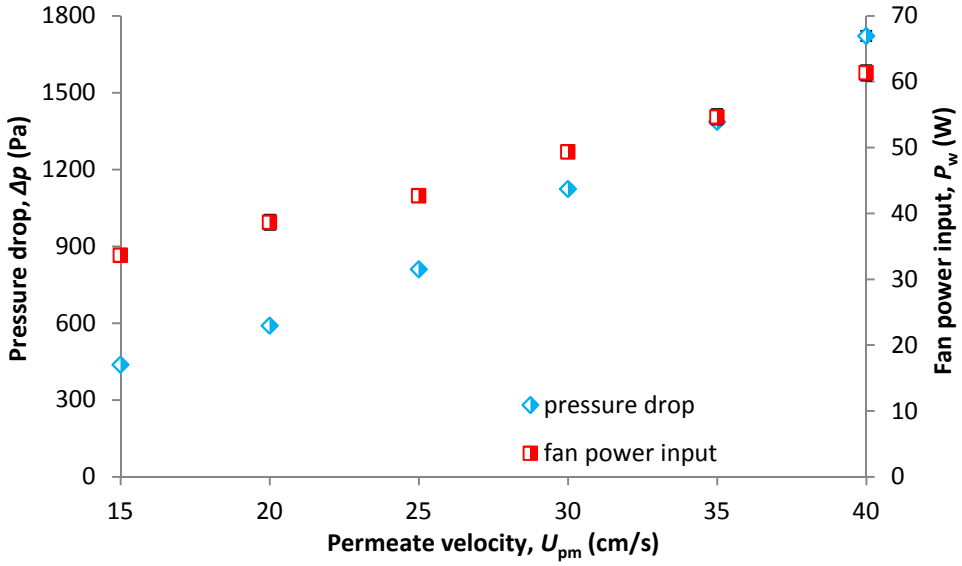

Fig. 5.5: *Pressure drop and fan power consumption vs permeate velocity of the tested HFM*

5.3.2 Particle separation efficiency of HFMs

Fig. 5.6 shows the filtration efficiency at a permeate velocity of 15 and 30 cm/s tested with different amounts of dispersed dust of 50 mg (Fig. 5.6a) and 100 mg (Fig. 5.6b). We can see high filtration efficiency of more than 99.97% for particles above 100 nm. Under 100 nm, it decreases to most penetrating particles size (MPPS) which is in 32–40 nm range.

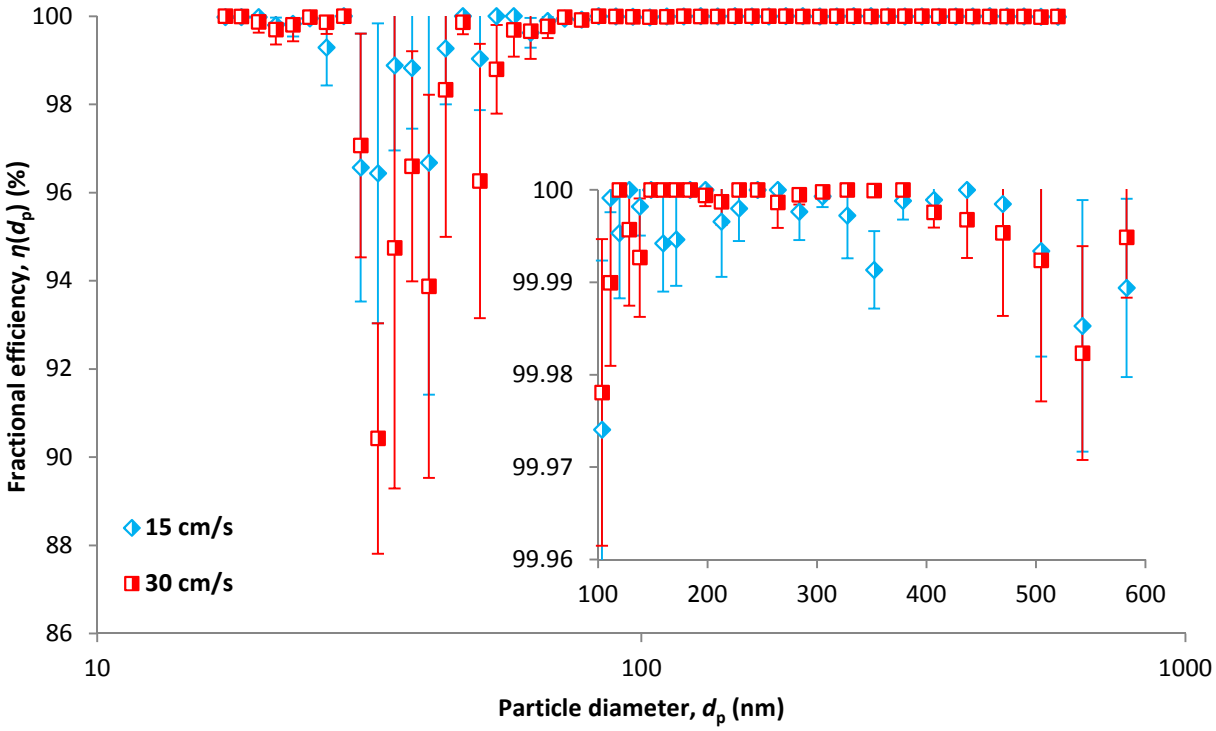

a)

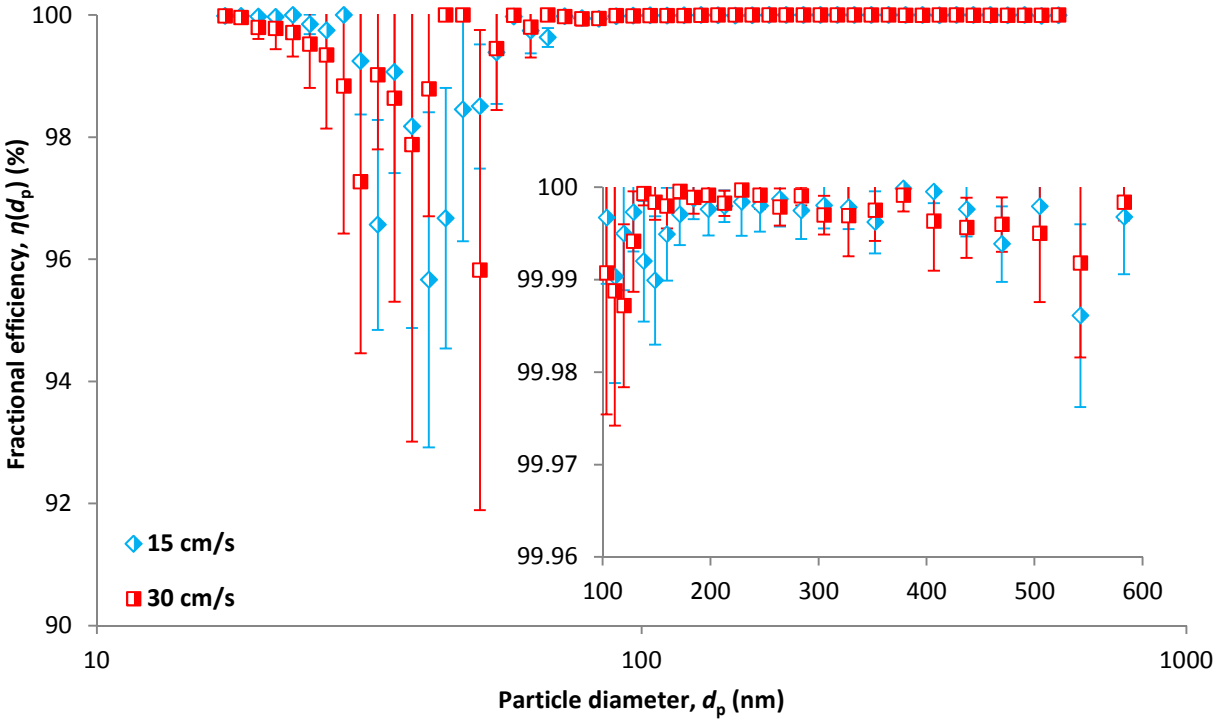

b)

Fig. 5.6: *Fractional efficiency for different dust amount – comparison by permeate velocity: 50 mg (a) and 100 mg (b)*

Comparing the efficiency curves between those two permeate velocities, we can see practically no difference when considering the standard deviation bars. The same is true if we compare the efficiency in terms of upstream particle concentration, i.e. different amount of test dust (Fig. 5.7). This was also confirmed using the Mann-Whitney test at the significance level of 0.05. Even though the data seems very scattered, all standard deviations were lower than 6% of the given efficiency value. For the conditions adopted in the filtration experiments, there is no or a minimal influence of permeate velocity and dust amount.

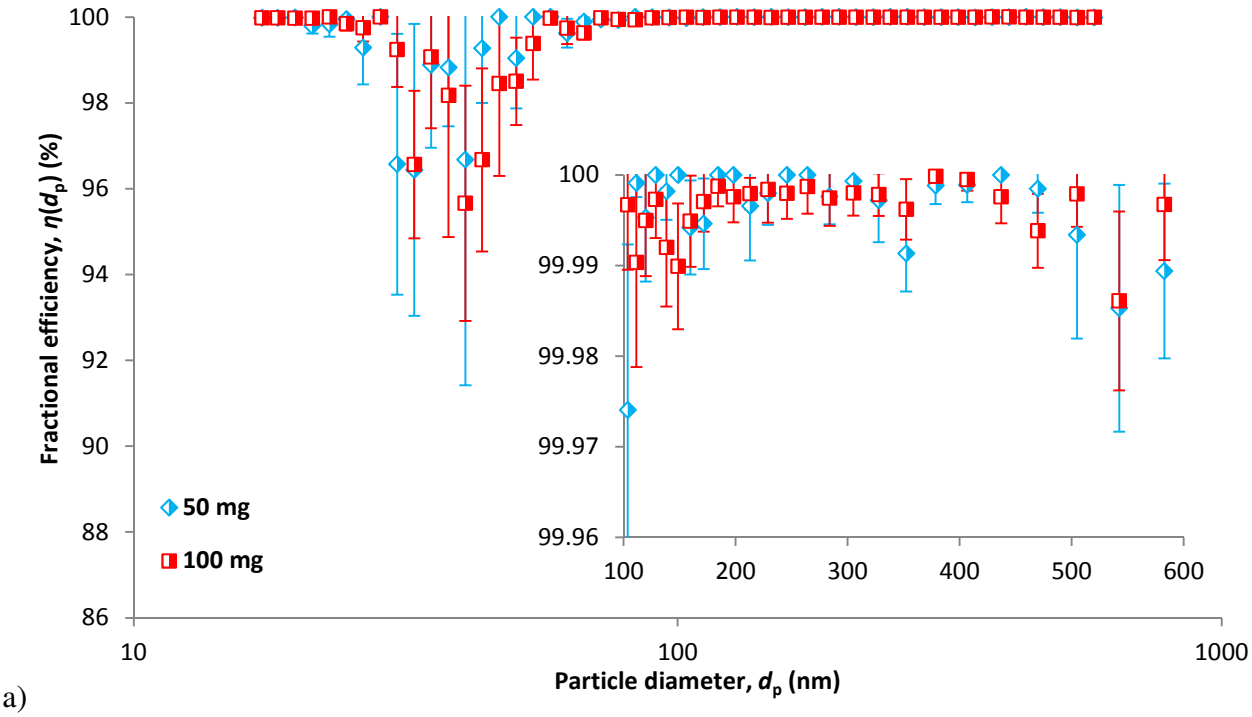

a)

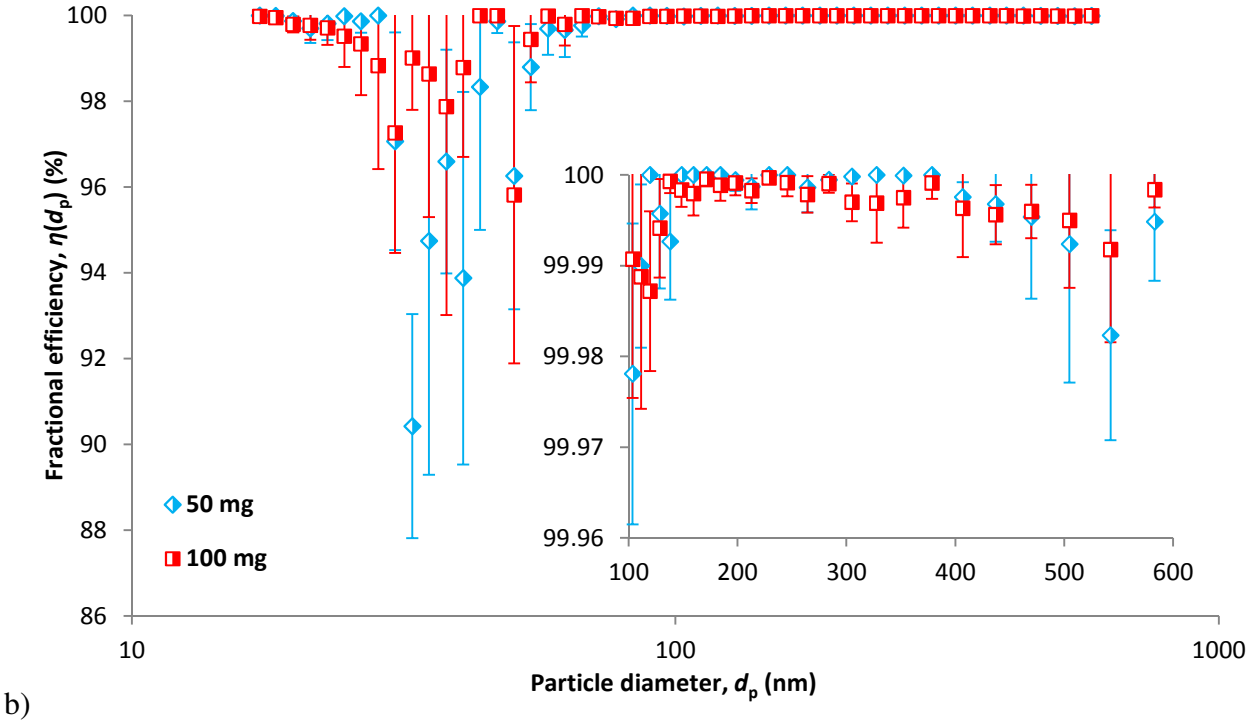

b)

Fig. 5.7: *Fractional efficiency for different permeate velocity – comparison by dust amount: 15 cm/s (a) and 30 cm/s (b)*

The above mentioned results may be attributed to pore structure of the used HFMs. The pores have elliptical shape with dimensions of about 50 nm × 600 nm (Fig. 3.4b). So the structure significantly differs from that of fibrous filters [135–137] where deep bed filtration dominates. So the main mechanism governing the separation of particles above 100 nm is sieving due to small pore diameter. However, for particles under 100 nm size, the mechanisms can be similar to those observed in fibrous filters. To describe which mechanisms actually took place in the experimental conditions adopted in this study, it was necessary to calculate dimensionless parameters characterizing the main filtration mechanisms. Peclet number (*Pe*), Stokes number (*Stk*), and interception parameter I were calculated to determine the influence of Brownian motion, inertial impaction and interception, using Eqs. (5.5), (5.6) and (5.7), respectively:

$$Pe = \frac{Ud_{\mathrm{f}}}{D} \tag{5.5}$$

$$Stk = \frac{d_{\mathrm{p}}^2 \rho_{\mathrm{p}} C_{\mathrm{s}} U}{18 \mu d_{\mathrm{f}}} \tag{5.6}$$

$$R = \frac{d_{\mathrm{p}}}{d_{\mathrm{f}}} \tag{5.7}$$

where U, d_{f}, d_{p}, and ρ_{p} are the face velocity, collector diameter (refer to Fig. 3.4a), particle diameter and particle density (TiO_2 = 4.23 g cm^{-3}), respectively, and D and C_{s} are the diffusion coefficient and Cunningham slip correction factor calculated using Eq. (5.8) and (5.9), respectively:

$$D = \frac{k_{\mathrm{B}} T C_{\mathrm{s}}}{3\pi\mu d_{\mathrm{p}}} \tag{5.8}$$

$$C_{\mathrm{s}} = 1 + Kn\left[1.207 + 0.44\exp\left(-\frac{0.78}{Kn}\right)\right] \tag{5.9}$$

where k_{B} is the Boltzmann constant and Kn is the particle Knudsen number which is the ratio of mean free path of gas molecules to particle diameter [122, 138].

Peclet number is used to consider relative importance of convection and diffusion. Peclet number was mostly lower than 20 (Fig. S5.3) for particles under 100 nm. This indicates Brownian motion to dominate the separation. The same is true for particle-size range from 100 to 220 nm at 15 cm/s and from 100 to 140 nm at 30 cm/s. Significant separation mechanism in the particle size range up to 100 nm is also interception with interception parameter from 0.1 to 0.89 for particle size up to 100 nm (Fig. S5.4). The interception mechanism starts to dominate at an interception parameter higher than 0.1 [108] which is true for our experimental conditions. Moreover, interception was found to play an important role in nanoparticle filtration for small collector diameters [41, 139] which is true for the porous structure of the HFM (Fig. 3.4a). For particles above 100 nm, the sieving effect occurs due to smaller pore sizes of the HFM (Fig. 3.4b). The interception enhances the particle separation but also compete with diffusion resulting in MPPS which was in the range from 32 to 40 nm. For larger particles, inertial impaction dominates as Stokes number was mostly higher than unity (Fig. S5.5) which was true for particles above 100 nm. As mentioned above the sieving effect will rather prevail over the inertial impaction mechanism when separating particles larger than 100 nm.

Fig. 5.8 shows *QF* for different particle sizes compared in terms of permeate velocity. *QF* increases with increasing particle size and practically follows the filtration efficiency/particle size

pattern. *QF* was generally lower than that of fibrous filters [116, 140–143] or comparable to those reported e.g. in [44, 126, 144] to other fibrous membranes as reported earlier. Even though the HFM has generally high efficiency, the filtration is accompanied by higher pressure drops; therefore the overall *QF* is rather lower.

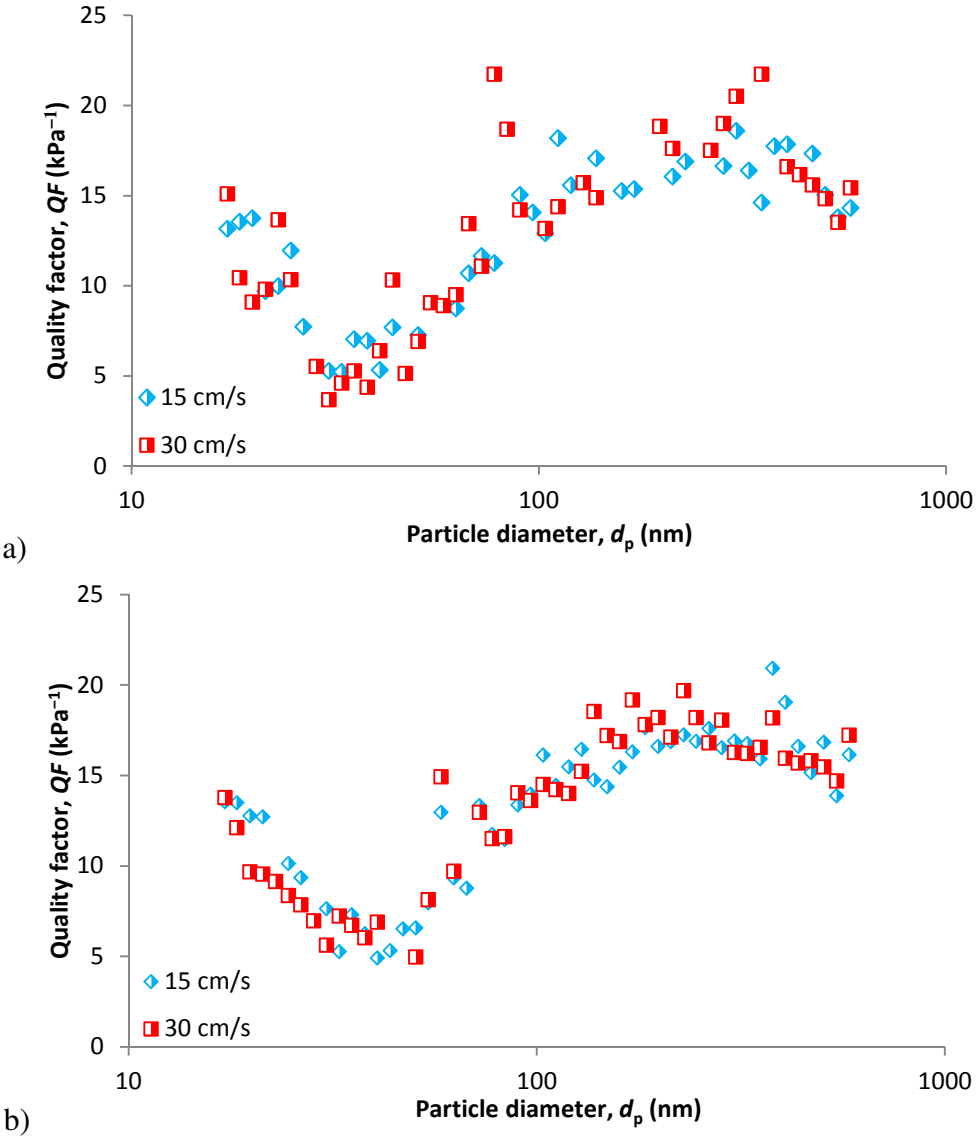

Fig. 5.8: *Quality factor for different amount of test dust: 50 mg (a) and 100 mg (b)*

5.3.3 HFM fouling by TiO_2 particles

We did a long term measurement of membrane fouling with SEM observation at defined intervals. 0.2 g per hour was fed to the chamber and samples of fouled membrane were observed after 25, 50 and 90 hours of experiment (Fig. 5.9a, b and c, respectively). We can see gradual fouling of HFM surface by TiO_2 particles with time. After longer time (90 hours), the presence of larger aggregates is obvious (Fig. 9c circled). However, there is probably still enough space for fluid to pass through the cake/membrane wall even after 90 hours of fouling as we did not noticed significant increase in pressure drop at these conditions (0.2 g/h). This could be caused by the space among particles which is still large for fluid to flow without any obstructions. Moreover, the HFM samples were cut from a fiber closer to the potting connected to the fan. This part of the membrane is fouled

more intensely and when completely clogged, the filtration will move to the middle part of the membrane which is less fouled. So to observe significant pressure drop increase, the HFM would have to be completely fouled over the whole surface area. Therefore, the concentration of dust dosed was increased to 2 g/h.

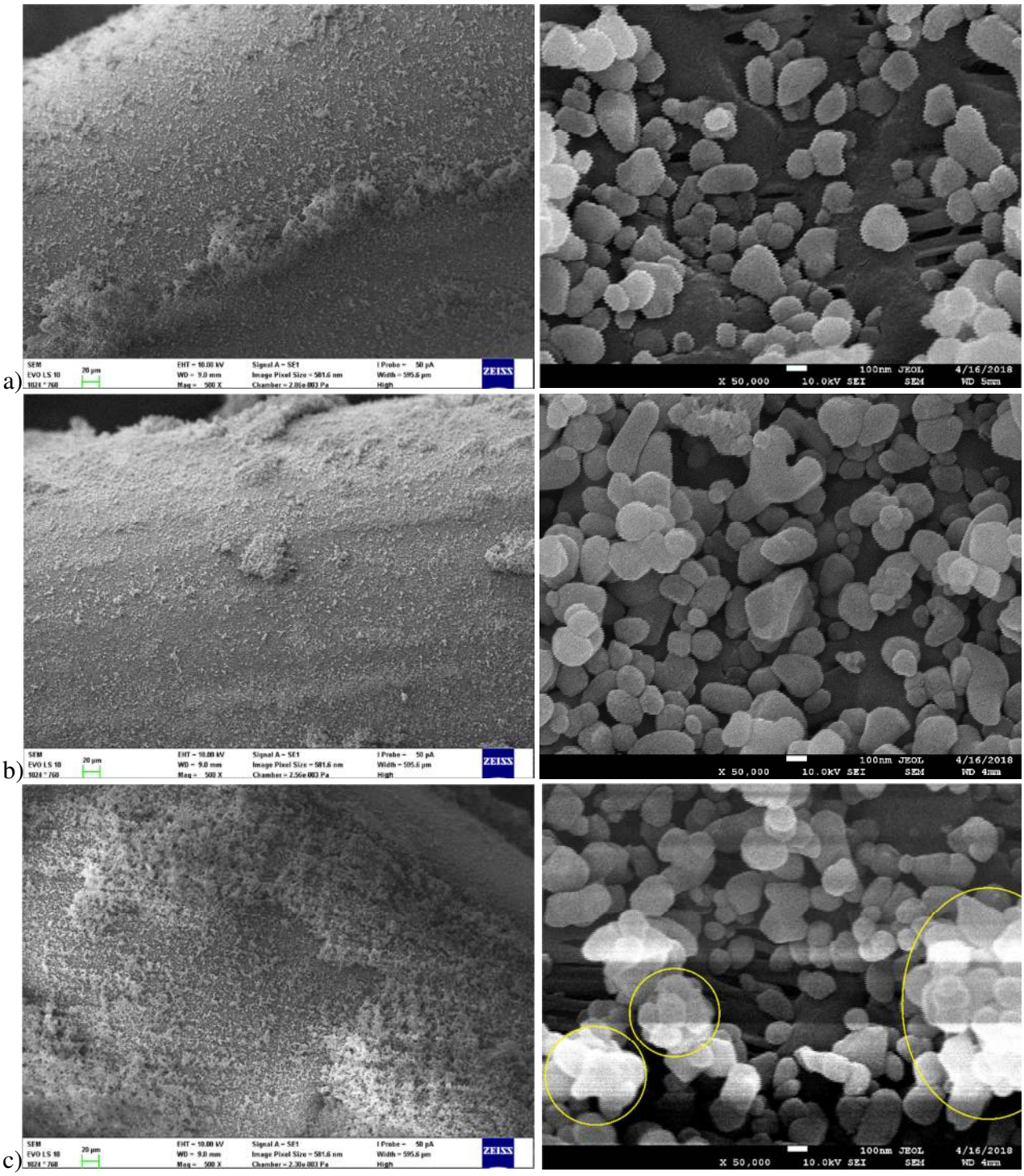

Fig. 5.9: *HFMs fouling by TiO_2 particles after 25 h (a), 50 h (b) and 90 h (c) of experiment*

At these conditions, we observed pressure drop to increase to double the initial value after 40 hours (Fig. 5.10). The pressure drop increase is smoothly linear up to filtration time of 14 hours, corresponding to dosed dust amount of 28 g. Then, the pressure drop increased exponentially up to

the final pressure drop of 1438 Pa (total dust dosed of 80 g). The amount of dust held by the membrane (dust holding capacity) was 24.7 g. Fouled and clean HFMs are compared in Fig. 5.11. The course of the pressure drop increase with particle loading is in agreement with other works carried out on planar high efficiency filter media, see e.g. [145–147].

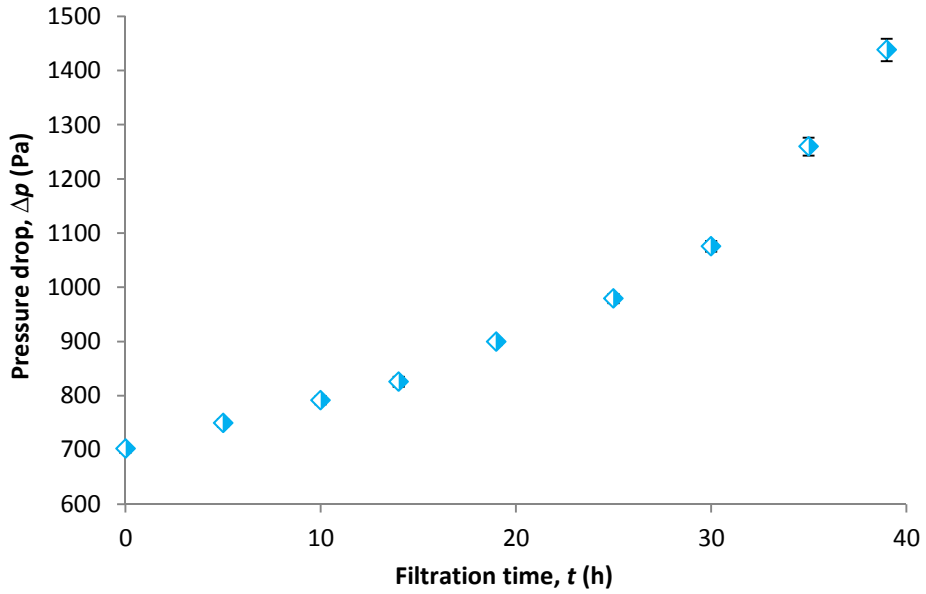

Fig. 5.10: *Pressure drop profile during fouling of the HFMs with 2 g/h of TiO_2 powder*

Fig. 5.11: *A comparison of a TiO_2 fouled (left) and a clean (right) HFM*

Generally, the dominating filtration type is the surface filtration although some of the smaller particles (mainly those smaller than 100 nm) might get caught inside the membrane wall porous structure. This is in agreement with works focused on fibrous filters where combination of surface and depth filtration occurs, see e.g. [41, 108, 148–150]. However, for larger particles, it is only the surface filtration as obvious from the SEM picture details (Fig. 5.9). This is a significant difference compared to works focused on fibrous filters where depth filtration is the main mechanism [44,

115, 126, 144] but in agreement with Nuclepore filters where solely surface filtration dominates [39, 77, 139, 151, 152].

5.4 Conclusion

Polypropylene HFMs are highly efficient in removal of ultrafine particles. The efficiency is higher than 99.97% for particles above 100 nm. Under 100 nm it decreases to most penetrating particle size which in the range of 32–40 nm with efficiency in the range of 90–96%. Different permeate velocity and dust amount were found to have no significant influence on the filtration efficiency. This proves HFMs to have stable properties during air filtration independent of different flow and particle concentration conditions. However, due to hollow fiber geometry, these membranes have higher pressure drops. It is 640 Pa at 20 cm/s permeate velocity for an active filtration area of 0.43 m^2. This can be eliminated by increasing the area of the membrane by connecting individual HFM bundles into larger modules (Fig. S5.0) and customization of fiber inner diameter.

Long term exposure did not prove significant pressure drop increase for given conditions. After 90 hours of fouling with dust feed of 0.2 g/h, no significant change in pressure drop was observed. The concentration of dust dosed was therefore increased to 2 g/h which caused pressure drop to increase to double the initial value after 40 hours of filtration.

6 Air filtration efficiency and particle loading behavior of closed hollow-fiber membrane air filter modules

6.1 Introduction

Here, measurement of size-resolved penetration of polypropylene HFM modules with different active surface area at different airflow velocities using a monodisperse and polydisperse ammonium sulfate aerosol is described. Monodisperse aerosol of different particle sizes (20, 35, 50, 70, 100, 140, 280 and 400 nm) was used. To obtain information about the pressure drop evolution during filtration cycle, we also did a particle loading filtration test using a polydisperse aerosol until reaching double the initial pressure drop of the HFM module. The results are then compared with theoretical models for most penetrating particle size (MPPS).

6.2 Predicting the minimum efficiency and MPPS

There are two possible ways to predict air filtration efficiency of HFMs using existing models, i.e. models for fibrous filters and for capillary pore membranes (CPMs) better known as Nuclepore filters. First, we can consider the fibrous-like formations in the HFM structure analogical to fibers, to evaluate their diameter using e.g. image analysis from SEM pictures (Fig. 3.4a) and calculate the efficiency. Such a prediction is, among many other parameters, dependent on filter solidity (solid volume fraction, i.e. 1 − filter porosity), and are mostly valid for a solidity range of 0.01 to 0.3 [4]. However, HFMs considered in this study have solidity as high as 0.48 which inevitably predicts the efficiency equaled to 100%. Second, we can use models developed for CPMs which appears to be more appropriate. CPMs are thin PC membranes with circular pores of uniform diameter (refer to Fig 2.5c and e.g. [39, 73, 153]) which have widely been used in air pollution monitoring [154–157] and other mainly microbiological applications [158–160] and aerosol filtration studies [77, 161, 162]. The theoretical prediction of the filtration efficiency is based on several mechanisms as shown in Fig. 3.3 and dependent on pore dimensions (Fig. 3.4b). The same is true for prediction of minimum efficiency (ME) and MPPS which were derived based on both approaches i.e. for fibrous and Nuclepore filters.

For fibrous filters, Lee and Liu [163] derived explicit expressions for ME and MPPS, considering Brownian motion and interception mechanisms depending on the ratio of mean free path of gas molecules to particle diameter λ/d_p. For $\lambda/d_p < 0.075$, the relationship is as follows:

$$d_{MPPS} = 0.541\left[\left(\frac{Ku}{1-\alpha}\right)\left(\frac{k_B T}{\mu}\right)\left(\frac{d_f^2}{U}\right)\right]^{0.25} \tag{6.1}$$

where k_B, T, d_f, α, μ, U are the Boltzmann constant, temperature, collector diameter, membrane solidity, gas viscosity and face velocity, respectively and Ku is the Kuwabara hydrodynamic factor calculate according to Eq. (3.15). For $0.075 < \lambda/d_p < 1.3$, the relationship is as follows:

$$d_{MPPS} = 0.885\left[\left(\frac{Ku}{1-\alpha}\right)\left(\frac{k_B T\sqrt{\lambda}}{\mu}\right)\left(\frac{d_f^2}{U}\right)\right]^{2/9} \tag{6.2}$$

and for $\lambda/d_p > 1.3$, the relationship has the following form:

$$d_{\mathrm{MPPS}} = 0.958\left[\left(\frac{Ku}{1-\alpha}\right)\left(\frac{\lambda k_{\mathrm{B}}T}{\mu}\right)\left(\frac{d_{\mathrm{f}}^2}{U}\right)\right]^{0.2} \tag{6.3}$$

Substituting these equations into basic relationship for efficiency one can easily obtain minimum efficiency (shown in supplementary Table S6.1). However, as mentioned above the efficiency for the adopted conditions will be equal or even higher than 100%, therefore it also seems to be senseless to calculate MPPS. However, in the absolute value there is always a particle size which tends to have the lowest theoretical efficiency even though its ME will be equal or higher than 100%. Here, an attempt to calculate the MPPS is made to compare with the results from experiments. Another relationship for MPPS of fibrous filters was derived analytically by Song and Park [138] who, unlike Lee and Liu [163], also considered inertial impaction regime. In their study they derived MPPS relationship for conditions in which interception is negligible and only diffusion and inertial impaction regime dominate:

$$d_{\mathrm{MPPS}} = d_{\mathrm{f}}^{8/51}\left(\frac{5X}{12Y}\right)^{5/12} \tag{6.4}$$

where X and Y are coefficients characterizing diffusion and inertial impaction-dominant size regime, respectively and can be calculated using following equations:

$$X = \frac{10.4\alpha}{\pi}\left(\frac{2\lambda}{Ku}\right)^{1/3}\left(\frac{2.609k_{\mathrm{B}}T}{3\pi\mu U}\right)^{2/3} \tag{6.5}$$

$$Y = \frac{0.3\alpha}{\pi(1-\alpha)}\left(\frac{\rho_{\mathrm{p}}U}{18\mu}\right)^{6/5} \tag{6.6}$$

MPPS can also be explicitly derived for membrane filters considering their pore diameters and porosity which is taken into account in Chen's et al. [123] explicit expressions for ME and MPPS for Nuclepore filters. The principle of derivation is the same as for fibrous filters. The minimum efficiency can be found by differentiating the basic equation for overall efficiency, i.e. Eq. (3.56) with respect to particle size and setting the derivatives equal to zero. However, such an equation is first necessary to simplify. Here, we are dealing with particles smaller than 1 μm for which the impaction efficiency is, at given experimental conditions, negligible (up to 0.8 %, refer to supplementary Fig. S6.1). Surface diffusion efficiency was also neglected in their derivation and for different ranges of interception parameter R_{o} (Eq. 3.52) and diffusion parameter N_{D} (Eq. 3.50) different relationships were derived. For $N_{\mathrm{D}} < 0.01$ and $R_{\mathrm{o}} \leq 0.6$, the formula is as follows:

$$d_{\mathrm{MPPS}} = 2\left(8.36\frac{Z\varepsilon}{Ud_{\mathrm{o}}}\frac{kT\sqrt{\lambda}}{\pi\mu}\right)^{2/5} \tag{6.7}$$

where Z, ε and d_{o} are the membrane thickness, porosity and pore diameter, respectively. For $0.01 \leq N_{\mathrm{D}} < 0.1$ and $R_{\mathrm{o}} \leq 0.6$, the relationship is as follows:

$$d_{\mathrm{MPPS}} = 2\left(2.78\frac{Z\varepsilon}{Ud_{\mathrm{o}}}\frac{kT\sqrt{\lambda}}{\pi\mu}\right)^{2/5} \tag{6.8}$$

and for $N_{\mathrm{D}} > 0.01$, $R_{\mathrm{o}} \leq 0.6$, the formula is of the following form:

$$d_{\mathrm{MPPS}} = 0.243d_{\mathrm{o}} \tag{6.9}$$

6.3 Materials and methods

6.3.1 HFM modules

HFMs modules from Zena Membranes s.r.o. [26] (Table 6.1) of different active filtration area were tested. The HFMs are made of polypropylene and were examined using classical bubble point test according to ASTM F316-03 (2011) [164]. The membranes are naturally hydrophobic and can be sterilized with standard ethylene-oxide procedure. Depending on the application, NaOH, H_2O_2, citric acid and enzymatic liquids can be used to clean the membrane. The used HFM modules are shown in Fig. 6.1.

Table 6.1 : *Parameters of HFM modules*

Module	small	large
Surface area (m^2)	0.22	3.1
Number of fibers	1385	9690
Length (mm)	150	475
Material of fittings	PVC	PVC
Potting material	polyurethane	polyurethane
HFM material	polypropylene	
Pore size (nm)	115	
Outer/inner diameter (µm)	305/230	
HFM wall thickness (µm)	37.5	
Surface treatment	none (hydrophobic)	
Fiber burst pressure (bar)	> 4.8	
Fiber collapse pressure (bar)	> 3.5	

a)

b)

Fig. 6.1: *Tested HFM modules: a) small module, b) large module*

6.3.2 Experimental setup

Penetration through the HFM module was measured using a modified method described elsewhere [165–167]. The experimental setup for testing using monodisperse particles is shown in Fig. 6.2. Testing aerosol particles were generated using a Palas AGK 2000 nebulizer from a 1 g/L ammonium sulfate solution under a pressure of 2 bars. Ammonium sulfate was chosen due mainly to the dodecahedron shape of generated particles. This is closer to spherical shape which is considered in theoretical assumptions adopted for particle sizing in electrostatic classifiers. The generated polydisperse aerosol is driven through a droplet separator and a diffusion dryer and brought to a size selector with a differential mobility analyzer of an active length of 110 mm. Here, a monodisperse aerosol of required size is separated. The size selector includes a 370 MBq ^{85}Kr neutralizer and a closed-loop airflow equipped with flow, temperature and pressure sensors. The sheath air flowrate is controlled using a 5 L/min critical orifice. The aerosol was kept at a flowrate of 1 L/min periodically checked using a Sensidyne Gilibrator-2 airflow calibrator.

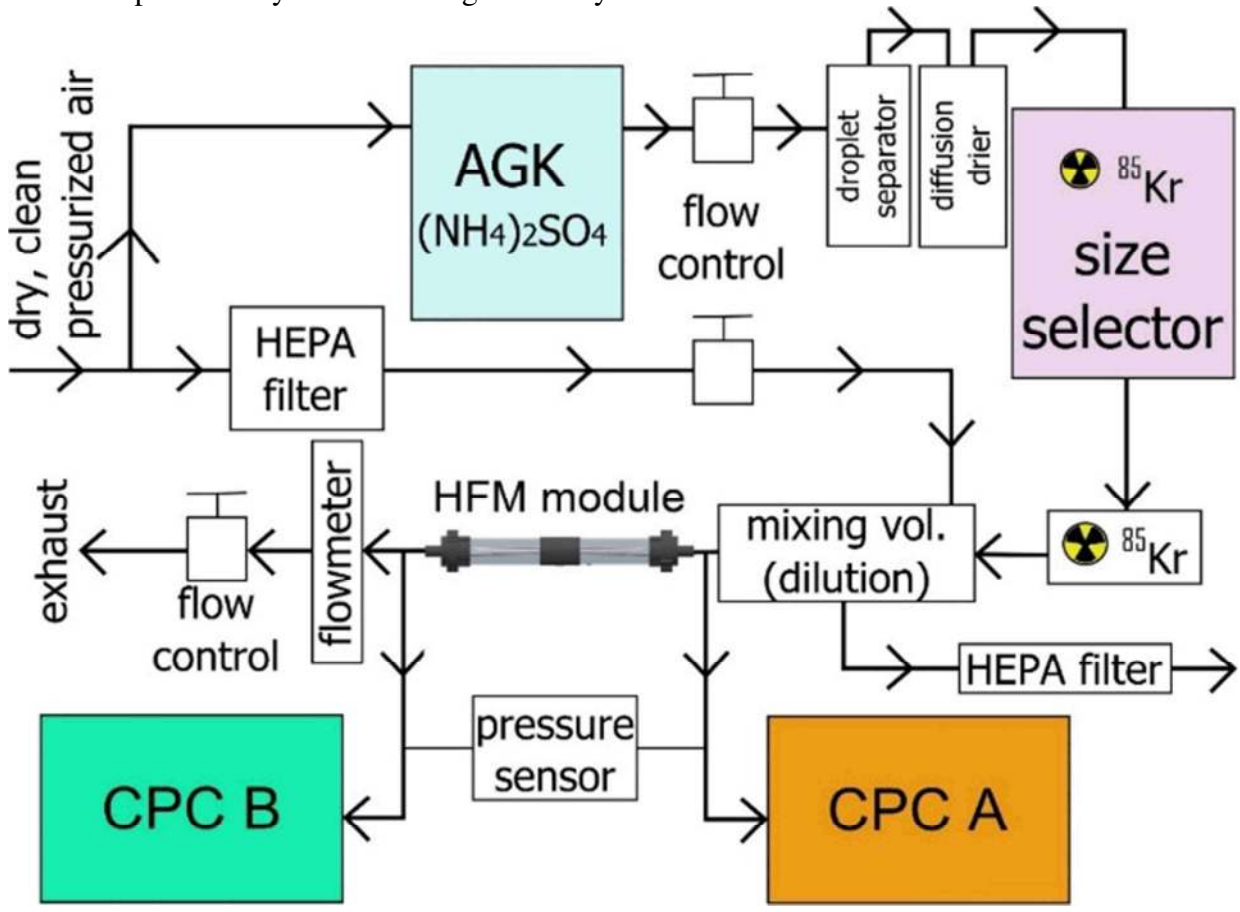

Fig. 6.2: *A scheme of experimental setup for filtration efficiency testing with monodisperse aerosol*

The selected monodisperse aerosol is neutralized using a second 370 MBq ^{85}Kr neutralizer and, after dilution, driven through the tested HFM module. The particle number concentration is then simultaneously measured using two TSI UCPC 3025A condensation particle counters (CPC), each at upstream and downstream side of the HFM module. The whole system was controlled using LabView software which operated the classifier, CPCs, electromagnetic valves, data management and processing. Prior to each measurement, five zero-count checks were done to control possible foreign particles in the system.

The experimental setup for testing with polydisperse aerosol (Fig. 6.3) is practically the same excluding size selector and having two SMPS/CPC systems instead of two CPC. The particle number concentrations upstream and downstream of the HFM module are shown in Fig. 6.4.

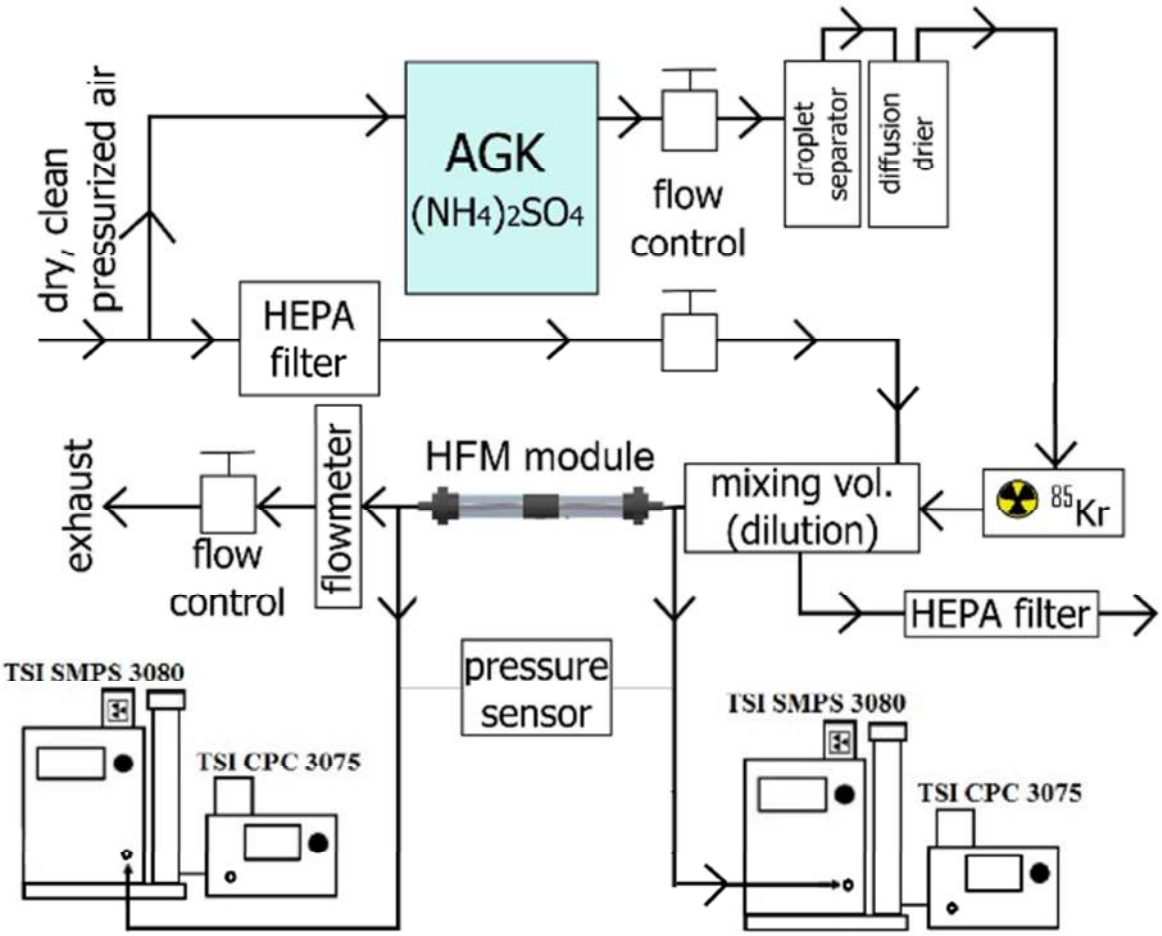

Fig. 6.3: *A scheme of experimental setup for filtration efficiency testing with polydisperse aerosol*

6.3.3 Data processing

Determining the collection efficiency using polydisperse aerosol was performed via simultaneous measurement of particle number concentration upstream and downstream of the HFM module. Both upstream and downstream particle size/concentration profile were measured eleven times and for each profile arithmetic average value and standard deviation were calculated (Fig. 6.4). The average particle concentration upstream/downstream of the HFM was then used to calculate the filtration efficiency. This was done two times and the arithmetic average of efficiency and its standard deviation were determined. The data was further processed using the StatSoft Statistica software. The efficiency data measured using polydisperse aerosol at different velocities was compared using Mann-Whitney test (non-parametric ANOVA). Non-parametric ANOVA was chosen based on the Shapiro-Wilk test which confirmed the efficiency data to be out of the normal distribution (for the results refer to supplementary material, Fig. S6.2).

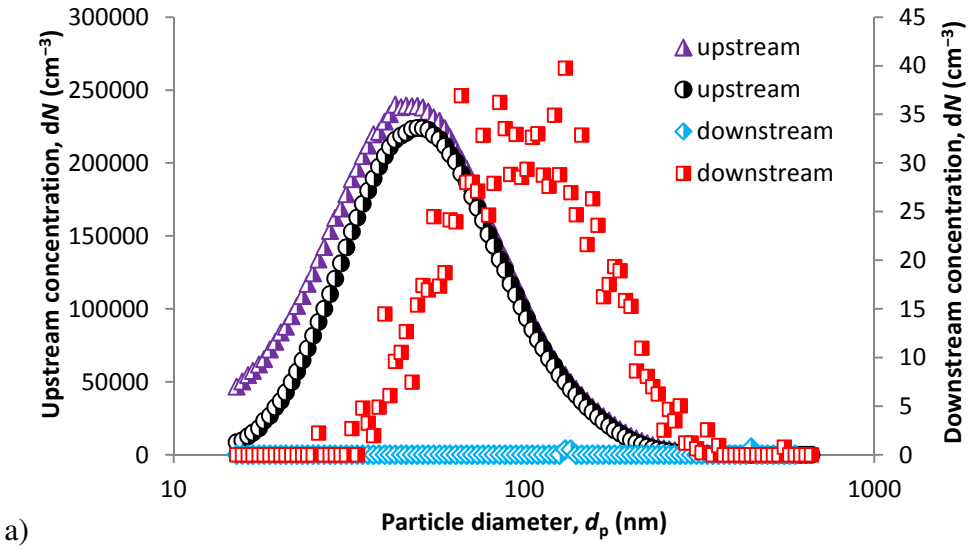

a)

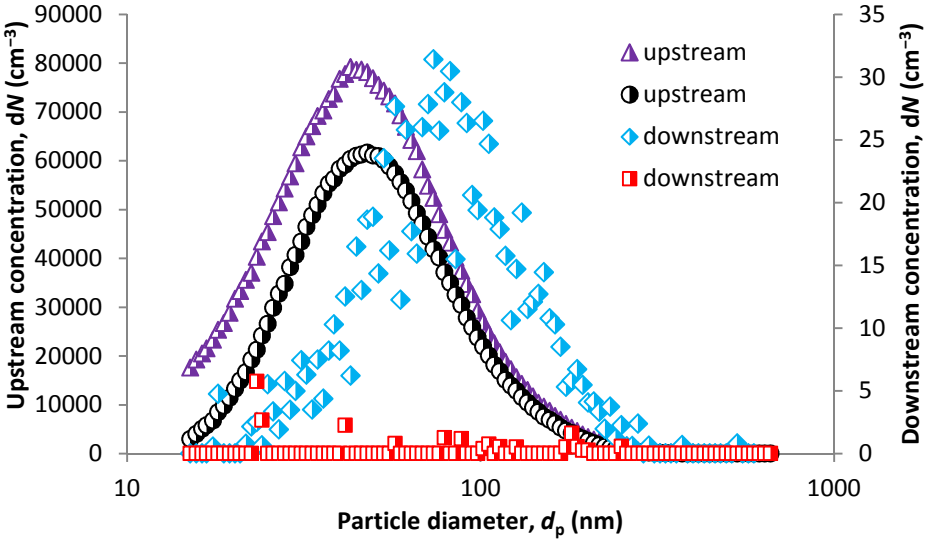

b)

Fig. 6.4: *Upstream and downstream particle number concentrations of polydisperse aerosol measured at different flowrates of 10 L/min (a) and 40 L/min (b)*

6.4 Results and discussion

6.4.1 Filtration efficiency

Fig. 6.5 and 6.6 shows the measured filtration efficiency of the HFM modules challenged with monodisperse and polydisperse aerosol, respectively. When challenged with monodisperse aerosol, eight different particle sizes from 20 to 400 nm were selected. For all these particle sizes, the HFM module showed 100% efficiency no matter of its surface area. However, due to size selection, the particle concentration of the monodisperse aerosol was rather low. Another important issue was the pressure drop of the tested modules which was rather higher and did not allow testing at higher face velocities as the testing apparatus was limited by the operation pressure drop at which the CPCs are able to sample the aerosol. The experiment with monodisperse aerosol was also limited by the detection limit of the used CPCs which is as low as 0.0001%. Below this limit, no particles are detected although some can physically be present in the downstream feed.

Therefore, it was decided to test the modules with high concentrations of polydisperse aerosol to verify if the HFM modules have the same efficiency.

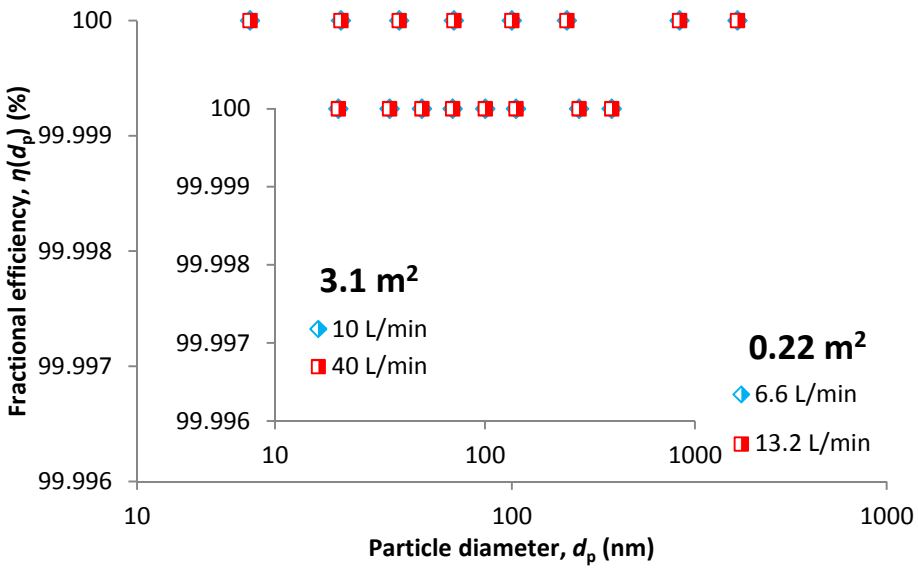

Fig. 6.5: *Filtration efficiency in relation to particle size of the tested modules challenged with monodisperse aerosol*

After challenging with polydisperse aerosol, some penetrations were observed. MPPS was found to be 334 nm with an efficiency of 99.9989% and 250.3 nm with an efficiency of 99.9982% at the flowrate of 10 and 40 L/min, respectively (Fig. 6.6). However, Mann-Whitney test has confirmed there is no statistically significant difference between the efficiency values measured at different flowrates (at a significance level of 0.05). Therefore, change of the face velocity in the present manner does not have significant effect on the filtration efficiency of the HFM modules.

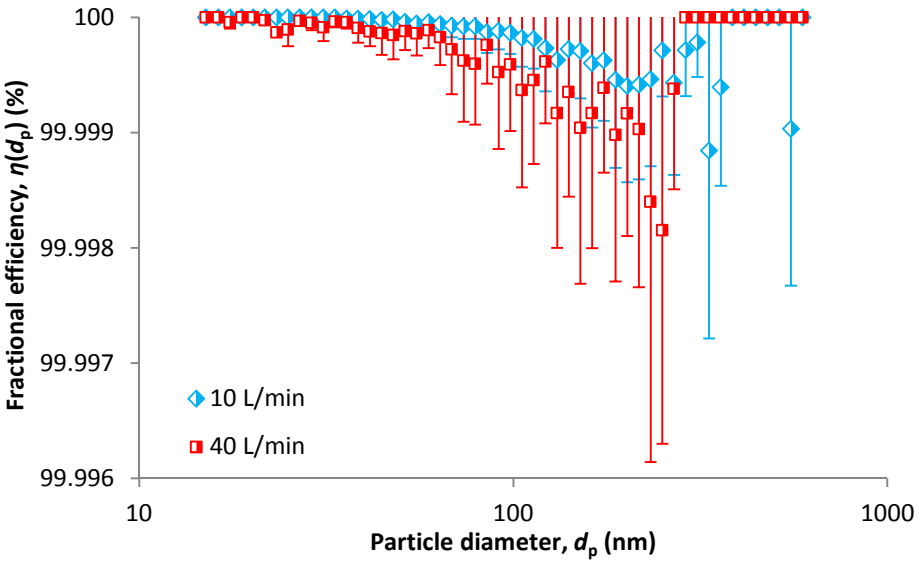

Fig. 6.6: *Filtration efficiency in relation to particle size of the tested modules challenged with polydisperze aerosol*

Table 6.2 shows measured MPPS compared with theoretical models found in literature. The best model which fit the experimental results is that of Lee and Liu [163] developed for MPPS prediction of fibrous filters considering the Brownian motion and interception as the main governing mechanisms.

Table 6.2 : *Comparison of experimental MPPS with existing models*

Q (L/min)	MPPS by Lee and Liu [163] (nm)		
	$\lambda/d_p < 0.075$	$0.075 < \lambda/d_p > 1.3$	$\lambda/d_p > 1.3$
10	351	392	303
40	265	287	213
	MPPS by Chen et al. [123] (nm)		
	$N_D < 0.01, R_o \leq 0.6$	$0.01 \leq N_D < 0.1, R_o \leq 0.6$	$N_D > 0.01, R_o \leq 0.6$
10	23330	15019	28
40	13302	8563	28
	MPPS by Song and Park [138] (nm)		
10	163316		
40	547724		
	MPPS experimental (nm)		
10	333		
40	250		

6.4.2 Pressure drop evolution with particle loading

Pressure drop increase during filtration of polydisperse aerosol was measured on both modules. Fig. 6.7 shows pressure drop with time, accumulated mass of the aerosol in the HFM module with time and the particle size/concentration profile of the aerosol with time. Generally, the highest particle concentrations were in the particle size range between 30 and 110 nm. Most of the pore sizes are in this range, so the loading rate and pressure drop evolution was assumed to be rather fast. However, the results have shown quite different behavior.

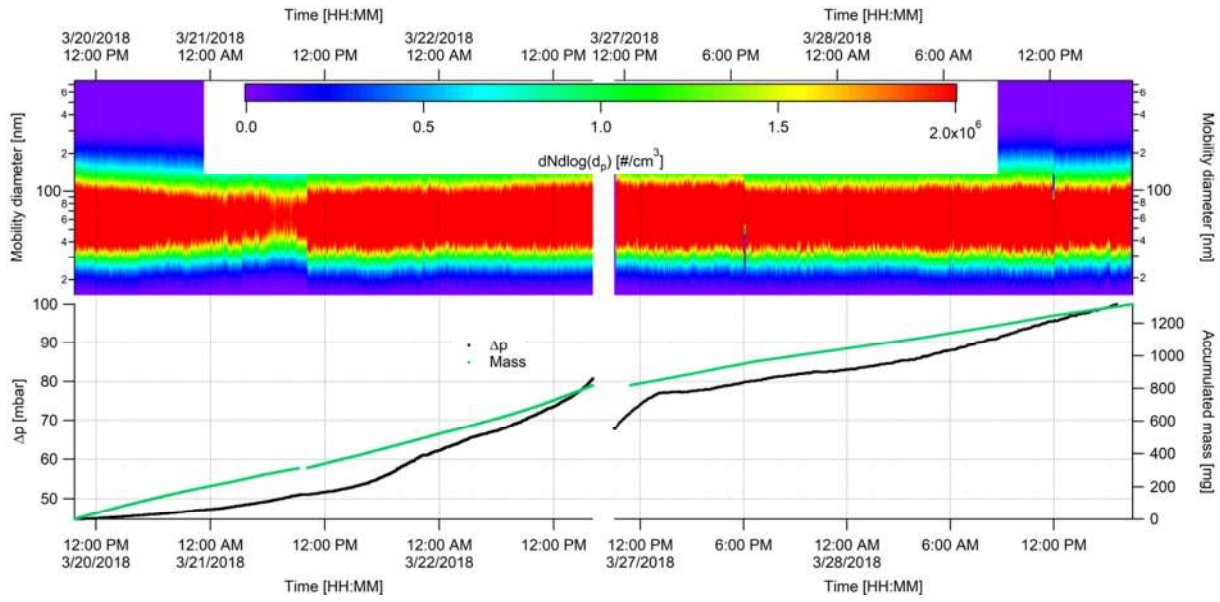

a)

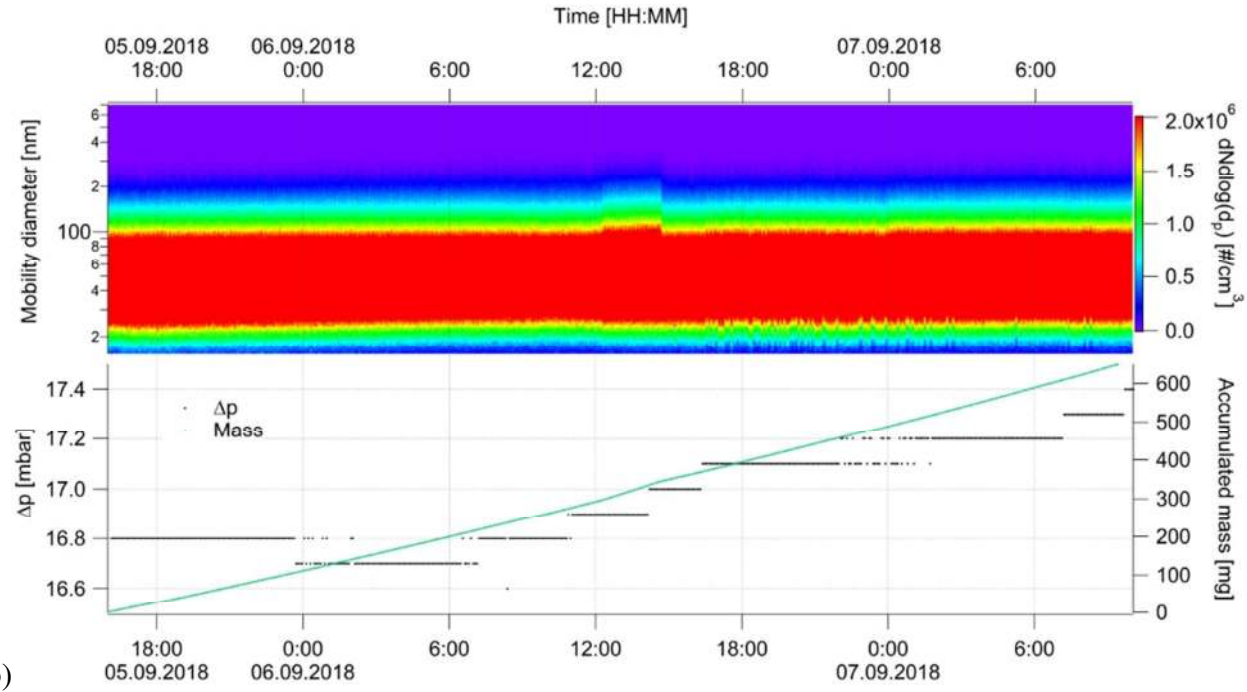

b)

Fig. 6.7: *Pressure drop evolution, course of accumulated mass of particles and particle size/concentration profile of challenge aerosol in time during long-term polydisperse aerosol loading for HFM module with an area of 0.22 m^2 (a) and 3.1 m^2 (b)*

The smaller module (0.22 m^2) was tested at a flowrate of 11 L/min and reached double the pressure drop after 75 hours (Fig. 6.7a). The whole experiment took 84 hours and the pressure drop increased from 44.7 to 99.8 mbar. The weight of the accumulated particles was 1.2 g. The other module with an area of 3.1 m^2 was tested at 40 L/min which after 42 hours increased from 16.7 to 17.4 mbar. Due to markedly larger filtration surface, significantly longer time to obtain double the initial pressure drop would be necessary.

6.5 Conclusion

HFM modules of two different surface areas were tested. When challenged with monodisperse aerosol, zero penetration was observed in both modules, i.e. 100% efficiency. However, due to the limitations of the experiments with monodisperse aerosol (low concentrations of classified aerosol, low face velocity together with the detection limit of the CPCs), the modules were further tested using polydisperse aerosol to confirm the excellent collection efficiency. When challenged with polydisperse aerosol, some penetrations were observed. MPPS was found to be 334 nm at 10 L/min and 250 nm at 40 L/min even though the differences between efficiency/particle size profiles at different velocities were statistically insignificant.

Pressure drop increase with particle loading showed the HFM modules are fouled very slowly even with high particle concentrations. The smaller area module needed 75 hours to reach double the initial pressure drop. In the larger module after more than 40 hours, practically no increase was observed. Therefore, the experiment was not continued until the twofold initial pressure drop value, as it would take significantly longer time.

7 Pressure drop evolution during dust loading of hollow-fiber membranes – energy requirements and life-cycle cost estimate

7.1 Introduction

The particle loading process was extensively studied in fibrous filters and is generally divided into three phases. First, the particle collection is in depth filtration regime, i.e. particles are captured inside the filter media. During this phase, the filter pressure drop gradually increases as particles are filling the space among the filter fibers. Second, a transitional regime occurs, i.e. a significant amount of the void space inside the filter is filled with particles. The filter pressure drop in this phase rises faster compared to depth filtration phase. The last stage of filtration is called surface filtration, i.e. particles are collected on the filter surface, a filtration cake is established and growing while rapidly increasing pressure drop. In high efficiency filters, the surface filtration is the main filtration mechanism while the previous two take only a short time. However, for certain type of membrane filters, the first two stages do completely not occur and the filtration solely takes place on the membrane surface. If we look at the structure of a PP HFM, which will be subject of this study (Fig. 7.1), we can consider them both filter with fibrous-like structure (Fig. 7.1a) and filter with capillary pore structure (Fig. 7.1b). Therefore, it is of interest to study, how the HFMs behave during long term dust loading and which mechanism will dominate.

In relation to long term air filter operation, a great attention is paid to energy requirements. Typical air filters in HVAC systems have very low initial pressure drop and are able to operate at very high air flowrates up to several thousand cubic meters per hour. Pressure drop increases with long term dust fouling and the power necessary to draw the required airflow through the filter increases too. When the pressure drop is at a certain level, mostly double the initial value, the filter is changed for a new one because most of the fibrous filters working in depth filtration regime cannot be regenerated. Membrane filters can be regenerated by back-pulse or back-blow [168, 169] or simply by blowing the surface using pressure air. This is, however, accompanied by a residual pressure drop as it is practically impossible to clean the membrane completely. The question remains how many cycles membrane can work without significant increase of residual pressure drop. This is very important due to energy use as it accounts for about 75% of total air filtration cost (refer to Fig. 2.4a) [35]. The main problem is the membrane itself because it usually has a very dense structure. If HFMs are considered, another contribution to pressure drop will come with their geometry. Hollow fiber geometry is significantly advantageous. HFMs are compact, self-supported and can be easily cleaned. These advantages are recognizable in liquid filtration but it is a significant shortcoming in air filtration due to high pressure drops. HFM pressure drop is a sum of contributions of transmembrane pressure, i.e. the pressure caused by the membrane wall pore structure, and mainly the pressure loss along the hollow fiber lumen. So it is not possible to operate HFMs at such high flowrates as filters for general ventilation purposes. Therefore the use of HFMs will be limited to low volume and/or short term applications and for special application like nanoaerosol separation or aerosols which are potentially toxic and must be captured with high efficiency no matter of the filtration costs. This work, therefore, aimed to study pressure drop evolution of HFMs during dust loading which has not been done so far. We used ASHRAE A2 test dust to simulate dust environment and recorded pressure drop, permeate velocity and fan power input until reaching final pressure drop. Furthermore, theoretical models for dust

cake pressure drop and energy requirements were compared with the experimental results. Finally, an attempt to estimate the life-cycle cost for operating the HFM air filter was made.

7.2 Theoretical considerations

Two possible approaches to assess the pressure drop of the considered HFMs. First, we can consider the segments in HFM pore structure analogically to fibers (Fig. 7.1a), to measure their diameter and assess pressure drop using mathematical models developed for fibrous filters. Second, we can consider pores of the HFM analogically to capillaries (Fig. 7.1b) as for capillary pore membranes (CPMs, also called Nuclepore filters) and analogically calculate pressure drop based on pore diameter using Hagen-Poiseuille equation. The former is based on calculation of dimensionless permeability $f(\alpha)$ and then recalculated to filter permeability using average fiber (collector) diameter d_f as follows:

$$k = \frac{d_f^2 f(\alpha)}{4} \tag{7.1}$$

The filter permeability is then used to calculate transmembrane pressure using Darcy equation as follows:

$$TMP = \frac{\mu U Z}{k} \tag{7.2}$$

where μ, U and Z are the gas dynamic viscosity, airflow face velocity and membrane wall thickness, respectively.

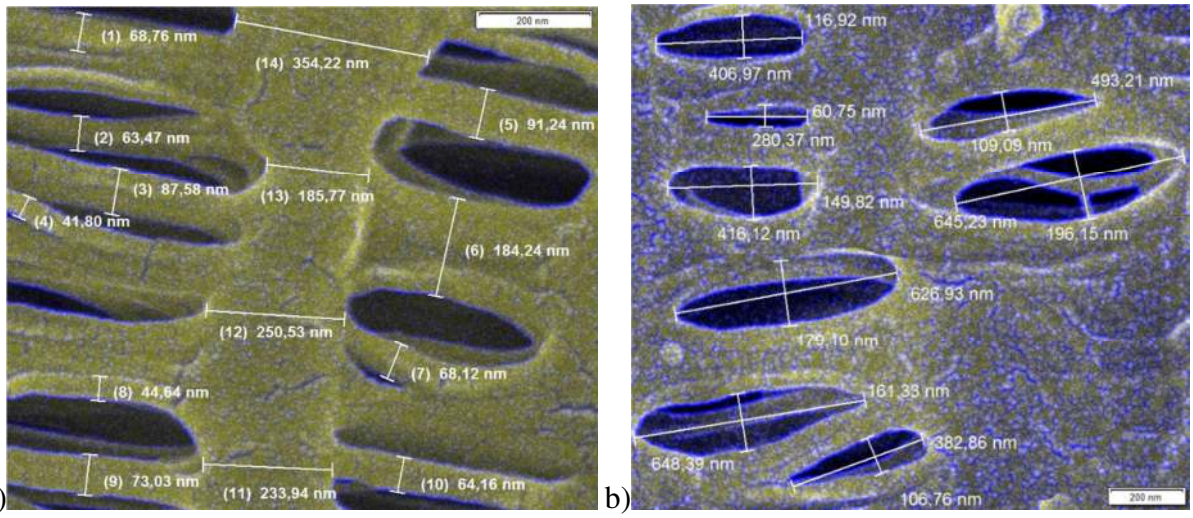

Fig. 7.1: *Evaluation of collector diameter (a) and pore size (b) from SEM images using Stream Motion software*

7.2.1 HFM gas permeability

Dimensionless permeability $f(\alpha)$ is a function of filter solidity α and various researchers have proposed different relationships for flow through fibrous structures. Woudberg [170] reviewed available models for predicting the dimensionless permeability for different fiber arrangements (1D, 2D and 3D) and flow direction (parallel and perpendicular to fibers). The author of [170] further proposed analytical models for 2D arrangements based on existing RUC (representative

unit cell) models for flow through 1D fiber arrangement and also considered effects of developing flow and pore blockage. Typical for all models is that they predict the dimensionless permeability to approach zero for filter solidity higher than 0.4. HFMs considered in this work have solidity as high as 0.46–0.48 thus predicting very low permeability in the order of 10^{-16}–10^{-17} m^2. Here, some of the dimensionless permeability models are presented and compared with permeability of the PP HFMs obtained experimentally.

Several assumptions were made. HFMs are assumed to be isotropic porous media with 3D fiber arrangement. The flow is fully developed and the RUC model (rectangular structure, refer to supplementary Fig. S7.0) of porous medium geometry is assumed. The flow through the cell is always parallel to one collector in the configuration and perpendicular to the other two irrespective of the flow direction. This means that 1/3 of the flow weight is parallel flow and the remaining 2/3 of the flow weight is assigned to transverse flow. The dimensionless permeability predicted using the isotropic RUC model is given as follows [170]:

$$f(\alpha)=\pi\left[\frac{1}{3}\left[\frac{48\alpha^2}{(1-\alpha)^3}\right]+\frac{2}{3}\left[\frac{13.5\alpha^{1.5}}{(1-\sqrt{\alpha})^3}\right]\right]^{-1} \tag{7.3}$$

The analytical model of Tomadakis and Robertson [171] considers the effect of overlapping fibers:

$$f(\alpha)=\frac{(1-\alpha)}{8\ln^2(1-\alpha)}\frac{(1-\alpha-\varepsilon_p)^{\omega+2}}{(1-\varepsilon_p)^{\omega}\left[(1+\omega)(1-\alpha)-\varepsilon_p\right]^2} \tag{7.4}$$

where ω is a constant equal 0.661 and ε_p is the percolation threshold porosity, equal 0.037 in this model. Analytically weighted models of Happel [172], Drummond and Tahir [173] and Gebart [174] for 3D isotropic media are represented by Eqs. (7.5), (7.6) and (7.7), respectively:

$$f(\alpha)=\pi\left[\frac{4}{3}\alpha\left(2\alpha-\ln\alpha-\frac{\alpha^2}{2}-1.5\right)^{-1}+\frac{16}{3}\alpha\left(\frac{\alpha^2-1}{\alpha^2+1}-\ln\alpha\right)^{-1}\right]^{-1} \tag{7.5}$$

$$f(\alpha)=\pi\left[\frac{4}{3}\alpha\left(2\alpha-\ln\alpha-\frac{\alpha^2}{2}-1.5\right)^{-1}+\frac{16}{3}\alpha\left(2\alpha-\ln\alpha-\frac{\alpha^2}{2}-0.739\alpha^4-1.5\right)^{-1}\right]^{-1} \tag{7.6}$$

$$f(\alpha)=\left[\frac{53}{24}\frac{\alpha^2}{(1-\alpha)^3}+\frac{3\pi\sqrt{6}}{8}\left(\sqrt{\frac{\pi}{2\sqrt{3}\alpha}}-1\right)^{-2.5}\right]^{-1} \tag{7.7}$$

Empirical models of Davies [175] and Clague et al. [176], i.e. Eqs. (7.8) and (7.9), respectively, are also mentioned to compare with the analytical models:

$$f(\alpha)=\left[16\alpha^{1.5}(1+56\alpha^3)\right]^{-1} \tag{7.8}$$

$$f(\alpha)=0.714\left[\frac{1}{2}\sqrt{\frac{\pi}{\alpha}}-1\right]^2 e^{-0.519\alpha} \tag{7.9}$$

7.2.2 HFM transmembrane pressure and pressure drop over the fiber length

The simplest way to estimate TMP is based on Hagen-Poiseuille equation which considers membrane pores as parallel channels of a defined diameter, similar to those in Nuclepore filters, as follows [177]:

$$TMP = \frac{128 \mu Z Q_f}{\pi d_o^4 N_p} \tag{7.10}$$

where Q_f is the feed flowrate, d_o is the pore diameter and N_p is the number of pores. This equation was further extended by Spurny [106] and Adzumi [178] to consider the pore Knudsen number, i.e the ratio of mean free path of gas molecules and pore diameter. These relationships were, however, derived for pore diameters in the order of units of micrometers, which is not suitable for HFMs considered in this work. The equations are listed in supplementary materials, Eqs. (S7.1)–(S7.3). The same principle as for Eq (7.10) is used to calculate the pressure drop over the length of hollow fiber lumen assuming that the fiber wall permeation fluxes are negligible [179]. This condition is fulfilled only in non-porous hollow fibers:

$$\Delta p = \frac{128 \mu L Q_p}{\pi D_i^4 N_f} \tag{7.11}$$

where Q_p, L, D_i and N_f are the permeate flowrate, fiber length, fiber inner diameter and number of fibers in the membrane module, respectively.

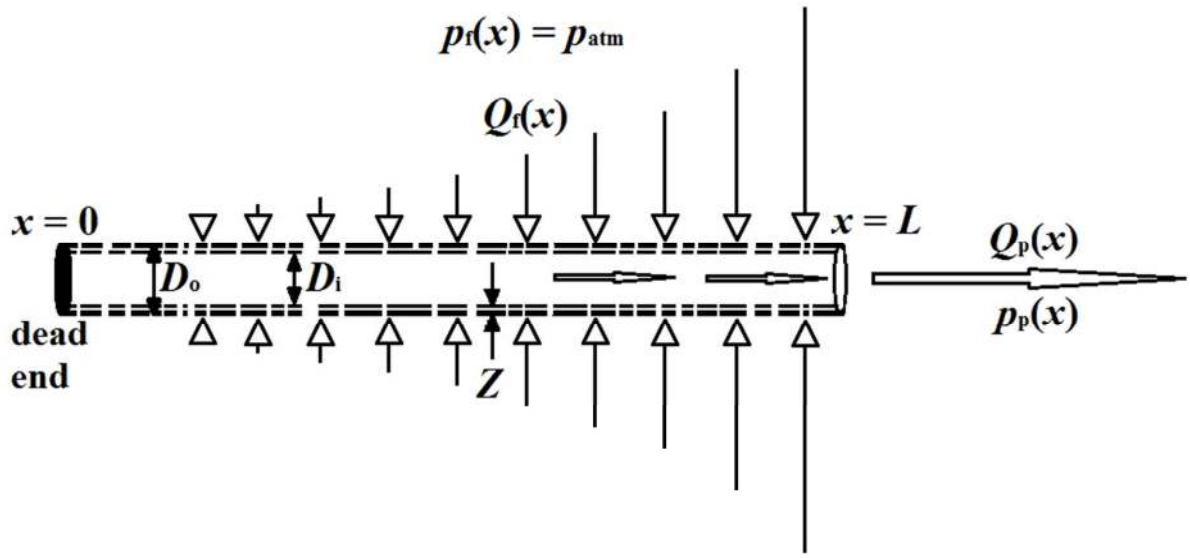

Fig. 7.2: *A scheme of dead-end filtration using a porous hollow fiber*

The overall pressure loss of a HFM is thus given by the transmembrane pressure *TMP* (i.e. the pressure caused by the membrane wall pore structure) and pressure drop over the length of the hollow fiber at the lumen side. However, pressure drop over the length of a porous hollow fiber is changing over the whole length of the fiber lumen. Therefore, variations of the flux through the wall at different points of the HFM length occur as shown in Fig. 7.2. To estimate the average pressure drop caused by a HFM, several models were developed for liquid filtration which can be, with some assumptions, applied for filtration of gases. These assumptions include incompressible fluid which is mostly not considered when dealing with gases. Gas compressibility can significantly influence the gas flow dynamics inside the fiber and affect the pressured drop. However, gas compression was not assumed at experimental conditions adopted in this work. A model developed for submerged HFM modules by Lim et al. [180] (refer to supplementary material, Eqs. S7.4–S7.14) is compared with experimental data in supplementary Fig. S7.1.

7.2.3 Dust cake pressure drop

Dust cake pressure drop is a significant part of the total pressure drop during filtration. As dust particles deposit onto the filter surface (Fig. 7.3), the cake thickness is increasing thus increasing the pressure drop but also increasing the overall filtration efficiency as the deposited particles form another active filtration layer. The cake pressure drop is dependent on dust characteristics, properties of the environment and filtration conditions. The filtration cake is possible to view as a layer of particles and any mathematical model used to describe pressure drop in a packed bed of particulates can be used analogically. Here, the basic mathematical models are reviewed and compared with experimental data.

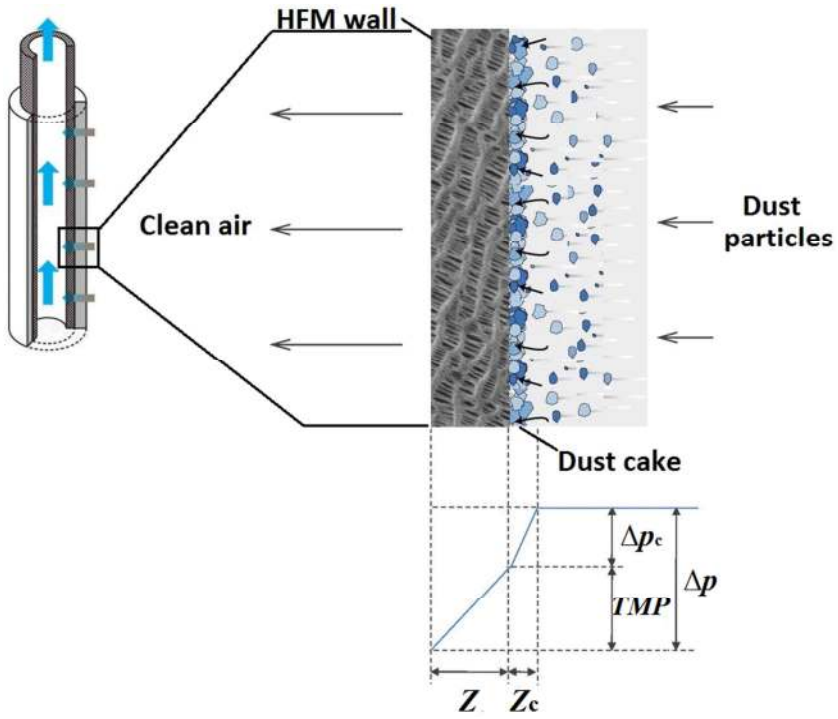

Fig. 7.3: *A scheme of cake filtration and related pressure drops*

Traditional Carman-Kozeny equation was used to calculate pressure drop for laminar flow through packed bed of solid particles [181–183]. Assuming spherical monodisperse particles this equation can be used to predict cake pressure drop (Δp_c) as follows:

$$\Delta p_c = 18 \mu U Z_c \frac{(1-\varepsilon_c)^2}{d_{p32}^2 \varepsilon_c^3} \tag{7.12}$$

where Z_c, ε_c, μ, U and d_{p32} are the cake thickness, cake porosity, fluid viscosity, face velocity, and Sauter mean particle diameter, respectively. Cake porosity can be determined using various direct and indirect methods, refer e.g. to [146, 184, 185]. Among indirect methods, a lot of studies used the Carman-Kozeny equation as a first approximation for estimate of filtration cake porosity. However, based on the study by Tien and Ramarao [181] the cake porosity results tend to be exceedingly low compared to results obtained from independent experiments. Therefore, the use of this equation to predict the cake porosity is rather inappropriate. In this study, the cake porosity was estimated based on the cake weight (m_c) and thickness using the equation as follows [146, 186, 187]:

$$\varepsilon_c = 1 - \frac{m_c}{\rho_p Z_c A} \tag{7.13}$$

where ρ_p and A are the particle density and HFM surface area, respectively. Another well-known correlation was proposed by Ergun as follows [188]:

$$\frac{\Delta p_c}{Z_c} = \frac{150\mu U(1-\varepsilon_c)^2}{\varepsilon_c^3 d_{p32}^2} + \frac{1.75\rho U^2(1-\varepsilon_c)}{\varepsilon_c^3 d_{p32}} \tag{7.14}$$

where ρ is the fluid density. The coefficients in both terms on the right-hand side of the equation (150 and 1.75) were obtained empirically for spherical particles. This equation is based on a modeling of interparticle space (packed bed of spheres) as parallel capillaries. The first term on the right hand side accounts for the viscous effects while the other for the inertial effects and the coefficients are correction factors accounting for geometrical differences between flow paths through packed spheres [189]. In most practical cases the inertial term is too small and can be omitted [184]. Another correlation comes from the Happel's cell model developed by solving the fundamental equations for an incompressible fluid flow through a bed of concentric spheres one of which is the inner solid sphere and the external one of a frictionless fluid [184, 190]:

$$\Delta p_c = \frac{18(1-\varepsilon_c)\mu U Z_c}{d_{p32}^2} \frac{3 + 2(1-\varepsilon_c)^{5/3}}{3 - 4.5(1-\varepsilon_c)^{1/3} + 4.5(1-\varepsilon_c)^{5/3} - 2(1-\varepsilon_c)^2} \tag{7.15}$$

In the dust cake filtration, the relationship between the cake pressure drop and cake structure must be discussed. From the previous works mentioned above, it is clear that their use is very limited to simplified systems, i.e. very narrow particle size distribution or even particle monodispersity and regular defined shape. In reality, however, majority of particulate systems are polydisperse with irregular particle shape. Endo et al. [191] solved this problem and derived a new relationship for random packing of polydisperse and non-spherical particles:

$$\Delta p_c = 18\mu U Z_c \frac{(1-\varepsilon_c) f(\varepsilon_c)}{\varepsilon_c^2} \frac{\gamma}{d_{pg}^2 \exp(4\ln^2 \sigma_{pg})} \tag{7.16}$$

where γ, d_{pg} and σ_{pg} are the particle shape factor, geometric average particle diameter and geometric standard deviation of particles, respectively and $f(\varepsilon_c)$ is so called void function. This formula was derived assuming a uniform cake structure (constant porosity), randomly packed particles, the void function is dependent only on the cake porosity and the particle sizes are governed by the log-normal distribution as follows:

$$f(\ln d_p) = \frac{1}{\sqrt{2\pi}\ln\sigma_g} \exp\left[-\frac{(\ln d_p - \ln d_{pg})^2}{2\ln^2 \sigma_g} \right] \tag{7.17}$$

Due to the HFM geometry, it was further necessary to transform the equations to include the change of the filtration velocity with the radial location. For the sake of brevity, an example is shown only for Eq. (7.16). This relationship was previously derived for hot gas filtration on ceramic filter candles, as follows [192]:

$$\Delta p_c = 9\mu U(D_o + Z_c)\ln\left(\frac{D_o + Z_c}{D_o}\right) \frac{(1-\varepsilon_c) f(\varepsilon_c)}{\varepsilon_c^2} \frac{\gamma}{d_{pg}^2 \exp(4\ln^2 \sigma_{pg})} \tag{7.18}$$

The void function $f(\varepsilon_c)$ describes the effect of neighboring particles and takes into account the change of apparent viscosity of fluid depending on the porosity or the particle concentration. The void function in Carman-Kozeny equation takes the following form:

$$f(\varepsilon_c) = \frac{10(1-\varepsilon_c)}{\varepsilon_c} \tag{7.19}$$

However, this form does not distinguish short-range and long-range effects which contribute to the overall void function. The short-range effect $f_s(\varepsilon_c)$ accounts for the shielding effect of the contacting neighbor particles and can be expressed as follows [186, 193]:

$$f_s(\varepsilon_c) = 1 - 0.6e^{-10(1-\varepsilon_c)} \tag{7.20}$$

The long range effect $f_l(\varepsilon_c)$ accounts for interaction of boundary layers of primary particles and three expressions were found in the literature. Brinkman [194], Happel [195] and Kim and Russel [196] proposed Eqs. 7.21, 7.22 and 7.23, respectively:

$$f_1(\varepsilon_c) = 1 + \frac{3}{4}(1-\varepsilon_c)\left(1 - \sqrt{\frac{8}{1-\varepsilon_c} - 3}\right) \tag{7.21}$$

$$f_1(\varepsilon_c) = \frac{3 - 4.5(1-\varepsilon_c)^{1/3} + 4.5(1-\varepsilon_c)^{5/3} - 3(1-\varepsilon_c)^2}{3 + 2(1-\varepsilon_c)^{5/3}} \tag{7.22}$$

$$f_1(\varepsilon_c) = \left[1 + \frac{3}{\sqrt{2}}(1-\varepsilon_c)^{0.5} + \frac{135}{64}(1-\varepsilon_c)\ln(1-\varepsilon_c) + 16.456(1-\varepsilon_c)\right]^{-1} \tag{7.23}$$

Combining the short-term and long-term effect coefficients, the void function takes the following form:

$$f(\varepsilon_c) = \frac{\varepsilon_c^2 f_s(\varepsilon_c)}{f_1(\varepsilon_c)} \tag{7.24}$$

7.2.4 Energy demands for fan operation

Air filtration performance is mostly determined in terms of filtration efficiency and pressure drop which is a subject of several standards including ANSI/ASHRAE 52.2-2017 (USA) [197], EN1822 [67] and ISO 29463 [198] (standards for high-efficiency air filters) and EN 779 [199] as of 7/2018 completely replaced by ISO 16890 [200] (filters for general ventilation). Based on the measured pressure difference averaged over the course of dust loading, the energy performance of a filter over an operating period can be simulated. Based on the energy consumption at a nominal air flowrate, a general ventilation filter can be classified according to Eurovent [201] certification into energy effectiveness class. Instantaneous power (P_w) required for delivering certain airflow through the filter can be calculated as follows:

$$P_w = \frac{\Delta p(t) Q}{\kappa_{fan}} \tag{7.25}$$

where $\Delta p(t)$, Q and κ_{fan} are the instantaneous pressure drop, volume flowrate (assumed to be constant) and fan efficiency, respectively. The average power consumption to deliver the air through the filter ($P_{w,avg}$) is determined using the following relationship:

$$P_{w\text{-}avg} = \frac{\Delta p_{avg} Q}{\kappa_{fan}} \tag{7.26}$$

where Δp_{avg} is the average pressure drop across the filter over the service life calculated as follows:

$$\Delta p_{\text{avg}} = \frac{1}{M}\int_0^M \Delta p(m)\mathrm{d}m \tag{7.27}$$

where M and $\Delta p(m)$ are the final dust load and instantaneous pressure drop across the filter as a function of dust load, respectively. The power consumption is then usually multiplied by the operation time, thus obtaining the overall energy demand:

$$E = \int_0^t P_{\text{w}}\mathrm{d}t = \frac{1}{\kappa_{\text{s}}}\int_0^t \Delta p(t) Q \mathrm{d}t \tag{7.28}$$

$$E = P_{\text{w-avg}}\, t = \frac{\Delta p_{\text{avg}} Q t}{\kappa_{\text{s}}} \tag{7.29}$$

where κ_{s} is the system efficiency. Generally, the power consumption/requirement determined by this method provides sufficient information about the energy consumption during the filter lifetime. However, based on the study by Montgomery et al. [202], such a simplification brings an error in the results as the relationship does not account for the actual pressure drop achieved in the filter or the effect of accumulated dust which is changing depending on location of the installed filter. It does not indicate anything about how long the filter should operate until exchange for a new one and neglects the rate of particle accumulation in the filter. The equation for the average pressure drop is then determined by integration to the final dust load [203, 204]:

$$\Delta p_{\text{avg}} = \frac{a}{bm}\left(\mathrm{e}^{bm} - 1\right) \tag{7.30}$$

where a and b are constants determined from dust holding capacity test results and m is the mass accumulation in the filter and is related to operation time t for constant volume systems as follows:

$$m = Qt\eta C_{\text{up}} \tag{7.31}$$

where η and C_{up} are the filtration efficiency and upstream particle concentration. If the dust holding capacity test results are not completely provided, an approximation can be obtained by curve fitting to the initial pressure drop of a clean filter and the final pressure drop at a given dust holding capacity as follows:

$$a = \Delta p_{\text{i}} \tag{7.32}$$

$$b = \frac{1}{DHC}\ln\left(\frac{\Delta p_{\text{f}}}{\Delta p_{\text{i}}}\right) \tag{7.33}$$

where Δp_{i} is the initial pressure drop of the clean filter, Δp_{f} is the final pressure drop at dust holding capacity and DHC is the filter dust holding capacity at the final pressure drop. The equations for pressure drop at filter change ($\Delta p_{\text{c-o}}$), average power and energy used to operate the fan can then be expressed as a function of operating time to change-out, using Eqs. (7.34)–(7.36), respectively:

$$\Delta p_{\text{c-o}} = \Delta p_{\text{i}} \mathrm{e}^{Bt} \tag{7.34}$$

$$P_{\text{w-avg}} = \frac{\Delta p_{\text{i}} Q}{\kappa_{\text{s}} Bt}\left(\mathrm{e}^{Bt} - 1\right) \tag{7.35}$$

$$E = \frac{\Delta p_i Q}{\kappa_s B}(e^{Bt} - 1) \tag{7.36}$$

where B is a constant calculated as follows:

$$B = \frac{Q \eta C_{up}}{DHC} \ln\left(\frac{\Delta p_f}{\Delta p_i}\right) \tag{7.37}$$

7.3 Materials and methods

7.3.1 Hollow-fiber membranes

Two types of HFMs were tested (Table 7.1) differing in fiber diameter and surface area. These HFMs are produced by Zena Membranes [26] and are made of polypropylene by extrusion and subsequent dry stretching technique. Such production is relatively simple, without producing any waste material. The polypropylene HFMs are naturally hydrophobic and have been used in various applications such as water/wastewater treatment, in membrane bioreactors, membrane distillation or medicine/biochemical laboratory applications etc.

Table 7.1 : *HFM parameters*

HFM	P60	P80
Fiber outer diameter, D_o (µm)	300	620
Fiber inner diameter, D_i (µm)	228	474
Fiber wall thickness, Z (µm)	36	73
Number of fibers, N_f	1380	300
Active length, L (mm)	730	730
Surface area, A (m^2)	0.95	0.43
Air permeability ($m^3m^{-2}h^{-1}bar^{-1}$)	139	240
Initial Δp at 20 cm/s (Pa)	1203 ± 14	714 ± 5
Initial Δp per unit area at 20 cm/s (Pa/m^2)	1143 ± 13	307 ± 2
Average pore diameter (nm)	87	95
Average collector diameter, d_f (nm)	90	112
Porosity, ε (%)	52	54

7.3.2 Test dust

An A2 fine test dust (Fig. 7.4a) defined by ANSI/ASHRAE 52.2 [197] was used in the experiments (particle-size distribution in Fig. 7.4b measured using a Sympatec HELOS KR laser diffraction analyzer). This product is designed for testing filters [205] and heating components in HVAC systems and has also been used for testing electronic equipment and other industrial and household components. The dust is a custom blend of 93.5 % of ISO 12103-1 A2 fine test dust (composition shown in supplementary material, Table S7.1) and 6.5 % milled cotton linters. The cotton linters are second cut cotton linters milled in a Willey mill fitted with a 4 mm screen [206].

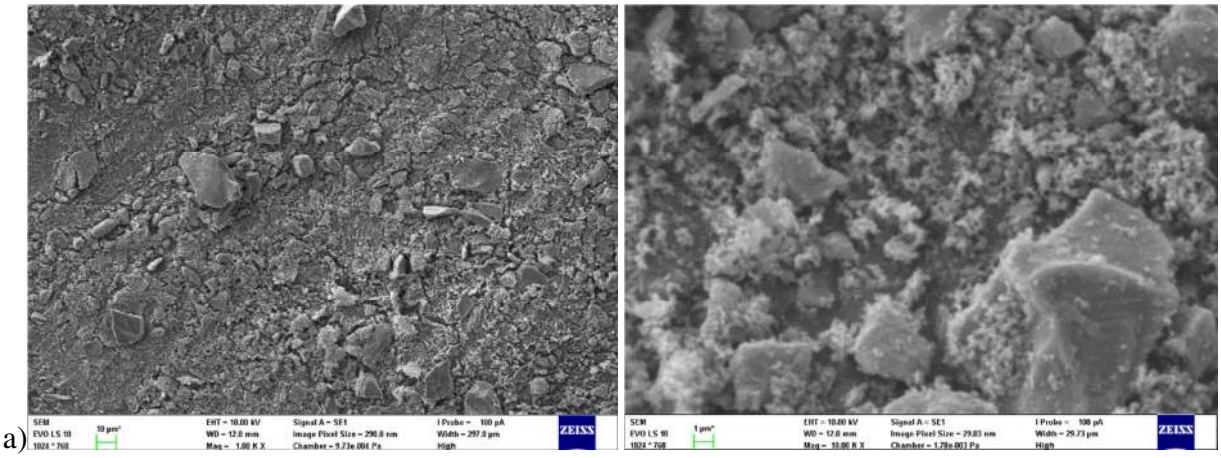

a)

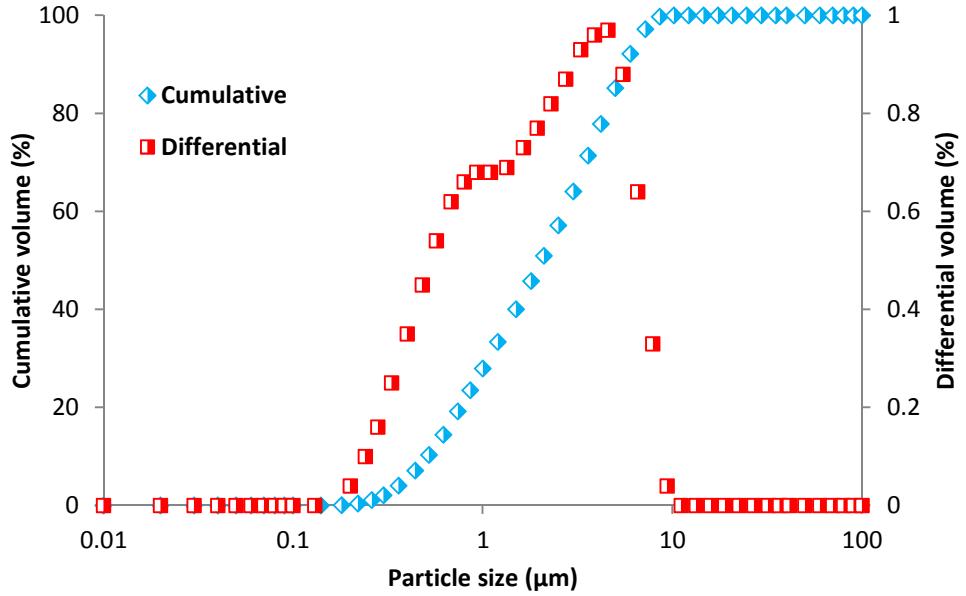

b)

Fig. 7.4: *SEM images of ASHRAE A2 dust used in filtration experiments (a) and particle size distribution of the ASHRAE A2 dust, d_{50} = 2.05 µm (b)*

7.3.3 Experimental setup

Filtration was carried out in a chamber of 70 L volume (Fig. 7.5). The chamber was connected to an ESAM Unijet 75-2V side channel blower (11) using a suction pipe (1), to which a HFM bundle (3) was linked. The blower frequency was controlled using a Siemens Sinamics V20 inverter (7). The test dust was fed through an opening in the chamber's wall (13) using pressure air nozzle. The suction pipe (1) was provided with an EE660 velocity probe (8) and an Omega PX277-05D5V differential pressure sensor (12). The second output of the differential pressure sensor was connected to the chamber thus obtaining pressure drop caused by the HFM. The fan was connected to the electricity through a Cost Control 3000 meter to record the electricity data over the period of the experiments. The fan power input is then obtained using the equation as follows [207]:

$$P_w = \sqrt{3} I_{avg} \tilde{U}_{avg} \cos\phi \tag{7.38}$$

where $I_{ave,}$ U_{ave} and $\cos\phi$ are the average current, average voltage at input and power factor, respectively. The sensors were connected to the LabView software via a data acquisition card

(National Instruments 9207 C Series Voltage/Current input module) and data was recorded with a frequency of 0.5 Hz. Due to long time measurement and high frequency of the data recording, the data were reduced. Data points for graphs were taken for each fifth hour of the experiment. The average with the standard deviation were calculated from ten values of raw data corresponding to a permeate velocity in the range of 0.199–0.201 m/s. This was necessary to avoid significant changes in pressure drop values caused by random velocity fluctuations in duct.

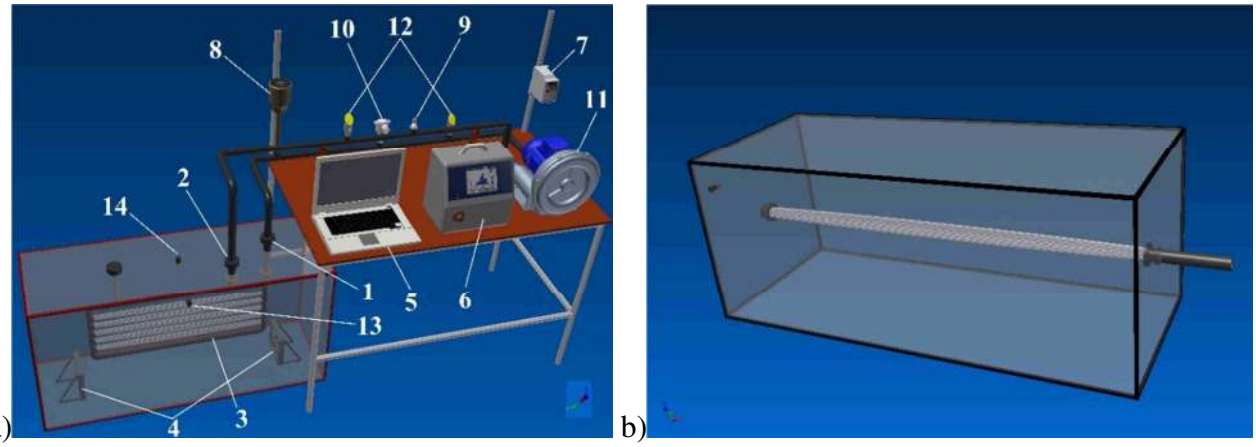

Fig. 7.5: *Experimental setup used for measuring the pressure drop evolution of HFMs (a) and a representation of the individual HFM in the chamber (b)*

7.4 Results and discussion

In this section, results from filtration experiments are compared for two different HFMs at two different permeate velocities (20 and 40 cm/s). Furthermore we tried to compare fouling behavior of a new HFM and a HFM after cleaning and at different dust loading rates. It is worth mentioning that in order to observe double the pressure drop increase in a not highly time-demanding manner, it was necessary to use extremely high dust concentrations. The dust loading rates adopted in the experiments were mostly as high as 4 g/h dosed continuously 1 g per 15 minutes into the chamber of a volume of 70 L. This corresponds to a dust concentration of 14.3 g m^{-3}. However, it is also important to note that the experiment arrangement was outside-in, i.e. a dust environment was created inside the chamber and the air was drawn through the HFM using the fan. This means that only a small portion of the dust dosed got attached to the HFM while the remaining part fell down to the chamber bottom due to sedimentation.

7.4.1 HFM permeability analysis

In this section, measured and theoretically predicted permeabilities are compared. Theoretical prediction is based on filter solidity approach, in which membrane solid volume fraction is used to calculate dimensionless permeability and then recalculated using the collector diameter to permeability k_α. This permeability is then converted to units of $m^3\ m^{-2}\ h^{-1}\ bar^{-1}$ in which the measured values are obtained from an air permeability experiment. Seven theoretical models which were developed assuming isotropic 3D pore structure were compared (Table 7.2).

Models which are closest to the measured value are that of Thomadakis and Robertson [171] and Clague et al. [176] for P60 and Thomadakis and Robertson [171] and Happel [172] for P80. A

model which is far from the measured values is that of Gebart [174]. This model was derived assuming a quadratic packing of cylinders for flow both parallel and transverse to the cylinders [208] which is quite different from the structure of considered HFMs. The favorite empirical formula of Davies also differs significantly, which is probably caused by a very high solidity of HFMs which is as high as 0.46–0.48. Davies derived this formula strictly for the solidity range of 0.01–0.3. The RUC model [170] under-predicts the results, the same is true for the model of Drummond and Tahir [173].

Table 7.2 : Comparison of measured HFM permeability with values obtained using different models for isotropic 3D porous media

	P60			P80		
Model	$f(\alpha)$ (10^{-2})	k_α (10^{-17} m^2)	k (m^{3}m^{-2}h^{-1}bar^{-1})	$f(\alpha)$ (10^{-2})	k_α (10^{-17} m^2)	k (m^{3}m^{-2}h^{-1}bar^{-1})
Measured	**3.81**	**7.66**	**139.0**	**4.22**	**13.2**	**240.0**
Tomadakis and Robertson [171]	3.29	6.61	120.1	3.96	12.4	225.4
RUC [170]	2.43	4.88	88.6	2.97	9.31	169.1
Happel [172]	3.15	6.34	115.1	3.81	11.9	216.8
Drummond and Tahir [173]	1.37	2.76	50.1	2.03	6.36	115.4
Gebart [174]	0.017	0.034	0.6	0.021	0.066	1.2
Clague et al. [176]	4.34	8.73	158.4	5.29	16.6	301.2
Davies [175]	2.61	5.26	95.4	3.11	9.74	176.8

7.4.2 Dust loading of HFMs

7.4.2.1 Experimental data

Tables 7.3 and 7.4 show an overview of the summarized data obtained experimentally. Both HFMs (P60 and P80, refer to Table 7.1) were submitted to filtration of high dust concentrations at two different permeate velocities (20 and 40 cm/s). Both HFMs at both permeate velocities were compared under the same loading rate (m_{load}) of 4 g/h in terms of initial and final pressure drop, average fan power input and DHC (Table 7.3). The same was done for P80 HFM at 20 cm/s but at different loading rates (2, 4 and 6 g/h) to compare its influence on the loading behavior and DHC (Table 7.4).

Table 7.3 : *Overview of the experimental data for different HFMs and the same loading rate*

HFM	U_{pm} (cm/s)	m_{load} (g/h)	*DHC* (g)	Δp_i (Pa)	Δp_f (Pa)	M_T (g)	t (h)	$P_{w\text{-}avg}$ (W)
P60	20	4	16.2	1204	2072	180	45	63
	40	4	4.7	3239	5581	24	6	132
P80	20	4	15.7	714	1453	192	48	39
	40	4	21.4	1870	3789	140	35	87

P80 at 20 cm/s was chosen to further evaluate due to an optimal loading behavior similar to the pressure drop/loading trends in planar filters and due to the most suitable fitting using exponential curve [202, 203]. Both tables also show the total amount of dust dosed during the experiments

(M_T). In further subsections individual parameters are discussed and some of them will be shown in other tables repeatedly due to further discussion and mainly comparison with predicted values.

Table 7.4 : *Overview of the experimental data for P80 HFMs at 20 cm/s at different loading rate*

HFM	U_{pm} (cm/s)	m_{load} (g/h)	*DHC* (g)	Δp_i (Pa)	Δp_f (Pa)	M_T (g)	*t* (h)	$P_{w\text{-}avg}$ (W)
P80	20	2	9	717	1115	66	33	40
		4	15.7	714	1453	192	48	39
		6	13.6	717	1318	180	30	41

7.4.2.2 Dust loading behavior of different HFMs

Fig. 7.6 shows a comparison of the tested HFMs at the velocity of 20 cm/s (Fig. 7.6a) and 40 cm/s (Fig. 7.6b). We can see the obvious difference caused mainly by the different hollow fiber diameter which is responsible for the different pressure drop behavior. P80 HFM has a slow linear increase until the clogging point at a filtration time of 30 hours at which the pressure drop starts to increase steeper. Quite the contrary can be observed for P60 which shows a steep increase within 5 hours and then increases slowly with a linear course. At a higher velocity of 40 cm/s, P80 is similar to P60 at 20 cm/s. However, at a higher velocity an increasing influence of the pressure drop along the length of the hollow fiber lumen is probably dominating over the increase caused by the cake resistance (discussed in next section).

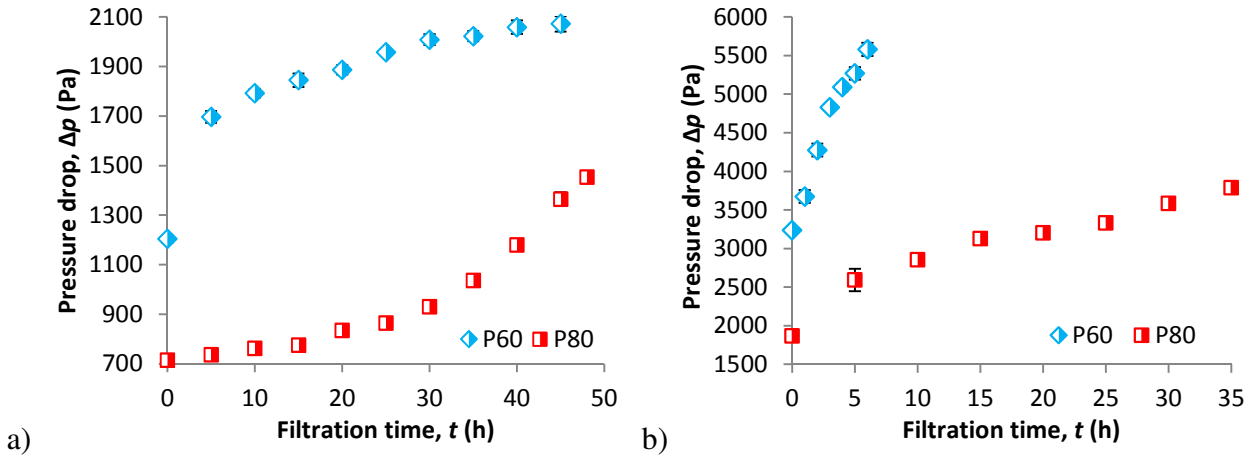

Fig. 7.6: *Comparison of fouling behavior of P60 and P80 HFMs at a permeate velocity of 20 cm/s (a) and 40 cm/s (b) at a dust concentration of 14.3 g/m³*

Tables 7.5 and 7.6 show the experimental results of pressure drop compared with that obtained using Eq. 7.30 and predicted pressure drop at which the filter should be changed out ($\Delta p_{c\text{-}o}$). Eq. 7.30 can be used as a correction of the average pressure drop including the effect of gradual dust accumulation on the HFM using the accumulated dust weight (m_{HFM}, also shown in Table 7.5). The average pressure drop after correction is even more than 30% higher in some cases. This prevents the results to be underestimated. For planar filter media Eq. 7.30 was used to predict pressure drop with assumption of the gradual accumulation of dust in the filter. The pressure drops were predicted with accuracy ± 10% using this formula [36].

The results of the pressure drop at change-out are reflecting dust accumulation in the filter media during filtration according to Eq. (7.34) in which the *B* coefficient (calculated using Eq. 7.37) is included. Therefore, the resulting values of pressure drop are higher compared to the experimental final pressure drop. However, the experimental value of final pressure drop was

obtained randomly and does not determine the real pressure drop at which the filter should be replaced. Eq. (7.34) presents an approximation which is overestimated in some cases mainly for higher permeate velocities (Table 7.5, P60 and P80 at 40 cm/s). In reality, no filter would be operated until reaching such a high value of pressure drop due to large energy requirements.

Table 7.5 : *Measured and predicted pressure drops for different HFMs at different flowrates, at the same loading rate of 4 g/h*

HFM	U_{pm} (cm/s)	m_{HFM} (g)	Experiment			Eq. (7.30)	Eq. (7.34)
			Δp_i (Pa)	Δp_f (Pa)	Δp_{avg} (Pa)	Δp_{avg} (Pa)	$\Delta p_{c\text{-}o}$ (Pa)
P60	20	20.4	1204	2072	1638	1728	2386
	40	11.8	3239	5581	4410	6945	12761
P80	20	23.7	714	1453	1042	1208	1861
	40	53.9	1870	3789	2830	5177	11084

Table 7.6 : *Measured and predicted pressure drops for P80 at 20 cm/s at different loading rates*

m_{load} (g/h)	m_{HFM} (g)	Experiment			Eq. (7.43)	Eq. (7.47)
		Δp_i (Pa)	Δp_f (Pa)	Δp_{avg} (Pa)	Δp_{avg} (Pa)	$\Delta p_{c\text{-}o}$ (Pa)
2	11.3	717	1115	916	959	2181
4	23.7	729	1355	1042	1208	1861
6	17.1	717	1318	1018	1078	1196

7.4.2.3 The effect of permeate velocity

The effect of face velocity was studied in previous works for planar filters [145, 147, 187, 209]. However, our experimental configuration does not allow to physically measure the face velocity. Therefore the results are compared based on permeate velocity, i.e. airflow velocity measured on the downstream side of the HFM using the velocity probe. In Fig. 7.7, the ratio of cake pressure drop to permeate velocity is used in y-axes. This ratio is based on the Darcy law where the filter pressure drop is linearly proportional to the flow velocity.

Based on this ratio, one can distinguish the influence of the filter pore structure. However, as previously mentioned, another significant influence comes with the hollow fiber geometry which even prevails over the pressure drop caused by the cake resistance. This is clearly visible for the higher permeate velocity in P60. P60 has two times smaller inner fiber diameter. As the pressure drop along the length of hollow fiber lumen is inversely proportional to the fourth power of the inner fiber diameter according to Hagen-Poiseuille equation (Eq. 7.11), the pressure drop is significantly higher compared to P80. Therefore, general pressure drop of a clean P80 is almost four times lower per unit area compared to P60 (Table 7.1). However, to exactly discover the influence of the hollow fiber geometry during the experiments is quite a difficult task. The only obvious thing is that the difference of pressure drop evolution per unit permeate velocity is so high that it cannot simply be attributed to the faster cake growth or the cake compression. Moreover, previous works related to planar filter media [145, 147, 209] have revealed no influence of filtration velocity on deposition patterns, i.e. the way how the particles settle down on the membrane surface. This means that the curves in Fig. 7.7 would be identical if the HFM pore structure was in the form of a planar filter.

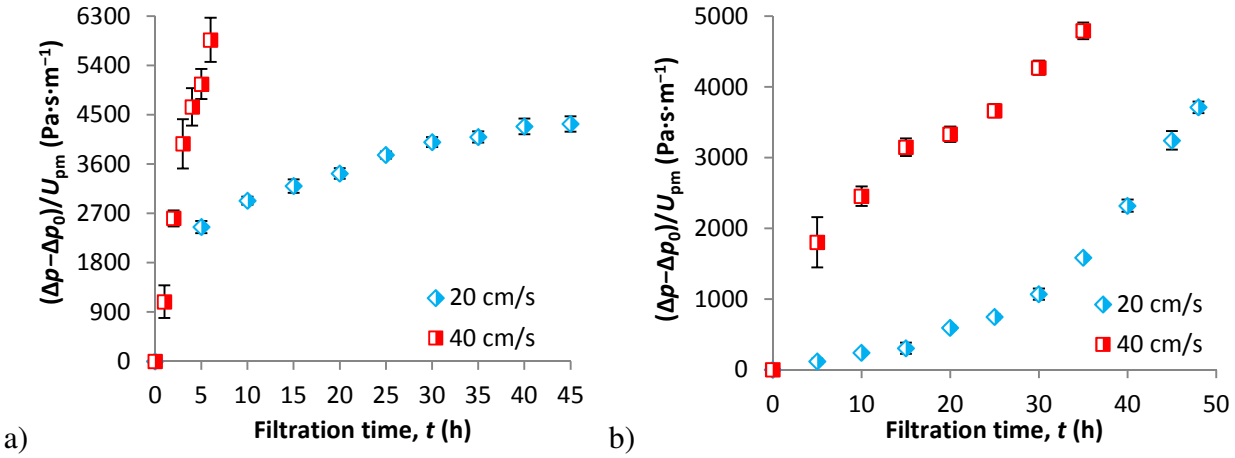

Fig. 7.7: *Comparison of fouling behavior of P60 (a) and P80 (b) HFMs at a permeate velocity of 20 cm/s and 40 cm/s at a dust concentration of 14.3 g/m^3*

7.4.2.4 Comparison of fouling behavior of new and regenerated HFM

Fig. 7.8 shows the fouling behavior of a new and a regenerated P80 membrane (by shaking the accumulated dust off) compared simply by pressure drop increase in time at a dust load of 4 g/h. The pressure drop of the new HFM linearly increased up to 30 hours of continuous filtration and then started to increase more steeply. The same is true for the HFM after cleaning with several differences.

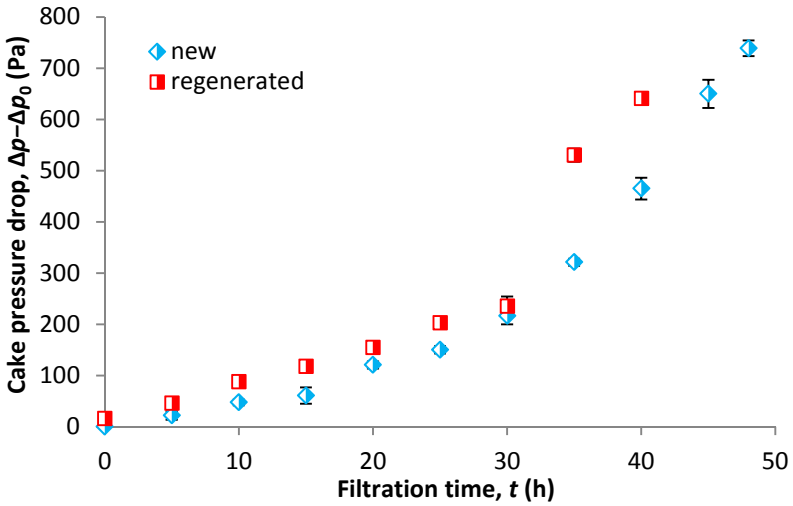

Fig. 7.8: *A comparison of pressure drop evolution of a new and a regenerated HFM at a dust concentration of 14.3 g/m^3 at a permeate velocity of 20 cm/s*

The initial pressure drop remained practically the same after regeneration. However, with the repeated dust loading the pressure drop is slightly higher and after 30 hours of continuous loading (in the same point as the new HFM) started to increased but significantly faster. The increase of pressure drop between 30 and 35th hour of operation was 105 and 295 Pa, for the new and cleaned HFM, respectively. This is caused by the residual particles on the membrane surface or the particles inside the structure after cleaning as obvious from SEM pictures (Fig. 7.9). Fig. 7.10 shows photographs of fouled membranes after the experiments. The dust forms a compact layer on the surface of the fibers which is, however, easily removable. Even during the manipulating the membranes for taking the pictures, the dust cake was very sensitive even to very small blowing or

shaking. This is obvious from Fig. 7.10a where clean fibers are visible due to the membrane manipulation.

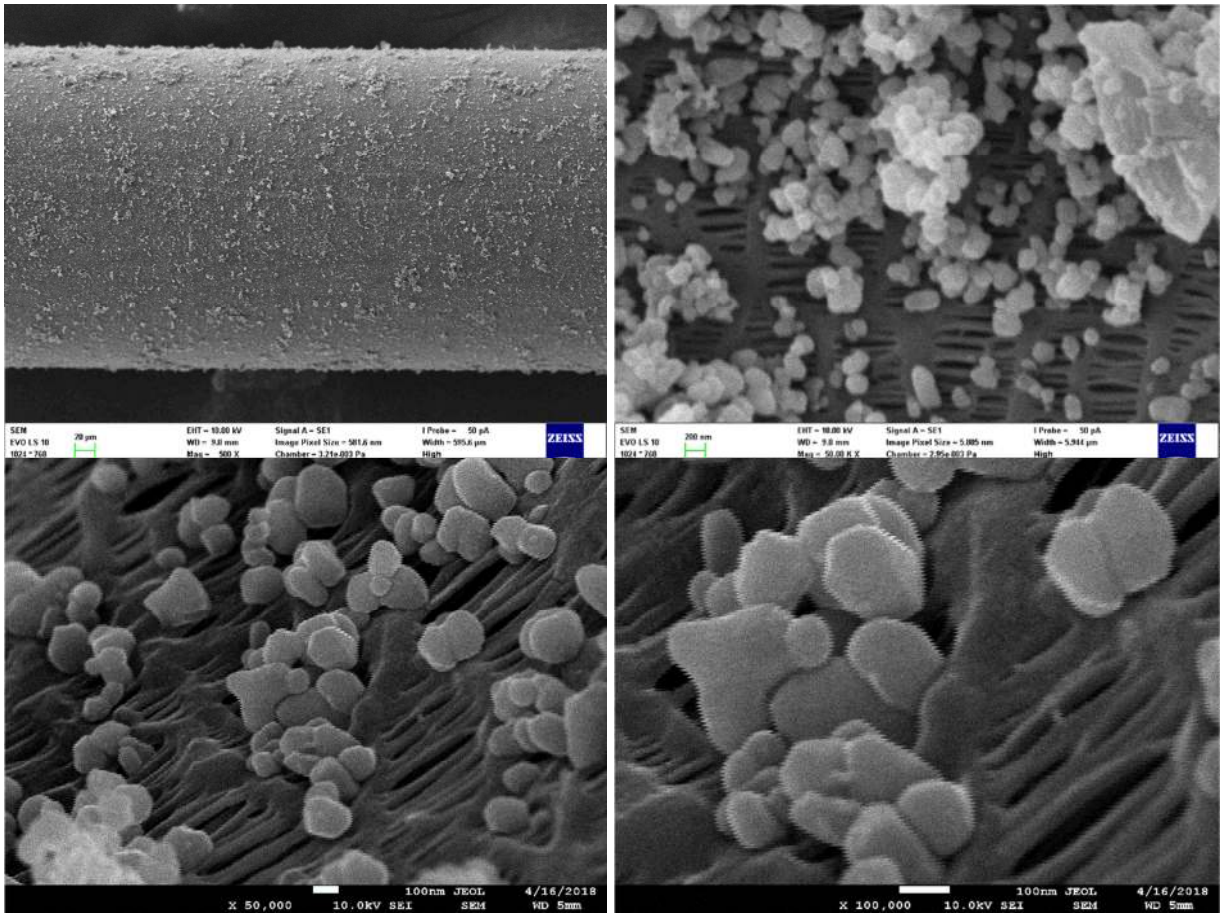

Fig. 7.9: *SEM pictures of cleaned membrane at various magnifications*

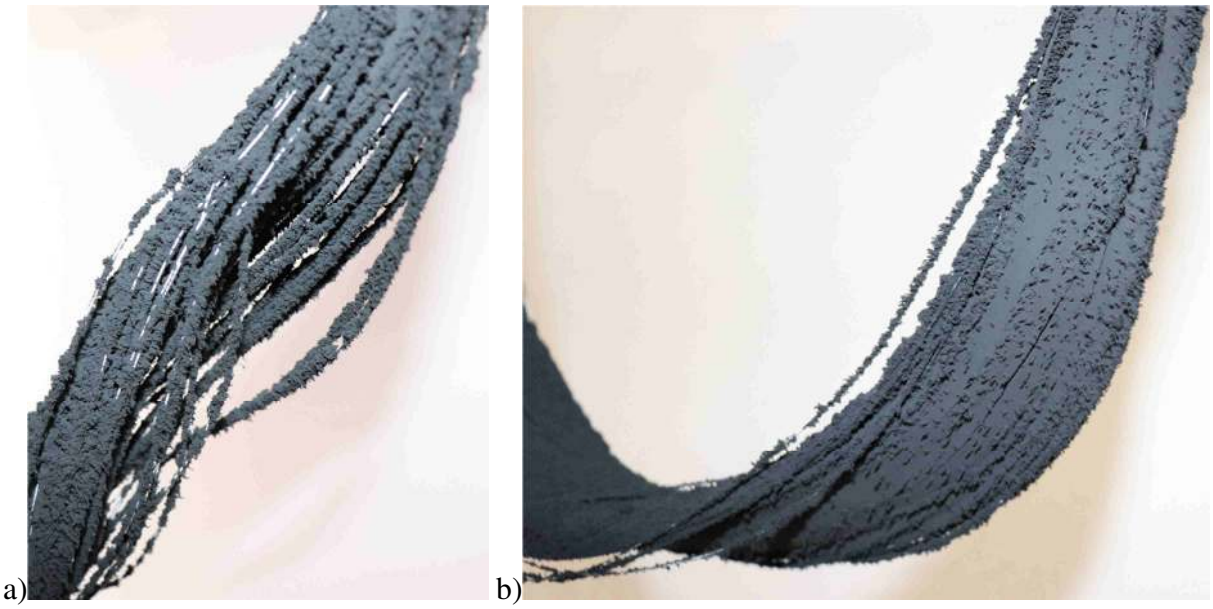

Fig. 7.10: *A real view of fouled HFMs after experiments: a) P80, b) P60*

7.4.2.5 Influence of dust concentration

Fig. 7.11 shows different behavior of the new and cleaned membrane when compared by dust concentration and filtration time and dust dose. Fig. 7.11a shows that the new HFM is fouled faster at higher dust concentration which is reasonable as more particles clog the membrane in a shorter time. However, if we compare the pressure drop/dust load dependence at the two different dust concentrations, we can see that the curves are very close to each other. This indicates that the pressure drop is practically identical at the same mass load of particles deposited on the HFM. This was also observed in a planar PTFE membrane when challenged with talc particles [147].

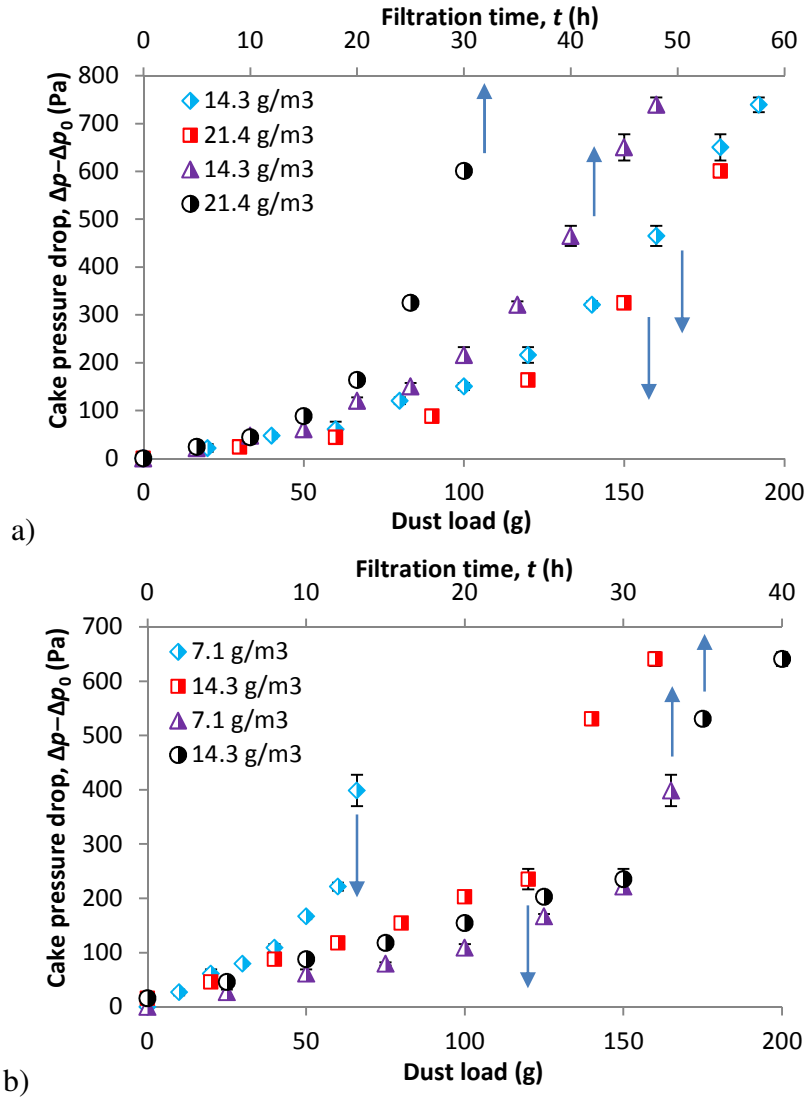

Fig. 7.11: *Fouling behavior of a new (a) and a regenerated HFM (b) at different dust doses at a permeate velocity of 20 cm/s: a comparison by filtration time and dust dose*

Different behavior, however, was observed by Wang et al. [145] who studied the effect of dust loading rate on the fouling of high efficiency filters. The authors hypothesized that at a lower dust concentration, the particles moving towards the filter surface had more time and space to arrange (without interfering by other incoming particles) into a denser cake microstructure. At high dust concentration, the high amount of particles interferes significantly each other at the moment of deposition onto the membrane surface. This results in an unconsolidated cake microstructure with higher permeability.

Fig. 7.11b shows the same but for regenerated membrane. We can see significantly different behavior. This is probably caused by residual particles on the membrane surface after cleaning. At first, we can see the curves very close to each other when compared by time axis while the pressure drop/mass load dependences are diverging from each other. Then the pressure drop in relation to dust load increased more rapidly at lower dust concentration. This behavior was also observed by Wang et al. [145] as described above. However, as clean HFM behaves in the opposite trend (i.e. at higher dust concentration, the fouling is faster), this can rather be attributed to the remaining layer of particles on the membrane surface even after cleaning.

7.4.2.6 Dust-holding capacity of HFMs

Dust-holding capacity (DHC) is the amount of dust kept on the filter after dust loading at the final pressure drop. Final pressure drop is mostly considered double the initial pressure drop value in high efficiency filter media [210]. Here we measured the weight of dust on the HFM after each experiment at double the initial pressure drop value, if allowed by the experimental conditions.

Table 7.7 shows an overview of the experimental DHC data. As the filtration area of HFMs and duration of experiments were different (due to various unspecified experiment related reasons), measured DHC values were related to unit area of the HFM and time. This was done to better compare among the experiments and to assess the influence of different experimental conditions (mainly flowrate and loading rate). Both, the absolute DHC measured and DHC converted per unit area and time, are shown in Table 7.7.

Table 7.7 : *Overview of the experimental data for different HFMs at a constant loading rate*

HFM	U_{pm} (cm/s)	t (h)	m_{load} (g/h)	M_T (g)	m_{HFM} (g)	DHC_{exp} (g)	DHC (g m^{-2} h^{-1})
P60	20	45	4	180	20.4	16.2	0.38
	40	6	4	24	11.8	4.7	0.82
P80	20	48	4	160	23.7	15.7	0.93
	40	35	4	140	53.9	21.4	1.42

Fig. 7.12 shows the relationship between pressure drop and dosed dust. The best curve fit for dependence of pressure drop on dust load was found through testing various filters and is of a common form [203]:

$$\Delta p = a\,\mathrm{e}^{bm} \tag{7.39}$$

with a and b as constants which are described by Eq. (7.32) and (7.33), respectively, and m is the mass accumulation in the filter (Eq. 7.31). The mass accumulation in the filter as described by Eq. (7.31) is, however, valid only for planar filters in which the majority of dosed dust is captured and kept on. If we refer to the DHC definition, which is the amount of dust the filter is able to capture and hold on its surface, certain corrections must be introduced for HFMs.

The experimental configuration was outside-in, which means that the HFM bundle was placed in a chamber where the dust was dispersed and the air in the chamber was then filtered. Considering the whole chamber with the HFM bundle inside as a filter unit, the whole dust amount which was actually fed into the chamber must be considered. However, objective of this section is

to assess the DHC of the membrane bundle itself, i.e. only the dust deposited and kept on the fibers' surface during the filtration and weighted after the experiments.

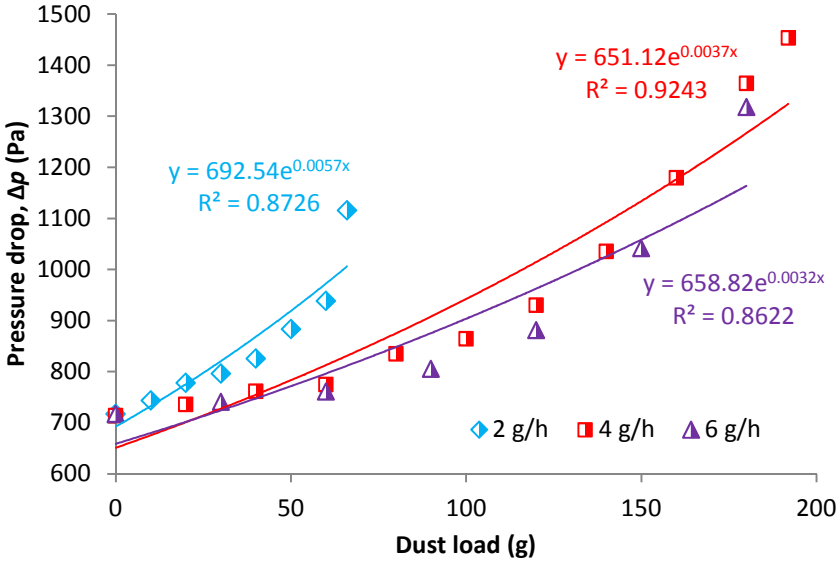

Fig. 7.12: *Pressure drop in relation to dosed dust weight – estimate of DHC from curve fit*

In planar filters, practically all dust carried by an air stream is deposited on the surface, except the particles which penetrate through the filter. So the real dust amount captured is related to the filter's efficiency (dust arrestance) according to Eq. (7.31). Unlike in planar filters, only partial amount of dust is deposited on HFM surface and the remaining dust will settle down in the chamber. Therefore, it is necessary to estimate the rate of dust deposition on the HFM bundle at given conditions. This is, however, a complicated task as most relationships describing filter fouling are of exponential dependence. As a first approximation, we multiplied the mass accumulation in the filter (Eq. 7.31) by a coefficient, i.e. the ratio of DHC_{exp} (DHC obtained experimentally) and total amount of dust fed (M_T) in the chamber, which reflects the real accumulation of dust deposited on the HFM bundle:

$$m_{HFM} = Qt\eta C_{up}\frac{DHC_{exp}}{M_T} \tag{7.40}$$

From Eq. 7.33, DHC_{reg} can be calculated using the b regression constant from the dependence between pressure drop and dosed dust (Fig. 7.12). DHC_{reg} is the real DHC which would be obtained if all the dust fed was deposited on the HFM (like in the planar filter). To obtain the modified DHC for the HFM (DHC_{HFM}), DHC_{reg} is multiplied by the ratio of DHC_{exp}/M_T. DHC_{HFM} presents a generalized real possible DHC which a HFM should be able to achieve at the final pressure drop. The results are summarized in Table 7.8 for P80 at different loading rates.

Table 7.8 : *Overview of the experimental data for P80 HFMs at 20 cm/s at different loading rates*

t (h)	M_T (g)	m_{load} (g/h)	m_{HFM} (g)	DHC_{exp} (g)	DHC (g m^{-2} h^{-1})	b (g^{-1})	DHC_{reg} (g)	DHC_{HFM} (g)
33	66	2	22.7	9.0	0.63	0.0057	77.4	10.6
48	160	4	23.7	15.7	0.78	0.0037	167.5	16.4
30	180	6	11.4	13.6	1.05	0.0032	190.3	14.4

The differences between experimentally obtained (DHC_{exp}) and predicted (DHC_{HFM}) values are up to 15%. This comparison was done only for P80 at 20 cm/s for which the exponential curve fit of pressure drop/dust load dependence (Eq. 7.39) was assured. This assumption was not fulfilled for the other experimental conditions, i.e. P60 at 20 and 40 cm/s and P80 at 40 cm/s (refer to supplementary Fig. S7.2). The approximation of the pressure drop/dust load dependence by an exponential curve fit shows low coefficient of determination. Therefore, assessing the dependences using the exponential fit was not considered sufficiently reliable.

7.4.2.7 Analysis on dust cake pressure drop

Dust cake pressure drop obtained experimentally is compared with existing models and discussed in this section. Table 7.9 shows the experimental parameters used for calculation of the theoretical dust cake pressure drop. Cake thickness was determined from photographs of the fouled HFMs using Stream Motion software as shown in supplementary Fig. S7.3. Thickness of the layer deposited on individual fibers was measured at various positions of the membrane fibers and an average thickness was calculated from at least 15 values. Cake mass corresponds to measured DHC, i.e. the mass of the dust deposited on the fiber bundle measured after the experiment (refer to DHC_{exp} in Table 7.7 and 7.8). Geometric average particle size of the test dust was determined using the laser diffraction analyzer and geometric standard deviation was calculated from the test dust particle size distribution (Fig. 7.4) as follows:

$$\sigma_{pg} = \exp\left(\sqrt{\frac{\sum n_{pi}(\ln d_{pi} - \ln d_{pg})^2}{\sum n_{pi}}}\right) \tag{7.41}$$

where n_{pi} is the number of particles in group i having a midpoint size d_{pi}. Void function was calculated based on the contributions from short-range and long-range effect according to Eq. (7.24). Long-range effect contribution was calculated using relationships from different researchers and compared (refer to supplementary Table S7.2). The lowest value (that calculated using the relationship according to Happel, refer to Eq. 7.22) was used for the calculation of the overall void function. The overall void function was thus the highest which should have ensured the results not to be underestimated. The value of particle shape factor was taken from [145].

Table 7.9: *Dust and cake parameters used for predicting the cake pressure drop*

HFM	P60	P80
Cake thickness, Z_c (μm)	333	829
Cake mass, m_c (g)	16.2	15.7
Dust density, ρ_p (kg m^{-3})	2100	2100
Permeate velocity, U_{pm} (cm s^{-1})	20	20
Geometric average particle size, d_{pg} (μm)	2.62	2.62
Geometric standard deviation, σ_{pg} (μm)	2.63	2.63
Cake porosity, ε_c (–)	0.9507	0.9790
Void function, $f(\varepsilon_c)$ (–)	1.257	0.838
Particle shape factor, γ (–)	1.5	1.5

Table 7.10 shows that the results calculated using various relationships strongly disagree with experimental data. This may be caused by several factors. The most important is the hollow fiber geometry instead of the planar one for which all the relationships were derived. The deposition on

the surface of hollow fibers can be governed by mechanisms, which can be similar to those occurring in planar filters, but their course, interactions and side effects can be totally different which have not been described anywhere in the literature thus far. The main problem remains in describing the HFM bundle as a whole. It is extremely difficult to describe several hundreds of porous fibers in terms of their particle loading behavior.

Table 7.10: *Comparison of the cake pressure drop obtained experimentally and predicted using different models*

Cake pressure drop, Δp_c (Pa)	P60	P80
Experimental	868.5	739.3
Endo et al. [191]	3.1	3.2
Happel [195]	36.8	37.9
Ergun [188]	77.3	77.6
Carman-Kozeny [182]	18.5	18.6

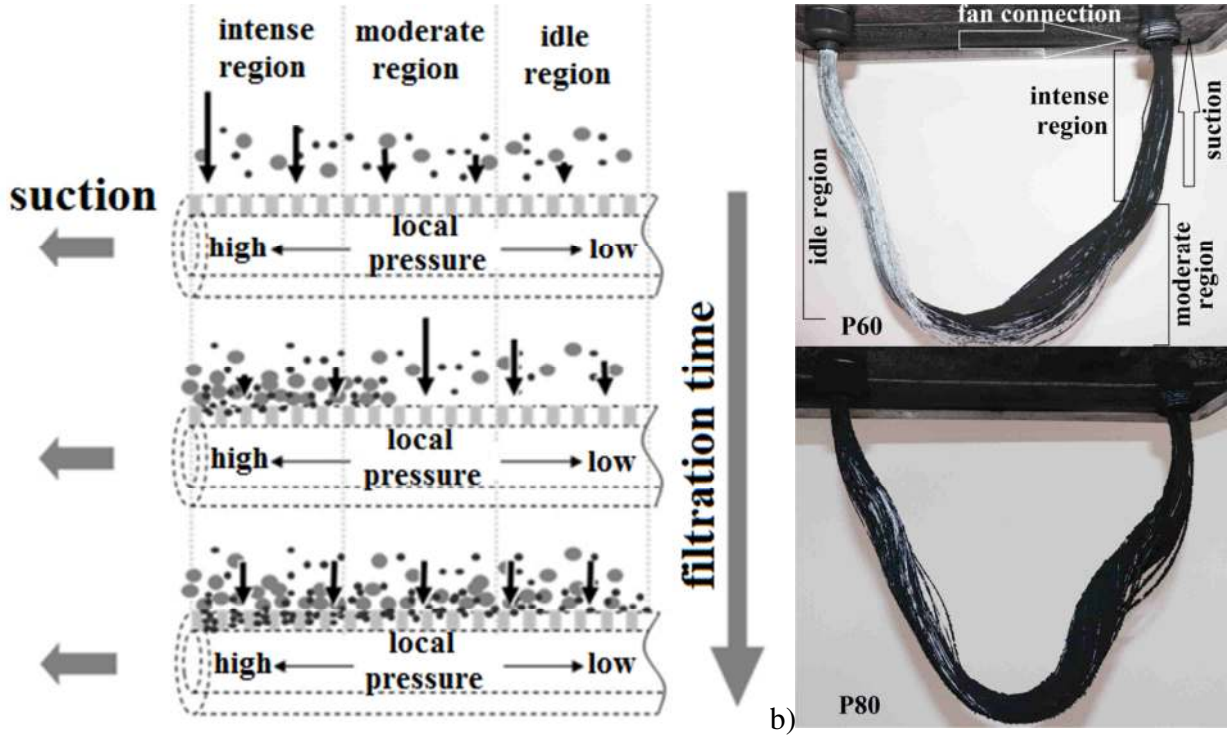

Fig. 7.13: *A simplified diagram of transient behavior of local fouling (a – adopted and adjusted from* **[211]***) and a real comparison of fouled P60 and P80 HFM with designated regions (b)*

HFM fouling is influenced by random motion of particles, random positions of fibers to each other and fiber-fiber interactions which have been found to significantly influence the HFM performance due to the permeate competition between the fibers [212]. Moreover, the fouling of HFM is mostly not uniform over the fiber length [211, 213] due to the axial distribution of permeate flux and local pressure in the hollow fiber lumen as shown in the model by Lee and Kim [211] (Fig. 7.13a). Comparing with the real photographs of fouled HFMs after the experiments (Fig. 7.13b), similar behavior can be seen especially in P60 HFM. The smaller fiber diameter of P60 causes so high pressure drop along the fiber length that half of the membrane (further from the suction end – the idle region) is practically inactive and minimal fouling is observed. This is also

obvious in P80 but not so markedly. The second half of P80 is partially fouled to the point that it cannot be caused by a simple sedimentation on the fibers' surface.

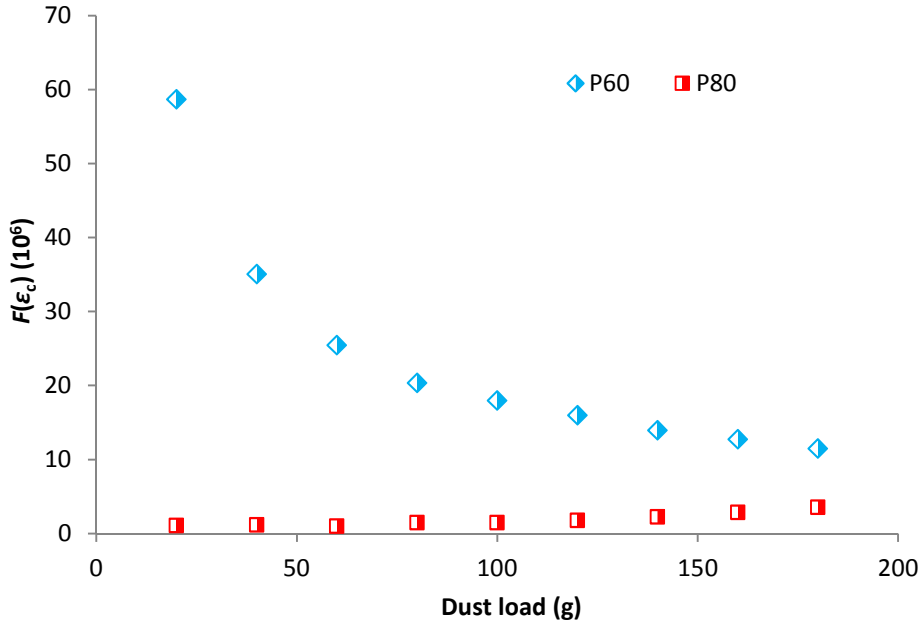

c)

Fig. 7.14: *The macroscopic function of the loaded HFMs*

The results in Table 7.10 clearly show that none of the presented models can reliably describe the fouling and formation of dust cake on HFMs and accurately predict the dust cake pressure drop. To prove that the pressure drop build-up was caused by the formation of dust cake during dust loading, further analysis must have been rendered. Eq. (7.16) can be rearranged as follows:

$$\Delta p_c = \mu U \gamma \frac{m_c}{\rho_p} \frac{1}{d_{pg}^2 \exp(4 \ln^2 \sigma_{pg})} \frac{18 f(\varepsilon_c)}{\varepsilon_c^2} \tag{7.42}$$

This equation can then be manipulated into the following form:

$$F(\varepsilon_c) = \frac{18 f(\varepsilon_c)}{\varepsilon_c^2} = \frac{\Delta p_c}{m_c} \frac{\rho_p d_{pg}^2 \exp(4 \ln^2 \sigma_{pg})}{\mu U \gamma} \tag{7.43}$$

This function can be considered for a macroscopic expression of particle-loaded membrane. Fig. 7.14 shows the macroscopic function of both HFMs for the permeate velocity of 20 cm/s. Significantly different behavior can be observed. P60 decreased significantly with increasing dust load while P80 slightly increased and was significantly lower than P60. The decreasing function of P60 indicates decreasing effect of the cake layer on the overall membrane resistance. This means that the pressure drop increase during the experiments was not primarily caused by the cake. Another effect is that of the increasing pressure drop along the fiber lumen with increasing flowrate. As the inverter increased fan rotations to keep the velocity constant, it caused a significant pressure drop increase along the fiber lumen and this increase even prevailed over the pressure drop increase caused by the cake itself. This effect was not obvious in P80 for which the function is slightly increasing. This indicates that a pressure contribution with each dust dose causes an overall pressure drop increase. So the pressure drop increase was primarily dominated by the growing cake layer even though the effect of pressure drop along the fiber could partially contribute to the overall pressure drop increase. It is, however, not as obvious as for P60 which has two times lower fiber diameter. This is also the reason for so different courses of loading curves

(refer to Fig. 7.6 and 7.7). However, to exactly distinguish between these two effects (i.e. the pressure drop caused by the cake and the pressure drop along the fiber lumen), it is necessary to thoroughly measure the pressure drop in relation to permeate velocity of a clean HFM with detailed resolution. Then the pressure drop of the clean HFM at the given velocity can exactly be subtracted from the HFM fouled with dust particles at the same velocity. This would need significantly large experimental effort. This was unfortunately not done. Even though we were well aware of this phenomenon, it was considered insignificant and only further analysis of experimental data presented here has shown its importance. Due to time issues and different specified aims of this work, further in-depth analysis of this phenomenon was not carried out and is considered for a suggestion for future research.

7.4.3 Power consumption for fan operation

Here the measured fan power inputs (P_w) under various conditions, calculated energy demands based on the measured fan power inputs and theoretical predictions are compared. Table 7.11 shows the measured fan power input and calculated energy consumption at the filtration experiments and predicted power and energy consumption. The experimental results show overall fan power input, i.e. the input necessary for the fan operation itself and the input necessary to draw the air through the membrane. The predicted fan power consumption is based on the pressure drop of the membrane and air flowrate through the membrane and fan efficiency according to Eqs. (7.26) and (7.29) and according to Eqs. (7.35) and (7.36).

Table 7.11: *Measured fan power input and predicted energy requirements for different HFMs at different flowrates*

HFM	U_{pm} (cm/s)	Experiment		Eq. (7.26), (7.29)		Eq. (7.35)–(7.37)	
		$P_{w\text{-}avg}$ (W)	E (kWh)	$P_{w\text{-}avg}$ (W)	E (kWh)	$P_{w\text{-}avg}$ (W)	E (kWh)
P60	20	63	2.835	0.321	0.014	0.236	0.011
	40	132	0.792	1.729	0.010	1.270	0.008
P80	20	36	1.440	0.204	0.010	0.143	0.007
	40	87	3.045	1.109	0.039	0.733	0.026

Table 7.12: *Measured and predicted energy requirements for P80 at 20 cm/s at different loading rates*

m_{load} (g/h)	Experiment		Eq. (7.26), (7.29)		Eq. (7.35)–(7.37)	
	$P_{w\text{-}avg}$ (W)	E (kWh)	$P_{w\text{-}avg}$ (W)	E (kWh)	$P_{w\text{-}avg}$ (W)	E (kWh)
2	40	1.320	0.180	0.006	0.141	0.005
4	36	1.728	0.204	0.010	0.143	0.007
6	41	1.230	0.199	0.006	0.141	0.004

The experimental values were measured directly using the electricity meter which measures the fan power input for the fan operation. The equations predict the fan power consumption necessary solely for drawing the air through the resistance caused by the membrane. However, the electricity meter measures the total power input necessary for the fun operation i.e. the sum of the power for drawing the air through the membrane and power for the operation of the fan itself. Therefore, there is so large difference between the measured and predicted values. However, to obtain a comparable difference between the prediction and experiment, larger flowrates must have been

involved in the experiments. At these experimental conditions, the predicted values are very low. This is rather a suggestion for another study. The same is shown in Table 7.12 where a comparison for different loading rates is shown.

Fig. 7.15 shows measured fan power input during dust loading. Generally, the fan power input follows similar trends as the pressure drop with dust load. This is given by gradual fouling of the HFM. The experiments were performed at a constant air flowrate. During the membrane fouling the airflow is gradually decreasing due to forming layer and the inverter automatically increases the fan frequency to keep the airflow constant. As there is now a new resistance on the membrane surface (the cake layer), increasing the flowrate increases the pressure drop thus the fan power input at the same time.

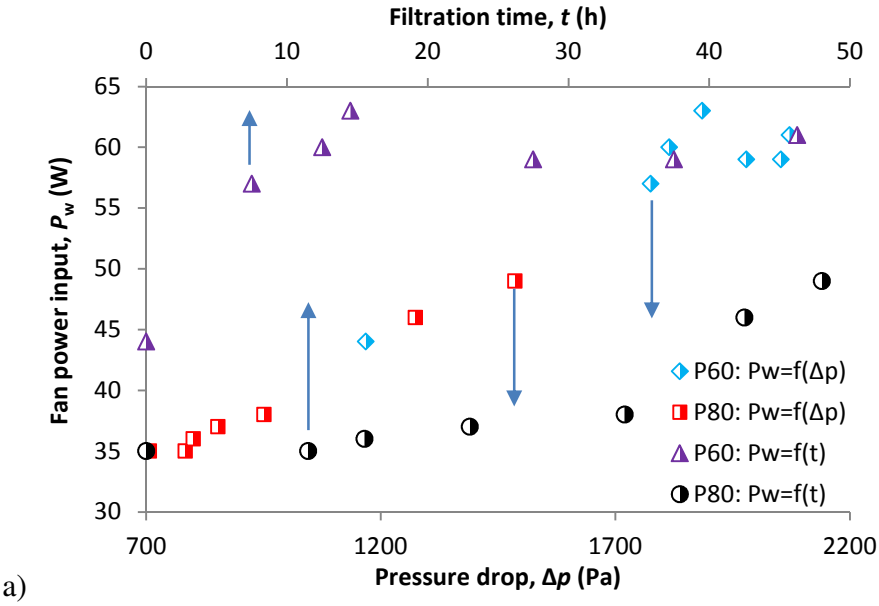

a)

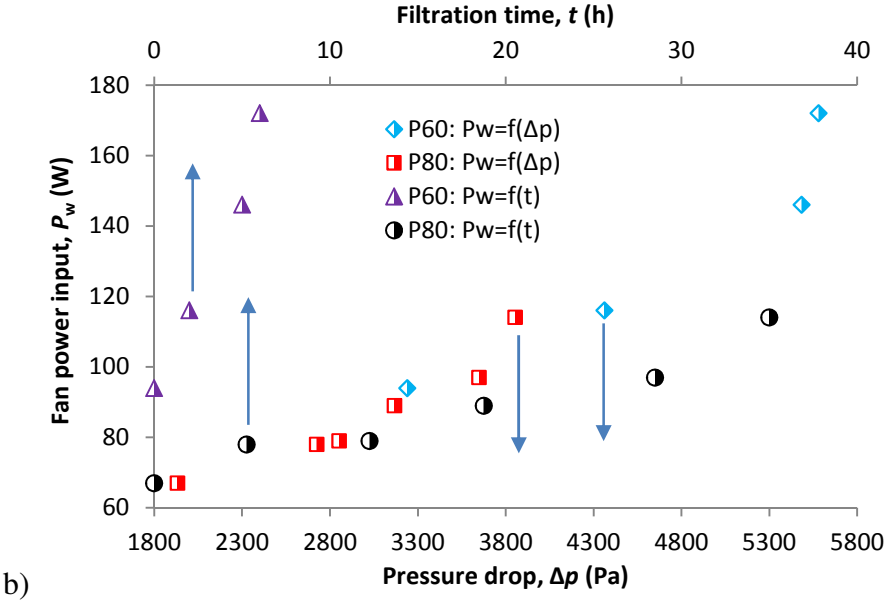

b)

Fig. 7.15: *Comparison of different HFMs in terms of fan power input by filtration time and pressure drop at 20 cm/s (a) and 40 cm/s (b)*

The power consumption can also be expressed using the Euler number (*Eu*). The Euler number (often referred to as dimensionless pressure drop) describes the relationship between pressure drop

and the kinetic energy. It was previously used to characterize rows of hollow-fiber membranes [214], in-line and staggered rows of tubes [215], tubes of a heat exchanger [216] or for characterization and design of cyclone separators [217–219] and filtering hydrocyclones [220]. Euler number is defined as the ratio of pressure forces to inertial forces [214, 215, 221]:

$$Eu = \frac{2\Delta p}{\rho U^2} \tag{7.44}$$

Fig. 7.16 shows a relationship between Euler and Reynolds number. Euler number is extremely high indicating large energy consumption even for low airflow velocities adopted in the experiments. It is, however, significantly decreasing with Reynolds number in which the fiber inner diameter is used as a characteristic dimension. This indicates that increasing the inner fiber diameter leads to significant reduction of power consumption regardless of increasing the airflow velocity.

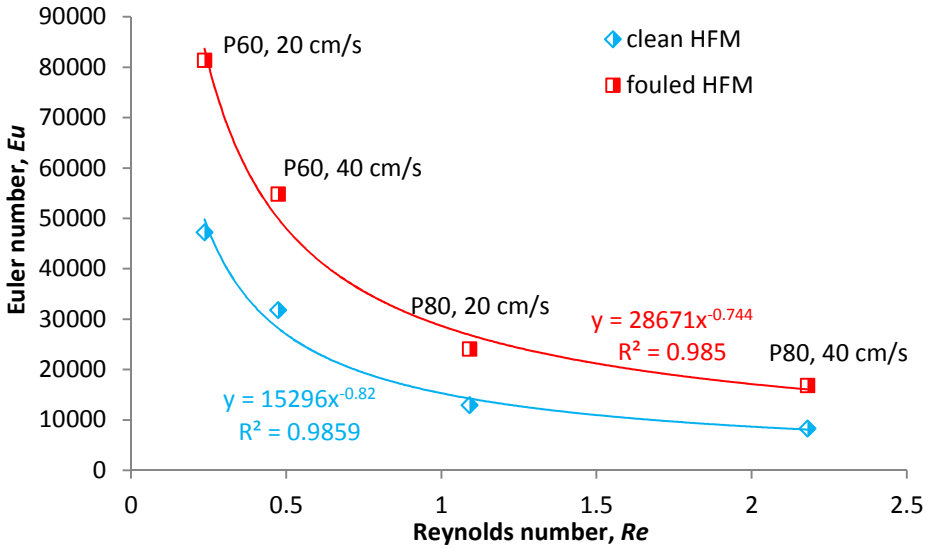

Fig. 7.16: *Euler number in relation to Reynolds number of clean and fouled HFM*

7.4.4 Life-cycle cost estimate

Life cycle cost (LCC) is the total cost of filtration operation and related activities including initial investments into the filtration equipment, installation, operation cost (energy demands), maintenance and final disposal. The LCC of continuous operation of a filter at a constant flowrate can be determined as follows, with I_{FI}, LCC_E, LCC_M and LCC_D as filter investment/installation cost, electricity cost, maintenance and disposal cost per life cycle, respectively:

$$LCC = I_{FI} + LCC_E + LCC_M + LCC_D \tag{7.45}$$

where I_{FI} is the cost of a new filter including frame, labor, filter housing, the building volume for the filters etc. LCC_E is the present total cost of energy to draw the air through the filter (the electricity to power the fan). The calculation of energy cost is mostly based on the average pressure drop calculated using initial and final pressure drop value at DHC (recommended by the filter manufacturer). Here, the average pressure drop values obtained from experiments are used to simulate the life cycle energy requirements as follows:

$$LCC_{\mathrm{E}} = Pr_{\mathrm{E}} P_{\mathrm{w\text{-}avg}} t_{\mathrm{LC}} \tag{7.46}$$

where Pr_{E} is the electricity price, $P_{\mathrm{w\text{-}avg}}$ is the average power consumption of the fan over the filter life cycle t_{LC} which is calculated as follows [222]:

$$t_{\mathrm{LC}} = \frac{DHC}{\eta QC_{\mathrm{up}}} \tag{7.47}$$

LCC_{M} is the total maintenance cost including labor cost, filter replacement and related activities. LCC_{D} is the total cost of filter disposal. This item is very important today because of the requirements on material recycling and waste volume reduction. However, it is important to express the price changes with time mostly in terms of price increase, inflation/interest rate and other economic indices. This means that money spent today may differ from the same amount of money spent in the future. Certain costs must be considered and paid regularly, e.g. for energy or routine maintenance, others occur less frequently or over a longer period of time, e.g. filter replacement. Other costs are paid only once, i.e. investment and disposal at the end of the life cycle or other extraordinary expenses. The present cost (Co_{p}) of a single cost item paid after n years (Co_{n}) can be estimated as follows:

$$\frac{Co_{\mathrm{p}}}{Co_{\mathrm{n}}} = \left(1 + i - PI\right)^{-n} \tag{7.48}$$

where PI is the price increase and i is the interest rate. This correction factor is calculated for each year and the sum of these factors is then used to calculate the total discounted costs [223]. For the sake of brevity, the LCC is calculated only for one case, i.e. HFM P80 at the velocity of 40 cm/s. Average price increase taken for calculation was 2.5% per year based on data released by Czech Statistical Office (a year-on-year comparison, August 2018) [224]. Interest rate was assumed to be 2% based on Czech National Bank forecast released in November 2018 [225]. The cost of individual items was assumed based on the actual prices. Electricity price was assumed to be 0.16 €/kWh [226], filter investment, maintenance and disposal were considered as high as 40 €, 15 € and 2.2 €, respectively. Filter investment cost is based on the price of one HFM bundle of 20 €, plus 20 € related to installations and associated accessories. Prices of maintenance and disposal are based on [223] and recalculated to current prices.

Fig. 7.17 shows the LCC estimate of the HFM filtration system. The course of individual cost items during 10 years is slightly increasing. This simulation of price increase over the use of the filter is based on the present price which is multiplied by the correction factor calculated using Eq. (7.48). The total LCC for the period of 10 years was estimated at 2026 euro, with the cost of investments, electricity, maintenance and disposal accounting for 19.5%, 72.1%, 7.3% and 1.1% of the total cost, respectively (Fig. 7.17b). This is in partial agreement with literature [35] where higher cost for maintenance and lower cost for investments are considered (refer to Fig. 2.4a). For general ventilation filters, the investments costs are about 6% of the total cost while maintenance accounts for 17%. This is not unusual as high-efficiency filter media, which HFMs are considered for, are generally more expensive. They also need less service because these filters are mostly used as a last stage of filtration where very small amount of most penetrating particles are filtered so the fouling is less intensive. Disposal and energy costs accounting for about 1% and 72%, respectively, are assumed to be about the same, with energy cost increasing for high-efficiency filters due to higher pressure drops. The period of 10 years is based on eight filter replacements,

one after 1.25 years of use (one cycle). The one filter-cycle length was taken as a half of the value calculated using Eq. (7.47) which is based on the experimentally measured DHC assuming an upstream particle concentration of 1 mg/m^3, an efficiency of 99.998% (MPPS efficiency measured at 40 L/min, refer to chapter 6, Fig. 6.6) and a flowrate of 12 L/min (corresponding to permeate velocity of 40 cm/s).

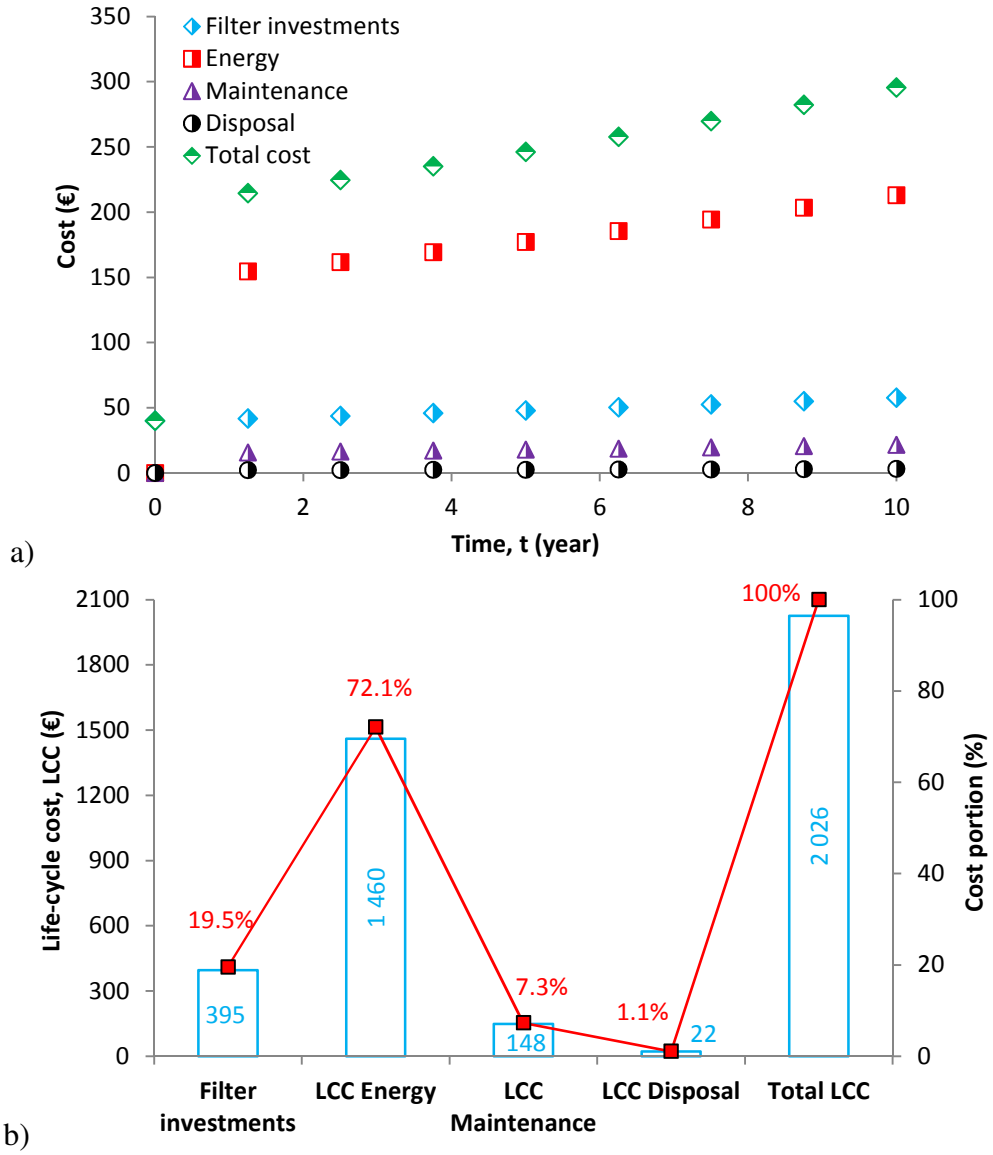

Fig. 7.17: *Cost development of individual items in time (a) and LCC of individual items and total LCC over 10-year period (b)*

7.5 Conclusion

HFMs exposed to extremely high dust concentrations showed very slow pressure drop increase. This was, however, true only for the lower permeate velocity (20 cm/s). The pressure drop increased linearly for 30 h and then an exponential increase occurred. At the higher velocity (40 cm/s) the pressure drop profile differs significantly as the effect of increasing pressure drop

along the length of hollow fiber lumen occurs. This might also be the main reason for different dust loading profiles of P60 and P80.

From the above mentioned, it is clear that the inner fiber diameter plays a vital role also in the membrane loading behavior and is thus a critical parameter for whole air filtration process unlike e.g. dust concentration which seems to have negligible effect. This is quite an exceptional behavior which is also confirmed by the relationship between Euler and Reynolds number for both HFMs at two different velocities. The energy consumption for the operation of the selected HFMs for adopted conditions is rather higher. However, it can be easily varied by changing the membrane parameters, mainly inner fiber diameter and surface area.

For the given conditions, an estimate of the life-cycle cost was outlined. The cost of the HFM air filtration will definitely be higher due mainly to operation cost arising from higher pressure drop. It is also worth mentioning that only two types of HFMs each of only one surface area were tested. Therefore, generalization of the results is rather a suggestion for future work including the HFM customization for air filtration applications. This will be possible as there is a large area for HFM optimization.

8 Summary and future work

This work appears to be a first attempt to use PP HFMs in aerosol filtration. As stated in the introduction, at the very beginning of this thesis proposal, no work had been found in literature on this topic. During evolvement of this thesis, several studies have emerged and are summarized in the first chapter. Unlike those previous studies, which were mainly focused on preparation of new HFMs customized for air filtration, this work was devoted to characterize HFMs commercially available for water treatment applications. For example, particle size resolved filtration efficiency was measured in all experiment configurations. This is quite different from the above mentioned studies where an unresolved aerosol defined by a geometric average diameter was used. Such an experiment, however, does not say anything about the factual filtration efficiency which is strictly different for different particle sizes. As a consequence, all standards for air filter testing require using of size segregated aerosol and define an exact particle size or particle size range for which the efficiency must be tested. It is for example twelve particle size ranges in the ASHRAE 52.2 standard or the MPPS for high-efficiency filters in the EN1822. Moreover, different types of aerosol were used and compared with the standardized method. Another contribution of this work is the comparison of existing models for air filtration efficiency and pressure drop of membrane and dust cake which were not dealt with in the aforementioned studies. This work has gone even further and tried to estimate life-cycle cost and outlined thus its possible utilization in a real application.

8.1 Summary

First chapter introduced the problem background and the research objectives were outlined. The second chapter was focused on the state of the art in the air filtration field where important knowledge about air filters, air filtration process generally, its application field and HFMs was summarized.

In the third chapter, models for predicting air filtration efficiency were reviewed and applied on the parameters of PP HFMs. Models developed for fibrous filters based on single fiber efficiency approach predicted 100% efficiency no matter of the face velocity. Using models for Nuclepore filters has given some penetrations which increased with increasing face velocity. Thus the Nuclepore models seem to be more appropriate as it gives more plausible results. Generally, the results rather indicate that there is no model suitable for prediction of filtration efficiency of the considered HFMs.

Chapters 4–6 focused on the filtration efficiency testing. The HFMs were challenged with a polydisperse incense stick and TiO_2 aerosol at different conditions. For both aerosols, an MPPS was found to be around 35 nm. These tests were performed to simulate different dust laden environment for comparison with semi-standardized experiments which is the subject of chapter 6. In chapter 6, closed HFM modules were tested using both the monodisperse and the polydisperse ammonium sulfate aerosol. Using the monodisperse aerosol, the HFM showed 100% efficiency for all particle sizes no matter of the flowrates and module surface area. To avoid the results overrating, we used HFM modules with a larger area, to obtain higher flowrates, and polydisperse aerosol with high particle concentration to check the efficiency at extreme conditions. At these conditions small penetrations were recognizable. To conclude on filtration efficiency testing, for

all conditions adopted, HFMs demonstrated very high efficiency comparable with HEPA and even with ULPA filters.

Another significant part of this work was to study the particle loading behavior of the HFMs which is described in chapters 5–7. This was studied using aerosol of TiO_2 particles, ammonium sulfate particles, and ASHRAE A2 fine dust. No matter of the used aerosol, the pressure drop/time profile had similar course, i.e. a moderate linear increase of pressure drop up to a certain time with a subsequent abrupt increase up to the final pressure drop value. The only difference was in the values of pressure drop itself due to different membrane filtration area and configuration used for different aerosols. The energy requirements for the operation of HFM air filter would definitely be higher. There is, however, large space for membrane optimization in terms of surface area, inner diameter, fiber wall thickness, porosity, pore size etc. These parameters can be adjusted to customize the HFM for particular air filtration applications.

8.2 Future work

The results obtained in the framework of this thesis have outlined a lot of suggestions for future work and further research in this field. No mathematical description for predicting the air filtration efficiency of HFMs is known. The current models are limited to fibrous or pore structures, which is sufficient for most cases. However, HFMs can demonstrate both types of structure or need other mechanisms to be included. An example of such a mechanism could be interception or diffusion capture at the lumen side surface of the fiber which cannot be considered in planar filters. Therefore, a development of accurate model generalizable for various air filtration conditions and HFM parameters or even various types of HFMs (made of different materials) is necessary. Another gap can be seen in the description of dust cake pressure drop which strongly disagrees with experimental data. This is due to the HFM geometry and the amount of hollow fibers in a bundle. Individual fibers, clean, slightly fouled or completely clogged, can interact among each other or even synergize the fouling effect. This means that a (clogged) fiber in an immediate vicinity of another one can act as another active filtration layer. Unlike for planar filters, for which the existing fouling models were developed, such a system is extremely difficult to describe as a whole. To be able to accurately describe this issue, it is necessary to exactly distinguish between TMP (caused by membrane wall) and lumen pressure drop (caused by extremely small fiber diameter) and the changes of their profiles during dust loading.

Concerning the practical issues of the HFM air filtration, it would be appropriate to develop a specific HFM customized for air filtration. This means a lot of optimization work and playing with HFM parameters to find an optimal tradeoff between membrane parameters, pressure drop, efficiency and price. At the current state, air filtration using the considered HFMs would be limited to very specific applications. To obtain other information about the practical importance of this system, it would be appropriate to develop a pilot scale unit with large filtration area and perform at least one year operation in a real polluted environment to obtain more complex filtration data. Based on this, it would be possible to evaluate the filtration behavior, fouling and also energy requirements which would be of practical importance even for higher volume applications.

9 References

[1] FUCHS, N. A. *The mechanics of aerosols*. 1. vyd. London: Pergamon Press, 1964. ISBN 978-0-486-66055-4.

[2] BROWN, Richard Colin. *Air Filtration: An Integrated Approach to the Theory and Applications of Fibrous Filters*. B.m.: Elsevier Science & Technology Books, 1993. ISBN 978-0-08-041274-0.

[3] HINDS, William C. *Aerosol technology: properties, behavior, and measurement of airborne particles*. B.m.: Wiley, 1999. ISBN 978-0-471-19410-1.

[4] WANG, Chiu-sen a Yoshio OTANI. Removal of Nanoparticles from Gas Streams by Fibrous Filters: A Review [online]. 2012, **52**(1), 5–17. ISSN 0888-5885. Dostupné z: doi:10.1021/ie300574m

[5] SHAFFER, Ronald E. a Samy RENGASAMY. Respiratory protection against airborne nanoparticles: a review. *Journal of Nanoparticle Research* [online]. 2009, **11**(7), 1661. ISSN 1388-0764, 1572-896X. Dostupné z: doi:10.1007/s11051-009-9649-3

[6] GALKA, Ned a Abhishek SAXENA. High efficiency air filtration: The growing impact of membranes. *Filtration* [online]. 2009, **46**(4), 22–25. Dostupné z: doi:10.1016/s0015-1882(09)70157-0

[7] ZHU, Miaomiao, Jingquan HAN, Fang WANG, Wei SHAO, Ranhua XIONG, Qilu ZHANG, Hui PAN, Yong YANG, Sangram Keshari SAMAL, Feng ZHANG a Chaobo HUANG. Electrospun Nanofibers Membranes for Effective Air Filtration. *Macromolecular Materials and Engineering* [online]. nedatováno, **302**(1), 1600353. ISSN 1439-2054. Dostupné z: doi:10.1002/mame.201600353

[8] SELATILE, Mantsopa Koena, Suprakas Sinha RAY, Vincent OJIJO a Rotimi SADIKU. Depth filtration of airborne agglomerates using electrospun bio-based polylactide membranes. *Journal of Environmental Chemical Engineering* [online]. 2018, **6**(1), 762–772. ISSN 22133437. Dostupné z: doi:10.1016/j.jece.2017.12.070

[9] MADUNA, Lebo a Asis PATNAIK. Textiles in air filtration. *Textile Progress* [online]. 2017, **49**(4), 173–247. ISSN 0040-5167, 1754-2278. Dostupné z: doi:10.1080/00405167.2018.1461921

[10] MAHON, Henry I. Permeability separatory apparatus, permeability separatory membrane element, method of making the same and process utilizing the same [online]. US3228876A. 11. leden 1966. [vid. 2018-06-23]. Dostupné z: https://patents.google.com/patent/US3228876/en

[11] PENG, Na, Natalia WIDJOJO, Panu SUKITPANEENIT, May May TEOH, G. Glenn LIPSCOMB, Tai-Shung CHUNG a Juin-Yih LAI. Evolution of polymeric hollow fibers as sustainable technologies: Past, present, and future. *Progress in Polymer Science* [online]. 2012, **37**(10), Topical Issue on Polymer Physics, 1401–1424. ISSN 0079-6700. Dostupné z: doi:10.1016/j.progpolymsci.2012.01.001

[12] FENG, C. Y., K. C. KHULBE, T. MATSUURA a A. F. ISMAIL. Recent progresses in polymeric hollow fiber membrane preparation, characterization and applications.

Separation and Purification Technology [online]. 2013, **111**, 43–71. ISSN 1383-5866. Dostupné z: doi:10.1016/j.seppur.2013.03.017

[13] JANG, Jeachul, Eun-Chul KANG, Hyung Keun LEE, Siyoung JEONG a Seong-Ryong PARK. Energy Demand Comparison between Hollow Fiber Membrane Based Dehumidification and Evaporative Cooling Dehumidification Using TRNSYS. *Energies* [online]. 2018, **11**(5), 1181. Dostupné z: doi:10.3390/en11051181

[14] ZHAO, Baiwang, Na PENG, Canzeng LIANG, Wai YONG a Tai-Shung CHUNG. Hollow Fiber Membrane Dehumidification Device for Air Conditioning System. *Membranes* [online]. 2015, **5**(4), 722–738. ISSN 2077-0375. Dostupné z: doi:10.3390/membranes5040722

[15] WANG, Liang-Yi, Wai Fen YONG, Liya E. YU a Tai-Shung CHUNG. Design of high efficiency PVDF-PEG hollow fibers for air filtration of ultrafine particles. *Journal of Membrane Science* [online]. 2017, **535**, 342–349. ISSN 0376-7388. Dostupné z: doi:10.1016/j.memsci.2017.04.053

[16] LI, Manqing, Yingnan FENG, Kaiyu WANG, Wai Fen YONG, Liya YU a Tai-Shung CHUNG. Novel Hollow Fiber Air Filters for the Removal of Ultrafine Particles in PM2.5 with Repetitive Usage Capability. *Environmental Science & Technology* [online]. 2017, **51**(17), 10041–10049. ISSN 0013-936X. Dostupné z: doi:10.1021/acs.est.7b01494

[17] WANG, Liang-Yi, Liya E. YU, Juin-Yih LAI a Tai-Shung CHUNG. Developing Ultra-High Gas Permeance PVDF Hollow Fibers for Air Filtration Applications. *Separation and Purification Technology* [online]. nedatováno [vid. 2018-05-25]. ISSN 1383-5866. Dostupné z: doi:10.1016/j.seppur.2018.05.036

[18] XU, Huan, Wangyong JIN, Feng WANG, Chengcai LI, Jieqi WANG, Hailin ZHU a Yuhai GUO. Preparation and properties of PTFE hollow fiber membranes for the removal of ultrafine particles in PM2.5 with repetitive usage capability. *RSC Advances* [online]. 2018, **8**(67), 38245–38258. ISSN 2046-2069. Dostupné z: doi:10.1039/C8RA07789D

[19] KITZ Micro Filter Corporation. 株式会社キッツマイクロフィルター [online]. [vid. 2018-06-27]. Dostupné z: http://www.kitzmf.com/english/

[20] *Regulators & Filters Hollow Fiber Membrane Filter | Pisco Pneumatic Equipment* [online]. [vid. 2018-06-23]. Dostupné z: http://www.pisco.com/products/Hollow_Fiber_Membrane_Filter

[21] *SMC Pneumatics Pvt. Ltd., Clean Air Filter/Hollow Fiber Element SFD,* [online]. [vid. 2018-06-27]. Dostupné z: http://www.smcin.com/content/clean-air-filterhollow-fiber-element-sfd

[22] *Mitsubishi Chemical* [online]. [vid. 2018-06-05]. Dostupné z: https://www.m-chemical.co.jp/sterapore/en/arf_spec.html

[23] *Koyo Industries Co., Ltd.* [online]. [vid. 2018-05-24]. Dostupné z: http://www.koyo-industries.jp/product/jopla/joplaxFilter.html

[24] *Hollow Fiber Filter, 0.2 um, Female/Male Luer; 12/Pk from Cole-Parmer* [online]. [vid. 2018-05-24]. Dostupné z: https://www.coleparmer.com/i/hollow-fiber-filter-0-2-um-female-male-luer-12-pk/2951050

[25] *FL0020 – Filter for Ionizing Nozzles | Transforming Technologies* [online]. [vid. 2018-05-24]. Dostupné z: http://transforming-technologies.com/product/fl0020-filter-for-ionizing-nozzles/

[26] *Zena Membranes s.r.o.* [online]. Dostupné z: www.zena-membranes.cz/

[27] EARNEST, G. a M. GRESSEL. *256. Guidance on the Use of Filtration and Air Cleaning Systems for Protecting Building Environments From Airborne Chemical, Biological, or Radiological Attacks*. 2003. ISBN 10.3320/1.2758028.

[28] SUTHERLAND, Ken. Air filtration: Keeping the air that we breathe clean. *Filtration Separation* [online]. 2013, **50**(4), 77–125. Dostupné z: doi:10.1002/9780470172926.ch4

[29] Practical filtration: Improving indoor air quality. *Filtration + Separation* [online]. 2013, **50**(1), 34–35. ISSN 0015-1882. Dostupné z: doi:10.1016/S0015-1882(13)70035-1

[30] SENNETT, Paul. Air filtration: All filters are not created equal. *Filtration & Separation* [online]. 2008, **45**(1), 24–26. ISSN 0015-1882. Dostupné z: doi:10.1016/S0015-1882(08)70026-0

[31] GINESTET, Alain, Dominique PUGNET a Laure MOURADIAN. Air filtration: Air filters for balanced ventilation systems. *Filtration + Separation* [online]. 2013, **50**(1), 30–33. ISSN 0015-1882. Dostupné z: doi:10.1016/S0015-1882(13)70034-X

[32] TOWNSEND, Terry. Indoor air quality: Clean, green HVAC machine. *Filtration* [online]. 2007, **44**(1), 24–26. ISSN 00151882. Dostupné z: doi:10.1016/S0015-1882(07)70022-8

[33] PAN, N. a W. ZHONG. Fluid Transport Phenomena in Fibrous Materials. *Textile Progress* [online]. 2006, **38**(2), 1–93. ISSN 0040-5167. Dostupné z: doi:10.1533/tepr.2006.0002

[34] PAN, Shu-Yuan, Pengchen WANG, Qian CHEN, Wenju JIANG, Ying-Hao CHU a Pen-Chi CHIANG. Development of high-gravity technology for removing particulate and gaseous pollutant emissions: Principles and applications. *Journal of Cleaner Production* [online]. 2017, **149**, 540–556. ISSN 0959-6526. Dostupné z: doi:10.1016/j.jclepro.2017.02.108

[35] New product: Filter media for High Efficiency Air filtration uses has energy-saving characteristics. *Filtration + Separation* [online]. 2013, **50**(6), 22–25. ISSN 0015-1882. Dostupné z: doi:10.1016/S0015-1882(13)70238-6

[36] MONTGOMERY, James F., Sheldon I. GREEN, Steven N. ROGAK a Karen BARTLETT. Predicting the energy use and operation cost of HVAC air filters. *Energy and Buildings* [online]. 2012, **47**, 643–650. ISSN 03787788. Dostupné z: doi:10.1016/j.enbuild.2012.01.001

[37] *Lydall Performance Materials | Filtration Media* [online]. [vid. 2018-06-28]. Dostupné z: http://lydallpm.com/

[38] LIU, Jingxian, David Y. H. PUI a Jing WANG. Removal of airborne nanoparticles by membrane coated filters. *Science of The Total Environment* [online]. 2011, **409**(22), 4868–4874. ISSN 0048-9697. Dostupné z: doi:10.1016/j.scitotenv.2011.08.011

[39] CHEN, Sheng-Chieh, Jing WANG, Heinz FISSAN a David Y. H. PUI. Exposure assessment of nanosized engineered agglomerates and aggregates using Nuclepore filter. *Journal of Nanoparticle Research* [online]. 2013, **15**(10). ISSN 1388-0764. Dostupné z: doi:10.1007/s11051-013-1955-0

[40] CIRQUEIRA, Samirys Sara Rodrigues, Eduardo Hiromitsu TANABE a Mônica Lopes AGUIAR. Evaluation of operating conditions during the pulse jet cleaning filtration using different surface treated fibrous filters. *Process Safety and Environmental Protection* [online]. 2017, **105**, 69–78. ISSN 09575820. Dostupné z: doi:10.1016/j.psep.2016.10.010

[41] WANG, Jing a Paolo TRONVILLE. Toward standardized test methods to determine the effectiveness of filtration media against airborne nanoparticles. *Journal of Nanoparticle Research* [online]. 2014, **16**(6). ISSN 1388-0764. Dostupné z: doi:10.1007/s11051-014-2417-z

[42] ZHU, Miaomiao, Dawei HUA, Hui PAN, Fei WANG, Bella MANSHIAN, Stefaan J. SOENEN, Ranhua XIONG a Chaobo HUANG. Green electrospun and crosslinked poly(vinyl alcohol)/poly(acrylic acid) composite membranes for antibacterial effective air filtration. *Journal of Colloid and Interface Science* [online]. 2018, **511**, 411–423. ISSN 0021-9797. Dostupné z: doi:10.1016/j.jcis.2017.09.101

[43] LI, Jing, Danzhen ZHANG, Tingting YANG, Shen YANG, Xudong YANG a Hongwei ZHU. Nanofibrous membrane of graphene oxide-in-polyacrylonitrile composite with low filtration resistance for the effective capture of PM2.5. *Journal of Membrane Science* [online]. 2018, **551**, 85–92. ISSN 0376-7388. Dostupné z: doi:10.1016/j.memsci.2018.01.025

[44] WANG, Zhe a Zhijuan PAN. Preparation of hierarchical structured nano-sized/porous poly(lactic acid) composite fibrous membranes for air filtration. *Applied Surface Science* [online]. 2015, **356**, 1168–1179. ISSN 01694332. Dostupné z: doi:10.1016/j.apsusc.2015.08.211

[45] ZHU, Miaomiao, Dawei HUA, Ming ZHONG, Lingfeng ZHANG, Fang WANG, Buhong GAO, Ranhua XIONG a Chaobo HUANG. Antibacterial and Effective Air Filtration Membranes by "Green" Electrospinning and Citric Acid Crosslinking. *Colloid and Interface Science Communications* [online]. 2018, **23**, 52–58. ISSN 2215-0382. Dostupné z: doi:10.1016/j.colcom.2018.01.002

[46] HU, Juanping, Xianfeng WANG, Bin DING, Jinyou LIN, Jianyong YU a Gang SUN. One-step Electro-spinning/netting Technique for Controllably Preparing Polyurethane Nano-fiber/net. *Macromolecular Rapid Communications* [online]. nedatováno, **32**(21), 1729–1734. ISSN 1521-3927. Dostupné z: doi:10.1002/marc.201100343

[47] WANG, Xianfeng, Bin DING, Gang SUN, Moran WANG a Jianyong YU. Electro-spinning/netting: A strategy for the fabrication of three-dimensional polymer nano-fiber/nets. *Progress in Materials Science* [online]. 2013, **58**(8), 1173–1243. ISSN 0079-6425. Dostupné z: doi:10.1016/j.pmatsci.2013.05.001

[48] ROSO, Martina, Carlo BOARETTI, Alessandra LORENZETTI a Michele MODESTI. Electrospun Nanofibrous Membranes. In: *Encyclopedia of Membranes* [online]. B.m.: Springer, Berlin, Heidelberg, 2016 [vid. 2018-06-28], s. 666–670. Dostupné z: doi:10.1007/978-3-662-44324-8_1545

[49] DING, Bin a Jianyong YU, ed. *Electrospun Nanofibers for Energy and Environmental Applications* [online]. Berlin, Heidelberg: Springer Berlin Heidelberg, 2014 [vid. 2018-06-28]. Nanostructure Science and Technology. ISBN 978-3-642-54159-9. Dostupné z: doi:10.1007/978-3-642-54160-5

[50] Nanofibrous Membrane with Functionalized Surface. In: *Surface Engineering of Polymer Membranes* [online]. B.m.: Springer, Berlin, Heidelberg, 2009 [vid. 2018-06-28], Advanced Topics in Science and Technology in China, s. 306–328. ISBN 978-3-540-88412-5. Dostupné z: doi:10.1007/978-3-540-88413-2_10

[51] FOCARETE, Maria Letizia, Chiara GUALANDI a Seeram RAMAKRISHNA. *Filtering Media by Electrospinning: Next Generation Membranes for Separation Applications*. B.m.: Springer, 2018. ISBN 978-3-319-78163-1.

[52] WANG, Zhen, Feng YAN, Hongchang PEI, Jianxin LI, Zhenyu CUI a Benqiao HE. Antibacterial and environmentally friendly chitosan/polyvinyl alcohol blend membranes for air filtration. *Carbohydrate Polymers* [online]. 2018, **198**, 241–248. ISSN 0144-8617. Dostupné z: doi:10.1016/j.carbpol.2018.06.090

[53] HUANG, Zhao-Xia, Xiaoxiao LIU, Xu ZHANG, Shing-Chung WONG, George G. CHASE, Jin-Ping QU a Avinash BAJI. Electrospun polyvinylidene fluoride containing nanoscale graphite platelets as electret membrane and its application in air filtration under extreme environment. *Polymer* [online]. 2017, **131**, 143–150. ISSN 0032-3861. Dostupné z: doi:10.1016/j.polymer.2017.10.033

[54] JIANG, Pan, Xinglei ZHAO, Yuyao LI, Yalong LIAO, Ting HUA, Xia YIN, Jianyong YU a Bin DING. Moisture and oily molecules stable nanofibrous electret membranes for effectively capturing PM2.5. *Composites Communications* [online]. 2017, **6**, 34–40. ISSN 2452-2139. Dostupné z: doi:10.1016/j.coco.2017.08.004

[55] SU, Jiafei, Guohong YANG, Cuilian CHENG, Chen HUANG, He XU a Qinfei KE. Hierarchically structured TiO2/PAN nanofibrous membranes for high-efficiency air filtration and toluene degradation. *Journal of Colloid and Interface Science* [online]. 2017, **507**, 386–396. ISSN 0021-9797. Dostupné z: doi:10.1016/j.jcis.2017.07.104

[56] LIU, Xiaobing, Hamid SOUZANDEH, Yudong ZHENG, Yajie XIE, Wei-Hong ZHONG a Cai WANG. Soy protein isolate/bacterial cellulose composite membranes for high efficiency particulate air filtration. *Composites Science and Technology* [online]. 2017, **138**, 124–133. ISSN 0266-3538. Dostupné z: doi:10.1016/j.compscitech.2016.11.022

[57] CAO, Jinshan, Zhiqiang CHENG, Lijuan KANG, Yingying ZHANG, Xiaodong ZHAO, Shengzhe ZHAO a Bo GAO. Novel anti-fouling polyethersulfone/polyamide 66 membrane preparation for air filtration by electrospinning. *Materials Letters* [online]. 2017, **192**, 12–16. ISSN 0167-577X. Dostupné z: doi:10.1016/j.matlet.2017.01.037

[58] ZHONG, Longgang, Tao WANG, Liyuan LIU, Wenhao DU a Sheng WANG. Ultra-fine SiO2 nanofilament-based PMIA: A double network membrane for efficient filtration of

PM particles. *Separation and Purification Technology* [online]. 2018, **202**, 357–364. ISSN 1383-5866. Dostupné z: doi:10.1016/j.seppur.2018.03.053

[59] AL-ATTABI, Riyadh, Ludovic F. DUMÉE, Jürg A. SCHÜTZ a Yosry MORSI. Pore engineering towards highly efficient electrospun nanofibrous membranes for aerosol particle removal. *Science of The Total Environment* [online]. 2018, **625**, 706–715. ISSN 0048-9697. Dostupné z: doi:10.1016/j.scitotenv.2017.12.342

[60] CHENG, Zhiqiang, Jinshan CAO, Lijuan KANG, Yunqing LUO, Tingting LI a Wencong LIU. Novel transparent nano-pattern window screen for effective air filtration by electrospinning. *Materials Letters* [online]. 2018, **221**, 157–160. ISSN 0167-577X. Dostupné z: doi:10.1016/j.matlet.2018.03.110

[61] CHANG, Meng-Jie, Xiao-Jiao CHAI, Wen-Na CUI a Jun LIU. Facile Fabrication of Electrospun Silica Nanofibrous Membrane with Hydrophobic, Oleophilic and Breathable Performances. *Fibers and Polymers* [online]. 2018, **19**(4), 760–766. ISSN 1229-9197, 1875-0052. Dostupné z: doi:10.1007/s12221-018-1021-8

[62] WONG, Dannee, Erwan VERRON, Andri ANDRIYANA a Bee Chin ANG. Constitutive modeling of randomly oriented electrospun nanofibrous membranes. *Continuum Mechanics and Thermodynamics* [online]. 2018, 1–13. ISSN 0935-1175, 1432-0959. Dostupné z: doi:10.1007/s00161-018-0687-x

[63] YANG, Guohong, Jiafei SU, Yaping GUO, He XU a Qinfei KE. Fabrication of TiO2/PI composite nanofibrous membrane with enhanced photocatalytic activity and mechanical property via simultaneous electrospinning. *Journal of Materials Science* [online]. 2017, **52**(9), 5404–5416. ISSN 0022-2461, 1573-4803. Dostupné z: doi:10.1007/s10853-017-0785-3

[64] DEUBER, Fabian, Sara MOUSAVI, Lukas FEDERER, Marco HOFER a Christian ADLHART. Exploration of Ultralight Nanofiber Aerogels as Particle Filters: Capacity and Efficiency. *ACS Applied Materials & Interfaces* [online]. 2018, **10**(10), 9069–9076. ISSN 1944-8244. Dostupné z: doi:10.1021/acsami.8b00455

[65] YI, Zhibing, Pan CHENG, Jiahui CHEN, Ke LIU, Qiongzhen LIU, Mufang LI, Weibing ZHONG, Wenwen WANG, Zhentan LU a Dong WANG. PVA-co-PE Nanofibrous Filter Media with Tailored Three-dimensional Structure for High Performance and Safe Aerosol Filtration via Suspension-drying Procedure. *Industrial & Engineering Chemistry Research* [online]. 2018 [vid. 2018-06-29]. ISSN 0888-5885. Dostupné z: doi:10.1021/acs.iecr.8b02523

[66] KIM, Han-Jung, Seon Joo PARK, Chul Soon PARK, Thanh-Hai LE, Sang HUN LEE, Tai Hwan HA, Hyoung-il KIM, Jinyeong KIM, Chang-Soo LEE, Hyeonseok YOON a Oh Seok KWON. Surface-modified polymer nanofiber membrane for high-efficiency microdust capturing. *Chemical Engineering Journal* [online]. 2018, **339**, 204–213. ISSN 1385-8947. Dostupné z: doi:10.1016/j.cej.2018.01.121

[67] *EN 1822:2009 - High efficiency air filters (EPA, HEPA and ULPA)*. 2009

[68] VINH, Nguyen a Hyung-Man KIM. Electrospinning Fabrication and Performance Evaluation of Polyacrylonitrile Nanofiber for Air Filter Applications. *Applied Sciences* [online]. 2016, **6**(9), 235-. ISSN 2076-3417. Dostupné z: doi:10.3390/app6090235

[69] ASMATULU, Ramazan, Harish MUPPALLA, Zeinab VEISI, Waseem KHAN, Abu ASADUZZAMAN a Nurxat NURAJE. Study of Hydrophilic Electrospun Nanofiber Membranes for Filtration of Micro and Nanosize Suspended Particles. *Membranes* [online]. 2013, **3**(4), 375–388. ISSN 2077-0375. Dostupné z: doi:10.3390/membranes3040375

[70] ZANDER, Nicole, Margaret GILLAN a Daniel SWEETSER. Recycled PET Nanofibers for Water Filtration Applications. *Materials* [online]. 2016, **9**(4), 247-. ISSN 1996-1944. Dostupné z: doi:10.3390/ma9040247

[71] BEATRIZ, Suárez-Peña, Negral LUIS, Castrillón LEONOR, Megido LAURA, Marañón ELENA a Fernández-Nava YOLANDA. Imaging Techniques and Scanning Electron Microscopy as Tools for Characterizing a Si-Based Material Used in Air Monitoring Applications. *Materials* [online]. 2016, **9**(2), 109-. ISSN 1996-1944. Dostupné z: doi:10.3390/ma9020109

[72] BALAMURUGAN, Ramalingam, Subramanian SUNDARRAJAN a Seeram RAMAKRISHNA. Recent Trends in Nanofibrous Membranes and Their Suitability for Air and Water Filtrations. *Membranes* [online]. 2011, **1**(4), 232–248. ISSN 2077-0375. Dostupné z: doi:10.3390/membranes1030232

[73] CYRS, W. D., D. A. BOYSEN, G. CASUCCIO, T. LERSCH a T. M. PETERS. Nanoparticle collection efficiency of capillary pore membrane filters. *Journal of Aerosol Science* [online]. 2010, **41**(7), 655–664. ISSN 00218502. Dostupné z: doi:10.1016/j.jaerosci.2010.04.007

[74] SPURNY, K. R. a J. W. GENTRY. Aerosol fractionization by graded nuclepore filters. A review. *Powder Technology* [online]. 1979, **24**(2), 129–142. ISSN 0032-5910. Dostupné z: doi:10.1016/0032-5910(79)87029-1

[75] SHAW, G. E. Nuclepore filters as diffusion screens: Effect of barrel-shaped pore distortions. *Journal of Aerosol Science* [online]. 1985, **16**(4), 307–313. ISSN 0021-8502. Dostupné z: doi:10.1016/0021-8502(85)90038-2

[76] GENTRY, J. W a K. R SPURNY. Measurements of collection efficiency of nuclepore filters for asbestos fibers. *Journal of Colloid and Interface Science* [online]. 1978, **65**(1), 174–180. ISSN 0021-9797. Dostupné z: doi:10.1016/0021-9797(78)90269-2

[77] ROMO-KRÖGER, Carlos M. A qualitative study of atmospheric aerosols and particles deposited on flat membrane surfaces by microscopy and other techniques. *Powder Technology* [online]. 2006, **161**(3), 235–241. ISSN 00325910. Dostupné z: doi:10.1016/j.powtec.2005.10.014

[78] MADDINENI, Ajay Kumar, Dipayan DAS a Ravi Mohan DAMODARAN. Air-borne particle capture by fibrous filter media under collision effect: A CFD-based approach. *Separation and Purification Technology* [online]. 2018, **193**, 1–10. ISSN 13835866. Dostupné z: doi:10.1016/j.seppur.2017.10.065

[79] KASPER, Gerhard, Stefan SCHOLLMEIER, Jörg MEYER a Jürgen HOFERER. The collection efficiency of a particle-loaded single filter fiber. *Journal of Aerosol Science* [online]. 2009, **40**(12), 993–1009. ISSN 00218502. Dostupné z: doi:10.1016/j.jaerosci.2009.09.005

[80] WANG, J., D. R. CHEN a D. Y. H. PUI. Modeling of filtration efficiency of nanoparticles in standard filter media. *Journal of Nanoparticle Research* [online]. 2007, **9**(1), 109–115. ISSN 1388-0764. Dostupné z: doi:10.1007/s11051-006-9155-9

[81] KIRSCH, A. A. a N. A. FUCHS. Studies on Fibrous Aerosol Filters—III Diffusional Deposition of Aerosols in Fibrous Filters. *The Annals of Occupational Hygiene* [online]. 1968, 299–304. ISSN 1475-3162. Dostupné z: doi:10.1093/annhyg/11.4.299

[82] STECHKINA, I., A. KIRSCH a N. FUCHS. Studies on Fibrous Aerosol Filters—IV Calculation of Aerosol Deposition in Model Filters in the Range of Maximum Penetration. *The Annals of Occupational Hygiene* [online]. 1969, **12**, 1–8. ISSN 1475-3162. Dostupné z: doi:10.1093/annhyg/12.1.1

[83] PICH, J. The filtration theory of highly dispersed aerosols. *Staub Reinhalt. Luft*. 1965, **5**, 16–23.

[84] LEE, K. W. a B. Y. H. LIU. Theoretical Study of Aerosol Filtration by Fibrous Filters. *Aerosol Science and Technology* [online]. 1982, **1**(2), 147–161. ISSN 0278-6826. Dostupné z: doi:10.1080/02786828208958584

[85] KIRSCH, A. A. a I. B. STECHKINA. The Theory of Aerosol Filtration with Fibrous Filters. In: *Fundamentals of Aerosol Science*. New York: Shaw, D.T. Ed. Viley, 1978.

[86] LIU, B. Y. H. a K. L. RUBOW. Efficiency, pressure drop and figure of merit of high efficiency fibrous and membrane filter media. In: *5th World filtration Congress, Nice, 5-8 Juin 1990*. B.m.: Société Francaise de Filtration, Paris, 1990, s. 112.

[87] PAYET, S., D. BOULAUD, G. MADELAINE a A. RENOUX. Penetration and pressure drop of a HEPA filter during loading with submicron liquid particles. *Journal of Aerosol Science* [online]. 1992, **23**(7), 723–735. ISSN 00218502. Dostupné z: doi:10.1016/0021-8502(92)90039-X

[88] KUWABARA, Sinzi. The Forces experienced by Randomly Distributed Parallel Circular Cylinders or Spheres in a Viscous Flow at Small Reynolds Numbers. *Journal of the Physical Society of Japan* [online]. 1959, **14**(4), 527–532. ISSN 0031-9015. Dostupné z: doi:10.1143/JPSJ.14.527

[89] BAŁAZY, Anna a Albert PODGÓRSKI. Deposition efficiency of fractal-like aggregates in fibrous filters calculated using Brownian dynamics method. *Journal of Colloid and Interface Science* [online]. 2007, **311**(2), 323–337. ISSN 00219797. Dostupné z: doi:10.1016/j.jcis.2007.03.008

[90] ZHANG, Yuanhui. *Indoor air quality engineering*. 1. vyd. Boca Raton, Florida: CRC Press, c2005. ISBN 978-1-56670-674-2.

[91] HORACE LAMB. *Hydrodynamics* [online]. B.m.: University Press, 1916 [vid. 2018-05-20]. Dostupné z: http://archive.org/details/hydrodynamics02lambgoog

[92] LANGMUIR, I. OSRD Report No. 865. 1942.

[93] STECHKINA, I. B. a N. A. F. FUCHS. Studies on Fibrous Aerosol Filters—I. Calculation of Diffusional Deposition of Aerosols in Fibrous Filters. *The Annals of Occupational Hygiene* [online]. 1966, 59–64. ISSN 1475-3162. Dostupné z: doi:10.1093/annhyg/9.2.59

[94] LEE, K. W. a J. A. GIESEKE. Note on the approximation of interceptional collection efficiencies. *Journal of Aerosol Science* [online]. 1980, **11**(4), 335–341. ISSN 00218502. Dostupné z: doi:10.1016/0021-8502(80)90041-5

[95] PICH, J. The effectiveness of the barrier effect in fiber filters at small Knudsen numbers. *Staub Reinhalt. Luft.* 1966, **26**, 1–4.

[96] LANDAHL, H. D. a R. G. HERRMANN. Sampling of liquid aerosols by wires, cylinders, and slides, and the efficiency of impaction of the droplets. *Journal of Colloid Science* [online]. 1949, **4**(2), 103–136. ISSN 00958522. Dostupné z: doi:10.1016/0095-8522(49)90038-0

[97] SALEH, A. M., S. A. HOSSEINI, H. Vahedi TAFRESHI a B. POURDEYHIMI. 3-D microscale simulation of dust-loading in thin flat-sheet filters: A comparison with 1-D macroscale simulations. *Chemical Engineering Science* [online]. 2013, **99**, 284–291. ISSN 00092509. Dostupné z: doi:10.1016/j.ces.2013.06.007

[98] GOUGEON, R., D. BOULAUD a A. RENOUX. Comparison of theory and experiment in stationary filtration. *Journal of Aerosol Science* [online]. 1993, **24**, S273–S274. ISSN 00218502. Dostupné z: doi:10.1016/0021-8502(93)90229-3

[99] FRIEDLANDER, S. K. Aerosol Filtration by Fibrous Filters. In: *Biochemical and Biological Engineering Science*. 1. vyd. London: Academic Press, 1967, s. 49–67. ISBN 978-0-12-103601-0.

[100] ZHU, Chao, Chao-Hsin LIN a Chun Shun CHEUNG. Inertial impaction-dominated fibrous filtration with rectangular or cylindrical fibers. *Powder Technology* [online]. 2000, **112**(1–2), 149–162. ISSN 00325910. Dostupné z: doi:10.1016/S0032-5910(99)00315-0

[101] SUNEJA, S. K. a C. H. LEE. Aerosol filtration by fibrous filters at intermediate Reynolds numbers ($\leq$ 100). *Atmospheric Environment (1967)* [online]. 1974, **8**(11), 1081–1094. ISSN 00046981. Dostupné z: doi:10.1016/0004-6981(74)90043-2

[102] ILIAS, Shamsuddin a Peter L. DOUGLAS. Inertial impaction of aerosol particles on cylinders at intermediate and high reynolds numbers. *Chemical Engineering Science* [online]. 1989, **44**(1), 81–99. ISSN 0009-2509. Dostupné z: doi:10.1016/0009-2509(89)85235-2

[103] PTAK, T. a T. JAROSZCZYK. Theoretical-Experimental Aerosol Filtration Model for Fibrous Filters at Intermediate Reynolds Numbers. In: *Proceedings of the Fifth World Filtration Congress*. 1990, s. 566–572.

[104] CHAMBERS, Frank W., Abdel AL-SARKHI a Shenghong YAO. Velocity distribution effects in air filter testing. *Particulate Science and Technology* [online]. 2001, **19**(1), 1–21. ISSN 0272-6351. Dostupné z: doi:10.1080/02726350109709744

[105] PICH, J. Impaction of aerosol particles in the neighbourhood of a circular hole. *Collection of Czechoslovak Chemical Communications* [online]. 1964, **29**(9), 2223–2227. ISSN 0010-0765. Dostupné z: doi:10.1135/cccc19642223

[106] SPURNY, Kvetoslav, James P. LODGE, Evelyn R. FRANK a David C. SHEESLEY. Aerosol filtration by means of Nuclepore filters: structural and filtration properties. *Environ. Sci. Technol.* [online]. 1969, **3**(5), 453–464. ISSN 0013-936x. Dostupné z: doi:10.1021/es60028a004

[107] MANTON, M. J. Brownian diffusion of aerosols to the face of a nuclepore filter. *Atmospheric Environment (1967)* [online]. 1979, **13**(4), 525–531. ISSN 00046981. Dostupné z: doi:10.1016/0004-6981(79)90146-X

[108] RAJAGOPALAN, Rajamani a Chi TIEN. Trajectory analysis of deep-bed filtration with the sphere-in-cell porous media model. *AIChE Journal* [online]. 1976, **22**(3), 523–533. ISSN 0001-1541. Dostupné z: doi:10.1002/aic.690220316

[109] ZHONG, Wen a Ning PAN. Aerosol Filtration by Fibrous Filters: A Statistical Mechanics Approach. *Textile Research Journal* [online]. 2007, **77**(5), 284–289. ISSN 0040-5175. Dostupné z: doi:10.1177/0040517507078041

[110] ISRAELACHVILI, Jacob N. *Intermolecular and surface forces*. 3rd ed. Amsterdam: Elsevier, 2011. ISBN 978-0-12-375182-9.

[111] KIRSH, V. A. Gravitational Deposition of Aerosol Particles on a Fibrous Filter with Account for the Effect of Van der Waals Force. *Colloid Journal* [online]. 2001, **63**(1), 68–73. ISSN 1061-933X, 1608-3067. Dostupné z: doi:10.1023/A:1009494309020

[112] RABIEE, Marzie Babaie, Shahram TALEBI, Omid ABOUALI a Ehsan IZADPANAH. Investigation of the characteristics of particulate flows through fibrous filters using the lattice Boltzmann method. *Particuology* [online]. 2015, **21**, 90–98. ISSN 16742001. Dostupné z: doi:10.1016/j.partic.2014.11.010

[113] TIEN, Chi a B. V. RAMARAO. Mechanisms of particle deposition. *Granular Filtration of Aerosols and Hydrosols* [online]. 2007, 117–168. Dostupné z: doi:10.1016/B978-185617458-9/50005-1

[114] LI, Dongfei, Rong WANG a Tai-Shung CHUNG. Fabrication of lab-scale hollow fiber membrane modules with high packing density. *Separation and Purification Technology* [online]. 2004, **40**(1), 15–30. ISSN 13835866. Dostupné z: doi:10.1016/j.seppur.2003.12.019

[115] BORTOLASSI, A. C. C., V. G. GUERRA a M. L. AGUIAR. Characterization and evaluate the efficiency of different filter media in removing nanoparticles. *Separation and Purification Technology* [online]. 2017, **175**, 79–86. ISSN 13835866. Dostupné z: doi:10.1016/j.seppur.2016.11.010

[116] HUNG, Chi-Ho a Wallace Woon-Fong LEUNG. Filtration of nano-aerosol using nanofiber filter under low Peclet number and transitional flow regime. *Separation and Purification Technology* [online]. 2011, **79**(1), 34–42. ISSN 13835866. Dostupné z: doi:10.1016/j.seppur.2011.03.008

[117] YAO, Kuan-Mu, Mohammad T. HABIBIAN a Charles R. O'MELIA. Water and waste water filtration. Concepts and applications [online]. 1971, **5**(11), 1105–1112. ISSN 0013-936x. Dostupné z: doi:10.1021/es60058a005

[118] LEUNG, Wallace Woon-Fong, Chi-Ho HUNG a Ping-Tang YUEN. Effect of face velocity, nanofiber packing density and thickness on filtration performance of filters with nanofibers coated on a substrate. *Separation and Purification Technology* [online]. 2010, **71**(1), 30–37. ISSN 13835866. Dostupné z: doi:10.1016/j.seppur.2009.10.017

[119] BAO, Li, Kazuya SEKI, Hitoshi NIINUMA, Yoshio OTANI, Ratna BALGIS, Takashi OGI, Leon GRADON a Kikuo OKUYAMA. Verification of slip flow in nanofiber filter media through pressure drop measurement at low-pressure conditions. *Separation and Purification Technology* [online]. 2016, **159**, 100–107. ISSN 1383-5866. Dostupné z: doi:10.1016/j.seppur.2015.12.045

[120] YUE, Chang, Quan ZHANG a Zhiqiang ZHAI. Numerical simulation of the filtration process in fibrous filters using CFD-DEM method. *Journal of Aerosol Science* [online]. 2016, **101**, 174–187. ISSN 00218502. Dostupné z: doi:10.1016/j.jaerosci.2016.08.004

[121] CAI, Rong-Rong, Li-Zhi ZHANG a Yuying YAN. Performance prediction of PM 2.5 removal of real fibrous filters with a novel model considering rebound effect. *Applied Thermal Engineering* [online]. 2017, **111**, 1536–1547. ISSN 13594311. Dostupné z: doi:10.1016/j.applthermaleng.2016.07.162

[122] SERRANO, José Ramón, Héctor CLIMENT, Pedro PIQUERAS a Emanuele ANGIOLINI. Filtration modelling in wall-flow particulate filters of low soot penetration thickness. *Energy* [online]. 2016, **112**, 883–898. ISSN 0360-5442. Dostupné z: doi:10.1016/j.energy.2016.06.121

[123] CHEN, Sheng-Chieh, Yaorui HU, David Y. H. PUI a Jing WANG. Explicit expressions for the minimum efficiency and most penetrating particle size of Nuclepore filters. *Journal of Aerosol Science* [online]. 2016, **100**, 108–117. ISSN 00218502. Dostupné z: doi:10.1016/j.jaerosci.2016.07.008

[124] JUNG, Chang H., Hyun-Seol PARK a Yong P. KIM. Theoretical study for the most penetrating particle size of dust-loaded fiber filters. *Separation and Purification Technology* [online]. 2013, **116**, 248–252. ISSN 13835866. Dostupné z: doi:10.1016/j.seppur.2013.05.045

[125] JABRI, W., P. VROMAN a A. PERWUELZ. Study of the influence of synthetic filter media compressive behavior on its dust holding capacity. *Separation and Purification Technology* [online]. 2015, **156**, 92–102. ISSN 13835866. Dostupné z: doi:10.1016/j.seppur.2015.09.068

[126] CHANG, Cheng, Zhongli JI a Fanyong ZENG. The effect of a drainage layer on filtration performance of coalescing filters. *Separation and Purification Technology* [online]. 2016, **170**, 370–376. ISSN 13835866. Dostupné z: doi:10.1016/j.seppur.2016.06.006

[127] GAC, Jakub M., Anna JACKIEWICZ, Łukasz WERNER a Szymon JAKUBIAK. Consecutive filtration of solid particles and droplets in fibrous filters. *Separation and Purification Technology* [online]. 2016, **170**, 234–240. ISSN 13835866. Dostupné z: doi:10.1016/j.seppur.2016.06.057

[128] SAMBAER, Wannes, Martin ZATLOUKAL a Dusan KIMMER. 3D air filtration modeling for nanofiber based filters in the ultrafine particle size range. *Chemical Engineering Science* [online]. 2012, **82**, 299–311. ISSN 00092509. Dostupné z: doi:10.1016/j.ces.2012.07.031

[129] POPOVIĆ, Svetlana, Marcel DITTRICH a Jiři CAKL. Modelling of fouling of outside-in hollow-fiber membranes by TiO2 particles. *Separation and Purification Technology* [online]. 2015, **156**, 28–35. ISSN 13835866. Dostupné z: doi:10.1016/j.seppur.2015.08.028

[130] PARK, Hyun-Seol a Young Ok PARK. Filtration properties of electrospun ultrafine fiber webs. *Korean Journal of Chemical Engineering* [online]. 2005, **22**(1), 165–172. ISSN 0256-1115. Dostupné z: doi:10.1007/BF02701480

[131] THÉRON, Félicie, Aurélie JOUBERT a Laurence Le COQ. Numerical and experimental investigations of the influence of the pleat geometry on the pressure drop and velocity field of a pleated fibrous filter. *Separation and Purification Technology* [online]. 2017, **182**, 69–77. ISSN 13835866. Dostupné z: doi:10.1016/j.seppur.2017.02.034

[132] SHAO, P. a R. Y. M. HUANG. An analytical approach to the gas pressure drop in hollow fiber membranes. *Journal of Membrane Science* [online]. 2006, **271**(1–2), 69–76. ISSN 03767388. Dostupné z: doi:10.1016/j.memsci.2005.06.058

[133] MUNSON-MCGEE, Stuart H. An approximate analytical solution for the fluid dynamics of laminar flow in a porous tube. *Journal of Membrane Science* [online]. 2002, **197**(1–2), 223–230. ISSN 03767388. Dostupné z: doi:10.1016/S0376-7388(01)00634-2

[134] YOON, Seong-Hoon, Sangho LEE a Ik-Tae YEOM. Experimental verification of pressure drop models in hollow fiber membrane. *Journal of Membrane Science* [online]. 2008, **310**(1–2), 7–12. ISSN 03767388. Dostupné z: doi:10.1016/j.memsci.2007.11.048

[135] WANG, Jing, Drew THOMPSON a David Y. H. PUI. Integrative filtration research and sustainable nanotechnology. *Particuology* [online]. 2013, **11**(1), 5–13. ISSN 16742001. Dostupné z: doi:10.1016/j.partic.2012.06.004

[136] XU, Bin, Ya WU a Pengyi CUI. Semi-analytical and computational investigation of different dust loading structures affecting the performance of a fibrous air filter. *Particuology* [online]. 2014, **13**, 60–65. ISSN 16742001. Dostupné z: doi:10.1016/j.partic.2013.05.004

[137] XU, Bin, Yu GONG a Ya WU. Charged ultrafine particle filtration through vehicular cabin air filters. *Particuology* [online]. 2016, **28**, 1–5. ISSN 16742001. Dostupné z: doi:10.1016/j.partic.2015.09.012

[138] SONG, C. B. a H. S. PARK. Analytic solutions for filtration of polydisperse aerosols in fibrous filter. *Powder Technology* [online]. 2006, **170**(2), 64–70. ISSN 00325910. Dostupné z: doi:10.1016/j.powtec.2006.08.011

[139] SCHILLER, Sascha a Hans-Joachim SCHMID. Highly efficient filtration of ultrafine dust in baghouse filters using precoat materials. *Powder Technology* [online]. 2015, **279**, 96–105. ISSN 00325910. Dostupné z: doi:10.1016/j.powtec.2015.03.048

[140] WANG, Na, Zhigao ZHU, Junlu SHENG, Salem S. AL-DEYAB, Jianyong YU a Bin DING. Superamphiphobic nanofibrous membranes for effective filtration of fine particles. *Journal of Colloid and Interface Science* [online]. 2014, **428**, 41–48. ISSN 0021-9797. Dostupné z: doi:10.1016/j.jcis.2014.04.026

[141] PODGÓRSKI, Albert, Anna BAŁAZY a Leon GRADOŃ. Application of nanofibers to improve the filtration efficiency of the most penetrating aerosol particles in fibrous filters. *Chemical Engineering Science* [online]. 2006, **61**(20), 6804–6815. ISSN 00092509. Dostupné z: doi:10.1016/j.ces.2006.07.022

[142] BALGIS, Ratna, Christina W. KARTIKOWATI, Takashi OGI, Leon GRADON, Li BAO, Kazuya SEKI a Kikuo OKUYAMA. Synthesis and evaluation of straight and bead-free nanofibers for improved aerosol filtration. *Chemical Engineering Science* [online]. 2015, **137**, 947–954. ISSN 00092509. Dostupné z: doi:10.1016/j.ces.2015.07.038

[143] NICOSIA, A., T. KEPPLER, F. A. MÜLLER, B. VAZQUEZ, F. RAVEGNANI, P. MONTICELLI a F. BELOSI. Cellulose acetate nanofiber electrospun on nylon substrate as novel composite matrix for efficient, heat-resistant, air filters: note II. *Chemical Engineering Science* [online]. 2016, **153**, 284–294. ISSN 00092509. Dostupné z: doi:10.1016/j.ces.2016.07.017

[144] ZHANG, Xu, Xi YANG a George G. CHASE. Filtration performance of electrospun acrylonitrile-butadiene elastic fiber mats in solid aerosol filtration. *Separation and Purification Technology* [online]. 2017, **186**, 96–105. ISSN 13835866. Dostupné z: doi:10.1016/j.seppur.2017.06.002

[145] WANG, Qiang, Xiuli LIN a Da-Ren CHEN. Effect of dust loading rate on the loading characteristics of high efficiency filter media. *Powder Technology* [online]. 2016, **287**, 20–28. ISSN 00325910. Dostupné z: doi:10.1016/j.powtec.2015.09.032

[146] BOURROUS, S., L. BOUILLOUX, F. -X. OUF, P. LEMAITRE, P. NERISSON, D. THOMAS a J. C. APPERT-COLLIN. Measurement and modeling of pressure drop of HEPA filters clogged with ultrafine particles. *Powder Technology* [online]. 2016, **289**, 109–117. ISSN 0032-5910. Dostupné z: doi:10.1016/j.powtec.2015.11.020

[147] JIANG, Deqiang, Weidong ZHANG, Junteng LIU, Wang GENG a Zhongqi REN. Filtration and regeneration behavior of polytetrafluoroethylene membrane for dusty gas treatment. *Korean Journal of Chemical Engineering* [online]. 2008, **25**(4), 744. ISSN 0256-1115, 1975-7220. Dostupné z: doi:10.1007/s11814-008-0122-2

[148] AKBARNEZHAD, S., A. AMINI, A. Soltani GOHARRIZI, T. RAINEY a L. MORAWSKA. Capacity of quartz fibers with high filtration efficiency for capturing soot aerosol particles. *International Journal of Environmental Science and Technology* [online]. nedatováno. ISSN 1735-1472. Dostupné z: doi:10.1007/s13762-017-1457-1

[149] CHATTOPADHYAY, Saptarshi, T. Alan HATTON a Gregory C. RUTLEDGE. Aerosol filtration using electrospun cellulose acetate fibers. *Journal of Materials Science* [online]. 2016, **51**(1), 204–217. ISSN 0022-2461. Dostupné z: doi:10.1007/s10853-015-9286-4

[150] WANG, Xinpeng, Kitai KIM, Changhwan LEE a Jooyong KIM. Prediction of air filter efficiency and pressure drop in air filtration media using a stochastic simulation. *Fibers*

and Polymers [online]. 2008, **9**(1), 34–38. ISSN 1229-9197. Dostupné z: doi:10.1007/s12221-008-0006-4

[151] LIND, Terttaliisa, Steffen DANNER a Salih GUENTAY. Monodisperse fine aerosol generation using fluidized bed. *Powder Technology* [online]. 2010, **199**(3), 232–237. ISSN 00325910. Dostupné z: doi:10.1016/j.powtec.2010.01.011

[152] LING, Tsz Yan, Jing WANG a David Y. H. PUI. Measurement of filtration efficiency of Nuclepore filters challenged with polystyrene latex nanoparticles: experiments and modeling. *Journal of Nanoparticle Research* [online]. 2011, **13**(10), 5415–5424. ISSN 1388-0764. Dostupné z: doi:10.1007/s11051-011-0529-2

[153] CHEN, Sheng-Chieh, Jing WANG, Heinz FISSAN a David Y. H. PUI. Use of Nuclepore filters for ambient and workplace nanoparticle exposure assessment—Spherical particles. *Atmospheric Environment* [online]. 2013, **77**, 385–393. ISSN 13522310. Dostupné z: doi:10.1016/j.atmosenv.2013.05.007

[154] VANDERSTAPPEN, M. a R. Van GRIEKEN. Trace metal analysis of sediments and particulate matter in sea water by energy-dispersive X-ray fluorescence. *Fresenius' Zeitschrift für analytische Chemie* [online]. 1976, **282**(1), 25–30. ISSN 0016-1152, 1618-2650. Dostupné z: doi:10.1007/BF00443774

[155] MIRANDA, Javier, Ihali CRESPO a Maria Angeles MORALES. Absolute principal component analysis of atmospheric aerosols in Mexico city. *Environmental Science and Pollution Research* [online]. 2000, **7**(1), 14–18. ISSN 0944-1344, 1614-7499. Dostupné z: doi:10.1065/espr199910.006

[156] ATHARI, M., M. SOHRABPOUR, M. SHAHRIARI a S. ROSTAMI. Elemental characterization of TSP and two size fractions of airborne particulate matter from Tehran by INAA and AAS. *Journal of Radioanalytical and Nuclear Chemistry* [online]. 2004, **260**(2), 351–356. ISSN 0236-5731, 1588-2780. Dostupné z: doi:10.1023/B:JRNC.0000027108.93111.1e

[157] GODOI, Ricardo H. M., Sérgio J. GONÇALVES, Célia SAYAMA, Gabriela POLEZER, José M. Reis NETO, Bálint ALFÖLDY, René Van GRIEKEN, Carlos A. RIEDI, Carlos I. YAMAMOTO, Ana F. L. GODOI a László BENCS. Health implications of atmospheric aerosols from asbestos-bearing road pavements traditionally used in Southern Brazil. *Environmental Science and Pollution Research* [online]. 2016, **23**(24), 25180–25190. ISSN 0944-1344, 1614-7499. Dostupné z: doi:10.1007/s11356-016-7586-0

[158] OBAYASHI, Yumiko a Satoru SUZUKI. Adsorption of extracellular proteases in seawater onto filters during size fractionation. *Journal of Oceanography* [online]. 2008, **64**(3), 367–372. ISSN 0916-8370, 1573-868X. Dostupné z: doi:10.1007/s10872-008-0029-x

[159] BUDINOFF, Charles R., Star N. LOAR, Gary R. LECLEIR, Steven W. WILHELM a Alison BUCHAN. A protocol for enumeration of aquatic viruses by epifluorescence microscopy using Anodisc™ 13 membranes. *BMC Microbiology* [online]. 2011, **11**(1), 168. ISSN 1471-2180. Dostupné z: doi:10.1186/1471-2180-11-168

[160] LAFLEUR, John E. a Scott A. RICE. Induction of resistance to S. aureus in an environmental marine biofilm grown in Sydney Harbor, NSW, Australia. *World Journal of*

Microbiology and Biotechnology [online]. 2015, **31**(2), 353–358. ISSN 0959-3993, 1573-0972. Dostupné z: doi:10.1007/s11274-014-1787-9

[161] FAN, K. C., C. LEASEBURGE, Y. HYUN a J. GENTRY. Clogging in nuclepore filters: Cap formation model. *Atmospheric Environment (1967)* [online]. 1978, **12**(8), 1797–1802. ISSN 0004-6981. Dostupné z: doi:10.1016/0004-6981(78)90329-3

[162] BUZZARD, G. H. a J. P. BELL. Experimental filtration efficiencies for large pore nuclepore filters. *Journal of Aerosol Science* [online]. 1980, **11**(5), 435–438. ISSN 0021-8502. Dostupné z: doi:10.1016/0021-8502(80)90115-9

[163] LEE, K. W. a B. Y. H. LIU. On the Minimum Efficiency and the Most Penetrating Particle Size for Fibrous Filters. *Journal of the Air Pollution Control Association* [online]. 1980, **30**(4), 377–381. ISSN 0002-2470. Dostupné z: doi:10.1080/00022470.1980.10464592

[164] *ASTM F316-03 (2011) Standard Test Methods for Pore Size Characteristics of Membrane Filters by Bubble Point and Mean Flow Pore Test* [online]. B.m.: ASTM International. 2011. Dostupné z: https://www.astm.org/Standards/F316.htm

[165] ZÍKOVÁ, N., J. ONDRÁČEK a V. ŽDÍMAL. Size-Resolved Penetration Through High-Efficiency Filter Media Typically Used for Aerosol Sampling. *Aerosol Science and Technology* [online]. 2015, **49**(4), 239–249. ISSN 0278-6826. Dostupné z: doi:10.1080/02786826.2015.1020997

[166] SERFOZO, Norbert, Jakub ONDRÁČEK, Petr OTÁHAL, Mihalis LAZARIDIS a Vladimír ŽDÍMAL. Manikin-based size-resolved penetrations of CE-marked filtering facepiece respirators. *Journal of Occupational and Environmental Hygiene* [online]. 2017, **14**(12), 965–974. ISSN 1545-9624. Dostupné z: doi:10.1080/15459624.2017.1358816

[167] SERFOZO, Norbert, Jakub ONDRACEK, Nadezda ZIKOVA, Mihalis LAZARIDIS a Vladimir ZDIMAL. Size-Resolved Penetration of Filtering Materials from CE-Marked Filtering Facepiece Respirators. *Aerosol and Air Quality Research* [online]. 2017, **17**(5), 1305–1315. ISSN 1680-8584. Dostupné z: doi:10.4209/aaqr.2016.09.0390

[168] LEUNG, Wallace Woon-Fong a Curie Wing-Yi HAU. A model of backpulse and backblow cleaning of nanofiber filter loaded with nano-aerosols. *Separation and Purification Technology* [online]. 2016, **169**, 171–178. ISSN 1383-5866. Dostupné z: doi:10.1016/j.seppur.2016.06.007

[169] LEUNG, Wallace Woon-Fong a Curie Wing Yi HAU. Skin layer in cyclic loading-cleaning of a nanofiber filter in filtering nano-aerosols. *Separation and Purification Technology* [online]. 2017, **188**, 367–378. ISSN 1383-5866. Dostupné z: doi:10.1016/j.seppur.2017.07.043

[170] WOUDBERG, S. Permeability prediction of an analytical pore-scale model for layered and isotropic fibrous porous media. *Chemical Engineering Science* [online]. 2017, **164**, 232–245. ISSN 0009-2509. Dostupné z: doi:10.1016/j.ces.2017.01.061

[171] TOMADAKIS, Manolis M. a Teri J. ROBERTSON. Viscous Permeability of Random Fiber Structures: Comparison of Electrical and Diffusional Estimates with Experimental and Analytical Results. *Journal of Composite Materials* [online]. 2005, **39**(2), 163–188. ISSN 0021-9983. Dostupné z: doi:10.1177/0021998305046438

[172] HAPPEL, John. Viscous flow relative to arrays of cylinders. *AIChE Journal* [online]. 1959, **5**(2), 174–177. ISSN 1547-5905. Dostupné z: doi:10.1002/aic.690050211

[173] DRUMMOND, J. E. a M. I. TAHIR. Laminar viscous flow through regular arrays of parallel solid cylinders. *International Journal of Multiphase Flow* [online]. 1984, **10**(5), 515–540. ISSN 0301-9322. Dostupné z: doi:10.1016/0301-9322(84)90079-X

[174] GEBART, B.R. Permeability of Unidirectional Reinforcements for RTM. *Journal of Composite Materials* [online]. 1992, **26**(8), 1100–1133. ISSN 0021-9983. Dostupné z: doi:10.1177/002199839202600802

[175] DAVIES, C. N. The Separation of Airborne Dust and Particles. *Proceedings of the Institution of Mechanical Engineers, Part B: Management and engineering manufacture* [online]. 1953, **1**(1–12), 185–213. ISSN 0263-7146. Dostupné z: doi:10.1177/095440545300100113

[176] CLAGUE, D. S., B. D. KANDHAI, R. ZHANG a P. M. A. SLOOT. Hydraulic permeability of (un)bounded fibrous media using the lattice Boltzmann method. *Physical Review E* [online]. 2000, **61**(1), 616–625. Dostupné z: doi:10.1103/PhysRevE.61.616

[177] SIOUTAS, Constantinos. Experimental Investigation of Pressure Drop with Particle Loading in Nuclepore Filters. *Aerosol Science and Technology* [online]. 1999, **30**(1), 71–83. ISSN 0278-6826. Dostupné z: doi:10.1080/027868299304895

[178] ADZUMI, Hiroshi. Studies on the Flow of Gaseous Mixtures through Capillaries. III. The Flow of Gaseous Mixtures at Medium Pressures. *Bulletin of the Chemical Society of Japan* [online]. 1937, **12**(6), 292–303. ISSN 0009-2673. Dostupné z: doi:10.1246/bcsj.12.292

[179] NORDON, Robert E. a Klaus SCHINDHELM. Design of Hollow Fiber Modules for Uniform Shear Elution Affinity Cell Separation. *Artificial Organs* [online]. 1997, **21**(2), 107–115. ISSN 1525-1594. Dostupné z: doi:10.1111/j.1525-1594.1997.tb00346.x

[180] LIM, Keng, Hui AN, Peng WANG, Guiqin LIU, Simon YU, Keng Boon LIM, Hui AN, Peng Cheng WANG, Guiqin LIU a Simon Ching Man YU. Theoretical and Computational Analysis on Double-End Submerged Hollow Fibre Membrane Modules. *Energies* [online]. 2018, **11**(5), 1042. Dostupné z: doi:10.3390/en11051042

[181] TIEN, Chi a Bandaru V. RAMARAO. Can filter cake porosity be estimated based on the Kozeny–Carman equation? *Powder Technology* [online]. 2013, **237**, 233–240. ISSN 0032-5910. Dostupné z: doi:10.1016/j.powtec.2012.09.031

[182] KRUCZEK, Boguslaw. Carman–Kozeny Equation. In: Enrico DRIOLI a Lidietta GIORNO, ed. *Encyclopedia of Membranes* [online]. Berlin, Heidelberg: Springer Berlin Heidelberg, 2015 [vid. 2018-11-27], s. 1–3. ISBN 978-3-642-40872-4. Dostupné z: doi:10.1007/978-3-642-40872-4_1995-1

[183] VALDES-PARADA, Francisco J., J. Alberto OCHOA-TAPIA a Jose ALVAREZ-RAMIREZ. Validity of the permeability Carman–Kozeny equation: A volume averaging approach. *Physica A: Statistical Mechanics and its Applications* [online]. 2009, **388**(6), 789–798. ISSN 03784371. Dostupné z: doi:10.1016/j.physa.2008.11.024

[184] AGUIAR, M. L. a J. R. COURY. Cake Formation in Fabric Filtration of Gases. *Industrial & Engineering Chemistry Research* [online]. 1996, **35**(10), 3673–3679. ISSN 0888-5885. Dostupné z: doi:10.1021/ie960042p

[185] ITO, L. X. a M. L. AGUIAR. A study of the porosity of gas filtration cakes. *Brazilian Journal of Chemical Engineering* [online]. 2009, **26**(2), 307–315. ISSN 0104-6632. Dostupné z: doi:10.1590/S0104-66322009000200008

[186] LIU, Jingxian, Jacob J. SWANSON, David B. KITTELSON, David Y. H. PUI a Jing WANG. Microstructural and loading characteristics of diesel aggregate cakes. *Powder Technology* [online]. 2013, **241**, 244–251. ISSN 0032-5910. Dostupné z: doi:10.1016/j.powtec.2013.03.028

[187] CHENG, Yu-Hsiang a Chuen-Jinn TSAI. Factors Influencing Pressure Drop through a Dust Cake during Filtration. *Aerosol Science and Technology* [online]. 1998, **29**(4), 315–328. ISSN 0278-6826. Dostupné z: doi:10.1080/02786829808965572

[188] ERGUN, S. Fluid flow through packed columns. *Chemical Engineering Progress*. 1952, **48**(2), 89–94.

[189] DUKHAN, Nihad, Özer BAĞCI a Mustafa ÖZDEMIR. Experimental flow in various porous media and reconciliation of Forchheimer and Ergun relations. *Experimental Thermal and Fluid Science* [online]. 2014, **57**, 425–433. ISSN 0894-1777. Dostupné z: doi:10.1016/j.expthermflusci.2014.06.011

[190] NEIVA, Antonio C. B a Leonardo GOLDSTEIN. A procedure for calculating pressure drop during the build-up of dust filter cakes. *Chemical Engineering and Processing: Process Intensification* [online]. 2003, **42**(6), 495–501. ISSN 0255-2701. Dostupné z: doi:10.1016/S0255-2701(02)00066-1

[191] ENDO, Yoshiyuki, Da-Ren CHEN a David Y. H. PUI. Effects of particle polydispersity and shape factor during dust cake loading on air filters. *Powder Technology* [online]. 1998, **98**(3), 241–249. ISSN 0032-5910. Dostupné z: doi:10.1016/S0032-5910(98)00063-1

[192] LIN, Justin Chun-Te, Ta-Chih HSIAO, Shu-San HSIAU, Da-Ren CHEN, Yen-Kai CHEN, Sheng-Hsiu HUANG, Chih-Chieh CHEN a Moo-Been CHANG. Effects of temperature, dust concentration, and filtration superficial velocity on the loading behavior and dust cakes of ceramic candle filters during hot gas filtration. *Separation and Purification Technology* [online]. 2018, **198**, Filtering a Better Future, 146–154. ISSN 1383-5866. Dostupné z: doi:10.1016/j.seppur.2017.06.014

[193] VANNI, Marco. Creeping flow over spherical permeable aggregates. *Chemical Engineering Science* [online]. 2000, **55**(3), 685–698. ISSN 0009-2509. Dostupné z: doi:10.1016/S0009-2509(99)00316-4

[194] BRINKMAN, H. C. A Calculation of The Viscous Force Exerted by a Flowing Fluid on a Dense Swarm of Particles. *Applied Scientific Research*. 1947, **A1**, 27–34.

[195] HAPPEL, John. Viscous flow in multiparticle systems: Slow motion of fluids relative to beds of spherical particles. *AIChE Journal* [online]. 1958, **4**(2), 197–201. ISSN 1547-5905. Dostupné z: doi:10.1002/aic.690040214

[196] KIM, Sangtae a William B. RUSSEL. Modelling of porous media by renormalization of the Stokes equations. *Journal of Fluid Mechanics* [online]. 1985, **154**, 269–286. ISSN 1469-7645, 0022-1120. Dostupné z: doi:10.1017/S0022112085001525

[197] *ASHRAE 52.2-2017 - Method of Testing General Ventilation Air-Cleaning Devices for Removal Efficiency by Particle Size (ANSI Approved)* [online]. 2017 [vid. 2018-12-05]. Dostupné z: https://www.techstreet.com/standards/ashrae-52-2-2017?product_id=1942059

[198] *ISO 29463:2017, High efficiency filters and filter media for removing particles from air* [online]. B.m.: International Organization for Standardization. 2017 [vid. 2018-12-07]. Dostupné z: https://www.iso.org/obp/ui/#iso:std:iso:29463:-1:ed-2:v1:en

[199] *EN 779:2012 - Air filters for general ventilation* [online]. 2012 [vid. 2018-12-05]. Dostupné z: http://www.generalfilter.com/en/norms/en-7792012/

[200] *ISO 16890:2016 - Air filters for general ventilation* [online]. B.m.: International Organization for Standardization. 2016 [vid. 2018-12-05]. Dostupné z: http://www.iso.org/cms/render/live/en/sites/isoorg/contents/data/standard/05/78/57864.html

[201] *Eurovent – klasifikace energetické efektivity vzduchových filtrů pro celkové větrání | 1Filter* [online]. [vid. 2018-12-05]. Dostupné z: http://1filter.cz/cz/uzitecne-informace/normy/eurovent-klasifikace-energeticke-efektivity-vzduchovych-filtru-pro-celkove-vetrani.html

[202] MONTGOMERY, James F., Sheldon I. GREEN, Steven N. ROGAK a Karen BARTLETT. Predicting the energy use and operation cost of HVAC air filters. *Energy and Buildings* [online]. 2012, **47**, 643–650. ISSN 0378-7788. Dostupné z: doi:10.1016/j.enbuild.2012.01.001

[203] SUN, Christine a Dan WOODMAN. Delivering Sustainability Promise to HVAC Air Filtration-Part I: Classification of Energy Efficiency for Air Filters. *ASHRAE Transactions; Atlanta*. 2009, **115**, 581–585. ISSN 00012505.

[204] SUN, Christine. Delivering Sustainability Promise to HVAC Air Filtration: Part II: Life Cycle Sustainability of Air Filters. *ASHRAE Transactions; Atlanta*. 2010, **116**, 25–32. ISSN 00012505.

[205] GUSTAVSSON, J. New developments in air filter test methods and classification. *Filtration & Separation* [online]. 1996, **33**(2), 155–154. ISSN 0015-1882. Dostupné z: doi:10.1016/S0015-1882(97)84207-3

[206] ASHRAE Test Dust #2 Per ANSI/ASHRAE 52.2P. *Powder Technology Inc.* [online]. [vid. 2018-12-06]. Dostupné z: https://www.powdertechnologyinc.com/product/ashrae-test-dust-2/

[207] KUBULE, Anna, Liga ZOGLA, Janis IKAUNIEKS a Marika ROSA. Highlights on energy efficiency improvements: a case of a small brewery. *Journal of Cleaner Production* [online]. 2016, **138**, Sustainable consumption and production - Research, experience, and development, 275–286. ISSN 0959-6526. Dostupné z: doi:10.1016/j.jclepro.2016.02.131

[208] VERLEYE, B, M KLITZ, R CROCE, M GRIEBEL, S V LOMOV, D ROOSE a I VERPOEST. Predicting the permeability of textile reinforcements via a hybrid Navier-Stokes/Brinkmann solver. In: *The 8th International Conference on Flow Processes in Composite Materials (FPCM8)*. 2006, s. 8.

[209] SONG, C. B., H. S. PARK a K. W. LEE. Experimental study of filter clogging with monodisperse PSL particles. *Powder Technology* [online]. 2006, **163**(3), 152–159. ISSN 0032-5910. Dostupné z: doi:10.1016/j.powtec.2006.01.016

[210] AZIMI, Parham a Brent STEPHENS. HVAC filtration for controlling infectious airborne disease transmission in indoor environments: Predicting risk reductions and operational costs. *Building and Environment* [online]. 2013, **70**, 150–160. ISSN 03601323. Dostupné z: doi:10.1016/j.buildenv.2013.08.025

[211] LEE, Mooseok a Jeonghwan KIM. Analysis of local fouling in a pilot-scale submerged hollow-fiber membrane system for drinking water treatment by membrane autopsy. *Separation and Purification Technology* [online]. 2012, **95**, 227–234. ISSN 1383-5866. Dostupné z: doi:10.1016/j.seppur.2012.04.017

[212] MA, Chunyan, Yanbiao LIU, Fang LI, Chensi SHEN, Manhong HUANG, Zhiwei WANG, Chun CAO, Qizhe ZHOU, Yingzi SHENG a Wolfgang SAND. CFD simulations of fiber-fiber interaction in a hollow fiber membrane bundle: Fiber distance and position matters. *Separation and Purification Technology* [online]. 2019, **209**, 707–713. ISSN 13835866. Dostupné z: doi:10.1016/j.seppur.2018.09.029

[213] MU, Situ, Kang XIAO, Huiju FAN, Chun LIU, Shuai LIANG, Feng XIAO, Xiaomao WANG a Xia HUANG. Non-uniform distribution of adsorptive fouling along hollow fiber membrane: Characterization and quantification. *Separation and Purification Technology* [online]. 2018, **205**, 159–168. ISSN 1383-5866. Dostupné z: doi:10.1016/j.seppur.2018.05.043

[214] WU, Su-En, Yi-Chun LIN, Kuo-Jen HWANG, Tung-Wen CHENG a Kuo-Lun TUNG. High-efficiency hollow fiber arrangement design to enhance filtration performance by CFD simulation. *Chemical Engineering and Processing - Process Intensification* [online]. 2018, **125**, 87–96. ISSN 0255-2701. Dostupné z: doi:10.1016/j.cep.2018.01.003

[215] BEALE, S. B. a D. B. SPALDING. A numerical study of unsteady fluid flow in in-line and staggered tube banks. *Journal of Fluids and Structures* [online]. 1999, **13**(6), 723–754. ISSN 0889-9746. Dostupné z: doi:10.1006/jfls.1999.0231

[216] FLOAN, Benjamin W. a Ephraim M. SPARROW. Fluid Flow in Heat Exchangers Whose Flow Passages Contain Periodically Deployed Tubes. *Numerical Heat Transfer, Part A: Applications* [online]. 2012, **62**(2), 81–94. ISSN 1040-7782. Dostupné z: doi:10.1080/10407790.2012.685125

[217] ELSAYED, Khairy a Chris LACOR. CFD modeling and multi-objective optimization of cyclone geometry using desirability function, artificial neural networks and genetic algorithms. *Applied Mathematical Modelling* [online]. 2013, **37**(8), 5680–5704. ISSN 0307-904X. Dostupné z: doi:10.1016/j.apm.2012.11.010

[218] ZHAO, Bingtao a Yaxin SU. Artificial neural network-based modeling of pressure drop coefficient for cyclone separators. *Chemical Engineering Research and Design* [online]. 2010, **88**(5), 606–613. ISSN 0263-8762. Dostupné z: doi:10.1016/j.cherd.2009.11.010

[219] BRAR, Lakhbir Singh a Khairy ELSAYED. Analysis and optimization of cyclone separators with eccentric vortex finders using large eddy simulation and artificial neural network. *Separation and Purification Technology* [online]. 2018, **207**, 269–283. ISSN 1383-5866. Dostupné z: doi:10.1016/j.seppur.2018.06.013

[220] OLIVEIRA, D. C., C. a. K. ALMEIDA, L. G. M. VIEIRA, J. J. R. DAMASCENO a M. a. S. BARROZO. Influence of geometric dimensions on the performance of a filtering hydrocyclone: an experimental and cfd study. *Brazilian Journal of Chemical Engineering* [online]. 2009, **26**(3), 575–582. ISSN 0104-6632. Dostupné z: doi:10.1590/S0104-66322009000300013

[221] TAHERINEJAD, Morteza, John GORMAN, Ephraim SPARROW a Shahram DERAKHSHAN. Porous medium model of a hollow-fiber water filtration system. *Journal of Membrane Science* [online]. 2018, **563**, 210–220. ISSN 0376-7388. Dostupné z: doi:10.1016/j.memsci.2018.05.048

[222] FISK, W. J., D. FAULKNER, J. PALONEN a O. SEPPANEN. Performance and costs of particle air filtration technologies. *Indoor Air* [online]. 2002, **12**(4), 223–234. ISSN 0905-6947. Dostupné z: doi:10.1034/j.1600-0668.2002.01136.x

[223] GUSTAVSSON, Jan. Software programme that calculates the life cycle cost of air filters. *Filtration* [online]. 2002, **39**(9), 22–26. Dostupné z: doi:10.1016/s0015-1882(02)80240-3

[224] *Consumer price indices - inflation - August 2018 | CZSO* [online]. [vid. 2018-11-26]. Dostupné z: https://www.czso.cz/csu/czso/ari/consumer-price-indices-inflation-august-2018

[225] Czech National Bank. *CNB current forecast* [online]. [vid. 2018-11-26]. Dostupné z: https://www.cnb.cz/en/monetary_policy/forecast/index.html

[226] *Cena 1 kWh elektřiny (aktuální) 2018* [online]. [vid. 2018-11-26]. Dostupné z: https://www.energie123.cz/elektrina/ceny-elektricke-energie/cena-1-kwh/

10 Nomenclature

10.1 Abbreviations

ANOVA	analysis of variance
ANSI	American National Standards Institute
ASHRAE	American Society of Heating, Refrigerating and Air Conditioning Engineers
ASTM	American Society for Testing and Materials
CPC	condensation particle counter
CPM	capillary pore membrane
DEHS	diethylhexyl sebacate
DHC	dust holding capacity
EPA	efficient particulate air
HEPA	high efficiency particulate air
HFM	hollow-fiber membrane
HVAC	heating, ventilation and air conditioning
IAQ	indoor air quality
ISO	International Organization for Standardization
LCC	life-cycle cost
ME	minimum efficiency
MERV	minimum efficiency reporting value
MPPS	most penetrating particle size
PAA	poly(acrylic acid)
PAN-GO	polyacrylonitril-graphene oxide
PC	polycarbonate
PEG	polyethylene glycol
PES	polyester
PESF	polyethersulfone
PI	price increase
PLA	poly(lactic acid)
PP	polypropylene
PTFE	polytetrafluorethylene
PU/SLS	polyurethane-sodium laurylsulfonate
PVA	polyvinylalcohol
PVC	polyvinylchloride
PVDF	polyvinylidenefluoride
QF	quality factor
RUC	representative unit cell
SCE	single collector efficiency
SEM	scanning electron microscopy
SMPS	scanning mobility particle sizer
TMP	transmembrane pressure
ULPA	ultra-low penetration air
UPE	ultra-high molecular weight polyethylene

10.2 Symbols

a	(Pa)	constant in the pressure drop/dust load relationship
A	(m^2)	membrane surface area
a_M	(–)	HFM packing density
a_0	(nm)	adhesion distance
b	(g^{-1})	constant in the pressure drop/dust load relationship
B	(s^{-1})	constant in theoretical power consumption relationship
C_a	(–)	integration constant in Eq. S7.9
C_b	(–)	integration constant in Eq. S7.9
C_{down}	(cm^{-3})	particle concentration downstream of the membrane
C_c	(–)	Cunningham slip correction factor
C_s	(–)	Cunningham slip correction factor according to Fuchs
C_{up}	(cm^{-3})	particle concentration upstream of the membrane
C_1	(–)	constant in the Payet's relationship for diffusion efficiency
C_2	(–)	constant in the Payet's relationship for diffusion efficiency
Co_n	(€)	cost paid after n years
Co_p	(€)	present cost
d_f	(nm)	collector diameter
d_{MPPS}	(nm)	most penetrating particle diameter
d_o	(nm)	pore diameter
d_p	(nm)	particle diameter
d_{pi}	(nm)	particle diameter of a given size
d_{pg}	(nm)	geometric average particle diameter
d_{p32}	(nm)	Sauter average particle diameter
D	($m^2\ s^{-1}$)	diffusion coefficient
D_{bi}	(mm)	inner diameter of HFM bundle
D_i	(µm)	fiber inner diameter
D_o	(µm)	fiber outer diameter
DHC	($g\ m^{-2}\ h^{-1}$)	dust-holding capacity per unit membrane area and unit time
DHC_{exp}	(g)	dust-holding capacity obtained experimentally
DHC_{HFM}	(g)	max possible dust-holding capacity of HFM
DHC_{reg}	(g)	dust-holding capacity obtained from curve fit (regression)
E	kWh	energy consumption of filter operation
E_a	(J)	adhesion energy
Eu	(–)	Euler number
$f(\alpha)$	(–)	dimensionless permeability
$f(\varepsilon_c)$	(–)	void function
$f_l(\varepsilon_c)$	(–)	long-range effect void function
$f_s(\varepsilon_c)$	(–)	short-range effect void function
$F(\varepsilon_c)$	(–)	macroscopic function of particle-loaded membrane
G	(–)	sedimentation parameter
h	$m^2\ kg\ s^{-1}$	Planck constant
H	(–)	Hamaker constant

i	(–)	interest rate
I_{avg}	(A)	average electric current
I_{FI}	(€)	filter and installation investment cost
J	(mol s^{-1})	molar flowrate of permeate
k	(m^3 m^{-2} h^{-1} bar^{-1})	measured permeability of HFM
k_α	(m^2)	predicted permeability of HFM
k_B	(J K^{-1})	Boltzmann constant
Kn	(–)	particle Knudsen number
Kn_f	(–)	fiber Knudsen number
Kn_o	(–)	pore Knudsen number
Ku	(–)	Kuwabara hydrodynamic factor
L	(m)	hollow fiber length
LCC_E	(€)	life-cycle cost of electricity for fan operation
LCC_M	(€)	life-cycle cost of maintenance
LCC_D	(€)	life-cycle cost of disposal
m	(g)	dust accumulation in a filter
m_c	(g)	cake weight
m_{HFM}	(g)	dust accumulation on HFM
m_{load}	(g h^{-1})	dust loading rate
M	(g)	final dust loading
M_T	(g)	total dust load
M_w	(g mol^{-1})	molecular weight
n	(–)	number of years in discount factor calculation
n_i	(–)	number of pores/collectors of a given size from SEM pictures
n_{pi}	(–)	number of particles of a given size
n_1	(–)	refractive index of particle
n_2	(–)	refractive index of membrane surface
n_3	(–)	refractive index of fluid
N	(cm^{-3})	particle number concentration
N_D	(–)	ratio of diffusion displacement and pore size
N_f	(–)	number of fibers in HFM bundle
$N_{f(o)}$	(–)	number of measurements of collector/pore diameter from SEM pictures
N_p	(–)	number of pores per unit area of membrane
p_{atm}	(Pa)	atmospheric pressure
p_{de}	(Pa)	dead-end pressure
p_f	(Pa)	feed pressure
p_p	(Pa)	permeate pressure
p_s	(Pa)	suction pressure
p_1	(Pa)	upstream gas pressure
$\Delta p(m)$	(Pa)	pressure drop as a function of dust load
$\Delta p(t)$	(Pa)	pressure drop as a function of time
Δp_{avg}	(Pa)	average pressure drop
Δp_c	(Pa)	cake pressure drop

$\Delta p_{\text{c-o}}$	(Pa)	pressure drop at change out
Δp_{f}	(Pa)	final pressure drop
Δp_{i}	(Pa)	initial pressure drop
P_{w}	(W)	instantaneous power input
$P_{\text{w-avg}}$	(W)	average power input
Pe	(–)	Peclet number
Pn	(–)	penetration
Pr_{E}	(€)	electricity price
Q	($\text{m}^3\ \text{s}^{-1}$)	air flowrate
Q_{f}	($\text{m}^3\ \text{s}^{-1}$)	feed flowrate
Q_{p}	($\text{m}^3\ \text{s}^{-1}$)	permeate flowrate
R	(–)	interception parameter
R_{m}	($\text{J mol}^{-1}\ \text{K}^{-1}$)	molar gas constant
R_{o}	(–)	pore interception parameter
Re_{f}	(–)	collector Reynolds number
Re_{p}	(–)	particle-fluid Reynolds number
Re_{pp}	(–)	particle Reynolds number
Stk	(–)	Stokes number
t	(s, min, h)	time
t_{LC}	(h)	life cycle time
T	(K)	temperature
U	(m s^{-1})	face velocity
U_{p}	(m s^{-1})	particle velocity
U_{pm}	(m s^{-1})	permeate velocity
$\tilde{U}_{\text{avg}}$	(V)	average electric voltage
x	(m)	random position along hollow fiber length
X	(–)	coefficient in the Song and Park formula for MPPS
Y	(–)	coefficient in the Song and Park formula for MPPS
Z	(µm)	filter/membrane wall thickness
Z_{c}	(µm)	cake thickness
α	(–)	membrane solidity
β_1	(–)	coefficient for calculation of surface diffusion efficiency
β_2	(–)	coefficient for calculation of surface diffusion efficiency
γ	(–)	particle shape factor
δ	(–)	coefficient for calculation of surface diffusion efficiency
ε	(–)	membrane porosity
ε_{c}	(–)	cake porosity
ε_{p}	(–)	percolation threshold porosity
η	(–)	overall filtration efficiency
η_{A}	(–)	single collector efficiency due to adhesion
η_{f}	(–)	single collector efficiency
η_{D}	(–)	single collector efficiency due to (pore) diffusion
η_{DS}	(–)	collection efficiency due to diffusion on membrane surface

η_I	(–)	single collector efficiency due to inertial impaction
$\eta_{I'}$	(–)	impaction parameter
η_{min}	(–)	minimum efficiency
η_R	(–)	single collector efficiency due to interception
ϑ_e	(s^{-1})	main electronic absorption frequency
κ_{fan}	(–)	fan efficiency
κ_s	(–)	system efficiency
λ	(m)	mean free path of air molecules
μ	(Pa s)	dynamic viscosity
v	(m s^{-1})	critical particle velocity
ξ	(–)	coefficient for calculation of impaction parameter
ρ	(kg m^{-3})	fluid density
ρ_p	(kg m^{-3})	particle density
σ_{pg}	(m)	particle size geometric standard deviation
φ_1	(–)	static dielectric constant of particle
φ_2	(–)	static dielectric constant of membrane surface
φ_3	(–)	static dielectric constant of fluid
ψ	(m^{-1})	parameter in Eq. (S7.12)
ω	(–)	constant in the Tomadakis and Robertson permeability model
Ω	(–)	Adzumi constant

11 List of figures

12 List of tables

Appendix I - Supplementary material

A I.1 Supplementary material to Chapter 3

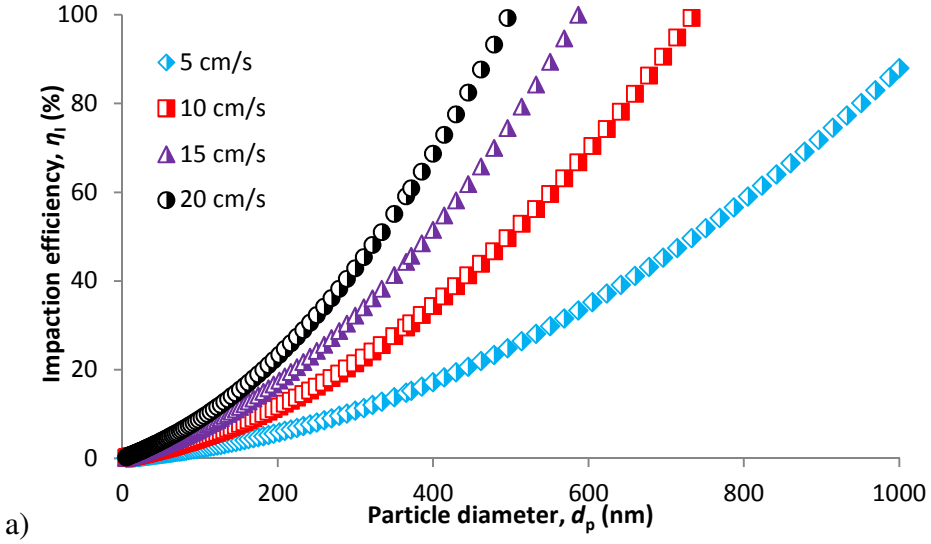

a)

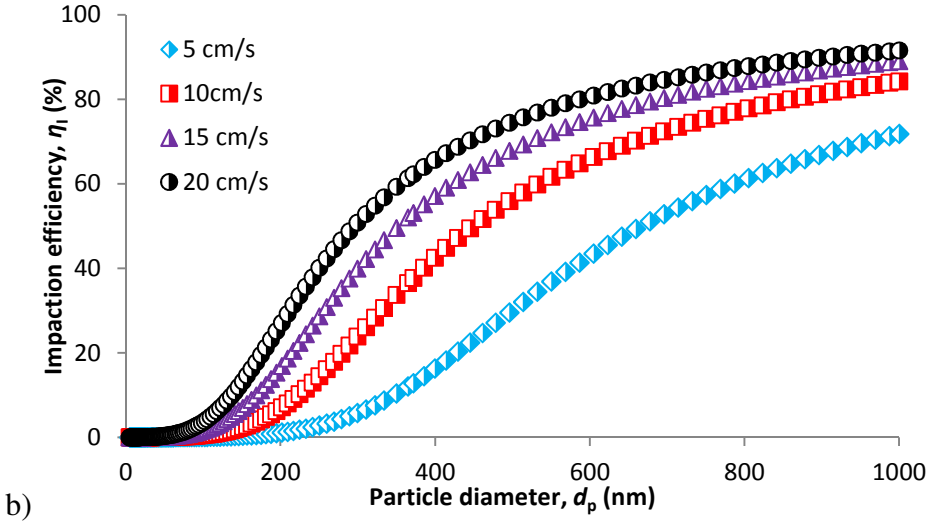

b)

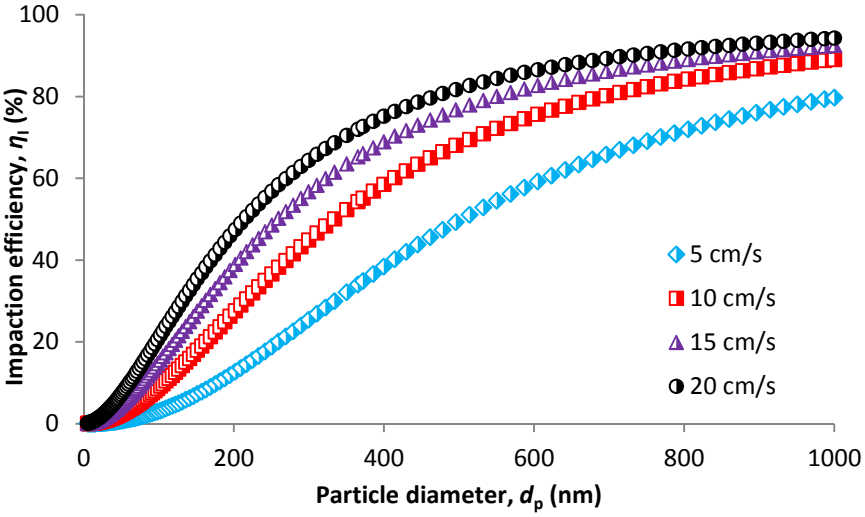

c)

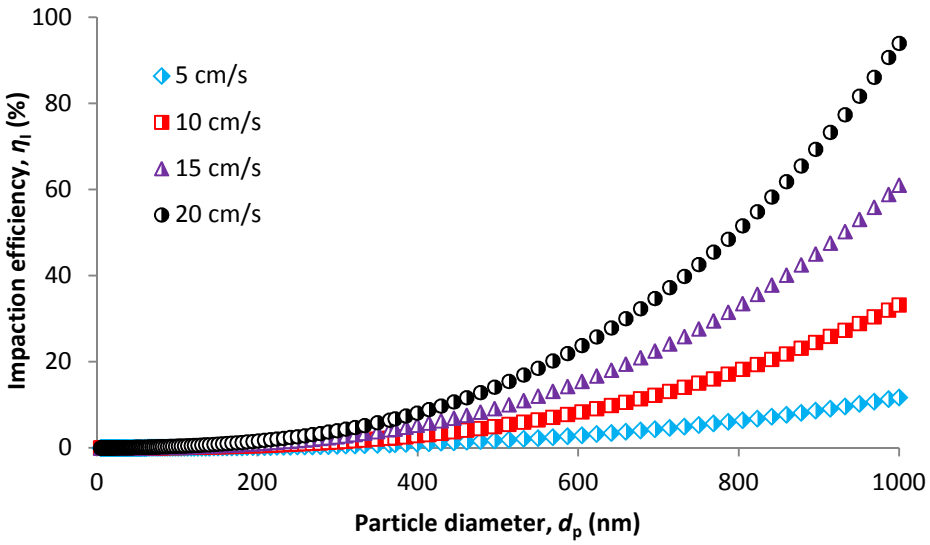
100
80
60
40
20
0
0
200
400
600
800
1000
5 cm/s
10 cm/s
15 cm/s
20 cm/s
Impaction efficiency, η_I (%)
Particle diameter, d_p (nm)

d)

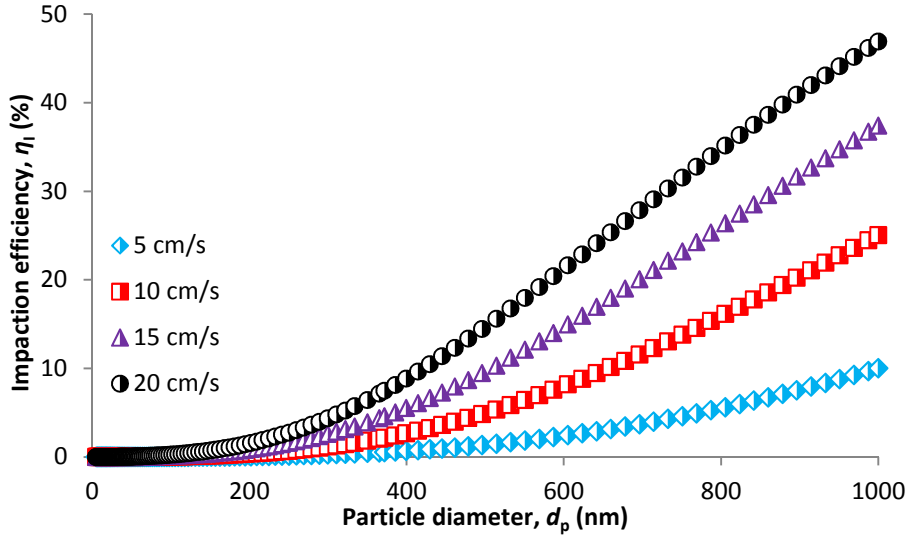
50
40
30
20
10
0
0
200
400
600
800
1000
5 cm/s
10 cm/s
15 cm/s
20 cm/s
Impaction efficiency, η_I (%)
Particle diameter, d_p (nm)

e)

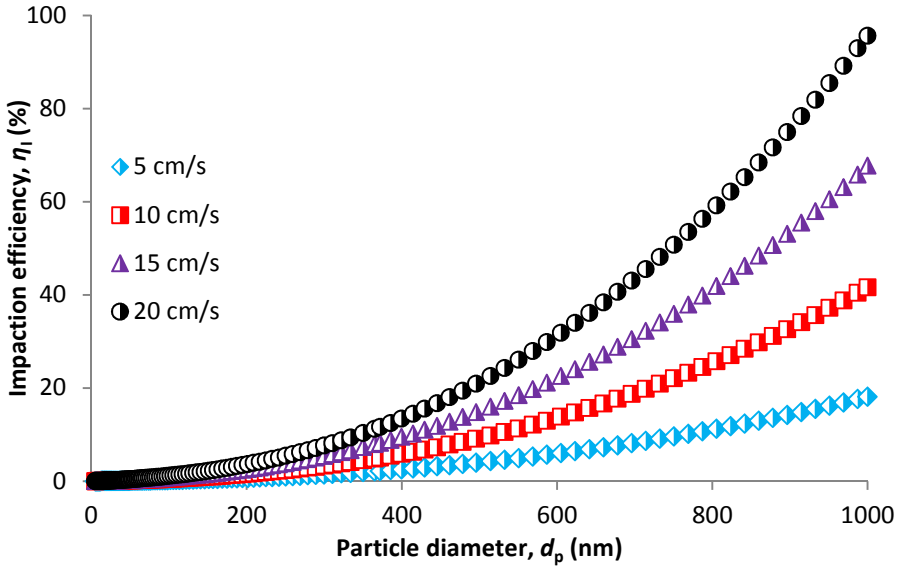
100
80
60
40
20
0
0
200
400
600
800
1000
5 cm/s
10 cm/s
15 cm/s
20 cm/s
Impaction efficiency, η_I (%)
Particle diameter, d_p (nm)

f)

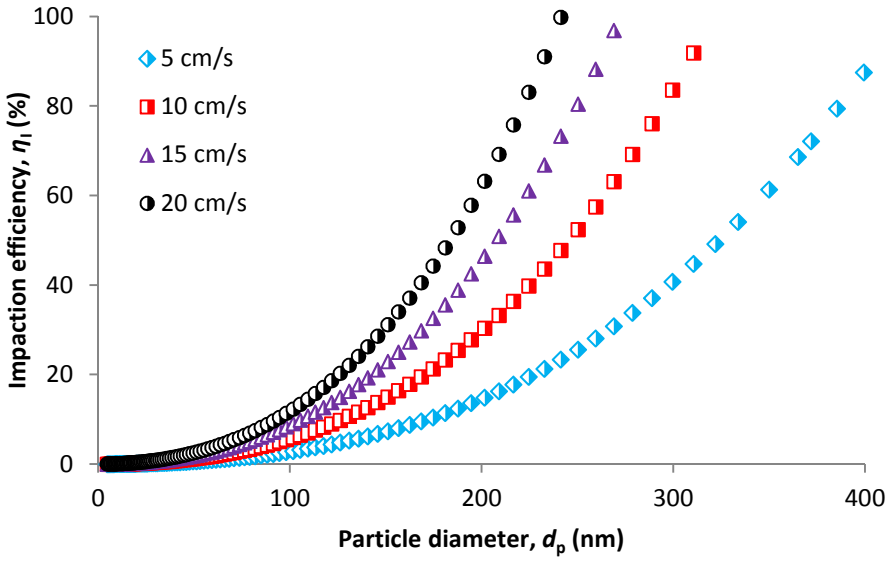

g)

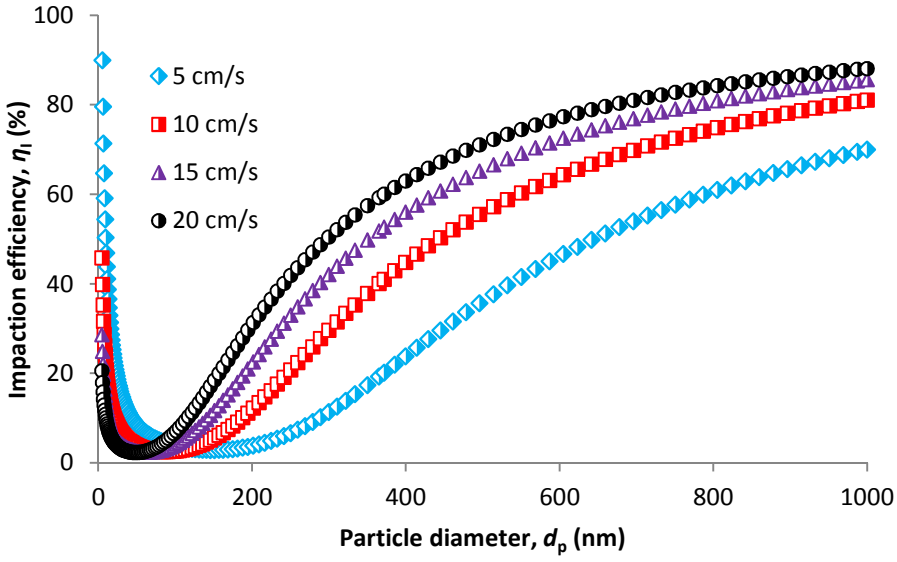

h)

Fig. S3.1: *SCE due to inertial impaction based on model of Stechkina et al. (a), Landahl and Herman (b), Fuchs (c), Gougeon et al. (d), Suneja and Lee (e), Friedlander (f), Zhu et al. (g) and Illias and Douglas (h)*

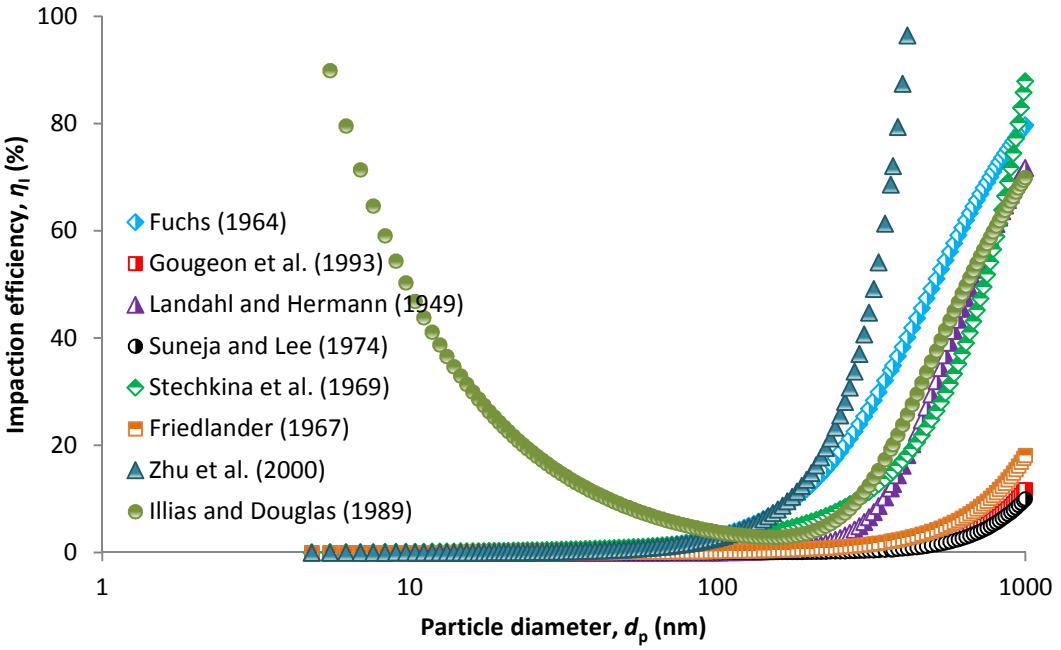

a)

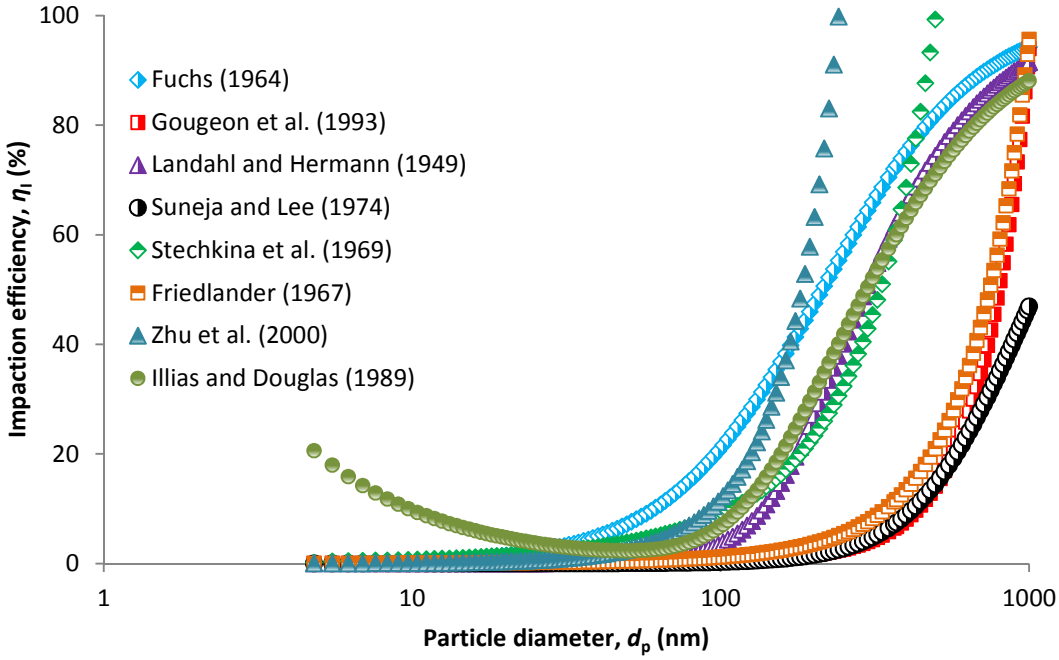

b)

Fig. S3.2: *Comparison of impaction efficiency based on different models and airflow velocity of 5 cm/s (a) and 20 cm/s (b)*

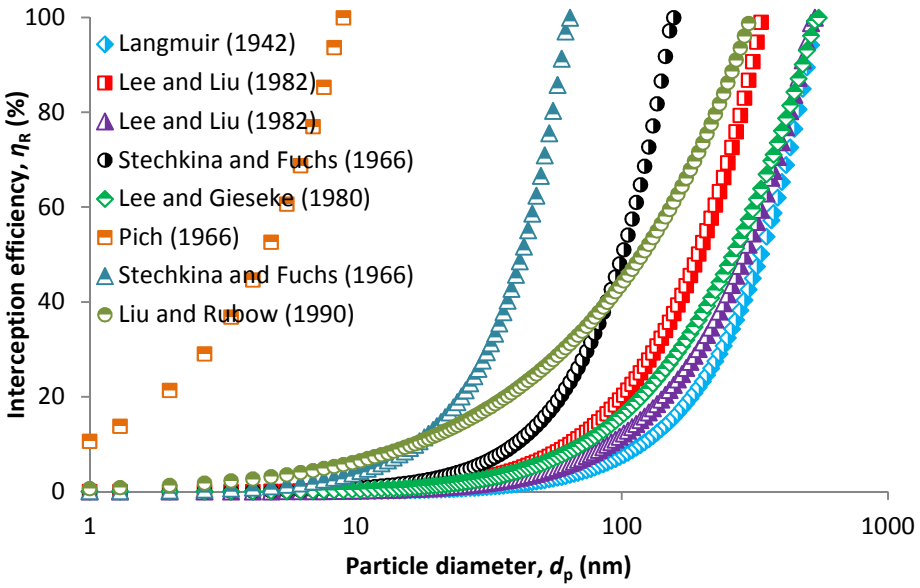

Fig. S3.3: *Comparison of SCE due to interception based on models developed by various researchers*

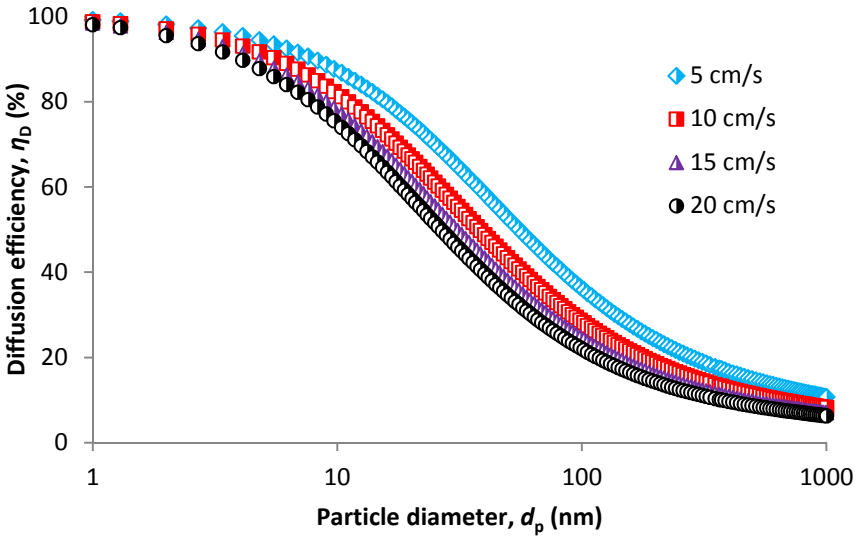

a)

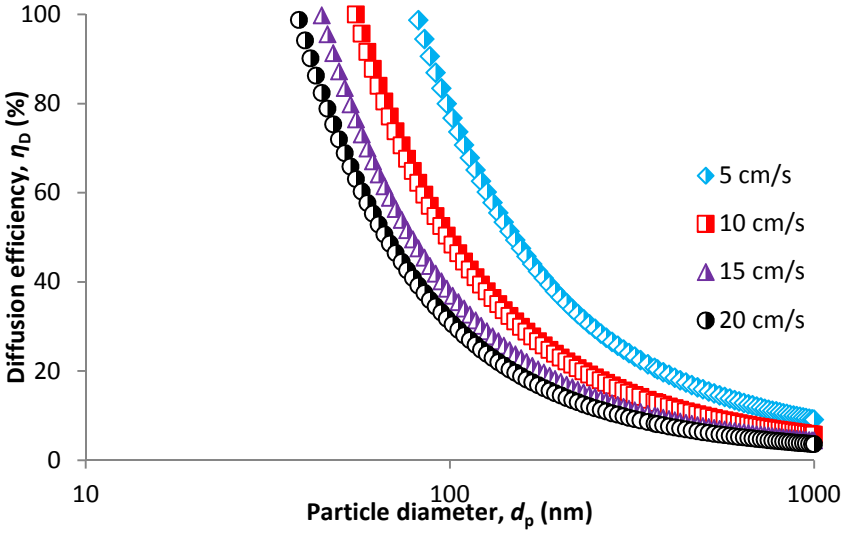

b)

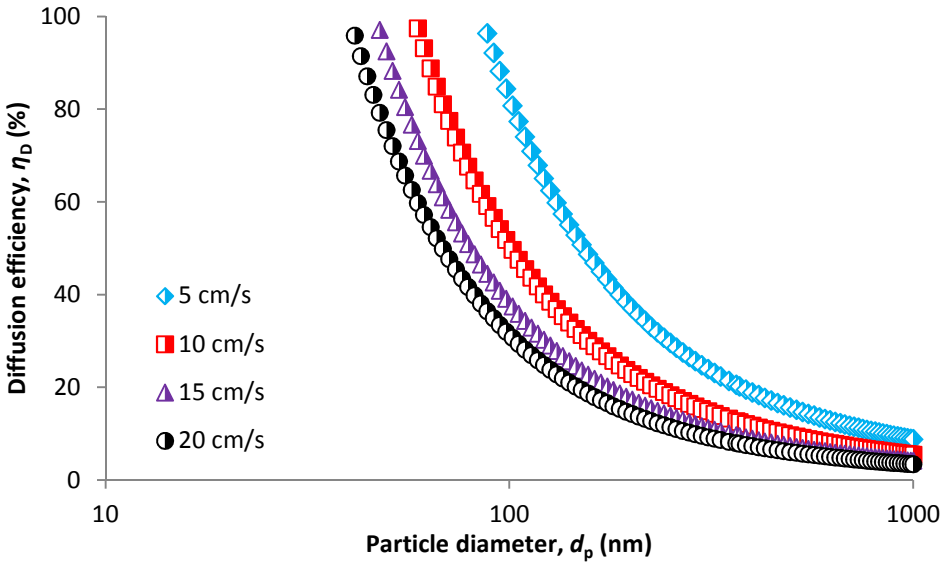
Diffusion efficiency, η_D (%)
100
80
60
40
20
0
10
100
1000
Particle diameter, d_p (nm)
5 cm/s
10 cm/s
15 cm/s
20 cm/s

c)

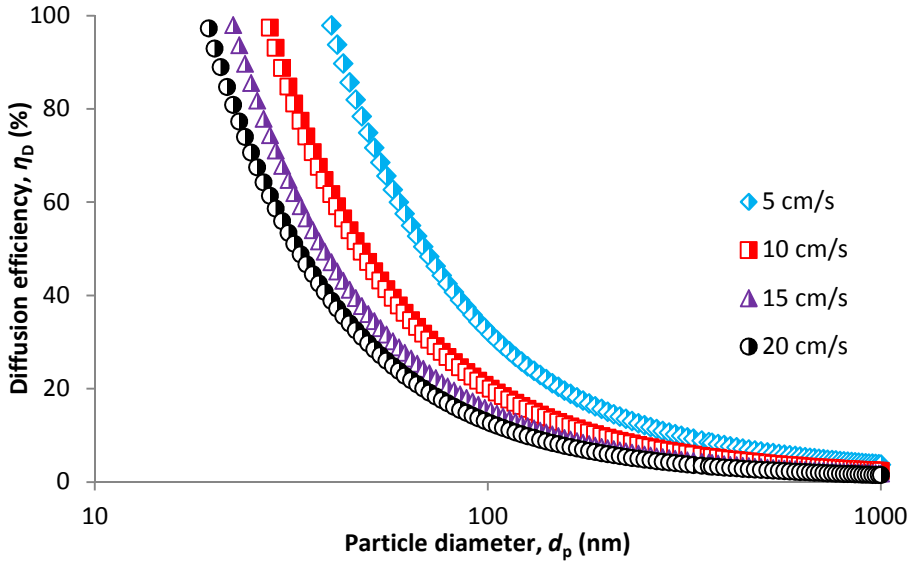
Diffusion efficiency, η_D (%)
100
80
60
40
20
0
10
100
1000
Particle diameter, d_p (nm)
5 cm/s
10 cm/s
15 cm/s
20 cm/s

d)

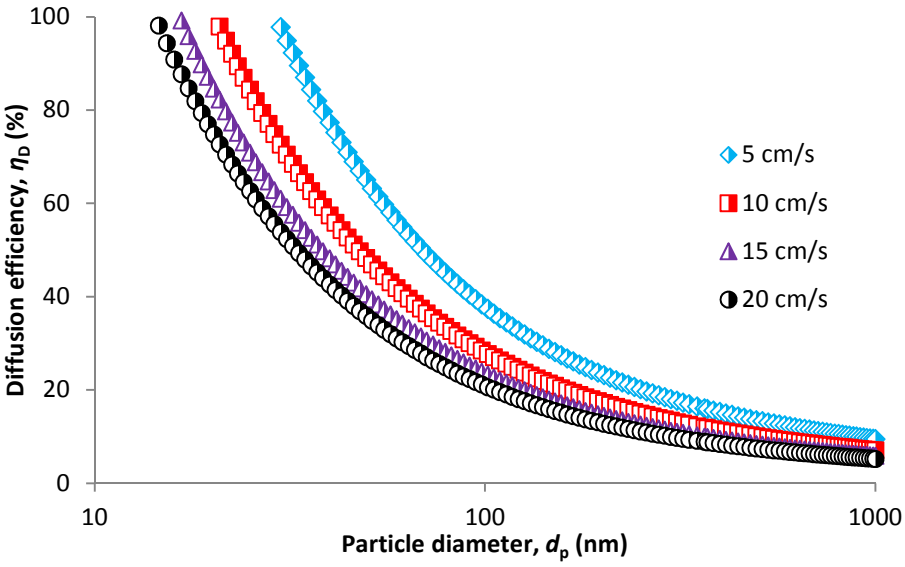
Diffusion efficiency, η_D (%)
100
80
60
40
20
0
10
100
1000
Particle diameter, d_p (nm)
5 cm/s
10 cm/s
15 cm/s
20 cm/s

e)

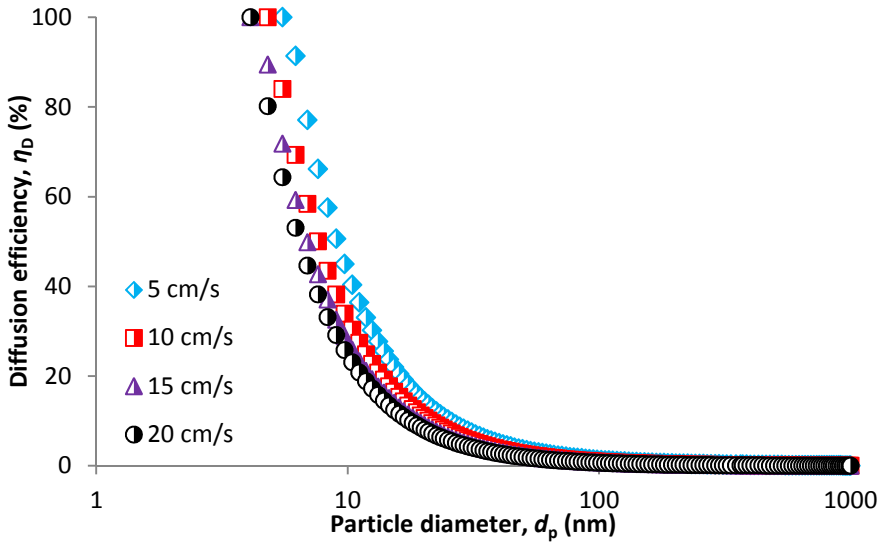

f)

Fig. S3.4: *SCE due to diffusion mechanism based on mathematical models developed by Payet et al. (a), Kirsch and Fuchs (b), Stechkina et al. (c), Lee and Liu (d), Wang et al. (e) and Pich (f)*

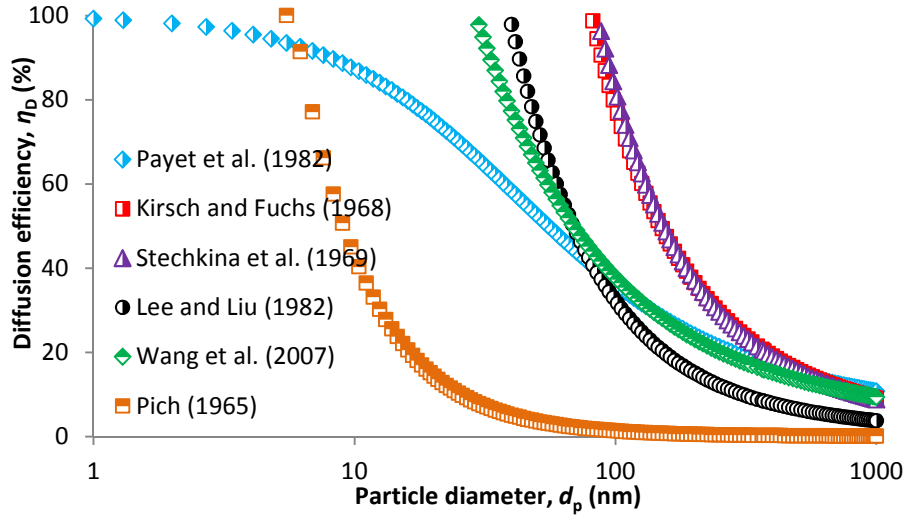

a)

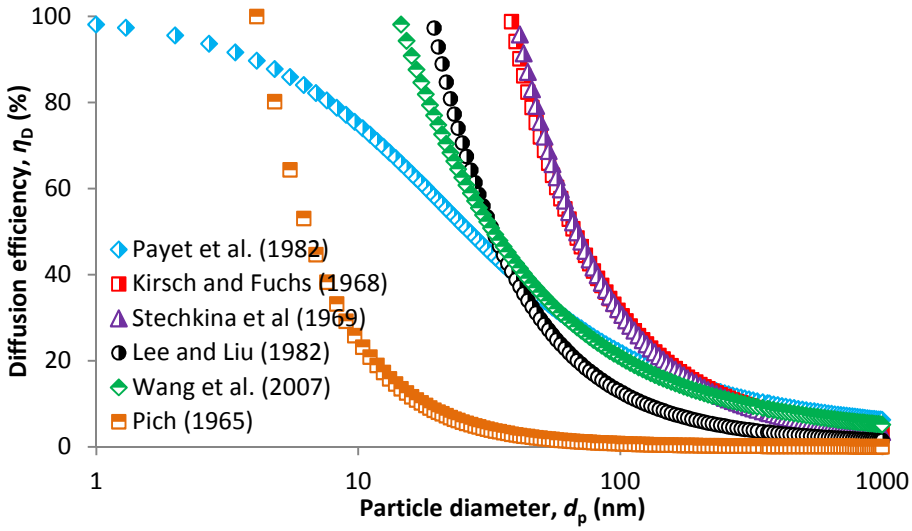

b)

Fig. S3.5: *Comparison of SCE due to diffusion mechanism based on different models for an airflow velocity of 5 cm/s (a) and 20 cm/s (b)*

A I.2 Supplementary material to Chapter 4

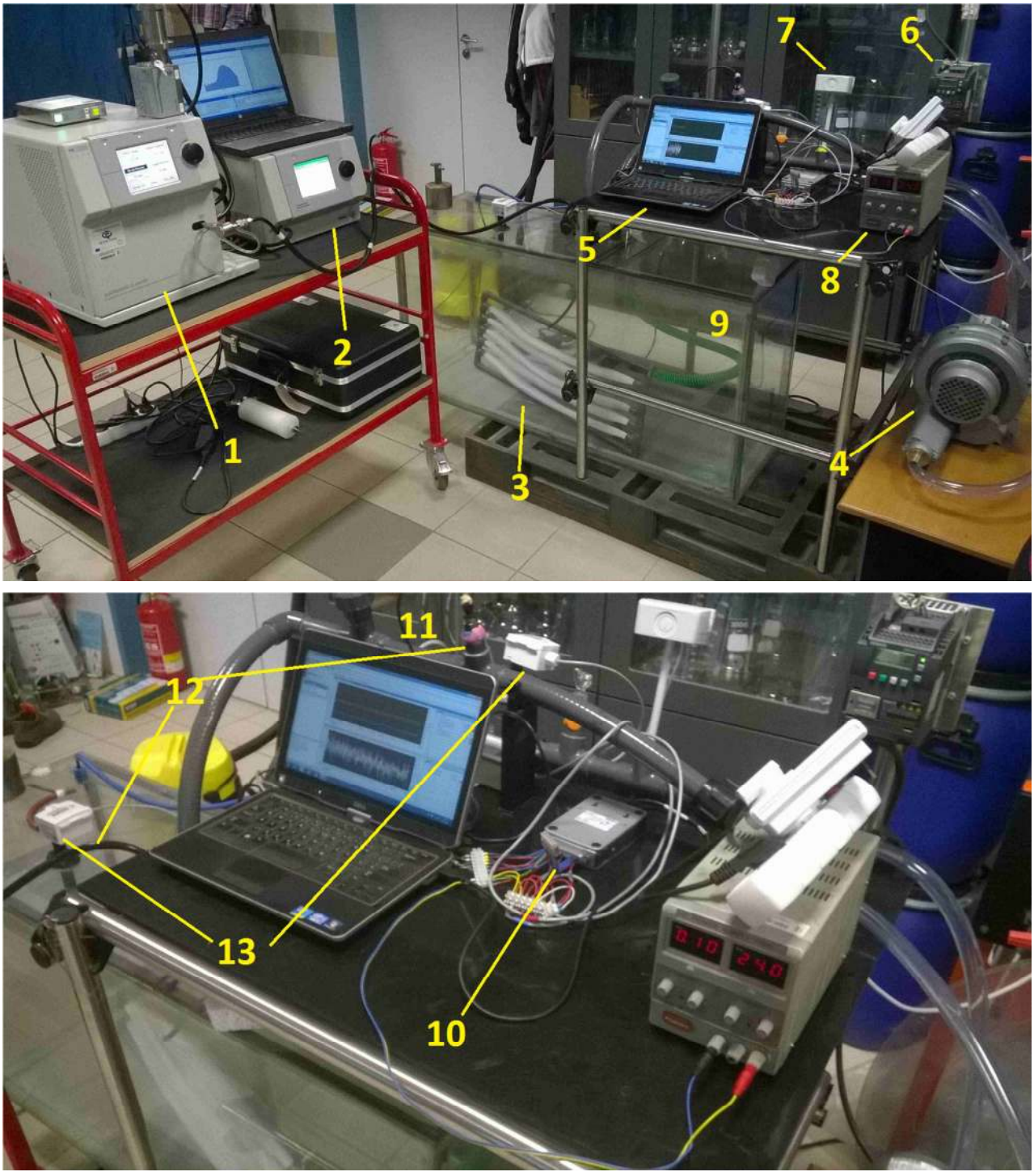

Fig. S4.00: *A real view of the experimental setup: SMPS (1), CPC (2), HFM module (3), fan (4), data recording (5), inverter (6), velocity probe (7), laboratory source (8), glass chamber (9), data acquisition card (10), differential pressure sensor (11), aerosol sampling spots (12), temperature and humidity sensors (13)*

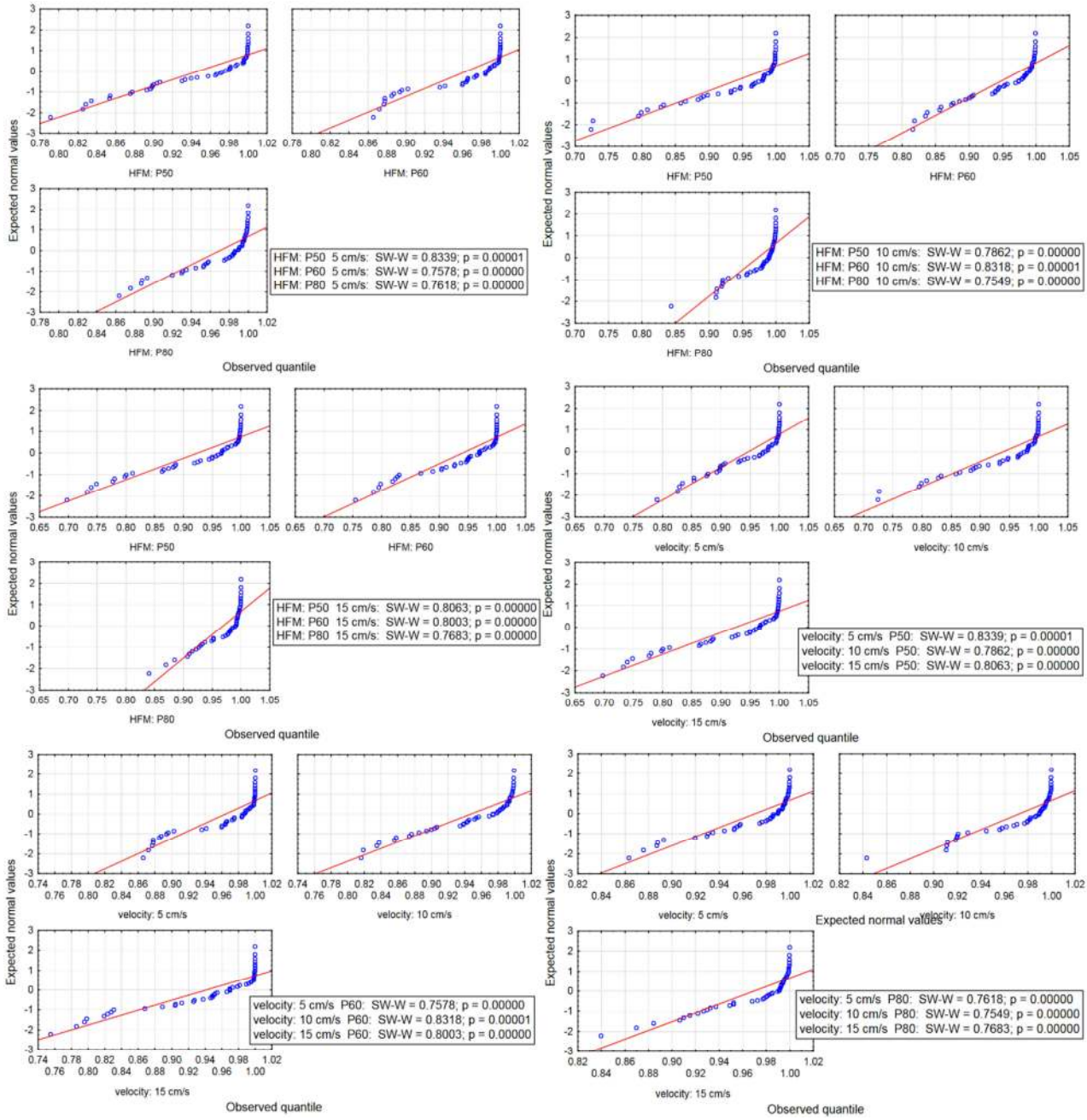

Fig. S4.0: *Shapiro-Wilk test on data normality: normal p-graphs from efficiency values categorized by permeate velocity and HFM type*

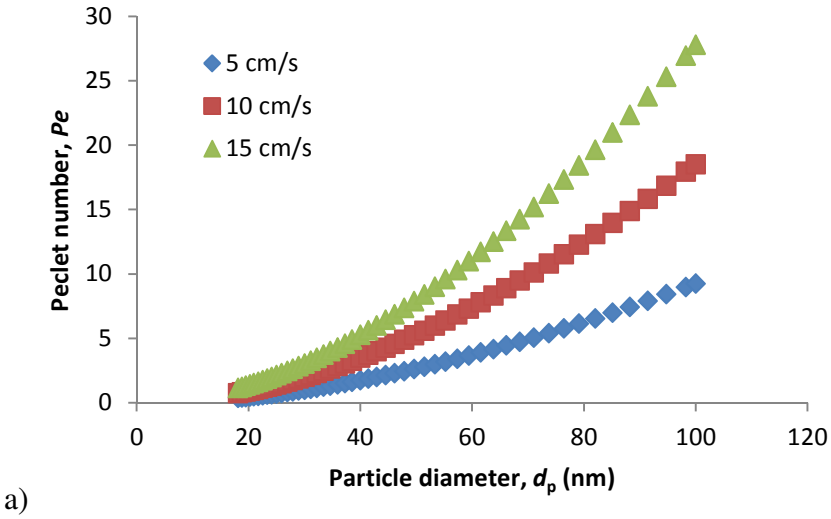

a)

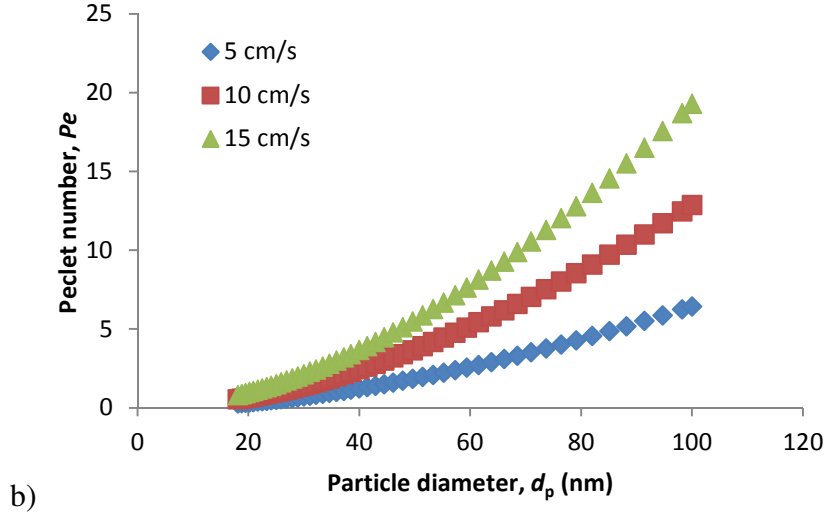

b)

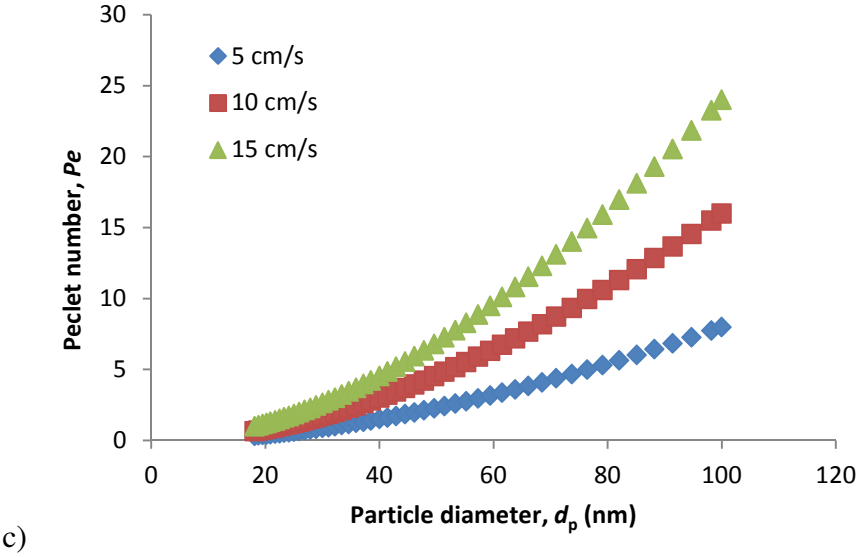

c)

Fig. S4.1: *Peclet number as a function of particle size at different permeate velocities for P50 (a), P60 (b) and P80 (c)*

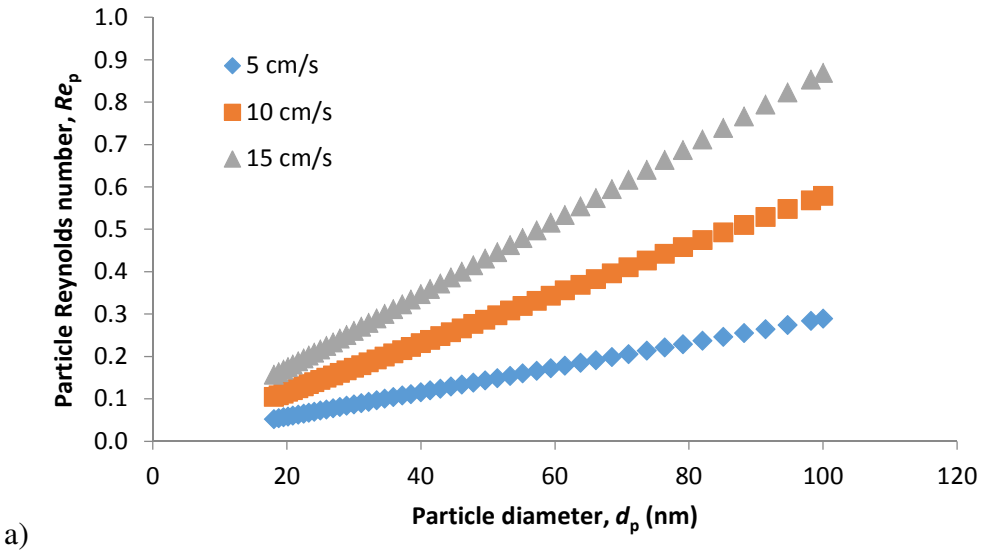

a)

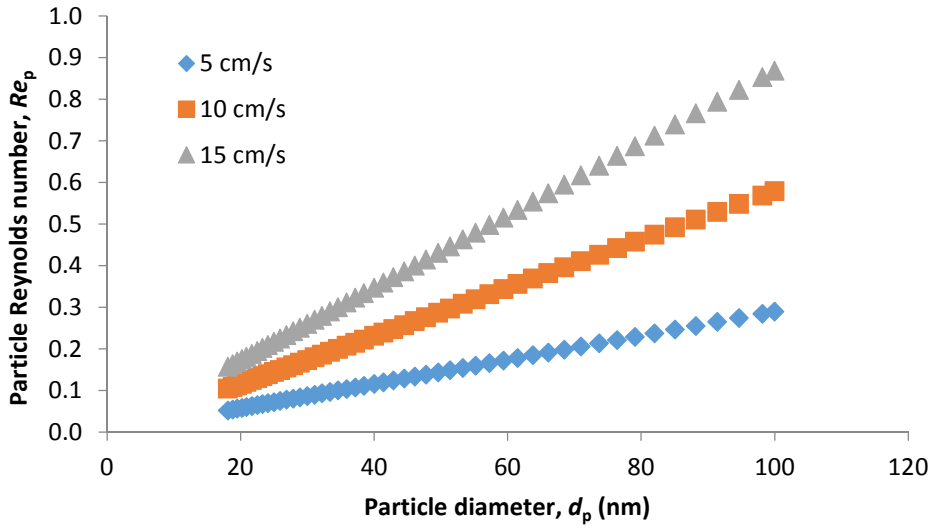

b)

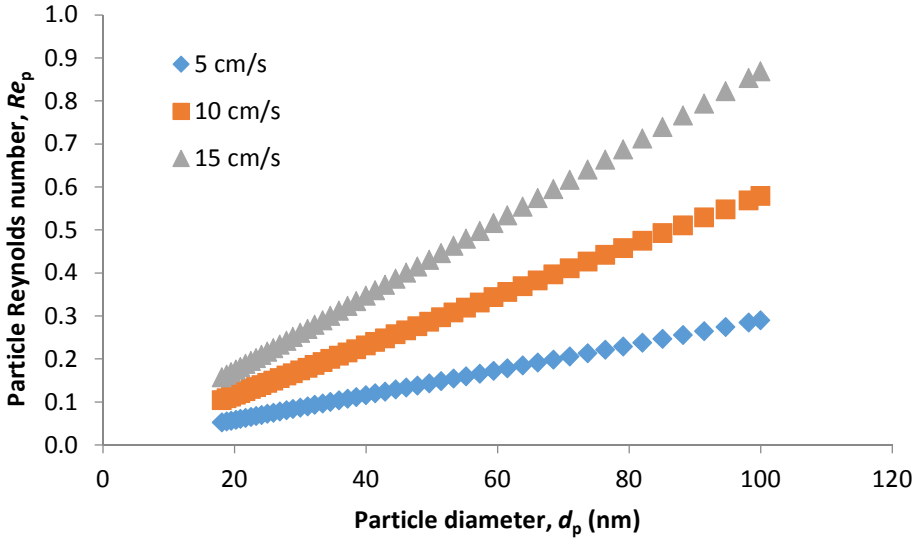

c)

Fig. S4.2: *Particle Reynolds number as a function of particle size at different permeate velocities for P50 (a), P60 (b) and P80 (c)*

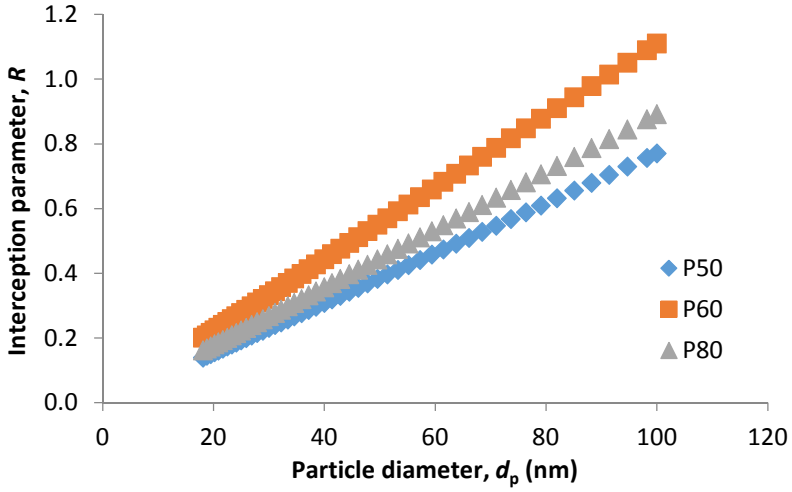

Fig. S4.3: *Interception parameter as a function of particle size*

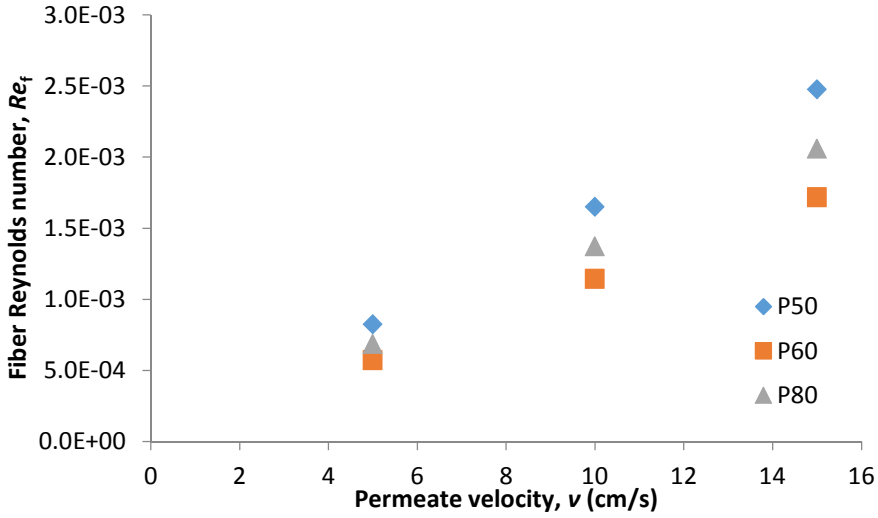

Fig. S4.4: *Fiber Reynolds number as a function of permeate velocity*

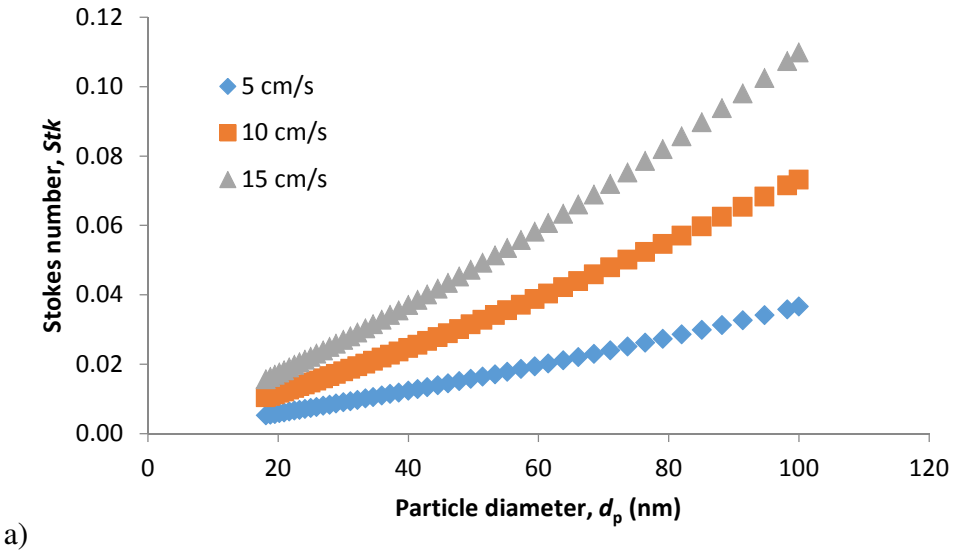

a)

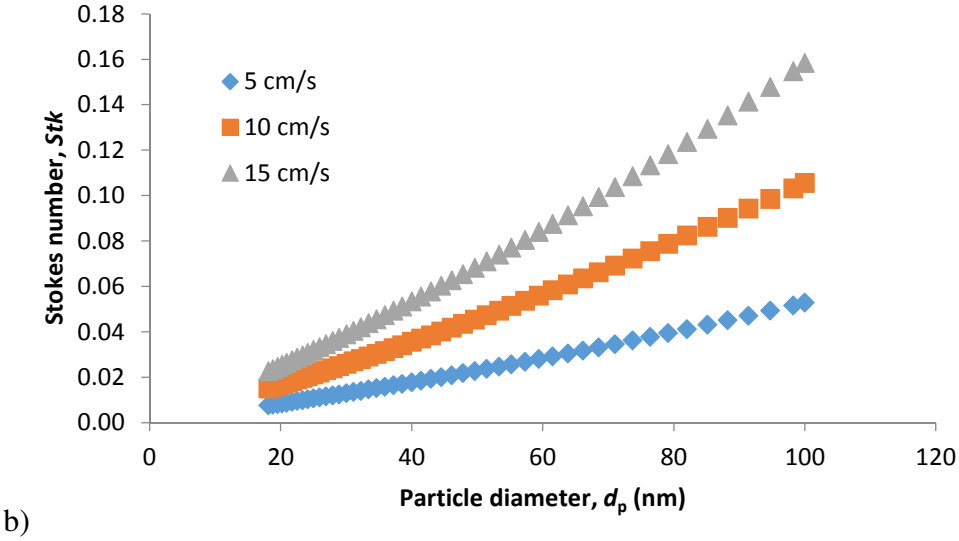

b)

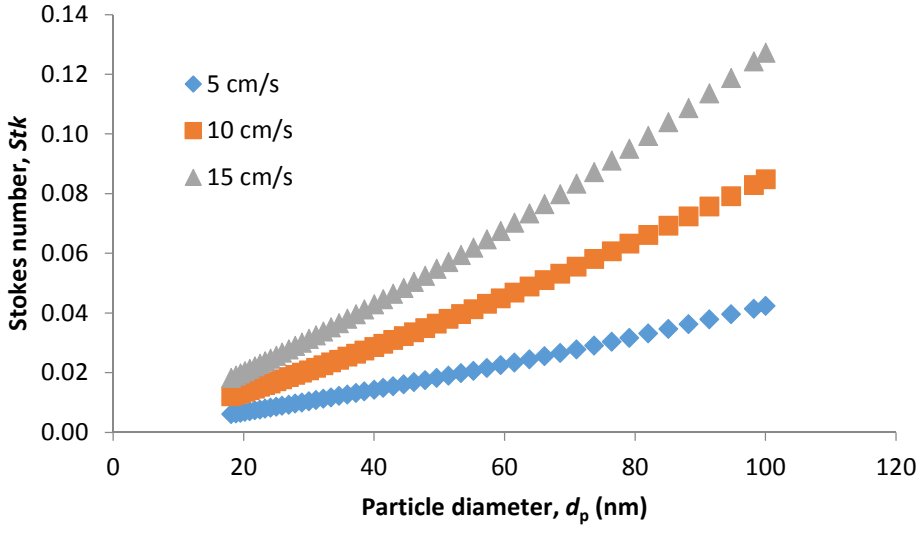

c)

Fig. S4.5: *Stokes number as a function of particle size at different permeate velocities for P50 (a), P60 (b) and P80 (c)*

A I.3 Supplementary material to Chapter 5

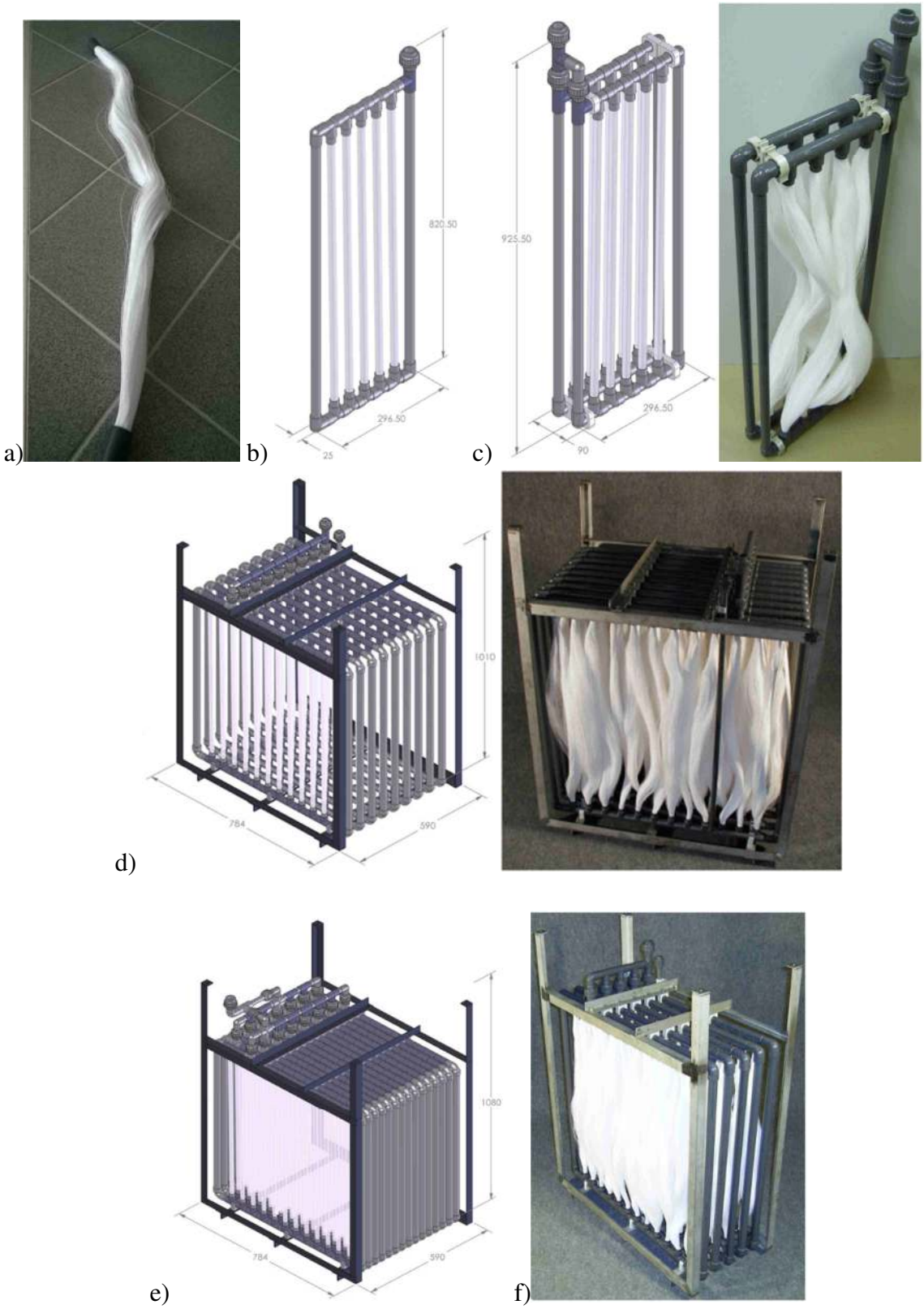

Fig. S5.0: *Scalability of HFMs filtration modules: individual HFM bundle (a), five bundle filtration frame of 4 m^2 area (b), 10 bundle filtration frame (c), membrane module 12x9, consists of 9 frames with 12 membrane bundles giving 86 m^2 filtration area (d) module 12x15 of 144 m^2 filtration area (e) and a real view of 12x5 module of 40 m^2 area (f)*

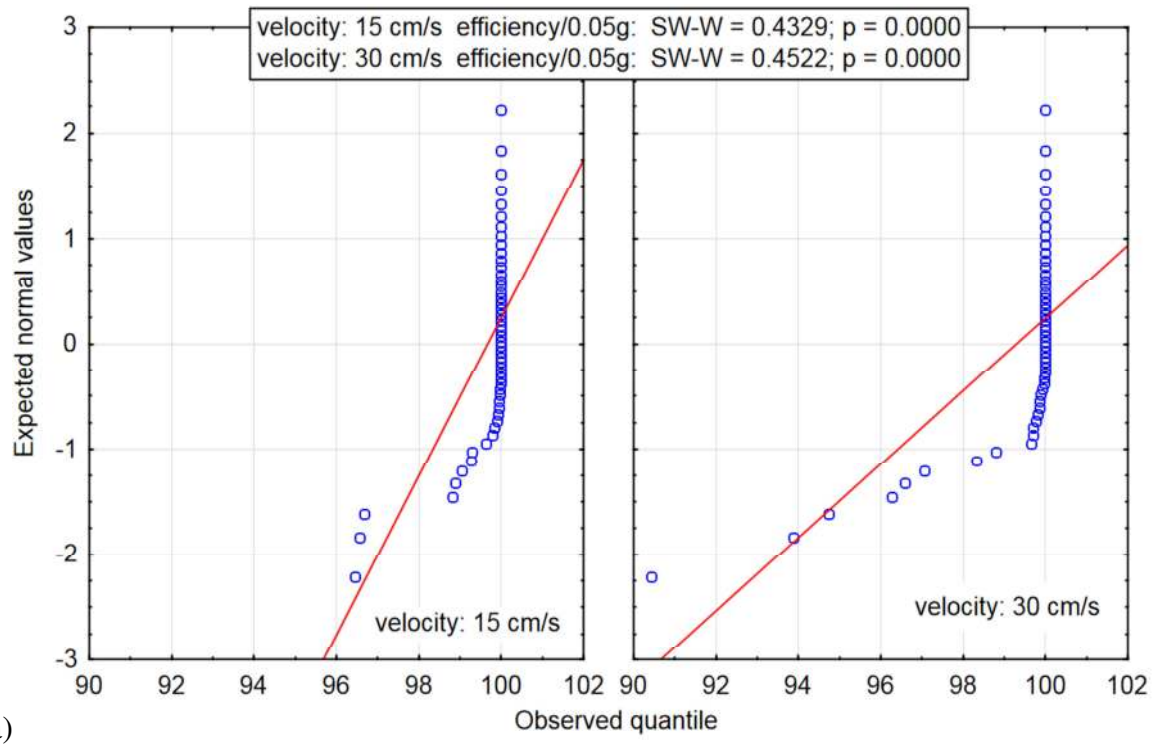

a)

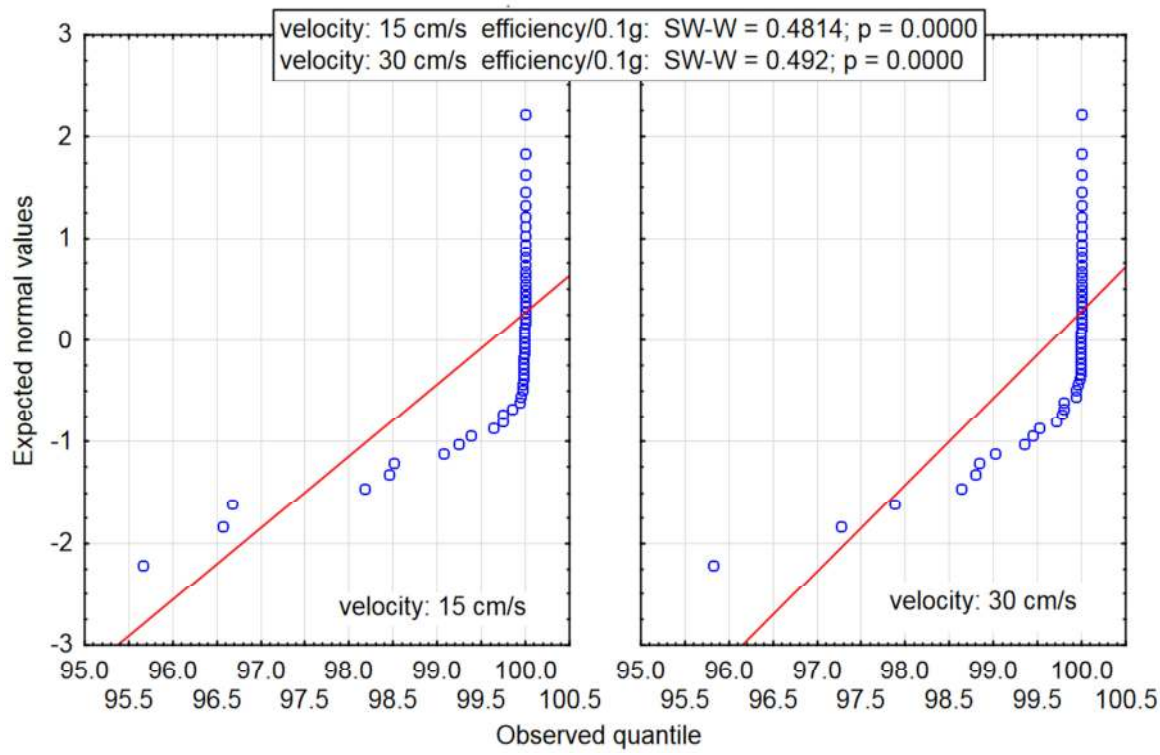

b)

Fig. S5.1: *Shapiro-Wilk test on data normality: normal p-graph from efficiency values categorized by permeate velocity for both dust doses of 50 mg (a) and 100 mg (b)*

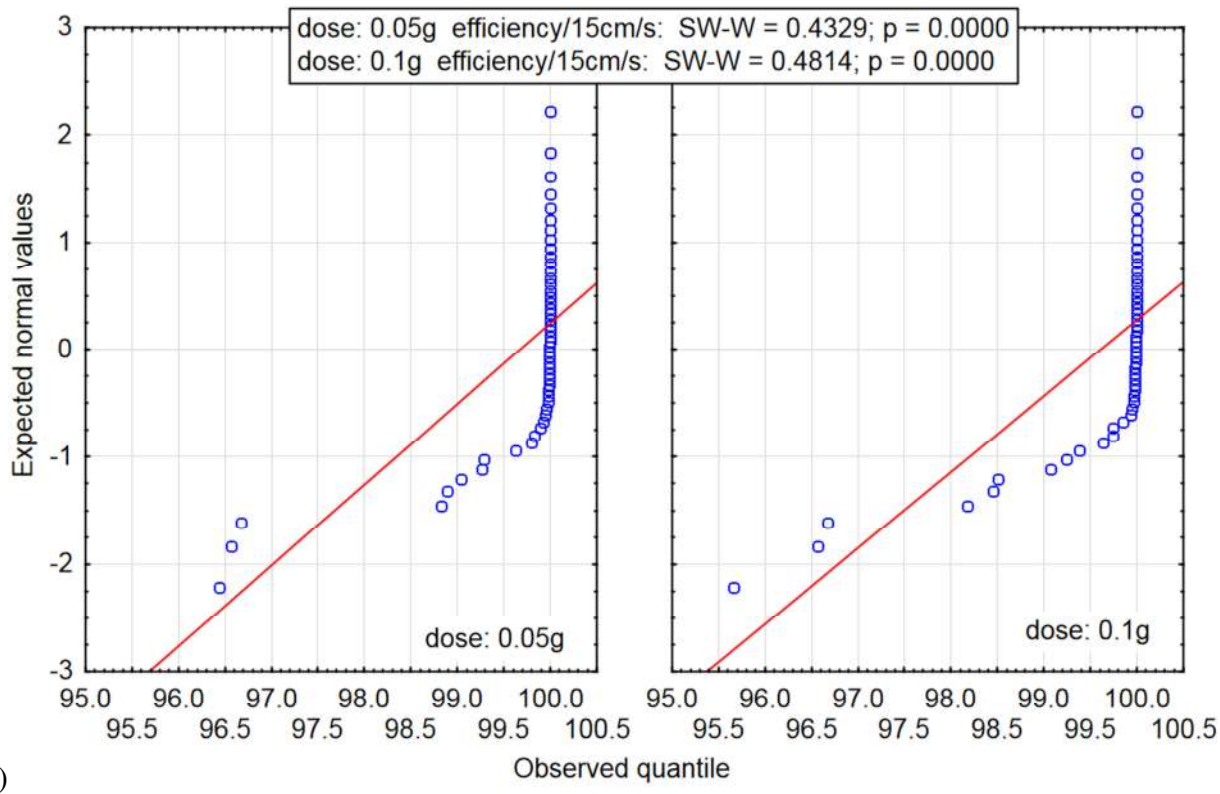

a)

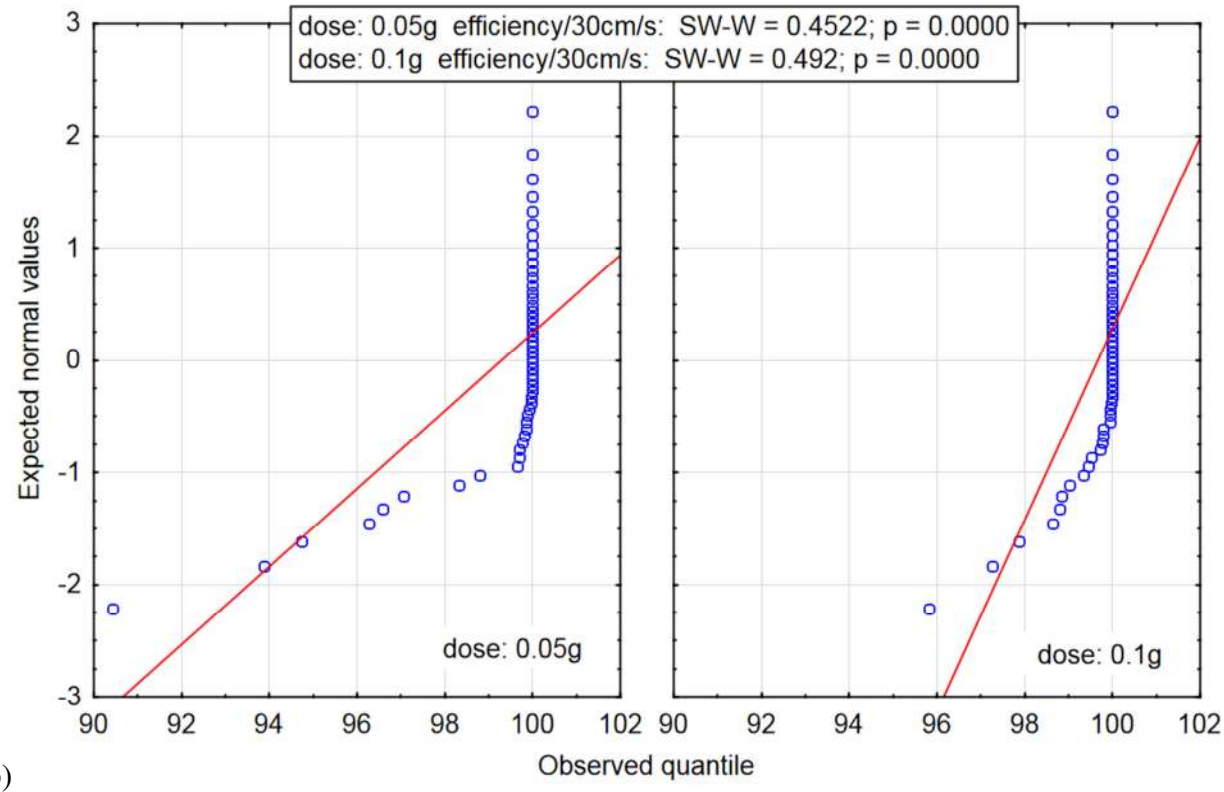

b)

Fig. S5.2: *Shapiro-Wilk test on data normality: normal p-graph from efficiency values categorized by dust dose for both permeate velocities of 15 cm/s (a) and 30 cm/s (b)*

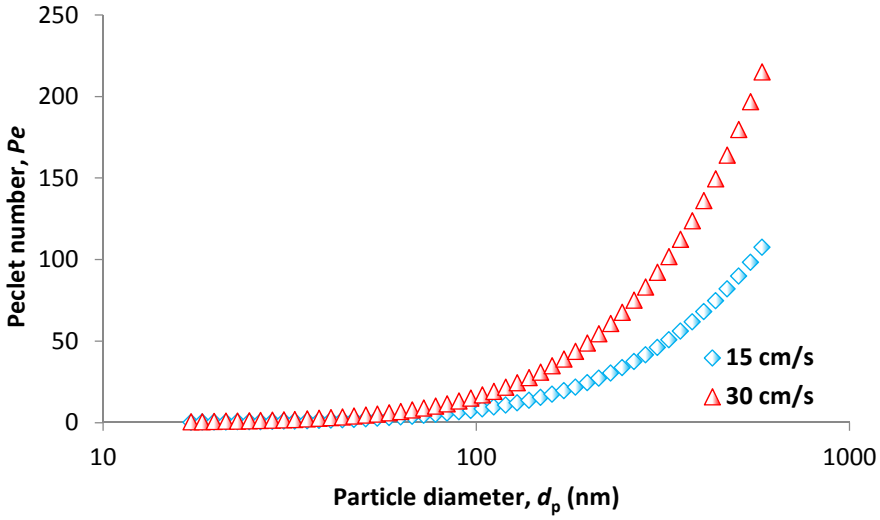

Fig. S5.3: *Peclet number vs particle diameter at given experimental conditions*

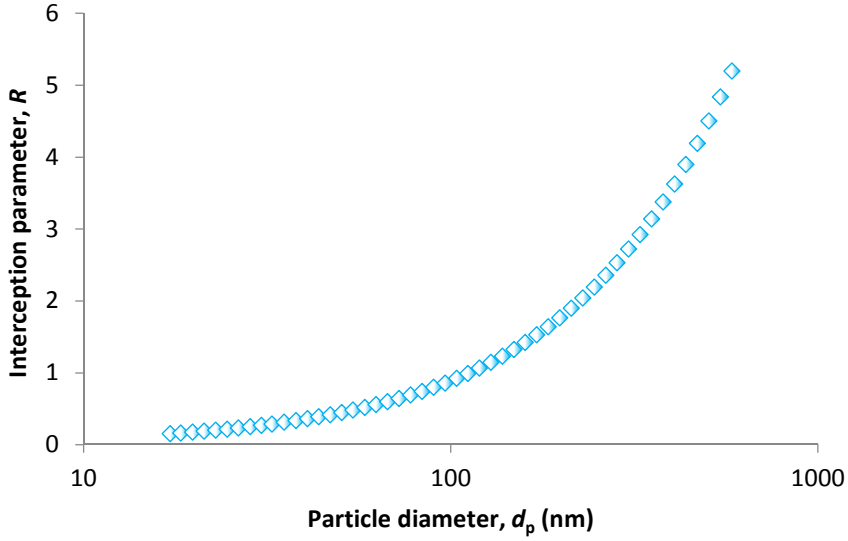

Fig. S5.4: *Interception parameter vs particle diameter*

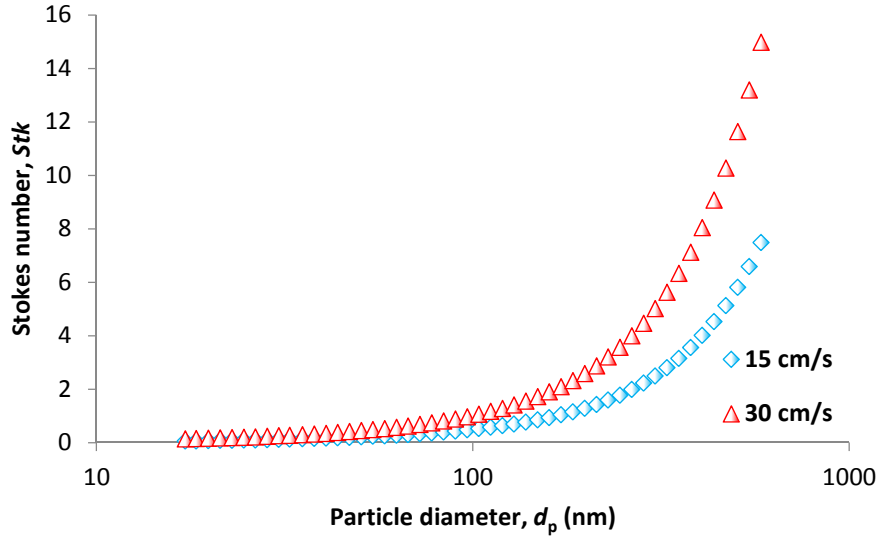

Fig. S5.5: *Stokes number vs particle diameter at given experimental conditions*

A I.4 Supplementary material to Chapter 6

Table S6.1: Various relationships for theoretical prediction of minimum efficiency

Range of validity	ME	Reference
$0.075 < \lambda/d_p < 1.3$	$\eta_{min} = 2.35\left[\left(\frac{1-\alpha}{Ku}\right)^5\left(\frac{kT\sqrt{\lambda}}{\mu}\right)^4\left(\frac{1}{U^4 d_f^{10}}\right)\right]^{1/9}$	[163]
$N_D < 0.01$, $N_R \leq 0.6$	$\eta_{min} = 4.63\left(\frac{Z\varepsilon}{U}\frac{kT\sqrt{\lambda}}{\pi\mu}\right)^{2/5}\left(\frac{d_o}{2}\right)^{-7/5} + 0.013$	[123]
$0.01 \leq N_D < 0.1$, $N_R \leq 0.6$	$\eta_{min} = 3\left(\frac{Z\varepsilon}{U}\frac{kT\sqrt{\lambda}}{\pi\mu}\right)^{2/5}\left(\frac{d_o}{2}\right)^{-7/5} + 0.1$	[123]
$N_D > 0.01$, $N_R \leq 0.6$	$\eta_{min} = 0.254\ln\left[0.11\left(\frac{d_o}{2}\right)^{-1.5}\right] + 0.38$	[123]

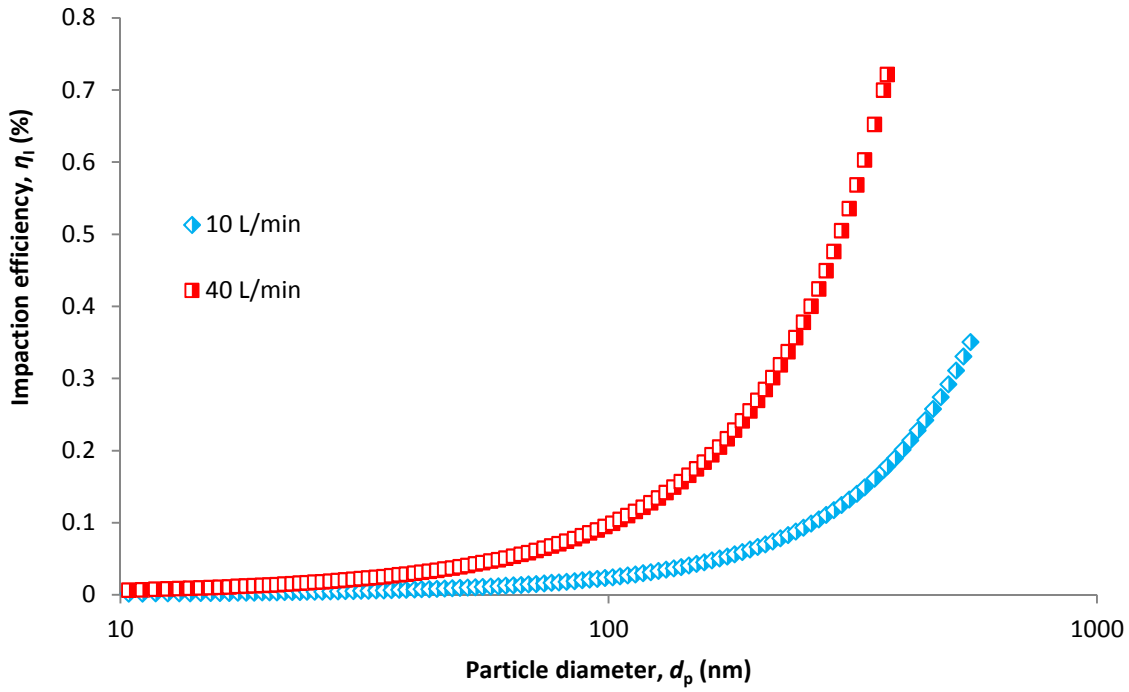

Fig. S6.1: *Impaction efficiency in relation to particle size at given experimental conditions*

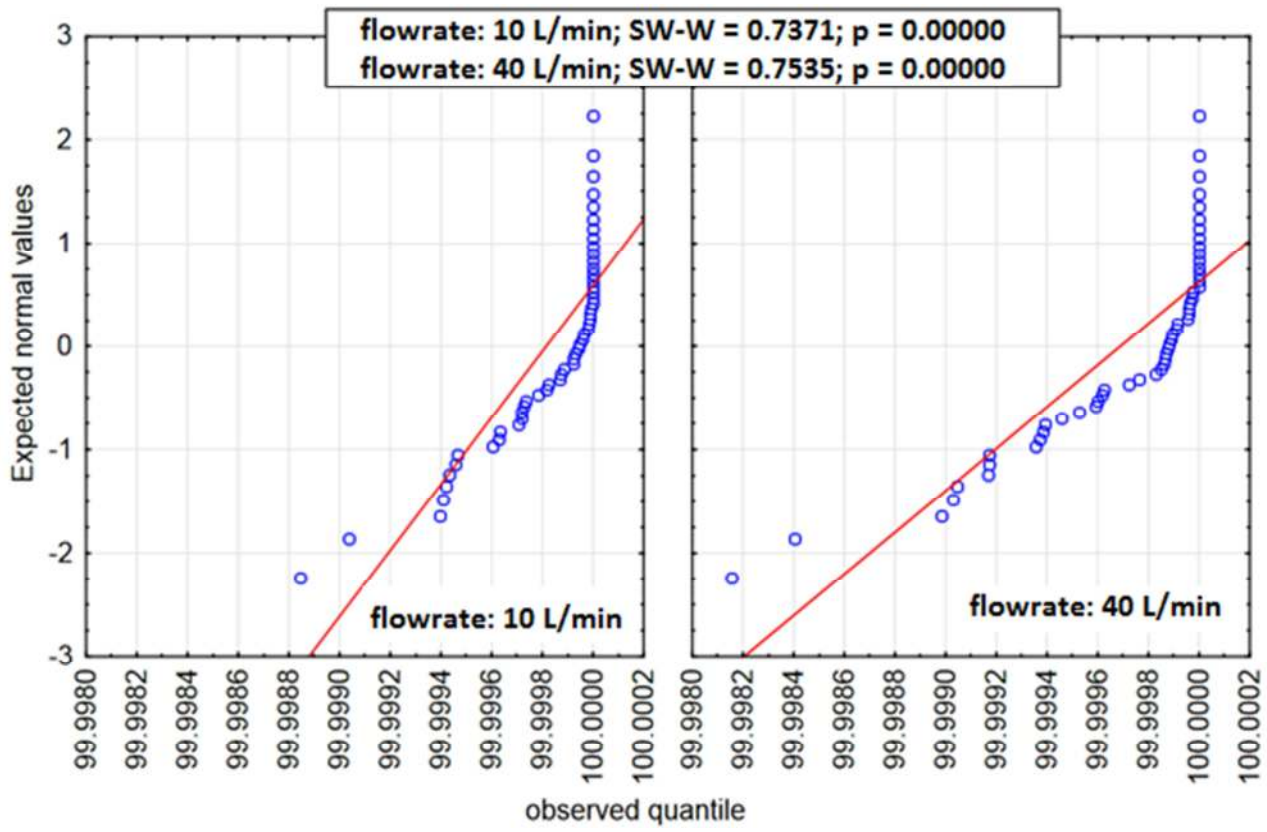

Fig. S6.2: *Normal p-graph of efficiency data categorized by air flowrate*

A I.5 Supplementary material to Chapter 7

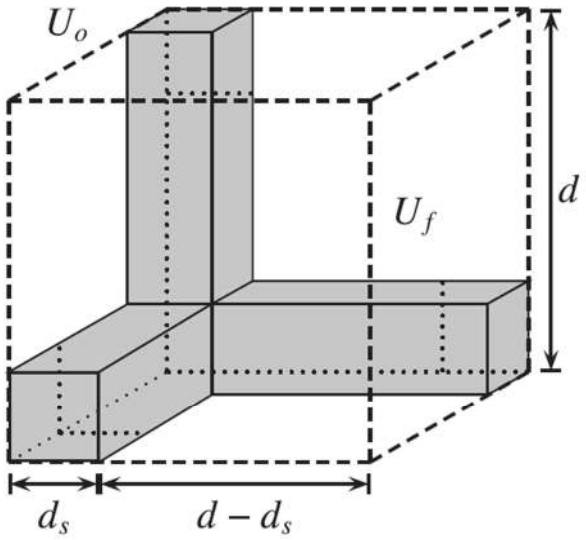

Fig. S7.0: *Representative unit cell (RUC) model resembling the average geometry of a 3D isotropic fibrous medium (adopted from* **[170]***)*

Equations derived for predicting the pressure drop of Nuclepore filters for different pore Knudsen numbers (Kn_p). For $Kn_p << 1$, the equation is as follows:

$$TMP = p_1 - p_1\sqrt{1 - 81.5\frac{\mu Z U}{p_1 d_o^4 N_p}} \tag{S7.1}$$

where p_1 is the gas pressure upstream of the filter, μ is the gas viscosity, Z is the filter thickness, U is the face velocity, N_p is the number of pores and d_o is the pore diameter. For $Kn_p < 1$ following equation can be used:

$$TMP = p_1 - p_1\sqrt{1-81.5\frac{\mu Z U}{p_1 d_o^4 N_p (1+11\lambda/d_o)}} \tag{S7.2}$$

where λ is mean free path of gas molecules. If Kn_p is near unity or > 1, the relationship is as follows:

$$TMP = p_1 + 6.84\frac{\Omega\mu}{d_o}\sqrt{\frac{2\pi R_m T}{M_w}} - \sqrt{\left[p_1 + 6.84\frac{\Omega\mu}{d_o}\sqrt{\frac{2\pi R_m T}{M_w}}\right]^2 - 81.5\frac{\mu Z p_1 U}{d_o^4 N_p}} \tag{S7.3}$$

where Ω is Adzumi's constant, M_w is molecular weight of gas, T is temperature and R_m is molar gas constant.

Air flowrate through the membrane wall (Q_f) can be described using Darcy equation (Eq. 7.2) in the form:

$$\frac{dQ_f(x)}{dx} = \frac{k\pi D_o\left[p_f(x) - p_p(x)\right]}{\mu Z} \tag{S7.4}$$

where $dQ_f(x)/dx$ is the membrane flux at a point x along the fiber length, D_o is the fiber outer diameter, $p_f(x)$ and $p_p(x)$ are the upstream air (feed) pressure (assumed to be equal to the atmospheric pressure) and permeate pressure at the point x along the fiber, respectively. The permeate flow in the fiber lumen can be estimated using the Hagen-Poiseuille equation for flow in a capillary as follows:

$$\frac{dp_p(x)}{dx} = -\frac{128\mu}{\pi D_i^4} Q_p(x) \tag{S7.5}$$

where $Q_p(x)$ is the permeate flowrate at the point x along the fiber. Relating the membrane flux and permeate flowrate along the fiber length with a mass balance gives:

$$\frac{dQ_f(x)}{dx} = \frac{dQ_p(x)}{dx} = \frac{k\pi D_o\left[p_f(x) - p_p(x)\right]}{\mu Z} \tag{S7.6}$$

Differentiating Eq. (S7.6) with $p_f(x) = p_{atm}$ = const. yields:

$$\frac{d^2Q_p(x)}{dx^2} = \frac{k\pi D_o}{\mu Z} - \frac{k\pi D_o}{\mu Z}\left(\frac{dp_p(x)}{dx}\right) \tag{S7.7}$$

Substituting $dp_p(x)/dx$ from Eq. (S7.5) into Eq. (S7.7) we obtain:

$$\frac{d^2Q_p(x)}{dx^2} = \frac{128 k D_o}{Z D_i^4} Q_p(x) \tag{S7.8}$$

This is a second order differential equation which after solving gives:

$$Q_p(x) = C_a e^{x\sqrt{\frac{128kD_o}{ZD_i^4}}} + C_b e^{-x\sqrt{\frac{128kD_o}{ZD_i^4}}} \tag{S7.9}$$

where C_a and C_b are constants which are found by applying boundary conditions as follows:

$$Q_p(0) = 0 \tag{S7.10}$$

$$p_{\mathrm{p}}(L) = p_{\mathrm{s}} \tag{S7.11}$$

where p_{s} is the suction pressure at the outlet induced by the fan. The permeate flowrate for given boundary conditions is then expressed as:

$$Q_{\mathrm{p}}(L) = \frac{k\pi D_{\mathrm{o}}}{\psi\mu Z} \frac{\left(p_{\mathrm{atm}} - p_{\mathrm{s}}\right)\left(\mathrm{e}^{\psi L} - \mathrm{e}^{-\psi L}\right)}{\left(\mathrm{e}^{\psi L} + \mathrm{e}^{-\psi L}\right)} \tag{S7.12}$$

where ψ is calculated as follows:

$$\psi = \sqrt{\frac{128 k D_{\mathrm{o}}}{Z D_{\mathrm{i}}^4}} \tag{S7.13}$$

Rearranging the Eq. S7.2 to derive the pressure drop, i.e. a difference between the ambient (atmospheric) pressure and suction pressure at the downstream side of the membrane ($p_{\mathrm{atm}} - p_{\mathrm{s}}$), gives:

$$\Delta p = \left(p_{\mathrm{atm}} - p_{\mathrm{s}}\right) = \frac{\psi\mu Z}{k\pi D_{\mathrm{o}}} \frac{Q_{\mathrm{p}}(L)\left(\mathrm{e}^{\psi L} + \mathrm{e}^{-\psi L}\right)}{\left(\mathrm{e}^{\psi L} - \mathrm{e}^{-\psi L}\right)} \tag{S7.14}$$

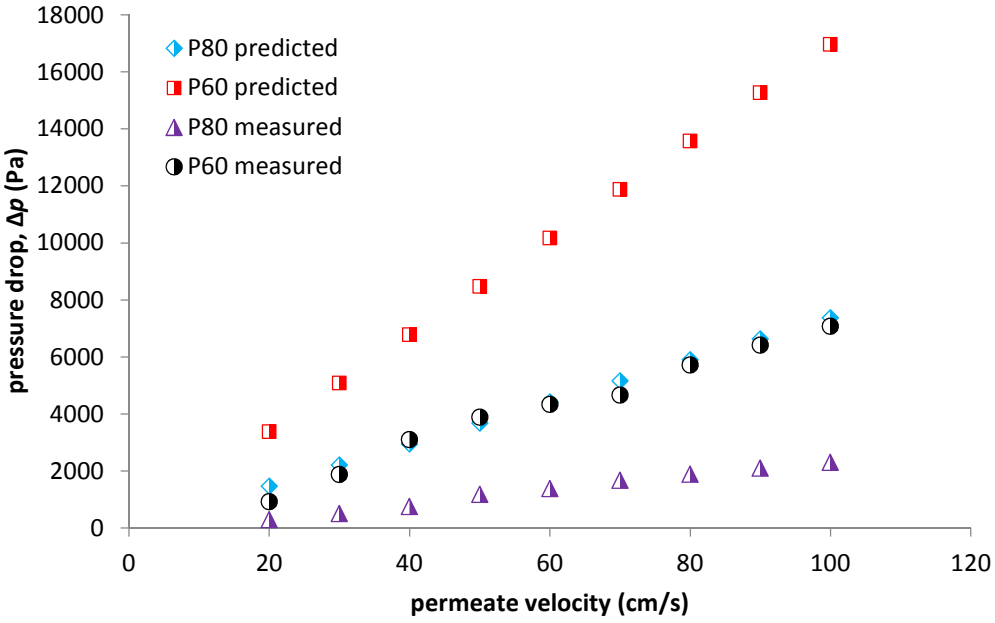

Fig. S7.1: *Comparison of experimental pressure drop with predicted values based on Eq. (S7.14)*

Table S7.1: *Composition of the ASHRAE A2 test dust*

Chemical ingredient	% of weight
SiO_2	68 – 76
Al_2O_3	10 – 15
Fe_2O_3	2 – 5
Na_2O	2 – 4
CaO	2 – 5
MgO	1 – 2

Table S7.2: *Comparison of long-range effect contributions to void function obtained using different models*

	P60	P80	Model
$f_l(\varepsilon_c)$	0.455	0.588	Happel [195]
	0.570	0.710	Brinkmann [194]
	0.508	0.675	Kim and Russel [196]

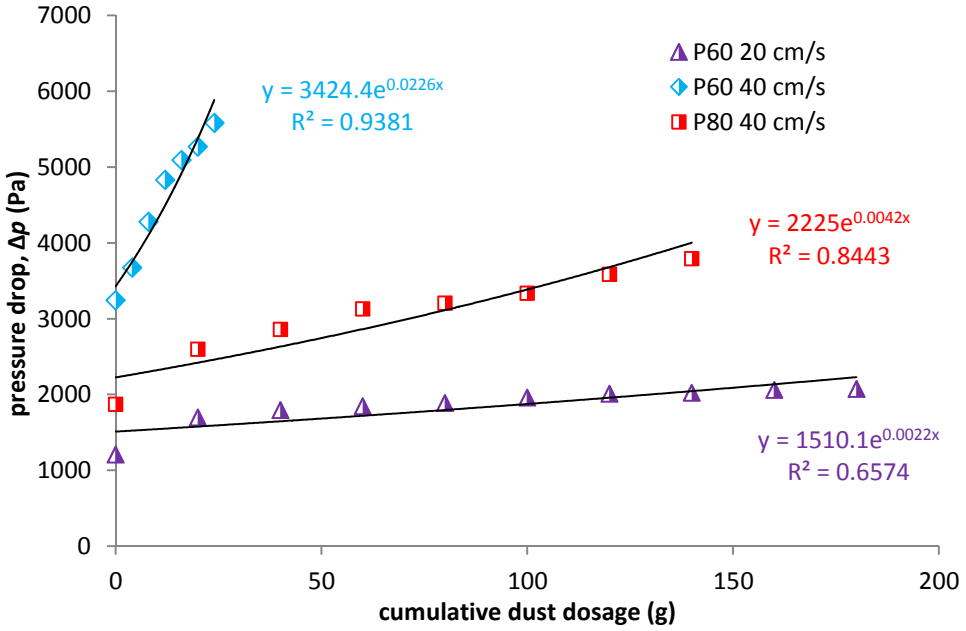

Fig. S7.2: *Pressure drop in relation to dosed dust weight with exponential curve fit*

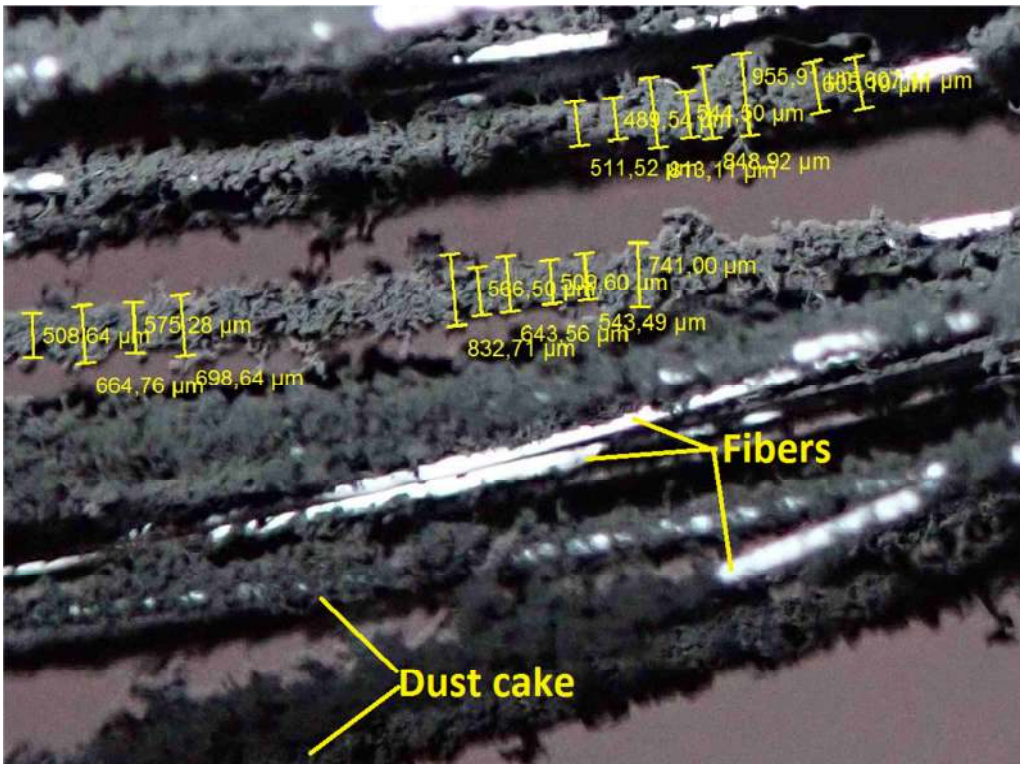

Fig. S7.3: *Determining the cake thickness using the Stream Motion software*

Appendix II – Author's publications and conference attendances

AII.1 Publications in impact journals related to this thesis

BULEJKO, P. Numerical Comparison of Prediction Models for Aerosol Filtration Efficiency Applied on a Hollow-Fiber Membrane Pore Structure. *Nanomaterials,* 2018, roč. 8, č. 6, s. 1-24.

BULEJKO, P.; SVĚRÁK, T.; DOHNAL, M.; POSPÍŠIL, J. Aerosol filtration using hollow-fiber membranes: Effect of permeate velocity and dust amount on separation of submicron TiO_2 particles. *Powder Technology,* 2018, roč. 340, č. 1, s. 344-353.

BULEJKO, P.; DOHNAL, M.; POSPÍŠIL, J.; SVĚRÁK, T. Air filtration performance of symmetric polypropylene hollow-fibre membranes for nanoparticle removal. *Separation and Purification Technology,* 2018, roč. 197, č. 1, s. 122-128.

AII.2 Other publications related to this thesis

BULEJKO, P.; SVĚRÁK, T.; KRIŠTOF, O.; DOHNAL, M.; ONDRÁČEK, J. Aerosol separation efficiency and pressure drop evolution with intense particle loading of hollow-fiber membranes. In *23rd International Congress of Chemical and Process Engineering CHISA 2018 Prague*. 2018. s. 1 (1 s.).

BULEJKO, P.; DOHNAL, M.; POSPÍŠIL, J.; KRIŠTOF, O.; SVĚRÁK, T.; KEJÍK, P. Air filtration using hollow-fibre membranes for nanoparticle removal. In *FILTECH 2018, March 13-15, Cologne – Germany.* 2018. s. 1-12. ISBN: 978-3-941655-15-7.

BULEJKO, P.; DOHNAL, M.; POSPÍŠIL, J.; KRIŠTOF, O.; KEJÍK, P.; SVĚRÁK, T. Efficiency of hollow-fiber membranes for air filtration of submicron particles. In *44th International Conference of the Slovak Society of Chemical Engineering*. 2017. s. 495-499. ISBN: 978-80-89597-58-1.

BULEJKO, P.; DOHNAL, M.; POSPÍŠIL, J.; SVĚRÁK, T. Air purification performance of polypropylene hollow-fibre membranes in submicron particle removal. In *Proceedings of 18th Annual Conference of the Czech Aerosol Society.* Praha: Česká aerosolová společnost, 2017. s. 88-91. ISBN: 978-80-270-2862-7.

BULEJKO, P.; SVĚRÁK, T.; DOHNAL, M.; POSPÍŠIL, J.; KRIŠTOF, O.; KEJÍK, P.; KALIVODA, J. Filtration efficiency of hollow-fiber membranes in airborne particle removal. In *Sborník XVII. výroční konference České aerosolové společnosti, 25.–26. října 2016, Mikulov.* Praha: Česká aerosolová společnost, 2016. s. 65-68. ISBN: 978-80-86186-85-6.

AII.3 Other publications in impact journals

BULEJKO, P., STRÁNSKÁ, E. Electrochemical properties and structural changes of anion-exchange membranes with varying anionic resin moistness. *Ionics* (In revision)

BULEJKO, P., STRÁNSKÁ, E. The effect of initial moisture content of cation-exchange resin on the preparation and properties of heterogeneous cation-exchange membranes. *Materials Chemistry and Physics,* 2018, roč. 205, č. 1, s. 470-479.

BULEJKO, P.; STRÁNSKÁ, E.; WEINERTOVÁ, K. Electrochemical and mechanical stability of ion-exchange membranes in alkaline solution. *Chemical Papers,* 2017, roč. 71, č. 7, s. 1303-1309.

BULEJKO, P.; ADAMEC, V.; SKEŘIL, R.; SCHÜLLEROVÁ, B. BENCKO, V. Levels and health risk assessment of PM10 aerosol in Brno, Czech Republic. *Central European Journal of Public Health,* 2017, roč. 25, č. 2, s. 129-134.

BULEJKO, P.; STRÁNSKÁ, E.; WEINERTOVÁ, K. Properties and structure of heterogeneous ion-exchange membranes after exposure to chemical agents. *Journal of Solid State Electrochemistry,* 2017, roč. 21, č. 1, s. 111-124.

SVĚRÁK, T.; BULEJKO, P.; KRIŠTOF, O.; KEJÍK, P.; KALIVODA, J.; HORSKÝ, J. Covering ability of aluminum pigments prepared by milling processes. *Powder Technology,* 2017, roč. 305, č. 1, s. 396-404.

BULEJKO, P.; BÍLEK, V. Influence of chemical additives and curing conditions on mechanical properties and carbonation resistance of alkali activated slag composites. *Materiali in Tehnologije,* 2017, roč. 51, č. 1, s. 49-53.

BULEJKO, P.; ADAMEC, V.; SCHÜLLEROVÁ, B.; SKEŘIL, R. Levels, sources and health risk assessment of polycyclic aromatic hydrocarbons in Brno, Czech Republic: A five year study. *Environmental Science and Pollution Research,* 2016, roč. 23, č. 20, s. 20462-20473.

AII.4 Other publications indexed in WoS and/or Scopus

ADAMEC, V.; SCHÜLLEROVÁ, B.; HRABOVÁ, K.; SKEŘIL,R.; KADLEC, R.; BULEJKO, P.; ADAM, V. Nanoparticle concentration in the traffic loaded urban area. In *Nanocon 2017.* Ostrava: TANGER Ltd., 2018. s. 698-703. ISBN: 978-80-87294-81-9.

BÍLEK Jr., V.; BULEJKO, P.; KEJÍK, P.; HAJZLER, J.; MÁSILKO, J.; BEDNÁREK, J.; TKACZ, J.; KALINA, L. Potential use of blast furnace slag for filtration membranes preparation: A pilot study. *IOP Conference Series: Materials Science and Engineering.* Bristol: IOP Publishing, 2018. s. 1-6.

KEJÍK, P.; BÍLEK Jr., V.; BULEJKO, P.; HAJZLER, J.; BŘEZINA, M.; GALVÁNKOVÁ, L.; KALINA, L. Porous Systems Based on Alkali-Activated Fly Ash. *Solid State Phenomena.* Switzerland: Trans Tech Publications, 2018. s. 179-184. ISBN: 978-3-0357-1348-0.

SVĚRÁK, T.; BULEJKO, P.; OSTREZI, J.; KRIŠTOF, O.; KALIVODA, J.; KEJÍK, P.; MAYEROVÁ, K.; ADAMČÍK, M. Separation of gaseous air pollutants using membrane contactors. *IOP Conference Series: Earth and Environmental Science,* 2017, roč. 92, č. 1, s. 1-5.

ADAMEC, V.; SCHÜLLEROVÁ, B.; BULEJKO, P.; DE LUCA, M.; RUSSO, F. Methodology of Environmental Damage Assessment Caused by Road Accidents. In *International Conference on Traffic and Transport Engineering ICTTE, November 24 - 25, 2016.* Belgrade, Serbia: City Net Scientific Research Center Ltd., 2016. s. 616-626. ISBN: 978-86-916153-3-8.

SVĚRÁK, T.; BULEJKO, P.; MAYEROVÁ, K.; KEJÍK, P.; KRIŠTOF, O.; RAUDENSKÝ, M. Hiding Power of Aluminum Metal Pigments Development in the Ball Mill Grinding Process. *Solid State Phenomena,* 2016, roč. 244, č. 1, s. 19-25.

VOTAVOVÁ, H.; POHANKA, M.; BULEJKO, P. Cooling homogeneity measurement during hydraulic descaling in spray overlapping area. In *METAL 2015 24th International Conference on Metallurgy and Materials.* 1. Ostrava: Tanger Ltd Ostrava, 2015. s. 265-270. ISBN: 978-80-87294-58-1.

BULEJKO, P.; SVĚRÁK, T.; KEJÍK, P.; KRIŠTOF, O.; SIKOROVÁ, K. The potential use of geopolymer-based materials in filtration applications. *21st International Congress of Chemical Engineering CHISA 2014, Praha, Czech Republic, Czech Society of Chemical Engineering.* 2014. ISBN: 978-80-02-02555-9.

SVĚRÁK, T.; KEJÍK, P.; SLANINA, O.; SIKOROVÁ, K.; BULEJKO, P.; KRIŠTOF, O. Bulk properties of micro-fine ligneous fillers. In *21st International Congress of Chemical and Process Engineering CHISA 2014 and 17th Conference PRES 2014,* Praha: Orgit Ltd., 2014. s. 1-10. ISBN: 978-80-02-02555-9.

BULEJKO, P.; SVĚRÁK, T. Mechanical and filtering properties of non-sintered porous solids for filtration applications. In *Engineering Mechanics 2014, 20th International Conference, May 12-15, 2014, Svratka, Czech Republic. Engineering mechanics 2014.* 2014. s. 112-115. ISBN: 978-80-214-4871-1.

AII.5 Other publications

BULEJKO, P.; ADAMEC, V.; SCHÜLLEROVÁ, B.; HRABOVÁ, K. Estimation of particulate matter (PM) deposition efficiency and PM-bound metals deposition fluxes in human respiratory tract. In *Proceedings of 27th International Scientific Conference of Forensic Engineering, Expert Forensic Science 2018.* Brno, 2018. s. 488-494. ISBN: 978-80-214-5600-6.

ADAMEC, V.; SCHÜLLEROVÁ, B.; BENCKO, V.; HRABOVÁ, K.; BULEJKO, P. Possible approaches to risk assessment of nanoparticles from the expert's point of view. In *Proceedings of 27th International Scientific Conference of Forensic Engineering, Expert Forensic Science 2018.* Brno, 2018. s. 9-21. ISBN: 978-80-214-5600-6.

KRIŠTOF, O.; BULEJKO, P.; SVĚRÁK, T. CFD simulation of a gas phase and spiral nozzle-sprayed liquid in a wet scrubber. In *23rd International Congress of Chemical and Process Engineering CHISA 2018 Prague*. 2018. s. 1-2.

BULEJKO, P.; BÍLEK, V. Ceramic membranes based on alkali- activated materials. In *44th International Conference of the Slovak Society of Chemical Engineering.* 2017. s. 501-507. ISBN: 978-80-89597-58-1.

KRIŠTOF, O.; SVĚRÁK, T.; BULEJKO, P.; KEJÍK, P.; KALIVODA, J. Experimental and CFD investigation of gas and liquid phase in scrubber for absorption processes. In *44th International Conference of the Slovak Society of Chemical Engineering.* 2017. s. 448-453. ISBN: 978-80-89597-58-1.

ADAMEC, V.; BULEJKO, P.; SCHÜLLEROVÁ, B.; ŠIMONÍKOVÁ, L.; SÁŇKA, M. Assessment of Heavy Metal Pollution in Surface Soils of Urban Areas in Brno. In *17th International Multidisciplinary Scientific Geoconference SGEM 2017, Vienna,* 2017. s. 317-324. ISBN: 978-619-7408-28-7.

SCHÜLLEROVÁ, B.; ADAMEC, V.; BULEJKO, P. Application of systemic approach for assessment of environmental damage using risk analysis methods. In *Proceedings of 26th*

International Scientific Conference of Forensic Engineering, Expert Forensic Science 2017. Brno, 2017. s. 512-521. ISBN: 978-80-214-5459-0.

BULEJKO, P.; ADAMEC, V.; SCHÜLLEROVÁ, B.; SKEŘIL, R. Health risk assessment of heavy metals bonded to airborne particulate matter. In *Proceedings of 26th International Scientific Conference of Forensic Engineering*. Brno, 2017. s. 320-326. ISBN: 978-80-214-5459-0.

KRIŠTOF, O.; SVĚRÁK, T.; KEJÍK, P.; BULEJKO, P.; MAYEROVÁ, K.; KALIVODA, J. Experimental investigation of the breakup of spiral-nozzle-produced liquid curtain for absorption processes. In *22nd International Congress of Chemical and Process Engineering CHISA 2016* Praha: Czech Society of Chemical Engineering, 2016.

BULEJKO, P.; ADAMEC, V.; SCHÜLLEROVÁ, B.; SKEŘIL, R. Levels, source apportionment and health risk assessment of polycyclic aromatic hydrocarbons fixed to airborne particulate matter in areas of Brno city. In *Proceedings of 25th International Scientific Conference of Forensic Engineering Expert Forensic Science 2016, Brno.* Brno: 2016. s. 414-427. ISBN: 978-80-214-5321-0.

KEJÍK, P.; BULEJKO, P.; SVĚRÁK, T.; KRIŠTOF, O.; MAYEROVÁ, K. Self-supported geopolymer-based barriers for filtration applications. *24th International Conference on Materials and Technology. Ljubljana, Slovenia: Inštitut za kovinske materiale in tehnologije*, 2016. ISBN: 978-961-94088-0-3.

BULEJKO, P.; KŘIVČÍK, J. Determination of milling performance of a GSM 06 laboratory vibrating mill with different grinding media. *Workshop of Students' presentations 2015: Membranes and membrane processes*. Česká Lípa: Czech Membrane Platform, 2015. s. 11-11. ISBN: 978-80-904517-4-2.

KEJÍK, P.; SVĚRÁK, T.; KRIŠTOF, O.; BULEJKO, P.; MAYEROVÁ, K. Attritor iron content measurement via objective colour determination. In *23rd International Conference on Materials and Technology. Portoroz, Slovenia*, 2015. s. 125-125. ISBN: 978-961-92518-8-1.

SVĚRÁK, T.; BULEJKO, P.; KEJÍK, P.; MAYEROVÁ, K.; KRIŠTOF, O.; RAUDENSKÝ, M. Bulk properties of surface treated limestone powders. In *1st International Conference on Applied Mineralogy & Advanced Materials – AMAM2015.* Digilabs S.a.s., 2015. s. 71-76. ISSN: 2283-5954.

SVĚRÁK, T.; BAKER, C. G. J.; SIKOROVÁ, K.; KEJÍK, P.; BULEJKO, P.; KRIŠTOF, O. Progress of the IR measurement in the area of the fine particulate material water content. *International Journal of Environmental Engineering,* 2015, roč. 2, č. 1, s. 146-149. ISSN: 2374-1724.

BULEJKO, P.; BÍLEK, V. Influence of Chemical Additives and Curing Conditions on Mechanical Properties and Carbonation Resistance of Alkali Activated Slag Composites. In *23rd International Conference on Materials and Technology. Portoroz, Slovenia*, 2015. s. 66-66. ISBN: 978-961-92518-8-1.

BULEJKO, P.; SVĚRÁK, T. Non-sintered porous barriers based on granular materials and inorganic binders. In *13th International Conference on Inorganic Membranes*, July 6-9, 2014, Brisbane, Australia, Book of Abstracts. 2014.

BULEJKO, P.; SIKOROVÁ, K.; KEJÍK, P.; KRIŠTOF, O.; SVĚRÁK, T. Filtration Membranes Based on Secondary Materials: Preparation, Characterization, and Properties. In *22nd*

International Conference on Materials and Technology. Portoroz, Slovenia, 2014. ISBN: 978-961-92518-7-4.

KRIŠTOF, O.; SVĚRÁK, T.; BULEJKO, P.; KEJÍK, P.; SIKOROVÁ, K. Pilot-plant shower scrubber for cleaning polluted gas. In *22nd International Conference on Materials and Technology*. *Portoroz, Slovenia*, 2014. s. 128-128. ISBN: 978-961-92518-7-4.

KRIŠTOF, O.; SVĚRÁK, T.; KEJÍK, P.; BULEJKO, P.; SIKOROVÁ, K. CO2 absorption to the NaOH solution using pilot-plant wet shower scrubber. In *21st International Congress of Chemical Engineering CHISA 2014*, Praha, Czech Republic, Czech Society of Chemical Engineering. 2014. ISBN: 978-80-02-02555-9.

KEJÍK, P.; SVĚRÁK, T.; SIKOROVÁ, K.; KRIŠTOF, O.; BULEJKO, P. Specific grinding energy and phase changes of the limestone and corundum ground stock in the ultrafine activated comminution process. In *21st International Congress of Chemical Engineering CHISA 2014*, Praha, Czech Republic, Czech Society of Chemical Engineering. 2014. s. 1. ISBN: 978-80-02-02555-9.

SVĚRÁK, T.; BULEJKO, P.; ŠÍPKOVÁ, H. Advances in Geopolymer Filtration Membranes Mechanical Properties. In *Membrane Technology Conference and Exposition*. Las Vegas, Nevada, USA, 2014: American Water Works Association.

KEJÍK, P.; SVĚRÁK, T.; SIKOROVÁ, K.; KRIŠTOF, O.; BULEJKO, P. Coir-based fillers grinding and bulk properties. In *22nd International Conference on Materials and Technology, Portoroz, Slovenia*, 2014. s. 111-111. ISBN: 978-961-92518-7-4.

SVĚRÁK, T.; DOHNAL, M.; BULEJKO, P.; SCHWARZEROVÁ, L. Effective use of the powdered coal process data by the fuzzy method, (In Czech). In *Kvalita cementu 2012*, VÚSTAH, Výzkumný ústav stavebních hmot. Brno: VÚSTAH a.s., 2012. s. 61-72. ISBN: 978-80-87397-10-7.

AII.6 Conference attendances

AII.6.1 Lectures

- Engineering Mechanics 2014, Svratka, Czech Republic
- 22nd International Conference on Materials and Technology 2014, Portorož, Slovenia
- 23rd International Conference on Materials and Technology 2015, Portorož, Slovenia
- International Conference Expert Forensic Science, ExFoS 2016, Brno, Czech Republic
- XVII. Annual Conference of the Czech Aerosol Society, 2016, Mikulov
- International Conference Expert Forensic Science, ExFoS 2017, Brno, Czech Republic
- XVIII. Annual Conference of the Czech Aerosol Society, 2017, Třešť, Czech Republic
- International Conference Expert Forensic Science, ExFoS 2018, Brno, Czech Republic
- Filtech 2018, Cologne, Germany
- 23rd International Congress of Chemical and Process Engineering CHISA 2018, Prague, Czech Republic

AII.6.2 Posters

- International Conference on Inorganic Membranes 2014, Brisbane, Australia

- 21st International Congress of Chemical and Process Engineering CHISA 2014, Prague, Czech Republic
- 44th International Conference of the Slovak Society of Chemical Engineering 2017, Demänovská Dolina, Slovakia
- 10th World Congress of Chemical Engineering 2017, Barcelona, Spain
- 23rd International Congress of Chemical and Process Engineering CHISA 2018, Prague, Czech Republic